INVESTIGATING THE IMPACTS OF AGRICULTURAL LAND USE CHANGE ON REGIONAL CLIMATE PROCESSES IN THE NORTHERN NORTH AMERICAN GREAT PLAINS

by

Gabriel Trees Bromley

A dissertation submitted in partial fulfillment
of the requirements for the degree

of

Doctor of Philosophy

in

Ecology and Environmental Science

MONTANA STATE UNIVERSITY
Bozeman, Montana

April 2021

©COPYRIGHT

by

Gabriel Trees Bromley

2021

All Rights Reserved

ACKNOWLEDGEMENTS

I'd like to thank my advisor, Dr. Paul Stoy for his tireless dedication to helping me achieve my full potential as a researcher. Dr. Stoy also funded me for most of my time at MSU and went above and beyond most advisors to make sure my funding was always secure. In addition, I'd like to thank the Montana Graduate School for awarding me a PhD Completion Grant that enabled me to finish my PhD and this thesis. I also received funding from the Montana Water Center and was supported by the National Center for Atmospheric Research as a Graduate Advanced Study Program awardee. I also would like to acknowledge high-performance computing support from Cheyenne (doi:10.5065/D6RX99HX) provided by NCAR's Computational and Information Systems Laboratory, sponsored by the National Science Foundation.

I'd like to thank Elizabeth Rehbein for her support as my partner during these final years of my PhD. She has helped keep me on track and has always been there to pull me out of a spiral. I received lots of support from friends and family, and I cannot thank you all enough for the encouragement.

Finally, I'd like to thank the other members of my committee, Dr. Jack Brookshire, Dr. Andreas Prein, Dr. Scott Powell, and Dr, Ankur Desai. You have all pushed me into becoming a better scientist.

TABLE OF CONTENTS

1. INTRODUCTION 1

Figures 6
References 7

2. RECENT TRENDS IN THE NEAR-SURFACE CLIMATOLOGY OF THE NORTHERN NORTH AMERICAN GREAT PLAINS 10

Contribution of Authors and Co-Authors 10
Manuscript Information Page 11
Abstract 12
Introduction 12
Methods 15
Study Area 15
Data 16
Analysis 17
Results 19
Seasonal Trends 19
Monthly Trends 20
Discussion 21
Climatological Seasons Mask Large Monthly Trends 22
Trends in Precipitation 23
Land Cover Change 24
Toward an understanding of the mechanisms underlying regional early-season cooling 27
Summary 29
Acknowledgements 30
Appendix 30
Data Coverage 30
Trend Verification 31
References 32
Figures 43

3. SIMULATING THE IMPACTS OF AGRICULTURAL LAND USE CHANGE ON THE CLIMATE OF THE NORTHERN NORTH AMERICAN GREAT PLAINS: VALIDATING A CONVECTION-PERMITTING CLIMATE MODEL 54

Contribution of Authors and Co-Authors 54
Manuscript Information Page 55
Abstract 56
Introduction 56

TABLE OF CONTENTS CONTINUED

Model Parameters and Observational Data 60
Model Setup and Domain Information 60
Creation of the Fallow Dataset 61
Observational Verification Data 63
Results 66
Seasonal Temperature 66
Seasonal Precipitation 67
Seasonal Vapor Pressure 68
Precipitation Intensities 69
Soundings 69
Surface Fluxes 70
Discussion 71
Comparison with other Convection-Permitting Simulations 71
Summer Warm Bias 72
Representation of Convective Precipitation 74
The Impact of Fallow Representation 74
Summary and Conclusion 75
Supplementary Information 76
Figures 78
Appendix 92
Refences 95

4. THE DECLINE IN SUMMER FALLOW IN THE NORTHERN PLAINS COOLED NEAR-SURFACE CLIMATE BUT HAD MINIMAL IMPACTS ON PRECIPITATION 102

Contribution of Authors and Co-Authors 102
Manuscript Information Page 103
Abstract 104
Introduction 104
Methods and Experimental Design 108
Study Area 108
Model Setup 109
Land Cover Experiments 110
Model Validation and Analysis 111
Results 112
Changes to Summer Fallow Extend and Representation in WRF 112
Changes to Near-Surface Energy and Humidity 113
Changes to Convective Environments 114
Changes to Precipitation 116
Discussion 116
Temperature and VPD 117

TABLE OF CONTENTS CONTINUED

Boundary Layer Changes 119
Precipitation 120

Summary and Conclusions 122
Tables 124
Figures 125
References 136

5. RECENT ENHANCEMENT OF THERMODYNAMIC ENVIRONMENTS IN THE NORTHERN NORTH AMERICAN GREAT PLAINS 142

Contribution of Authors and Co-Authors 142
Manuscript Information Page 143
Abstract 144
Introduction 144
Materials and Methods 147
Observational and Reanalysis Data 147
Simulation Data 148
Results 150
Recent and Future Changes to Thermodynamic Environments: CAPE 150
Recent and Future Changes to Thermodynamic Environments: CIN 151
Results from Climate Reanalysis 152
Discussion 152
Conclusions 155
Acknowledgments 156
Figures 157
References 163

6. CONCLUSION 167

References 170

REFERENCES CITED 173

LIST OF TABLES

Table Page

3.S1 Names and parameters for each simulation..... 65

4.1 Abbreviations and explanations for each model simulation..... 115

LIST OF FIGURES

Figure Page

1.1 Land cover in the NNAGP estimated by the European Space Agency 6

2.1 A map of the region considered to be the northern North American GreatPlains (NNAGP) for the purposes of this study 43

2.2 Trends in 2 m air temperature (T_{air}) from 1970 to 2015 across the northern North American Great Plains and surrounding regions 44

2.3 Trends in vapor pressure deficit (VPD) from 1970 to 2015 across the northern North American Great Plains and surrounding regions 45

2.4 Trends in precipitation (P) from 1970 to 2015 across the northern North American Great Plains and surrounding regions 46

2.5 Monthly trends in near-surface (2 m) air temperature between 1970 and 2015 for the northern North American Great Plains..... 47

2.6 May and June trends in 2 m air temperature (a), vapor pressure deficit (b), and precipitation (c) from 1970-2015 in the Northern North American Great Plains 48

2.7 Monthly trends in vapor pressure deficit between 1970 and 2015 for the northern North American Great Plains 49

2.8 Monthly trends in precipitation between 1970 and 2015 for the northern North American Great Plains 50

2.9 Trends in near surface air temperature from the CESM-LE ensemble 39

2.A1 Trends in air temperature from 1970-2015 in the Northern North American Great Plains using Berkley Earth Surface Temperature data 51

2.A2 Near-surface (2 m) air temperature trends from 270 Global Historical Climatology Network (GHCN) sites within the NNAGP 52

3.1 WRF landcover and vegetation fractions for the C11 and C84 simulations ... 78

3.2 Two-meter temperature comparison between C11 and Daymet 79

3.3 Two-meter temperature comparison between C84 and Daymet 80

LIST OF FIGURES CONTINUED

Figure Page

3.4 Precipitation comparison between C11 and Daymet 81

3.5 Precipitation comparison between C84 and Daymet 82

3.6 Vapor pressure comparison between C11 and Daymet 83

3.7 Vapor pressure comparison between C84 and Daymet 84

3.8 Probability densities of hourly precipitation from the C11 simulations and the U.S. hourly station observations. 85

3.9 Probability densities of hourly precipitation from the C84 simulations and the U.S. hourly station observations. 86

3.10 Vertical profiles from C11 of dewpoint temperature compared to the Glasgow, MT sounding location (GGW), the Bismarck, ND sounding location (BIS), Edmonton, AB, sounding location (WSE). 87

3.11 Vertical profiles from C11 of temperature compared to the Glasgow, MT sounding location (GGW), the Bismarck, ND sounding location (BIS), Edmonton, AB, sounding location (WSE). 88

3.12 Vertical profiles from C84 of dewpoint temperature compared to the Glasgow, MT sounding location (GGW), the Bismarck, ND sounding location (BIS), Edmonton, AB, sounding location (WSE). 89

3.13 Vertical profiles from C84 of temperature compared to the Glasgow, MT sounding location (GGW), the Bismarck, ND sounding location (BIS), Edmonton, AB, sounding location (WSE). 90

3.14 Comparison of sensible and latent heat flux between WRF and CA-Leth ... 91

3.S1 Two-meter temperature comparison between C11 and the CRU dataset 92

3.S2 Precipitation comparison between C11 and the CRU dataset 93

3.S3 Vapor pressure comparison between C11 and the CRU dataset 94

4.1 Time series of summer fallow for Canada and the U.S. 125

LIST OF FIGURES CONTINUED

Figure Page

4.2 Differences between the 2010 fallow and 1984 vegetation fraction..... 126

4.3 Two-meter temperature (T2) differences between modern (2011) fallow (F11) and control (C11) simulations..... 127

4.4 Monthly differences in T2 between F11 and C11 128

4.5 Difference in sensible and latent heat flux between F11 and C11..... 129

4.6 Two-meter vapor pressure deficit difference between the modern fallow (F11) and control (C11) simulations 130

4.7 Differences in convective parameters between F11 and C11 for May and June 131

4.8 Differences in convective parameters between F11 and C11 for July and August..... 132

4.9 Changes to precipitation for May and June, and July and August 133

4.10 Vertical cross-section of 1979-2020 May and June meridional wind trends (black contours) and specific humidity trends for the levels between 925 hPa to 800 hPa..... 134

4.11 Vertical cross-section of 1979-2020 July and August meridional wind trends (black contours) and specific humidity trends for the levels between 925 hPa to 800 hPa..... 135

5.1 Empirical probability distributions of CAPE for Glasgow, MT and Bismarck, ND..... 157

5.2 Generalized extreme value distributions of monthly maximum CAPE for Glasgow, MT and Bismarck, ND..... 158

5.3 Empirical probability distributions of CIN for Glasgow, MT and Bismarck, ND..... 159

5.4a Trends in May and June monthly mean CAPE from the ERA5 reanalysis for the 1979-2020 period 160

LIST OF FIGURES CONTINUED

Figure Page

5.4b Trends in July and August monthly mean CAPE from the ERA5 reanalysis for the 1979-2020 period 161

5.5 Trends in AMJ horizontal moisture convergence from ERA5 1979-2020 ... 162

ABSTRACT

The northern North American Great Plains (NNAGP) is the area defined by the Upper Missouri River Basin and the Canadian Prairies. It is a semi-arid region categorized by large stretches of grassland, pasture, and crops. During the last century and extending to the present day, a standard agricultural practice was to utilize a wheat-summer fallow rotation schedule, where the fields were left unplatted and an herbicide was often applied to keep weeds at bay. Concerns over soil health and profitability have led to the systematic decline of summer fallow, and nearly 116,000 km^2 that used to be fallow during the summer in the 1970s are now planted.

An observational analysis discovered that from 1970-2015, during the early warm season, the NNAGP have cooled at −0.18 °C $decade^{-1}$, nearly the same magnitude as the annual global warming rate. The near-surface atmosphere also moistened, evidenced by a decreasing vapor pressure deficit (VPD) trend, and monthly mean precipitation increased in excess of 8 mm per decade. Monthly mean convective available potential energy (CAPE) increased by 80% at Glasgow, MT and by 35% at Bismarck, ND based on atmospheric sounding observations.

To test whether a reduction in summer fallow is responsible for these observed changes, a set of convection-permitting model experiments were performed over the NNAGP. Two sets (4 total) of three-year simulations were driven by ERA5 data with the vegetative fraction adjusted using satellite estimated fallow amounts for 2011 and 1984. The control simulations were extensively validated against an ensemble of observations with large temperature biases in Winter by ~ -3 ºC and Summer by ~3ºC.

The areas where fallow area declined from 1984-2011 were cooler by about 1.5 °C and had a lower VPD by 0.15 kPa compared to where it did not. CAPE increased where fallow declined from 1984-2011 but so did convective inhibition (CIN). These findings insinuate that the observed change to monthly mean precipitation cannot be explained by summer fallow reduction alone. Trends in observed low level moisture transport show that the Great Plains Low Level Jet has been intensifying, bringing increased moisture to the NNAGP and partially responsible for the precipitation increase.

CHAPTER ONE

INTRODUCTION

Global near surface temperatures have been rising since the industrial revolution and are projected to keep increasing (IPCC 2013; Karl and Trenberth 2003). Mean annual global temperatures have increased by at least ~1°C since 1950 but this varies from region to region and season to season (Blunden and Arndt 2020). The land surface can be an important driver of these variations due to differences in how their reflectivity (known as albedo) reflects solar radiation back into space, how their evapotranspiration cools the surface and adds water to the atmosphere, and how their solar heating adds heat to the atmosphere (known as sensible heat flux). For example, temperate forests have a low albedo that absorbs a large proportion of incident solar radiation, but they also often have a large surface area of leaves and deeper roots, meaning that evapotranspiration and latent heat flux are relatively large and lead to a net cooling compared to areas with without forests, at least in many temperate and tropical zones (Bonan 2008; Manoli et al. 2016). Humans have intentionally modified the land surface for activities like agriculture and urban development. This land use and land cover change (LULCC) can have equal or larger impacts on regional temperatures compared to the greenhouse gas radiative forcing of anthropogenic climate change (Betts et al. 2013c; Mahmood et al. 2010). Characterizing the feedbacks between the land surface and climate processes is critical to better understanding the anthropogenic impacts on the climate.

In this volume, I focus on land use-climate interactions in the northern North American Great Plains (NNAGP) (Figure 1.1) a region that I define in the 2nd chapter as a combination of

the Canadian Prairies and the U.S. northern Great Plains. In the 21st century, the NNAGP is an important agricultural area in the U.S. with the primary commodity being wheat, and increasingly corn and soy. Grassland, shrubland, and a limited extent of forest and urban ecosystems and barren lands exist as well (Stoy et al. 2018; Dolan et al. 2020; Long et al. 2014b). The agricultural areas of the NNAGP used to be primarily grassland but were largely converted to a dryland wheat-fallow crop rotation during the late 1800s and early 1900s, which lead to a lower Bowen ratio during summer, and an increase in precipitation (Chen and Dirmeyer 2017; Pielke et al. 2007).

Since the 1970s, alternate cropping sequences that have replaced summer fallow with crops across more than a hundred thousand square kilometers as detailed in Chapter 3. These large-scale land management changes will impact regional climate for the reasons discussed above, but how? Multiple studies have demonstrated that the conversion of summer fallow to crops impacts near-surface climate and planetary boundary layer processes including convective precipitation as detailed in Chapters 2-5. But most modeling studies are unable to explicitly resolve the impacts of land use change on convective precipitation because they are run at a spatial scale that is too coarse to capture the processes involved. Resolving convection at regional scales requires a spatial scale of 4 km or smaller that can capture weather dynamics (Prein et al. 2015). Understanding the impacts of land cover change on climate processes requires that such models be run with different land cover fractions and across multi-year time periods to account for the impacts of large-scale climate features like ENSO. Running weather models over large areas to understand climate processes is a very computationally expensive exercise, requiring supercomputers.

To study the impacts of land cover change on climate processes across a large region (Figure 1), I ran the Weather Research and Forecasting Model (WRF), as described in Chapters 3-4 using past

and present land cover observations. Doing so revealed that planting crops instead of leaving fields barren cooled near-surface climate and added moisture to the atmosphere, resulting in more favorable conditions for crop growth. Landcover change alone appeared to have minimal impacts on regional precipitation, which instead was enhanced by additional moisture transport, mostly from the south, via the impacts of climate change on the Great Plains Low Level Jet. Combined, my findings revealed that changes to land use that have benefitted soil conservation (fallow increases erosion and carbon loss via respiration without plant input) and economic outcomes (producers usually make more money by planting crops instead of leaving fields bare) have also cooled the climate. This represents a 'win-win-win' for environmental and societal outcomes (Foley et al., 2005), but the details need to be disentangled. At a minimum, they have placed the NNAGP in a unique position amongst wheat-growing areas across the globe.

Globally, yields of important crops are expected to decrease with rising temperatures by as much as 30% under the Relative Concentration Pathway 8.5 scenario (Zhao et al. 2017). The climate impacts on wheat production are uncertain and is somewhat moderated by the development of new cultivars (Asseng et al. 2013a; Ortiz et al. 2008), but yields are thought to decline in the future (Zhao et al. 2017) and some critical wheat-growing regions such as Australia have already experienced stalled or declining yield trends(Hochman et al. 2017; Lobell et al. 2011). The temperature impacts on wheat are non-linear, meaning that wheat yields are resistant to temperatures up to ~28 °C, and decline rapidly thereafter, but the impacts of temperature also depend on the growing stage and cultivar (Asseng et al. 2015a; Schlenker et al. 2009). In some areas, such as the NNAGP, the growing season is lengthening and also moving earlier in the year

(Mueller et al. 2015a). Even though my work has demonstrated that reducing the amount of land held in fallow has cooled near-surface climate, future trends are uncertain.

The climate feedbacks of agriculture might offer a respite to the negative impacts of anthropogenic global warming. In North America, agricultural areas have led to a cooling of summer temperatures and as a result the impacts on yield have been minimal or even beneficial (Lobell et al. 2011; Butler et al. 2018). In the Midwest of the United States, increased productivity of corn crops have cooled summertime maximum temperatures by –0.5°C decade^{-1} and have increased precipitation by 10-15mm decade^{-1} (Mueller et al. 2015b; Bonan 2001). Agricultural expansion and intensification also increases the local near-surface humidity, especially in irrigated areas (Mahmood et al. 2008). More moisture at the surface can also impact precipitation processes such that rainfall is more likely, and also potentially more intense (Mahmood et al. 2008; Alter et al. 2015a; Chen et al. 2017; Collow et al. 2014). More moisture also decreases the vapor pressure deficit (VPD); plant stomata will close if VPD is too high to preserve water which then shuts off carbon uptake (Novick et al. 2016a). This lower VPD therefore reduces plant hydraulic stress and increases plant carbon uptake and grain yields (López et al., 2021).

Is it possible that, with careful consideration of the processes involved, agriculture can be beneficial to climate? I seek to understand the relationship between agricultural management and climate across an international region that is a globally-important source of key crops wheat, pulses, oilseeds. In Chapter 2, the regional climate trends of the NNAGP will be discussed and a hypothesis will be presented as to how changes wheat-fallow agriculture might affect regional climate. Chapter 3 and 4 test the hypothesis introduced in Chapter 2 with a state-of-the-art high-resolution climate model. Chapter 5 discusses how the environments of strong convective

precipitation are changing in the NNAGP. Throughout, I emphasize how agriculture and climate are coupled through the exchange of water and energy and how mechanistic and process-based studies of their interplay improve our understanding of both.

Figures

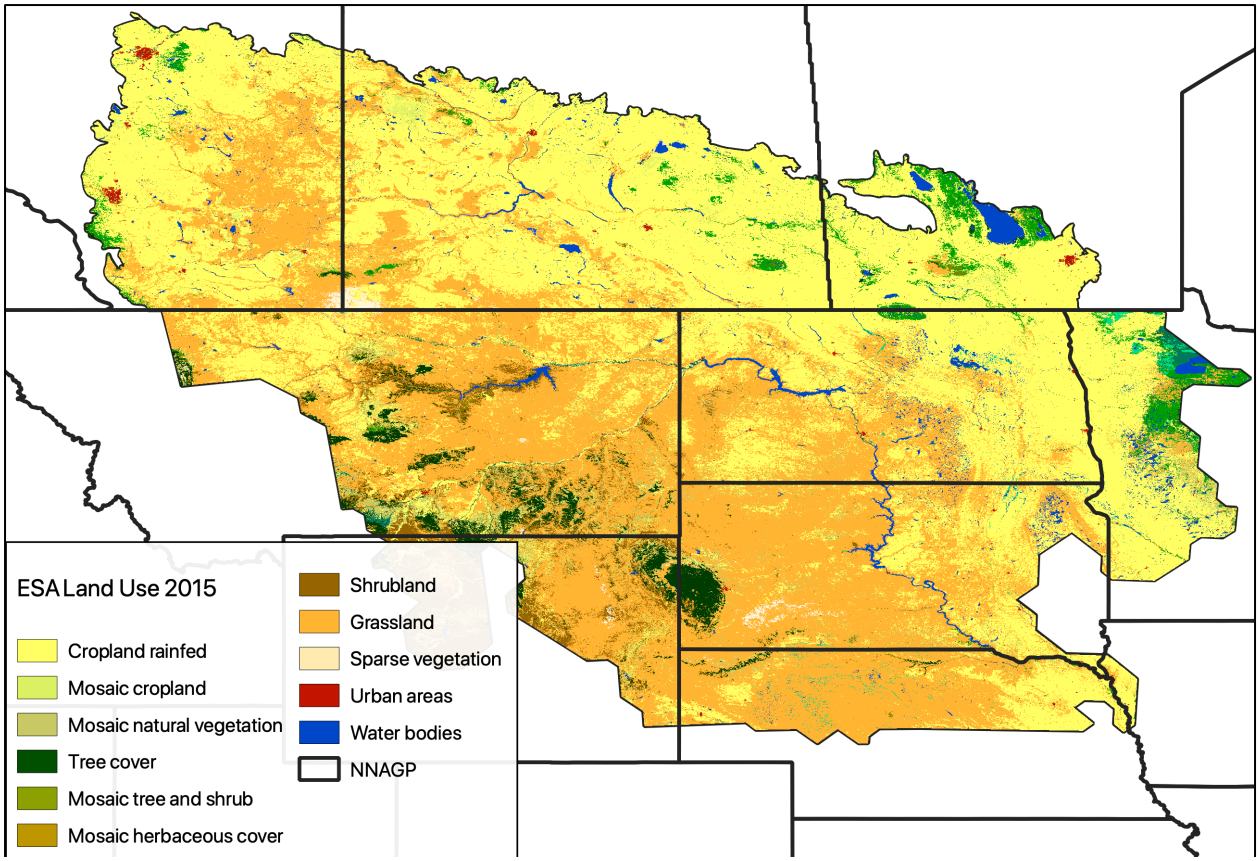


Figure 1: Land cover in the NNAGP estimated by the European Space Agency (ESA 2017).

References

Alter, R. E., Y. Fan, B. R. Lintner, C. P. Weaver, R. E. Alter, Y. Fan, B. R. Lintner, and C. P. Weaver, 2015: Observational Evidence that Great Plains Irrigation Has Enhanced Summer Precipitation Intensity and Totals in the Midwestern United States. *J. Hydrometeorol.*, **16**, 1717–1735, https://doi.org/10.1175/JHM-D-14-0115.1.

Asseng, S., and Coauthors, 2013: Uncertainty in simulating wheat yields under climate change. *Nat. Clim. Change*, **3**, 827–832, https://doi.org/10.1038/nclimate1916.

——, and Coauthors, 2015: Rising temperatures reduce global wheat production. *Nat. Clim. Change*, **5**, 143–147, https://doi.org/10.1038/nclimate2470.

Betts, A. K., R. Desjardins, D. Worth, and D. Cerkowniak, 2013: Impact of land use change on the diurnal cycle climate of the Canadian Prairies. *J. Geophys. Res. Atmospheres*, **118**, 11996–12011, https://doi.org/10.1002/2013JD020717.

Blunden, J., and D. S. Arndt, eds., 2020: State of the Climate in 2019. *Bull. Am. Meteorol. Soc.*, **101**, S1–S429, https://doi.org/10.1175/2020BAMSStateoftheClimate.1.

Bonan, G. B., 2001: Observational Evidence for Reduction of Daily Maximum Temperature by Croplands in the Midwest United States. *J. Clim.*, **14**, 2430–2442, https://doi.org/10.1175/1520-0442(2001)014<2430:OEFROD>2.0.CO;2.

——, 2008: Forests and Climate Change: Forcings, Feedbacks, and the Climate Benefits of Forests. *Science*, **320**, 1444–1449, https://doi.org/10.1126/science.1155121.

Butler, E. E., N. D. Mueller, and P. Huybers, 2018: Peculiarly pleasant weather for US maize. *Proc. Natl. Acad. Sci.*, **115**, 11935–11940, https://doi.org/10.1073/pnas.1808035115.

Chen, L., and P. A. Dirmeyer, 2017: Impacts of Land-Use/Land-Cover Change on Afternoon Precipitation over North America. *J. Clim.*, **30**, 2121–2140, https://doi.org/10.1175/JCLI-D-16-0589.1.

——, ——, A. Tawfik, and D. M. Lawrence, 2017: Sensitivities of Land Cover–Precipitation Feedback to Convective Triggering. *J. Hydrometeorol.*, **18**, 2265–2283, https://doi.org/10.1175/JHM-D-17-0011.1.

Collow, T. W., A. Robock, and W. Wu, 2014: Influences of soil moisture and vegetation on convective precipitation foerecasts over the United States Great Plains. *J. Geophys. Res. Atmospheres*, **119**, 9338–9358, https://doi.org/10.1002/2014JD021454.Received.

Dolan, K. A., P. C. Stoy, and B. Poulter, 2020: Land management and climate change determine second-generation bioenergy potential of the US Northern Great Plains. *GCB Bioenergy*, **12**, 491–509, https://doi.org/10.1111/gcbb.12686.

ESA, 2017: Land Cover CCI Product User Guide Version 2.

Hochman, Z., D. L. Gobbett, and H. Horan, 2017: Climate trends account for stalled wheat yields in Australia since 1990. *Glob. Change Biol.*, **23**, 2071–2081, https://doi.org/10.1111/gcb.13604.

IPCC, ed., 2013: *Climate Change 2013 - The Physical Science Basis: Working Group I Contribution to the Fifth Assessment Report of the Intergovernmental Panel on Climate Change*. Cambridge University Press,.

Karl, T. R., and K. Trenberth, 2003: Modern Global Climate Change. *Science*, **302**, 1719–1723.

Lobell, D. B., W. Schlenker, and J. Costa-Roberts, 2011: Climate Trends and Global Crop Production Since 1980. *Science*, **333**, 616–620, https://doi.org/10.1126/science.1204531.

Long, J. A., R. L. Lawrence, P. R. Miller, L. A. Marshall, and M. C. Greenwood, 2014: Adoption of cropping sequences in northeast Montana: A spatio-temporal analysis. *Agric. Ecosyst. Environ.*, **197**, 77–87, https://doi.org/10.1016/j.agee.2014.07.022.

López, J., D. A. Way, and W. Sadok, 2021: Systemic effects of rising atmospheric vapor pressure deficit on plant physiology and productivity. *Glob. Change Biol.*, gcb.15548, https://doi.org/10.1111/gcb.15548.

Mahmood, R., K. G. Hubbard, R. D. Leeper, and S. A. Foster, 2008: Increase in Near-Surface Atmospheric Moisture Content due to Land Use Changes: Evidence from the Observed Dewpoint Temperature Data. *Mon. Weather Rev.*, **136**, 1554–1561, https://doi.org/10.1175/2007MWR2040.1.

——, and Coauthors, 2010: Impacts of Land Use/Land Cover Change on Climate and Future Research Priorities. *Bull. Am. Meteorol. Soc.*, **91**, 37–46, https://doi.org/10.1175/2009BAMS2769.1.

Manoli, G., J. C. Domec, K. Novick, A. C. Oishi, A. Noormets, M. Marani, and G. Katul, 2016: Soil-plant-atmosphere conditions regulating convective cloud formation above southeastern US pine plantations. *Glob. Change Biol.*, **22**, 2238–2254, https://doi.org/10.1111/gcb.13221.

Mueller, B., M. Hauser, C. Iles, R. H. Rimi, F. W. Zwiers, and H. Wan, 2015a: Lengthening of the growing season in wheat and maize producing regions. *Weather Clim. Extrem.*, **9**, 47–56, https://doi.org/10.1016/j.wace.2015.04.001.

Mueller, N. D., E. E. Butler, K. A. Mckinnon, A. Rhines, M. Tingley, N. M. Holbrook, and P. Huybers, 2015b: Cooling of US Midwest summer temperature extremes from cropland intensification. https://doi.org/10.1038/NCLIMATE2825.

Novick, K. A., and Coauthors, 2016: The increasing importance of atmospheric demand for ecosystem water and carbon fluxes. *Nat. Clim. Change*, **6**, 1023–1027, https://doi.org/10.1038/nclimate3114.

Ortiz, R., and Coauthors, 2008: Climate change: Can wheat beat the heat? https://doi.org/10.1016/j.agee.2008.01.019.

Pielke, R. A., J. Adegoke, A. Beltrán-Przekurat, C. A. Hiemstra, J. Lin, U. S. Nair, D. Niyogi, and T. E. Nobis, 2007: An overview of regional land-use and land-cover impacts on rainfall. *Tellus Ser. B Chem. Phys. Meteorol.*, **59**, 587–601, https://doi.org/10.1111/j.1600-0889.2007.00251.x.

Prein, A. F., and Coauthors, 2015: A review on regional convection-permitting climate modeling: Demonstrations, prospects, and challenges. *Rev. Geophys.*, **53**, 323–361, https://doi.org/10.1002/2014RG000475.

Schlenker, W., M. J. Roberts, and V. K. Smith, 2009: Nonlinear temperature effects indicate severe damages to U.S. crop yields under climate change.

Stoy, P. C., and Coauthors, 2018: Opportunities and Trade-offs among BECCS and the Food, Water, Energy, Biodiversity, and Social Systems Nexus at Regional Scales. *BioScience*, **68**, 100–111, https://doi.org/10.1093/biosci/bix145.

Zhao, C., and Coauthors, 2017: Temperature increase reduces global yields of major crops in four independent estimates. *Proc. Natl. Acad. Sci.*, **114**, 9326–9331, https://doi.org/10.1073/pnas.1701762114.

CHAPTER TWO

RECENT TRENDS IN THE NEAR-SURFACE CLIMATOLOGY OF THE NORTHERN NORTH AMERICAN GREAT PLAINS

Contribution of Authors and Co-Authors

Manuscript in Chapter 2

Author: Gabriel T. Bromley
Contributions: Analyzed the data, wrote the first draft of the manuscript.
Co-Author: Tobias Gerken
Contributions: Provided feedback on the analysis methods, results, and edited the manuscript at all stages.

Co-Author: Andreas Prein
Contributions: Provided feedback on the analysis methods, results and edited the manuscript at all stages. Created a figure for the manuscript.

Co-Author: Paul C. Stoy
Contributions: Conceived of the study, obtained funding, provided feedback on the analysis methods and results, and edited the manuscript at all stages.

Manuscript Information

Gabriel T. Bromley, Tobias Gerken, Andreas F. Prein, Paul C. Stoy
Journal of Climate

Status of Manuscript:
____ Prepared for submission to a peer-reviewed journal
____ Officially submitted to a peer-reviewed journal
____ Accepted by a peer-reviewed journal
___X_ Published in a peer-reviewed journal

American Meteorology Society
33, 461–475,
https://doi.org/10.1175/JCLI-D-19-0106.1.

CHAPTER TWO

RECENT TRENDS IN THE NEAR-SURFACE CLIMATOLOGY OF THE NORTHERN NORTH AMERICAN GREAT PLAINS

Abstract

We examined climate trends in the northern North American Great Plains (NNAGP) from 1970-2015, a period that aligns with widespread land use changes in this globally-important agricultural region. Trends were calculated from the Climatic Research Unit (CRU) and other climate datasets using a linear regression model that accounts for temporal autocorrelation. The NNAGP warmed on an annual basis, with the largest change occurring in winter (DJF) at 0.4 °C decade^{-1}. January in particular warmed at nearly 0.9 °C decade^{-1}. The NNAGP cooled by −0.18 °C decade^{-1} during May and June, nearly the opposite of global warming trends during the study period. The atmospheric vapor pressure deficit (VPD), which can limit crop growth, decreased in excess of −0.4 hPa decade^{-1} during climatological summer in the southeastern part of the study domain. Precipitation (*P*) increased in the eastern portion of the NNAGP during all seasons except Fall and increased during May and June in excess of 8 mm decade^{-1}. Climate trends in the NNAGP largely followed global trends except during the early warm season (May and June) during which 2 m air temperature (T_{air}) became cooler, VPD lower, and *P* greater across large parts of the study region. These changes are consistent with observed agricultural intensification during the study period, namely the reduction of summer fallow and expansion of agricultural land use. Global climate model simulations indicate that observed T_{air} trends cannot be explained by natural climate variability. However, further climate attribution experiments are necessary to understand if observed changes are caused by increased agricultural intensity or other factors.

1. Introduction

Global near-surface temperatures have increased by nearly 0.2 °C decade^{-1} since the mid 1970s, with concurrent increases in global atmospheric moisture content (IPCC 2013; Dai 2006). Global climate trends are important to understand, but regional climate often departs from global trends due to regional variations in water and energy dynamics. Characterizing regional climate change is an important first step toward understanding the mechanisms that underlie these changes to further improve our understanding of the climate system and to provide information for decision

makers (Abatzoglou et al. 2009; Xie et al. 2015). Of particular importance is an improved understanding of climate dynamics in food-producing regions, identified by the World Climate Research Programme as the *Water for the Food Baskets of the World* grand challenge.

At regional scales, climate is often strongly influenced by land surface processes (Seneviratne et al. 2006) in addition to the general circulation. Anthropogenic modifications including irrigation and other agricultural land use and land cover changes can alter this connection (Couzin 1999), and numerous recent studies have reiterated that agricultural intensification, i.e. cropland expansion and/or increasing crop yields, often results in regional cooling during the vegetative growing season (Mahmood et al. 2014a; Mueller et al. 2015b; Alter et al. 2017; Mueller et al. 2017; Gameda et al. 2007). Increases in agricultural intensity often alter the surface energy balance such that latent heat flux to the atmosphere is increased, sensible heat flux is reduced, and maximum temperatures are suppressed (Huber et al. 2014; Diffenbaugh 2009). These changes to the surface energy balance can increase precipitation by increasing atmospheric moisture content and enhancing convective initiation through increased moist static energy (Pielke 2001; Pielke et al. 2007; Gerken et al. 2018b; Vick et al. 2016; Gentine et al. 2013; Gameda et al. 2007). The increase in latent heat flux decreases the Bowen ratio, which lowers the height of the planetary boundary layer (PBL) and simultaneously lowers the lifted condensation level (LCL) (Juang et al. 2007; Alter et al. 2015; Gerken et al. 2018a). LCLs that exceed the PBL height are associated with cloud development and constitute a 'necessary but not sufficient condition' for convective precipitation (Juang et al. 2007b; Bonetti et al. 2015; Manoli et al. 2016), noting additional requirements such as a minimum CAPE of ~ 400 J kg^{-1} (Yin et al. 2015) and positive convective triggering potential (Findell and Eltahir 2003a,b). Changes in PBL processes from agricultural

management also modify local and downwind air temperature (T_{air}) and precipitation (Diffenbaugh 2009; Lu et al. 2017), emphasizing their importance to regional climate. Understanding how agriculture interacts with regional climate processes is a critical step for developing sustainable management practices to help avoid deleterious impacts of climate change on agricultural production (e.g. Asseng et al. 2013, 2015), which have already been observed across multiple crop producing regions (IPCC 2014).

The Canadian Prairies (hereafter CP) are a notable example of a region that has experienced a simultaneous change in agricultural intensity and regional climate. The CP have undergone substantial changes in land surface composition since the 1970s, driven by a shift away from wheat / summer fallow cropping sequences to more diversified cropping systems that replaced summer fallow with oilseeds, pulses, and other crops (Campbell et al. 2002; Bradshaw et al. 2004). The area of summer fallow in the CP has decreased from nearly 160,000 km^2 in 1970 to less than 20,000 km^2 at present (Vick et al. 2016), which has increased moisture flux to the atmosphere and altered regional climate during the vegetative growing season (Gameda et al. 2007). Maximum summer temperatures have decreased by 1.2 °C since the 1970s, driven by a reduction in surface net radiation of −6 $W\ m^{-2}$ (Betts et al. 2013d). The decrease in net radiation is attributed to increased cloud cover as a result of shifting land use and increases in surface relative humidity of up to 7% (Betts et al. 2013a,d; Mahmood et al. 2008). These changes in near-surface moisture have also increased the potential for convective precipitation during the growing season (Raddatz 1998, 2000).

Summer fallow in the U.S. decreased gradually from over 160,000 km^2 to 60,000 km^2 during a similar time frame but starting in the mid 1980s (Vick et al. 2016), a large part of which

has occurred in the U.S. Northern Great Plains (NGP) adjacent to the CP (Figure 1). Convective likelihood has increased across parts of the NGP during the vegetative growing season (Gerken et al. 2018a), but it is otherwise unclear if the mechanisms causing regional climate changes in the NGP have followed those of the CP. It is difficult to understand the mechanisms causing regional cooling in the combined CP and NGP (hereafter the northern North American Great Plains, NNAGP) without first characterizing regional climate observations. Here, we describe changes in observed near-surface (2 m) air temperature (T_{air}), vapor pressure deficit (VPD), and precipitation (*P*) in the NNAGP at annual, seasonal, and monthly time scales from 1970 until 2015 by analyzing global climatic databases. Changes in T_{air} and *P* are commonly studied, and we additionally study VPD given its important role in crop yields ([CSL STYLE ERROR: reference with no printed form.]) and increasingly important role in controlling water transport from the soil through transpiration (Novick et al. 2016b). VPD is the difference between vapor pressure and saturation vapor pressure at the surface such that a decrease in 2 m VPD can be interpreted as more atmospheric moisture near the surface, all else being equal. We focus on the period from the 1970s until the present to study the time period characterized by increasing agricultural intensity (Alter et al. 2017; Vick et al. 2016) to improve our understanding of regional climate changes that have impacted – and appear to be impacted by – land and water management in the NNAGP.

2. Methods

a. Study Area

The NNAGP has no formal definition. For the purposes of this study we consider it to be the area encompassed by the National Ecological Observatory Network (NEON) Northern Plains Domain

in the U.S. (Domain 9) (Keller et al. 2008) and the Prairies Ecozone in Canada (Figure 1) (Wiken and Canadian Council on Ecological Areas 1996). The entire domain largely encompasses what is often called the 'Prairie Pothole' region with the inclusion of semi-arid areas dominated by rangeland toward the west (Millett et al. 2009) and the 'Northern Short Grasslands' defined by the World Wide Fund for Nature. The Northern Plains Domain encompasses most of the Upper Missouri River Basin (Stoy et al. 2018) as well as the U.S. portions of the Red River of the North and the Nebraska Sandhills. The Prairies Ecozone encompasses most major grassland and agricultural regions of the Prairie Provinces with the exception of the Peace River Country in Alberta and British Columbia.

The NNAGP was comprised largely of native shortgrass and mixed-grass prairie before the advent of widespread agriculture. Row crop agriculture, largely maize (hereafter corn) and soy, now dominate the eastern region of the NNAGP. A diverse mixture of wheat, pulse crops, oilseeds, and cover crops now dominate the northern and western regions, with rangeland dominating in areas unsuited to row crop agriculture, largely in the western part of the study region, with minor contributions of forests, urban areas, and lands developed for energy extraction, largely overlying the Bakken formation and within the Powder River Basin of Wyoming and Montana. The Canadian Prairies are broken into two distinct zones: the semi-arid prairies and the temperate prairies, with the latter forming the boundary between prairie and boreal forest (Gauthier and Wiken 2003; Hammermeister 2001).

b. Data

Station observations and gridded observational data products are used to study trends in T_{air}, VPD, and P in the NNAGP. Gridded monthly T_{air} and P come from the Climatic Research Unit (CRU)

TS 4.01 (Harris et al. 2014). VPD was calculated by subtracting vapor pressure obtained from the CRU dataset from saturation vapor pressure calculated using the CRU T_{air} data product. The CRU dataset is in good agreement with other commonly used temperature and precipitation datasets (Sun et al. 2018; Jones 2016) though does not contain as many source observations (Harris et al. 2014). The CRU dataset is also not homogeneous, though the source observations are often homogenized by the original data collection organization, and thus better-suited for trend analysis (Harris et al. 2014). The CRU dataset compiles observations from up to eight climate stations per grid cell from World Meteorological Organization (WMO) stations, a density that is achieved for most of North America. We use the independent Berkeley Earth dataset (Rohde et al. 2013) to corroborate the major findings from the CRU dataset in the Appendix.

Data from the Community Earth System Model Large Ensemble (CESM-LE) experiment (Kay et al. 2015) were used to determine if observed trends can be explained by natural climate variability (e.g. Deser et al. 2012). The ensemble contains 39 simulations with a 1° horizontal grid spacing, a length scale twice that of the CRU dataset, and uses historical forcings until 2005 at which point they are run under the RCP 8.5 scenario. Each model's initial conditions were slightly varied to create an ensemble that captures internal climate variability (Kay et al. 2015). The grid points containing the NNAGP were selected and averaged creating monthly time series for each model. Linear trends were then calculated from the monthly data.

c. Analysis

Anomalies in T_{air}, VPD, and P were calculated by first averaging monthly data for each grid point in the CRU dataset for the period 1980-2010. The means were then subtracted from the values of the time period of interest to create the anomaly value. Trends in the anomalies were calculated

for the variables of interest using an ordinary least squares (OLS) regression for the time period 1970-2015. The OLS function from the Statsmodels (Seabold and Perktold 2010) package in Python (Rossum 1995) was used to calculate trends. For the case of T_{air} during May and June, a one-sided lower-tailed Student's t-test was used to compare the calculated trends to the observed global annual average T_{air} trend of 0.2 °C decade^{-1} for the study period calculated using the CRU database, a similar but more conservative trend to the 0.26 °C decade^{-1} that is found by the IPCC (IPCC, 2013). A two-tailed Student's t-test was used when comparing against a null trend for VPD, P and T_{air} for seasonal analyses. We use the adjusted standard error to account for effects of temporal autocorrelation on standard error (Ramsey and Schafer 2012):

$$S_{adj} = S\sqrt{\frac{1+r_1}{1-r_1}} \qquad Eq.\ (1)$$

where S is the standard error and r_1 is the lag-1 autocorrelation coefficient calculated using the 'acf' function in the Statsmodels package. Without the adjustment, the calculated p-values are often too low resulting in more frequently rejecting the null hypothesis of no trend or, for the case of T_{air}, rejecting significantly different trends from the observed global increase of 0.2 °C decade^{-1} (Santer et al. 2000). We study trends in T_{air}, VPD, and P for standard climatological seasons as well as individual months to better-identify periods that are exhibiting exceptional change. We also test the sensitivity of trends to the start date of the study period using the Global Historical Climatology Network (GHCN) dataset (Lawrimore et al. 2011) in the Appendix.

3. Results

a. Seasonal trends

The greatest increases in T_{air} occurred during climatological Winter (DJF), with some areas experiencing significant ($p < 0.05$) warming in excess of 0.4 °C decade^{-1} (Figure 2), especially in the CP and the eastern portion of the NGP. Spring (MAM) and Summer (JJA) show no significant positive or negative warming trends in aggregate but Fall (SON) warmed at approximately the global average trend of 0.2 °C decade^{-1} over the measurement period, which is significantly different from no trend across most of the U.S. Northern Plains.

VPD decreased across most of the NNAGP during Winter and across its eastern half during Summer (Figure 3). The southeastern NGP experienced the greatest negative trend of −0.4 hPa decade^{-1} or less. The mountainous regions to the west of the NNAGP experienced large and significant positive trends of VPD in excess of 0.4 hPa decade^{-1} during Summer. VPD decreased during Winter across the entire region, with the greatest decrease in the south. Spring and Fall experienced no significant trends in VPD in the study area over the measurement period.

P increased by 1 mm decade^{-1} or more across the eastern Dakotas during Winter, by 2 mm decade^{-1} or more in western Minnesota during MAM, and by 4 mm decade^{-1} or more across the central and eastern Dakotas during Summer (Figure 4).

b. Monthly trends

Analyzing T_{air} trends by month across the measurement period for the NNGAP reveals patterns of significant warming and cooling that are not apparent in the analysis by climate season (Figure 5). Median T_{air} across the entire NNAGP increased by ~0.9 °C decade^{-1} in January. February experienced no significant trend and March warmed by 0.3 °C decade^{-1}. April experienced no T_{air} trend, but May and June cooled by about −0.2 °C decade^{-1} on average. In other words, warming in March masked cooling in May in the analysis by climatological Spring (MAM, Figure 2). July and August have warmed by ~0.2 °C decade^{-1} on average, masking June cooling in the seasonal analysis. Likewise, the lack of T_{air} trend in October masked warming in September and November on the order of 0.3-0.4 °C decade^{-1}, with similar mean warming in December, slightly greater than the global annual warming trend across the study period on the order of 0.2 °C decade^{-1}.

The greatest May and June cooling trends on the order of −0.25 °C decade^{-1} are found in eastern Montana, western North Dakota, and the CP, and extends to the Canadian Shield north of the study domain and the Rocky Mountains to the west of the study domain (Figure 6a). The Rocky Mountains are important for storm generation in the NNAGP (Carbone and Tuttle 2008), but are outside of the study area. Mean cooling across the entire NNAGP during May and June from 1970-2015 averaged −0.1 °C decade^{-1} compared to a mean global warming of 0.3 °C decade^{-1} over the same period.

VPD decreased by −0.2 hPa decade^{-1} in May and −0.3 hPa decade^{-1} in June which, coupled with decreases in T_a, result in cooler and moister conditions (Figure 6b). VPD in July and August show high spatial variability with large positive and negative VPD trends across different parts of the study region (Figure 7). The dipole feature of Figure 3c explains why there is so much

variability in July and August: The eastern half of the study area exhibited negative VPD trends and the western half experienced positive trends. *P* increased across the entire NNAGP at 3 mm decade^{-1} and 4 mm decade^{-1} during May and June, respectively, and *P* in eastern North Dakota has increased in excess of 8 mm decade^{-1} (Fig. 6c). October also exhibits a positive trend in *P* of 2 mm decade^{-1}, but trends in *P* during other months are not different from zero (Figure 8).

4. Discussion

The research conducted here demonstrates that the annual climate of the NNAGP followed global T_{air} trends from 1970-2015 with important seasonal exceptions that require further analysis to ascertain the responsible mechanisms. The analysis of standard climatological seasons shows that warming occurred across the study area, exceeding the global average trend during most of the Winter but less than the global average trend during early Summer. The northern hemisphere winter is warming at the greatest rate globally, particularly in the extratropical and arctic regions (IPCC 2013). The NNAGP follows this pattern, with the greatest Winter warming trend exceeding 0.4 °C decade^{-1} in the northern part of the study domain (Abatzoglou et al. 2014) (Fig. 2). VPD has decreased during Winter and Summer, with the largest changes occurring in the southern part of the NNAGP during summer (Fig. 3). *P* has increased during much of the warm season, primarily in the eastern NNAGP; the only significant negative trend in *P* is in the western half of the study area during Winter (Fig. 4).

To provide context to the results, we analyzed the temperature trends for the NNAGP using 39 members from the CESM-LE ensemble, an experiment designed to put bounds on internal climate variability (Kay et al. 2015). The trends show that the observed May-June cooling trends

are outside the spread of simulated trends and the ensembles of T_{air} trends are higher for most months than observations with a median of 0.6 to 1.25 ℃ decade^{-1} (Figure 9). This indicates that the observed trends in the NNAGP are outside of natural climate variability and might be forced by processes that are not captured in the CESM-LE simulations including those that are local in nature. These could include an inaccurate representation of agricultural intensification and other land use changes that have occurred over the study period (e.g. Stoy et al. 2018) and errors in simulating convective processes (e.g., Prein et al. 2015) and associated land surface atmosphere feedbacks (Hohenegger et al. 2009) due to the coarse model resolution. It is important to note that the CESM-LE simulations were run at 1° horizontal grid spacing and are limited in their ability to simulate the mechanisms that give rise to convective cloud formation and precipitation, which are known to be important features of the growing season climate of the NNAGP (Betts et al. 2013a). One can infer therefore that important climate mechanisms in the NNAGP are not captured by existing global climate models, at least during some seasons.

a. Climatological seasons mask large monthly trends

There was little to no trend in T_{air} in the NNGAP during the summer months in the analysis of standard climatological seasons (Figure 2). Significant cooling became apparent across much of the NNAGP during May and June after disaggregating the analysis into months to identify if the seasonal analyses were averaging out important information (Figure 5). Stronger May and June cooling trends result if the 1980s were chosen as a start date (Appendix A2), suggesting that the cooling effect is not an artifact of choosing 1970 as a start date. It is difficult to attribute the significant May and June T_{air} decrease to any particular mechanism in an empirical study except to note that the CESM-LE fails to capture the observations (Figure 9), but observations are broadly

consistent with research on land-atmosphere coupling to date. A reduction in the area of summer fallow since the 1970s has been identified as a contributor to summer cooling and cloud development in the Canadian Prairies (Gameda et al. 2007; Betts et al. 2013d; Raddatz 1998a) and is consistent with the increase in likelihood of convective precipitation due in part to the lowering of the Bowen Ratio across parts of the U.S. Northern Plains (Gerken et al. 2018a). That being said, changes in irrigation in the Ogallala Aquifer region south of the study domain, increased land surface albedo due to the advent of no-till agriculture (Seneviratne et al. 2018; Davin et al. 2014; Lobell et al. 2006), ongoing increases in water table height and thereby surface water extent across much of the study region (Rodell et al. 2018), and changes in the general circulation are likely to interact with land cover change to cause the unique May and June temperature trends, and we discuss each in the context of regional climate modeling below after discussing trends in *P* to which trends in T_{air} are coupled (e.g. Prein et al. 2016).

b. Trends in precipitation

P increased in the eastern part of the NNAGP during most of the warm season including climatological Spring and Summer (Figure 4). Further evidence of increased *P* manifests itself in the fact that groundwater storage is increasing across the northern Great Plains (Rodell et al. 2018); these changes in groundwater are likely due to an increase in water inputs to the land surface rather than decreased outputs given that latent heat flux has increased across parts of the NNAGP (Gerken et al. 2018a; Vick et al. 2016). While not explicitly studied here, there is evidence that precipitation intensity has increased more than the Clausius-Clapeyron relationship would suggest with a 16% increase in rainfall amount occurring during the heaviest precipitation events (Reidmiller et al. 2018; Mishra et al. 2012). Recent studies have demonstrated that increased precipitation and

precipitation intensity, especially during the early warm season, are partly due to stronger convective systems (Prein et al. 2017b, 2016; Feng et al. 2016). It is important to note that the NNAGP is characterized by considerable year-on-year variability in *P* which can mask trends (Muhlbauer et al. 2009) and has wide ranging impacts for agriculture and water resources. A recent reminder of this was given in 2016 and 2017, when parts of the NNAGP experienced 150% of normal *P* for the 2016 calendar year followed by a severe 'flash' drought in the western NGP during the 2017 growing season, noting that our study period ends in 2015 due to data availability. This drought was preceded by a period of anomalously low likelihood of convective precipitation (Gerken et al. 2018b), further emphasizing the important role that locally-triggered convective *P* plays in the NNGAP during climatological spring and summer.

c. Land cover change

The early warm season of May and June is a period of considerable vegetative activity and alone comprises one half or more of the total growing season net carbon uptake by winter and spring wheat in central Montana, USA, with rapid crop growth during this period giving rise to substantial latent heat fluxes (Vick et al. 2016). The eddy covariance measurements described by Vick et al. (2016) demonstrate that a spring wheat field had nearly double the evapotranspiration as a nearby fallow field and half the sensible heat flux from planting to harvest. The simulated height of the atmospheric boundary layer on account of these differences in surface-atmosphere energy exchange differed by nearly 1 km between the wheat and fallow treatments during the mid-growing season, suggesting a substantial impact of agricultural management on boundary-layer climate, consistent with observations in the Canadian Prairies (Betts et al. 2013b; Gameda et al. 2007). Given the decline in summer fallow area in the NNAGP on the order of over 200,000 km^2

(Vick et al., 2016), a potential mechanism for the May and June cooling trend emerges if the lower, more humid boundary layer more readily produces clouds and precipitation (Gerken et al. 2018a), which would also help explain May – June decreases in VPD.

That being said, the reduction of summer fallow is not the only change occurring in the NNAGP. Shrubs and croplands have increased in aerial extent the U.S. Northern Plains since 2001, while the extent of forest, pasture, and Conservation Reserve Program areas have decreased (Stoy et al. 2018). No-till agriculture has increased albedo, but the magnitude and location of these changes are difficult to quantify and the reanalysis data products that may be able to estimate these changes often struggle to correctly estimate changes to net radiation as cloud fields are not sufficiently resolved in the reanalysis modeling systems (e.g. Draper et al. 2017). Warming temperatures associated with global climate change have created conditions conducive to corn and soy agriculture in the NNAGP (Smith et al. 2013; Kucharik 2008; Butler et al. 2018) and corn and soy acreage has also increased in the Prairie Pothole region of the Dakotas since the 2000s (Lark et al. 2015). The growing season for corn/soy as well as wheat has been extended by up to 10 days in some areas contributing to an increase in yields (Lanning et al. 2010; Kucharik 2008; Hu et al. 2005; Sacks and Kucharik 2011). An increase in corn-soy production in the U.S. Central Plains (i.e. the "Corn Belt") resulted in a similar cooling trend to what we observe in the NNAGP, although it has occurred later in the warm season (Mueller et al. 2015b) consistent with seasonal growth patterns of maize, a C4 plant. It is important to note that the replacement of one land cover type in favor of another does not always result in a consistent effect on regional temperature and precipitation (Garcia-Carreras et al. 2010; Bright et al. 2017; Fall et al. 2010) and surface-atmosphere interactions may be dominated by soil moisture state rather than vegetation

composition (Desai et al. 2006; Collow et al. 2014), highlighting the importance of coupled energy and water fluxes to regional climate processes.

Another influence on ABL processes is the addition of moisture by way of irrigation which lowers the Bowen ratio by favoring latent heat flux at the surface (Adegoke et al. 2003; Lobell and Bonfils 2008; Lobell et al. 2008; Mahmood et al. 2013). The addition of surface moisture tends to increase *P* by way of increasing moist static energy available for convection, particularly downstream of irrigated areas (DeAngelis et al. 2010; Huber et al. 2014; Harding et al. 2012; Yang et al. 2017; Segal et al. 1998). Irrigation in the NNAGP is far less common than the U.S. Southern Plains, especially areas overlying the Ogallala Aquifer (Dickens et al. 2011), but could be influenced by advection of moisture from the south (Rodell and Famiglietti 2002; Rodell et al. 2018) – especially given the influence of the nocturnal jet in the central U.S. – which might be the water source for the observed increase in *P*. Such changes to water cycling immediately outside the NNAGP emphasize the importance of understanding external vs internal inputs to the climate system.

Ongoing climate warming has increased the importance of VPD to plant stomatal function, transpiration, and the assimilation of carbon across global biomes (Novick et al. 2016b). Much of the United States has exhibited near-surface drying (i.e. an increase in VPD) with climate change – with deleterious consequences for agriculture (Seager et al. 2018a) – with the exception of parts of the U.S. portion of the NNAGP (Ficklin and Novick 2017; Seager et al. 2018b). Our analysis supports the notion that aridity is increasing in the NNAGP on an annual basis because of the increase in T_{air} and lack of trend in *P*. However, there are two signals in the monthly VPD trends that are consistent with agricultural intensification or other changes to regional water cycling. First,

the decrease in VPD during May and June (Figure 6b) is consistent with increased evapotranspiration resulting from a larger planted area as noted. Second, there is a significant decrease in VPD in the south-eastern part of the study area during climatological summer (Figure 3c) which is consistent with an increase in agricultural intensification within the study region (Mueller et al. 2015b) and/or an increase in moisture transport from the surrounding region that has experienced an increase in irrigation.

d. Toward an understanding of the mechanisms underlying regional early-season cooling

Results here are broadly consistent with the notion that agricultural intensity within and/or external to the NNAGP have caused a cooling trend during parts of the vegetative growing season, but also point to the need for process-based regional climate studies to identify the causes that underlie these observations. The NNAGP is a dynamic region that receives advected moisture and energy from the Arctic, Pacific, and the Gulf of Mexico in addition to internal water and energy cycling (Bonsal et al. 1999; Raddatz 2000a; Quiring and Kluver 2009) of which locally-recycled convective precipitation is an important part (Raddatz 2000a). The NNAGP is also influenced by global oscillations including ENSO and the PDO, and the MJO, and teleconnections that result in variable weather patterns and precipitation (Quiring and Papakyriakou 2005; Bonsal et al. 1999; Li et al. 2018). Climate change is also increasing the variability of the polar jet, which may be partially responsible for changes in surface temperature across the continent due to changes in meridional flow patterns (Francis and Vavrus 2015; Partridge et al. 2018). Despite the notion that early growing season changes in regional climate are consistent with the impacts of an intensifying agriculture system either within or external to the NNAGP, we cannot exclude other features of the climate system may be responsible for observed changes in T_{air}, VPD, and P.

Targeted climate change attribution experiments could help to quantify the contribution of different processes to the observed trends by modifying energy and moisture fluxes from the land surface to mimic past, present, and projected future changes in agricultural intensity while controlling for large-scale weather conditions. Of particular importance to the NNAGP is the use of convection-permitting climate models (CPM) that run on spatial scales of 4 km or less (e.g., Prein et al. 2015) considering the importance of land-atmosphere feedbacks and convective precipitation in the NNAGP (Gerken et al. 2018a; Betts et al. 2013a) and the failure of current climate models to simulate observed May – June T_{air} trends (Figure 9). Early simulations demonstrated that parameterizations were inadequate for modeling atmospheric circulations associated with heterogeneous landscapes (Avissar and Pielke 1989, 1991; Pielke et al. 1998). Therefore, to successfully model these changes using a CPM, the model would need to accurately represent the land surface and the resulting land-atmosphere interactions. A commonly used CPM, the Weather Research and Forecasting model (WRF) (Skamarock et al. 2008) contains land cover data products that are accurate for homogenous landscapes but often need to be addressed for heterogeneous landscapes and landscapes that exhibit interannual variability such as agricultural areas (Spera et al. 2018; Sertel et al. 2010; Gao and Jia 2013). It is also important to track moisture sources in such a modeling exercise to determine the roles of internal *versus* external water cycle dynamics in determining ongoing climate changes in the NNAGP. Determining the precipitation recycling ratio (Raddatz 2000a; Prasanna and Yasunari 2009; Kanamori et al. 2018) would help with source attribution, as would using Lagrangian methods such as the HYSPLIT model (Stein et al. 2015). Given the use of a convection permitting model however, tracing water vapor within the model framework might give detailed insight into the water balance of the NNAGP

(Dominguez et al. 2016; Chug and Dominguez 2019). Such an effort would require extensive computational resources but would also be critical given the importance of the NNAGP to the global food system.

5. Summary

Regional climate trends influence perception of climate change and subsequent management decisions by local and regional stakeholders (Abatzoglou et al. 2009; Grimberg et al. 2018) for whom sub-seasonal climate variability is important (Asseng et al. 2015b; Klemm and McPherson 2017). The results of this study demonstrate the importance of studying climate trends at time scales that are more finely resolved than standard climatological seasons. From a global perspective, much of the NNAGP has responded to climate change as expected. However, there are stark changes within standard climatological seasons that are not captured by the CESM-LE simulations (Fig. 9): May and June have cooled at nearly the opposite rate of observed global warming, and January warmed much more than the global average (Fig. 5). The May – June cooling trend is centered within the NNAGP, but the warming in the winter and shoulder seasons has occurred in the Rocky Mountains to the west and areas further north (Fig. 2). VPD is generally not changing with the exception of the warm season; May and June have experienced a decrease in VPD with variable trends during July and August (Fig. 6). The negative summer VPD trend is found across the eastern half of the domain – largest in the southeast – and like many trends observed here spills across the study region, in this case toward the northeast (Fig. 3). *P* has increased across the early warm season, with the largest positive trends found in May and June (Fig. 7). Generally, the positive trends in *P* are located in the eastern half of the domain but extend

outside of the study area as well (Fig. 8c) and it is unclear if this is part of a common climate trend. Our observational study demonstrates that the NNAGP largely followed annual average global climate trends with many exceptions including cooler and wetter conditions during May and June whose causes must be investigated using mechanistic studies to understand if they were caused by agricultural intensification, and to disentangle the interaction between land management and climate in this globally-important agricultural region.

Acknowledgements

We thank NOAA, NASA, as well as many others for decades of data collection and management and acknowledge support from the National Science Foundation (NSF) Office of Integrated Activities (OIA) award 1632810, the NSF Division of Environmental Biology (DEB) award 1552976, the U.S. Department of Agriculture (USDA) National Institute of Food and Agriculture (NIFA) Hatch project 228396 and multistate project W3188, the Graduate School at Montana State University, and the Montana Wheat and Barley Committee. Dr. Ankur Desai, James T. Douglas, Shaelyn Meyer, Rebecca Pappas (†), Elizabeth Rehbein, Dr. Amy Trowbridge, and Dr. Perry Miller provided valuable comments on earlier drafts of the manuscript and we would like to thank Referees for constructive comments.

Appendix

Data Coverage

The CRU dataset is a gridded observational dataset that integrates observations from the World Meteorological Organization (WMO) and other sources (Harris et al. 2014). The CRU dataset

contains a source observation density data product that shows how many unique stations were interpolated to each grid cell. Each grid cell in the NNAGP (and most of North America) have eight stations contributing to each grid cell, which is the maximum that the CRU algorithms incorporate.

Trend Verification

We repeated the analysis of T_{air} trends using the Berkley Earth Surface Temperature data (Rohde et al. 2013) to critique results from the CRU dataset (Fig. 5). The same monthly T_{air} patterns hold (Fig. A1). We also used the Global Historical Climatology Network (GHCN) dataset (Lawrimore et al. 2011) to critique the start date of the analysis (Fig. A2). The May and June cooling trend across all GHCN stations in the NNAGP is larger if the analysis starts in 1980, suggesting that beginning the analysis in 1970 results in a conservative interpretation of observed May and June cooling trends.

References

Abatzoglou, J. T., K. T. Redmond, and L. M. Edwards, 2009: Classification of regional climate variability in the state of California. *J. Appl. Meteorol. Climatol.*, **48**, 1527–1541, https://doi.org/10.1175/2009JAMC2062.1.

Abatzoglou, J. T., D. E. Rupp, and P. W. Mote, 2014: Seasonal climate variability and change in the Pacific Northwest of the United States. *J. Clim.*, **27**, 2125–2142, doi:10.1175/JCLI-D-13-00218.1.

Adegoke, J. O., R. A. Pielke, J. Eastman, R. Mahmood, and K. G. Hubbard, 2003: Impact of Irrigation on Midsummer Surface Fluxes and Temperature under Dry Synoptic Conditions: A Regional Atmospheric Model Study of the U.S. High Plains. *Mon. Weather Rev.*, **131**, 556–564, https://doi.org/10.1175/1520-0493(2003)131<0556:IOIOMS>2.0.CO;2.

Alter, R. E., Y. Fan, B. R. Lintner, C. P. Weaver, R. E. Alter, Y. Fan, B. R. Lintner, and C. P. Weaver, 2015: Observational evidence that Great Plains irrigation has enhanced summer precipitation intensity and totals in the midwestern United States. *J. Hydrometeorol.*, **16**, 1717–1735, doi:10.1175/JHM-D-14-0115.1.

——, H. C. Douglas, J. M. Winter, and E. A. B. Eltahir, 2017: 20th-century regional climate change in the central United States attributed to agricultural intensification. *Geophys. Res. Lett.*, 1–9, https://doi.org/10.1002/2017GL075604.

Asseng, S., and Coauthors, 2013: Uncertainty in simulating wheat yields under climate change. *Nat. Clim. Change*, **3**, 827–832, https://doi.org/10.1038/nclimate1916.

——, and Coauthors, 2015: Rising temperatures reduce global wheat production. *Nat. Clim. Change*, **5**, 143–147, https://doi.org/10.1038/nclimate2470.

Avissar, R., and R. A. Pielke, 1989: A Parameterization of Heterogeneous Land Surfaces for Atmospheric Numerical Models and Its Impact on Regional Meteorology. *Mon. Weather Rev.*, **117**, 2113–2136, https://doi.org/10.1175/1520-0493(1989)117<2113:APOHLS>2.0.CO;2.

Avissar, R., and R. A. Pielke, 1991: The impact of plant stomatal control on mesoscale atmospheric circulations. *Agric. For. Meteorol.*, **54**, 353–372, https://doi.org/10.1016/0168-1923(91)90013-G.

Betts, A. K., R. Desjardins, and D. Worth, 2013a: Cloud radiative forcing of the diurnal cycle climate of the Canadian Prairies. *J. Geophys. Res. Atmospheres*, **118**, 8935–8953, https://doi.org/10.1002/jgrd.50593.

Betts, A. K., R. Desjardins, D. Worth, and D. Cerkowniak, 2013b: Impact of land use change on the diurnal cycle climate of the Canadian Prairies. *J. Geophys. Res. Atmospheres*, **118**, 11996–12011, https://doi.org/10.1002/2013JD020717.

Bonetti, S., G. Manoli, J. Domec, M. Putti, M. Marani, and G. G. Katul, 2015: The influence of water table depth and the free atmospheric state on convective rainfall predisposition. *Water Resour. Res.*, **51**, 2283–2297, https://doi.org/10.1002/2014WR016431.

Bonsal, B. R., X. Zhang, and W. D. Hogg, 1999: Canadian Prairie growing season precipitation variability and associated atmospheric circulation. *Clim. Res.*, **11**, 191–208.

Bradshaw, B., H. Dolan, and B. Smit, 2004: Farm-level adaptation to climatic variability and change: crop diversification in the Canadian Prairies. *Clim. Change*, **67**, 119–141, doi:10.1007/s10584-004-0710-z.

Bright, R. M., E. Davin, T. O'Halloran, J. Pongratz, K. Zhao, and A. Cescatti, 2017: Local temperature response to land cover and management change driven by non-radiative processes. *Nat. Clim. Change*, **7**, 296–302, https://doi.org/10.1038/nclimate3250.

Butler, E. E., N. D. Mueller, and P. Huybers, 2018: Peculiarly pleasant weather for US maize. *Proc. Natl. Acad. Sci.*, **115**, 11935–11940, https://doi.org/10.1073/pnas.1808035115.

Campbell, C. A., R. P. Zentner, S. Gameda, B. Blomert, and D. D. Wall, 2002: Production of annual crops on the Canadian prairies: Trends during 1976–1998. *Can. J. Soil Sci.*, **82**, 45–57, https://doi.org/10.4141/S01-046.

Carbone, R. E., and J. D. Tuttle, 2008: Rainfall Occurrence in the U.S. Warm Season: The Diurnal Cycle. *J. Clim.*, **21**, 4132–4146, https://doi.org/10.1175/2008JCLI2275.1.

Chug, D., and F. Dominguez, 2019: Isolating the observed influence of vegetation variability on the climate of La Plata River Basin. *J. Clim.*, https://doi.org/10.1175/JCLI-D-18-0677.1.

Collow, T. W., A. Robock, and W. Wu, 2014: Influences of soil moisture and vegetation on convective precipitation foerecasts over the United States Great Plains. *J. Geophys. Res. Atmospheres*, **119**, 9338–9358, https://doi.org/10.1002/2014JD021454.Received.

Couzin, J., 1999: Landscape changes make regional climate run hot and cold. *Science*, **283**, 317–319, doi:10.1126/science.283.5400.317.

Dai, A., 2006: Recent climatology, variability, and trends in global surface humidity. *J. Clim.*, **19**, 3589–3606, https://doi.org/10.1175/JCLI3816.1.

Davin, E. L., S. I. Seneviratne, P. Ciais, A. Olioso, and T. Wang, 2014: Preferential cooling of hot extremes from cropland albedo management. *Proc. Natl. Acad. Sci.*, **111**, 9757–9761, https://doi.org/10.1073/pnas.1317323111.

DeAngelis, A., F. Dominguez, Y. Fan, A. Robock, M. D. Kustu, and D. Robinson, 2010: Evidence of enhanced precipitation due to irrigation over the Great Plains of the United States. *J. Geophys. Res. Atmospheres*, **115**, https://doi.org/10.1029/2010JD013892.

Desai, A. R., K. J. Davis, C. J. Senff, S. Ismail, E. V. Browell, D. R. Stauffer, and B. P. Reen, 2006: A case study on the effects of heterogeneous soil moisture on mesoscale boundary-layer structure in the Southern Great Plains, U.S.A. Part I: Simple prognostic model. *Bound.-Layer Meteorol.*, **119**, 195–238, https://doi.org/10.1007/s10546-005-9024-6.

Deser, C., A. Phillips, V. Bourdette, and H. Teng, 2012: Uncertainty in climate change projections: the role of internal variability. *Clim. Dyn.*, **38**, 527–546, https://doi.org/10.1007/s00382-010-0977-x.

Dickens, J. M., B. T. Forbes, D. S. Cobean, and S. Tadayon, 2011: *Documentation of methods and inventory of irrigation data collected for the 2000 and 2005 U.S. Geological Survey Estimated use of water in the United States, comparison of USGS-compiled irrigation data to other sources, and recommendations for future compilations*. http://pubs.usgs.gov/sir/2011/5166/.

Diffenbaugh, N. S., 2009: Influence of modern land cover on the climate of the United States. *Clim. Dyn.*, **33**, 945–958, https://doi.org/10.1007/s00382-009-0566-z.

Dominguez, F., G. Miguez-Macho, and H. Hu, 2016: WRF with Water Vapor Tracers: A Study of Moisture Sources for the North American Monsoon. *J. Hydrometeorol.*, **17**, 1915–1927, https://doi.org/10.1175/JHM-D-15-0221.1.

Draper, C. S., R. H. Reichle, and R. D. Koster, 2017: Assessment of MERRA-2 Land Surface Energy Flux Estimates. *J. Clim.*, **31**, 671–691, https://doi.org/10.1175/JCLI-D-17-0121.1.

Fall, S., D. Niyogi, A. Gluhovsky, R. A. Pielke, E. Kalnay, and G. Rochon, 2010: Impacts of land use land cover on temperature trends over the continental United States: assessment using the North American Regional Reanalysis. *Int. J. Climatol.*, **30**, 1980–1993, https://doi.org/10.1002/joc.1996.

Feng, Z., L. R. Leung, S. Hagos, R. A. Houze, C. D. Burleyson, and K. Balaguru, 2016: More frequent intense and long-lived storms dominate the springtime trend in central US rainfall. *Nat. Commun.*, **7**, 13429, https://doi.org/10.1038/ncomms13429.

Ficklin, D. L., and K. A. Novick, 2017: Historic and projected changes in vapor pressure deficit suggest a continental-scale drying of the United States atmosphere. *J. Geophys. Res. Atmospheres*, **122**, 2061–2079, https://doi.org/10.1002/2016JD025855.

Findell, K. L., and E. a. B. Eltahir, 2003a: Atmospheric controls on soil moisture–boundary layer interactions. Part II: feedbacks within the continental United States. *J. Hydrometeorol.*, **4**, 570–583, doi:10.1175/1525-7541(2003)004<0570:ACOSML>2.0.CO;2.

Findell, K. L., and E. A. B. Eltahir, 2003b: Atmospheric controls on soil moisture–boundary layer interactions. Part I: framework development. *J. Hydrometeorol.*, **4**, 552–569, doi:10.1175/1525-7541(2003)004<0552:ACOSML>2.0.CO;2.

Francis, J. A., and S. J. Vavrus, 2015: Evidence for a wavier jet stream in response to rapid Arctic warming. *Environ. Res. Lett.*, **10**, 014005, https://doi.org/10.1088/1748-9326/10/1/014005.

Friedl, M. A., D. Sulla-Menashe, B. Tan, A. Schneider, N. Ramankutty, A. Sibley, and X. Huang, 2010: MODIS Collection 5 global land cover: algorithm refinements and characterization of new datasets. *Remote Sens. Environ.*, **114**, 168–182, doi:10.1016/j.rse.2009.08.016.

Gameda, S., B. Qian, C. A. Campbell, and R. L. Desjardins, 2007: Climatic trends associated with summerfallow in the Canadian Prairies. *Agric. For. Meteorol.*, **142**, 170–185, https://doi.org/10.1016/j.agrformet.2006.03.026.

Gao, H., and G. Jia, 2013: Assessing disagreement and tolerance of misclassification of satellite-derived land cover products used in WRF model applications. *Adv. Atmospheric Sci.*, **30**, 125–141, https://doi.org/10.1007/s00376-012-2037-4.

Garcia-Carreras, L., D. J. Parker, C. M. Taylor, C. E. Reeves, and J. G. Murphy, 2010: Impact of mesoscale vegetation heterogeneities on the dynamical and thermodynamic properties of the planetary boundary layer. *J. Geophys. Res. Atmospheres*, **115**, 1–12, https://doi.org/10.1029/2009JD012811.

Gauthier, D. A., and E. . Wiken, 2003: Monitoring the conservation of grassland habitats, Prairie Ecozone, Canada. *Environ. Monit. Assess.*, **88**, 343–364.

Gentine, P., A. A. M. Holtslag, F. D'Andrea, and M. Ek, 2013: Surface and atmospheric controls on the onset of moist convection over land. *J. Hydrometeorol.*, **14**, doi:10.1175/JHM-D-12-0137.1.

Gerken, T., G. T. Bromley, B. L. Ruddell, S. Williams, and P. C. Stoy, 2018a: Convective suppression before and during the United States Northern Great Plains flash drought of 2017. *Hydrol. Earth Syst. Sci.*, **22**, 4155–4163, https://doi.org/10.5194/hess-22-4155-2018.

——, ——, and P. C. Stoy, 2018b: Surface moistening trends in the northern North American Great Plains increase the likelihood of convective initiation. *J. Hydrometeorol.*, **19**, 227–244, doi:10.1175/JHM-D-17-0117.1.

Grimberg, B., S. Ahmed, C. Ellis, Z. Miller, and F. Menalled, 2018: Climate change perceptions and observations of agricultural stakeholders in the Northern Great Plains. *Sustainability*, **10**, 1687, doi:10.3390/su10051687.

Hammermeister, A. M., 2001: An ecological analysis of prairie rehabilitation on petroleum wellsites in southeast Alberta. *Can. Univ. Alta.*,.

Harding, K. J., P. K. Snyder, K. J. Harding, and P. K. Snyder, 2012: Modeling the Atmospheric Response to Irrigation in the Great Plains. Part II: The Precipitation of Irrigated Water and Changes in Precipitation Recycling. *J. Hydrometeorol.*, **13**, 1687–1703, https://doi.org/10.1175/JHM-D-11-099.1.

Harris, I., P. D. Jones, T. J. Osborn, and D. H. Lister, 2014: Updated high-resolution grids of monthly climatic observations - the CRU TS3.10 Dataset. *Int. J. Climatol.*, **34**, 623–642, https://doi.org/10.1002/joc.3711.

Hohenegger, C., P. Brockhaus, C. S. Bretherton, and C. Schär, 2009: The Soil Moisture–Precipitation Feedback in Simulations with Explicit and Parameterized Convection. *J. Clim.*, **22**, 5003–5020, https://doi.org/10.1175/2009JCLI2604.1.

Hu, Q., A. Weiss, S. Feng, and P. S. Baenziger, 2005: Earlier winter wheat heading dates and warmer spring in the U.S. Great Plains. *Agric. For. Meteorol.*, **135**, 284–290, https://doi.org/10.1016/j.agrformet.2006.01.001.

Huber, D., D. Mechem, and N. Brunsell, 2014: The effects of great plains irrigation on the surface energy balance, regional circulation, and precipitation. *Climate*, **2**, 103–128, doi:10.3390/cli2020103.

IPCC, ed., 2013: *Climate Change 2013 - The Physical Science Basis: Working Group I Contribution to the Fifth Assessment Report of the Intergovernmental Panel on Climate Change*. Cambridge University Press,.

——, 2014: *AR5 Climate Change 2014: Impacts, Adaptation, and Vulnerability — IPCC*. IPCC, https://www.ipcc.ch/report/ar5/wg2/ (Accessed January 8, 2019).

Jones, P., 2016: The reliability of global and hemispheric surface temperature records. *Adv. Atmospheric Sci.*, **33**, 269–282, https://doi.org/10.1007/s00376-015-5194-4.

Juang, J. Y., A. Porporato, P. C. Stoy, M. S. Siqueira, A. C. Oishi, M. Detto, H. S. Kim, and G. G. Katul, 2007: Hydrologic and atmospheric controls on initiation of convective precipitation events. *Water Resour. Res.*, **43**, 1–10, https://doi.org/10.1029/2006WR004954.

Kanamori, H., T. Kumagai, H. Fujinami, T. Hiyama, and T. Yasunari, 2018: Effects of Long- and Short-Term Atmospheric Water Cycles on the Water Balance over the Maritime Continent. *J. Hydrometeorol.*, **19**, 1413–1427, https://doi.org/10.1175/JHM-D-18-0052.1.

Kay, J. E., and Coauthors, 2015: The Community Earth System Model (CESM) Large Ensemble Project: A Community Resource for Studying Climate Change in the Presence of Internal

Climate Variability. *Bull. Am. Meteorol. Soc.*, **96**, 1333–1349, https://doi.org/10.1175/BAMS-D-13-00255.1.

Keller, M., D. S. Schimel, W. W. Hargrove, and F. M. Hoffman, 2008: A continental strategy for the National Ecological Observatory Network. *Front. Ecol. Environ.*, **6**, 282–284, https://doi.org/10.1890/1540-9295(2008)6[282:ACSFTN]2.0.CO;2.

Klemm, T., and R. A. McPherson, 2017: The development of seasonal climate forecasting for agricultural producers. *Agric. For. Meteorol.*, **232**, 384–399, https://doi.org/10.1016/j.agrformet.2016.09.005.

Kucharik, C. J., 2008: Contribution of Planting Date Trends to Increased Maize Yields in the Central United States. *Agron. J.*, **100**, 328–336, https://doi.org/10.2134/agronj2007.0145.

Lanning, S. P., K. Kephart, G. R. Carlson, J. E. Eckhoff, R. N. Stougaard, D. M. Wichman, J. M. Martin, and L. E. Talbert, 2010: Climatic Change and Agronomic Performance of Hard Red Spring Wheat from 1950 to 2007. *Crop Sci.*, **50**, 835, https://doi.org/10.2135/cropsci2009.06.0314.

Lark, T. J., J. Meghan Salmon, and H. K. Gibbs, 2015: Cropland expansion outpaces agricultural and biofuel policies in the United States. *Environ. Res. Lett.*, **10**, 044003, https://doi.org/10.1088/1748-9326/10/4/044003.

Lawrimore, J. H., M. J. Menne, B. E. Gleason, C. N. Williams, D. B. Wuertz, R. S. Vose, and J. Rennie, 2011: An overview of the Global Historical Climatology Network monthly mean temperature data set, version 3. *J. Geophys. Res. Atmospheres*, **116**, 1–18, https://doi.org/10.1029/2011JD016187.

Li, Z., Y. Li, B. Bonsal, A. H. Manson, and L. Scaff, 2018: Combined impacts of ENSO and MJO on the 2015 growing season drought on the Canadian Prairies. *Hydrol. Earth Syst. Sci.*, **22**, 5057–5067, https://doi.org/10.5194/hess-22-5057-2018.

Lobell, D. B., and C. Bonfils, 2008: The Effect of Irrigation on Regional Temperatures: A Spatial and Temporal Analysis of Trends in California, 1934–2002. *J. Clim.*, **21**, 2063–2071, https://doi.org/10.1175/2007JCLI1755.1.

Lobell, D. B., G. Bala, and P. B. Duffy, 2006: Biogeophysical impacts of cropland management changes on climate. *Geophys. Res. Lett.*, **33**, https://doi.org/10.1029/2005GL025492.

Lobell, D. B., C. J. Bonfils, L. M. Kueppers, and M. A. Snyder, 2008: Irrigation cooling effect on temperature and heat index extremes. *Geophys. Res. Lett.*, **35**, https://doi.org/10.1029/2008GL034145.

Lobell, D. B., M. J. Roberts, W. Schlenker, N. Braun, B. B. Little, R. M. Rejesus, and G. L. Hammer, 2014: Greater sensitivity to drought accompanies maize yield increase in the U.S. Midwest. *Science*, **344**, 516–519, doi:10.1126/science.1251423.

Lu, Y., K. Harding, and L. Kueppers, 2017: Irrigation effects on land-atmosphere coupling strength in the United States. *J. Clim.*, **30**, 3671–3685, https://doi.org/10.1175/JCLI-D-15-0706.1.

Mahmood, R., K. G. Hubbard, R. D. Leeper, and S. A. Foster, 2008: Increase in near-surface atmospheric moisture content due to land use changes: evidence from the observed dewpoint temperature data. *Mon. Weather Rev.*, **136**, 1554–1561, doi:10.1175/2007MWR2040.1.

——, T. Keeling, S. A. Foster, and K. G. Hubbard, 2013: Did irrigation impact 20th century air temperature in the High Plains aquifer region? *Appl. Geogr.*, **38**, 11–21, https://doi.org/10.1016/j.apgeog.2012.11.002.

——, and Coauthors, 2014: Land cover changes and their biogeophysical effects on climate. *Int. J. Climatol.*, **34**, 929–953, https://doi.org/10.1002/joc.3736.

Manoli, G., J. C. Domec, K. Novick, A. C. Oishi, A. Noormets, M. Marani, and G. Katul, 2016: Soil-plant-atmosphere conditions regulating convective cloud formation above southeastern US pine plantations. *Glob. Change Biol.*, **22**, 2238–2254, https://doi.org/10.1111/gcb.13221.

Millett, B.,W Carter Johnson, G. Guntenspergen, W. C. Johnson, and G. Guntenspergen, 2009: Climate trends of the North American prairie pothole region 1906–2000. *Clim. Change*, **93**, doi:10.1007/s10584-008-9543-5.

Mishra, V., J. M. Wallace, and D. P. Lettenmaier, 2012: Relationship between hourly extreme precipitation and local air temperature in the United States. *Geophys. Res. Lett.*, **39**, https://doi.org/10.1029/2012GL052790.

Mueller, N. D., E. E. Butler, K. A. Mckinnon, A. Rhines, M. Tingley, N. M. Holbrook, and P. Huybers, 2015: Cooling of US Midwest summer temperature extremes from cropland intensification. https://doi.org/10.1038/NCLIMATE2825.

Mueller, N. D., A. Rhines, E. E. Butler, D. K. Ray, S. Siebert, N. M. Holbrook, and P. Huybers, 2017: Global Relationships between Cropland Intensification and Summer Temperature Extremes over the Last 50 Years. *J. Clim.*, **30**, 7505–7528, https://doi.org/10.1175/JCLI-D-17-0096.1.

Muhlbauer, A., P. Spichtinger, and U. Lohmann, 2009: Application and Comparison of Robust Linear Regression Methods for Trend Estimation. *J. Appl. Meteorol. Climatol.*, **48**, 1961–1970, https://doi.org/10.1175/2009JAMC1851.1.

Novick, K. A., and Coauthors, 2016: The increasing importance of atmospheric demand for ecosystem water and carbon fluxes. *Nat. Clim. Change*, **1**, 1–5, https://doi.org/10.1038/nclimate3114.

Partridge, T. F., J. M. Winter, E. C. Osterberg, D. W. Hyndman, A. D. Kendall, and F. J. Magilligan, 2018: Spatially distinct seasonal patterns and forcings of the U.S. warming hole. *Geophys. Res. Lett.*, **45**, 2055–2063, doi:10.1002/2017GL076463.

Pielke, R. A., 2001: Influence of the spatial distribution of vegetation and soils on the predictions of cumulus convective rainfall. *Rev. Geophys.*, **39**, 151–177, doi:10.1029/1999RG000072.

——, Sr, R. Avissar, M. Raupach, A. J. Dolman, X. Zeng, and A. S. Denning, 1998: Interactions between the atmosphere and terrestrial ecosystems: influence on weather and climate. *Glob. Change Biol.*, **4**, 461–475, https://doi.org/10.1046/j.1365-2486.1998.t01-1-00176.x.

Pielke, R. A., J. Adegoke, A. Beltrán-Przekurat, C. A. Hiemstra, J. Lin, U. S. Nair, D. Niyogi, and T. E. Nobis, 2007: An overview of regional land-use and land-cover impacts on rainfall. *Tellus Ser. B Chem. Phys. Meteorol.*, **59**, 587–601, https://doi.org/10.1111/j.1600-0889.2007.00251.x.

Prasanna, V., and T. Yasunari, 2009: Time-Space Characteristics of Seasonal and Interannual Variations of Atmospheric Water Balance over South Asia. *J. Meteorol. Soc. Jpn. Ser II*, **87**, 263–287, https://doi.org/10.2151/jmsj.87.263.

Prein, A. F., and Coauthors, 2015: A review on regional convection-permitting climate modeling: Demonstrations, prospects, and challenges. *Rev. Geophys.*, **53**, https://doi.org/10.1002/2014RG000475.

——, R. M. Rasmussen, K. Ikeda, C. Liu, M. P. Clark, and G. J. Holland, 2016: The future intensification of hourly precipitation extremes. *Nat. Clim. Change*, https://doi.org/10.1038/nclimate3168.

——, C. Liu, K. Ikeda, S. B. Trier, R. M. Rasmussen, G. J. Holland, and M. P. Clark, 2017: Increased rainfall volume from future convective storms in the US. *Nat. Clim. Change*, **7**, 880–884, https://doi.org/10.1038/s41558-017-0007-7.

Quiring, S. M., and T. N. Papakyriakou, 2005: Characterizing the spatial and temporal variability of June-July moisture conditions in the Canadian prairies. *Int. J. Climatol.*, **25**, 117–138, https://doi.org/10.1002/joc.1104.

Quiring, S. M., and D. B. Kluver, 2009: Relationship between Winter/Spring snowfall and Summer precipitation in the Northern Great Plains of North America. doi:10.1175/2009JHM1089.1.

Raddatz, R. L., 1998: Anthropogenic vegetation transformation and the potential for deep convection on the Canadian prairies. *Can. J. Soil Sci.*, **78**, 657–666, https://doi.org/10.4141/S98-011.

——, 2000: Summer rainfall recycling for an agricultural region of the Canadian prairies. *Can. J. Soil Sci.*, **80**, 367–373, https://doi.org/10.4141/S99-016.

Ramsey, F., and D. Schafer, 2012: *The Statistical Sleuth: A Course in Methods of Data Analysis*. 4th ed.

Reidmiller, D. R., C. W. Avery, D. R. Easterling, K. E. Kunkel, K. L. M. Lewis, T. K. Maycock, and B. C. Stewart, 2018: *Impacts, Risks, and Adaptation in the United States: The Fourth National Climate Assessment, Volume II*. U.S. Global Change Research Program,.

Rodell, M., and J. S. Famiglietti, 2002: The potential for satellite-based monitoring of groundwater storage changes using GRACE: the High Plains aquifer, Central US. *J. Hydrol.*, **263**, 245–256, https://doi.org/10.1016/S0022-1694(02)00060-4.

——, ——, D. N. Wiese, J. T. Reager, H. K. Beaudoing, F. W. Landerer, and M. H. Lo, 2018: Emerging trends in global freshwater availability. *Nature*, **557**, 651–659, https://doi.org/10.1038/s41586-018-0123-1.

Rohde, R., R. A. Muller, R. Jacobsen, E. Muller, and C. Wickham, 2013: A new estimate of the average earth surface land temperature spanning 1753 to 2011. *Geoinformatics Geostat. Overv.*, **01**, doi:10.4172/2327-4581.1000101. http://www.scitechnol.com/2327-4581/2327-4581-1-101.php (Accessed January 18, 2019).

Rossum, G., 1995: *Python Reference Manual*. CWI (Centre for Mathematics and Computer Science),.

Sacks, W. J., and C. J. Kucharik, 2011: Crop management and phenology trends in the U.S. Corn Belt: Impacts on yields, evapotranspiration and energy balance. *Agric. For. Meteorol.*, **151**, 882–894, https://doi.org/10.1016/j.agrformet.2011.02.010.

Santer, B. D., T. M. L. Wigley, J. S. Boyle, D. J. Gaffen, J. J. Hnilo, D. Nychka, D. E. Parker, and K. E. Taylor, 2000: Statistical significance of trends and trend differences in layer-average atmospheric temperature time series. *J. Geophys. Res.*, **105**, 7337–7356, https://doi.org/10.1029/1999JD901105.

Seabold, S., and J. Perktold, 2010: Statsmodels: Econometric and statistical modeling with python. *Proc. 9th Python Sci. Conf.*, **2010**.

Seager, R., J. Feldman, N. Lis, M. Ting, A. P. Williams, J. Nakamura, H. Liu, and N. Henderson, 2018a: Whither the 100th meridian? The once and future physical and human geography of america's arid–humid divide. Part II: The meridian moves east. *Earth Interact.*, **22**, 1–24, doi:10.1175/EI-D-17-0012.1.

——, N. Lis, J. Feldman, M. Ting, A. P. Williams, J. Nakamura, H. Liu, and N. Henderson, 2018b: Whither the 100th meridian? The once and future physical and human geography

of america's arid–humid divide. Part I: The story so far. *Earth Interact.*, **22**, 1–22, doi:10.1175/EI-D-17-0011.1.

Segal, M., Z. Pan, R. W. Turner, and E. S. Takle, 1998: On the Potential Impact of Irrigated Areas in North America on Summer Rainfall Caused by Large-Scale Systems. *J. Appl. Meteorol.*, **37**, 325–331, https://doi.org/10.1175/1520-0450-37.3.325.

Seneviratne, S. I., D. Lüthi, M. Litschi, and C. Schär, 2006: Land-atmosphere coupling and climate change in Europe. *Nature*, **443**, 205–209, https://doi.org/10.1038/nature05095.

Seneviratne, S. I., and Coauthors, 2018: Land radiative management as contributor to regional-scale climate adaptation and mitigation. *Nat. Geosci.*, **11**, 88–96, https://doi.org/10.1038/s41561-017-0057-5.

Sertel, E., A. Robock, and C. Ormeci, 2010: Impacts of land cover data quality on regional climate simulations. *Int. J. Climatol.*, **30**, 1942–1953, https://doi.org/10.1002/joc.2036.

Skamarock, W. C., and Coauthors, 2008: A description of the advanced research WRF version 3, NCAR Technical Note. *Natl. Cent. Atmospheric Res. Boulder CO USA*,.

Smith, W. N., and Coauthors, 2013: Assessing the effects of climate change on crop production and GHG emissions in Canada. *Agric. Ecosyst. Environ.*, **179**, 139–150, https://doi.org/10.1016/j.agee.2013.08.015.

Spera, S. A., J. M. Winter, and J. W. Chipman, 2018: Evaluation of Agricultural Land Cover Representations on Regional Climate Model Simulations in the Brazilian Cerrado. *J. Geophys. Res. Atmospheres*, **123**, 5163–5176, https://doi.org/10.1029/2017JD027989.

Stein, A. F., R. R. Draxler, G. D. Rolph, B. J. B. Stunder, M. D. Cohen, and F. Ngan, 2015: NOAA's HYSPLIT Atmospheric Transport and Dispersion Modeling System. *Bull. Am. Meteorol. Soc.*, **96**, 2059–2077, https://doi.org/10.1175/BAMS-D-14-00110.1.

Stoy, P. C., and Coauthors, 2018: Opportunities and trade-offs among BECCS and the food, water, energy, biodiversity, and social systems nexus at regional scales. *BioScience*, **68**, 100–111, doi:10.1093/biosci/bix145.

Sun, Q., C. Miao, Q. Duan, H. Ashouri, S. Sorooshian, and K.-L. Hsu, 2018: A Review of Global Precipitation Data Sets: Data Sources, Estimation, and Intercomparisons. *Rev. Geophys.*, **56**, 79–107, https://doi.org/10.1002/2017RG000574.

Vick, E. S. K., P. C. Stoy, A. C. I. Tang, and T. Gerken, 2016: The surface-atmosphere exchange of carbon dioxide, water, and sensible heat across a dryland wheat-fallow rotation. *Agric. Ecosyst. Environ.*, **232**, 129–140, https://doi.org/10.1016/j.agee.2016.07.018.

Wiken, E. B., and Canadian Council on Ecological Areas, eds., 1996: *A perspective on Canada's ecosystems: an overview of the terrestrial and marine ecozones*. Canadian Council on Ecological Areas, 95 pp.

Xie, S.-P., and Coauthors, 2015: Towards predictive understanding of regional climate change. *Nat. Clim. Change*, **5**, 921–930, https://doi.org/10.1038/nclimate2689.

Yang, Z., F. Dominguez, X. Zeng, H. Hu, H. Gupta, and B. Yang, 2017: Impact of Irrigation over the California Central Valley on Regional Climate. *J. Hydrometeorol.*, **18**, 1341–1357, https://doi.org/10.1175/JHM-D-16-0158.1.

Yin, J., J. D. Albertson, J. R. Rigby, and A. Porporato, 2015: Land and atmospheric controls on initiation and intensity of moist convection: CAPE dynamics and LCL crossings. *Water Resour. Res.*, **51**, 8476–8493, https://doi.org/10.1002/2015WR017286.

Figures

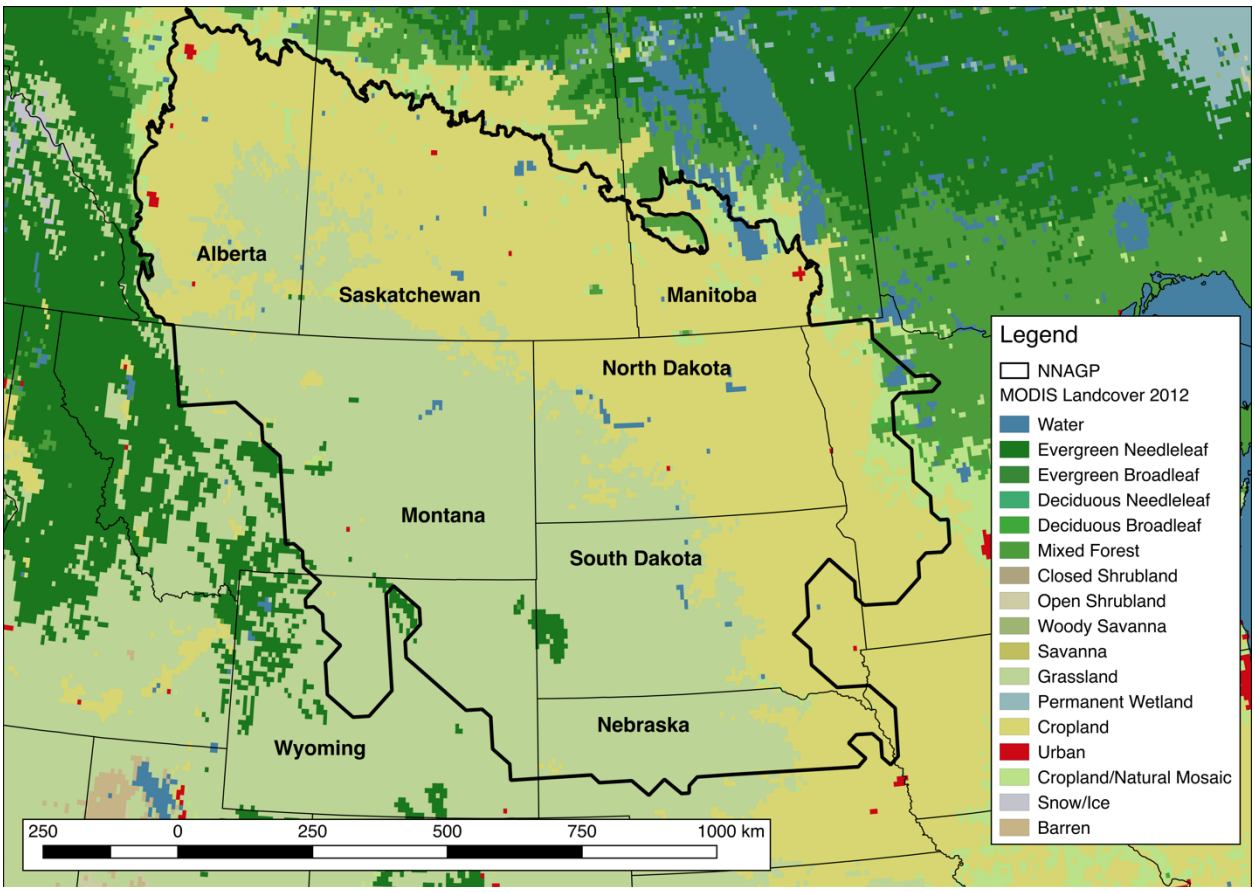


Figure 1: A map of the region considered to be the northern North American Great Plains (NNAGP) for the purposes of this study, which comprises the NEON Northern Plains Domain 9 in the United States and the Environment Canada Prairies Terrestrial Ecozone. Landcover as ascertained by MODIS are broken up into categories using the International Geosphere–Biosphere Programme (IGBP) classification system (Friedl et al. 2010).

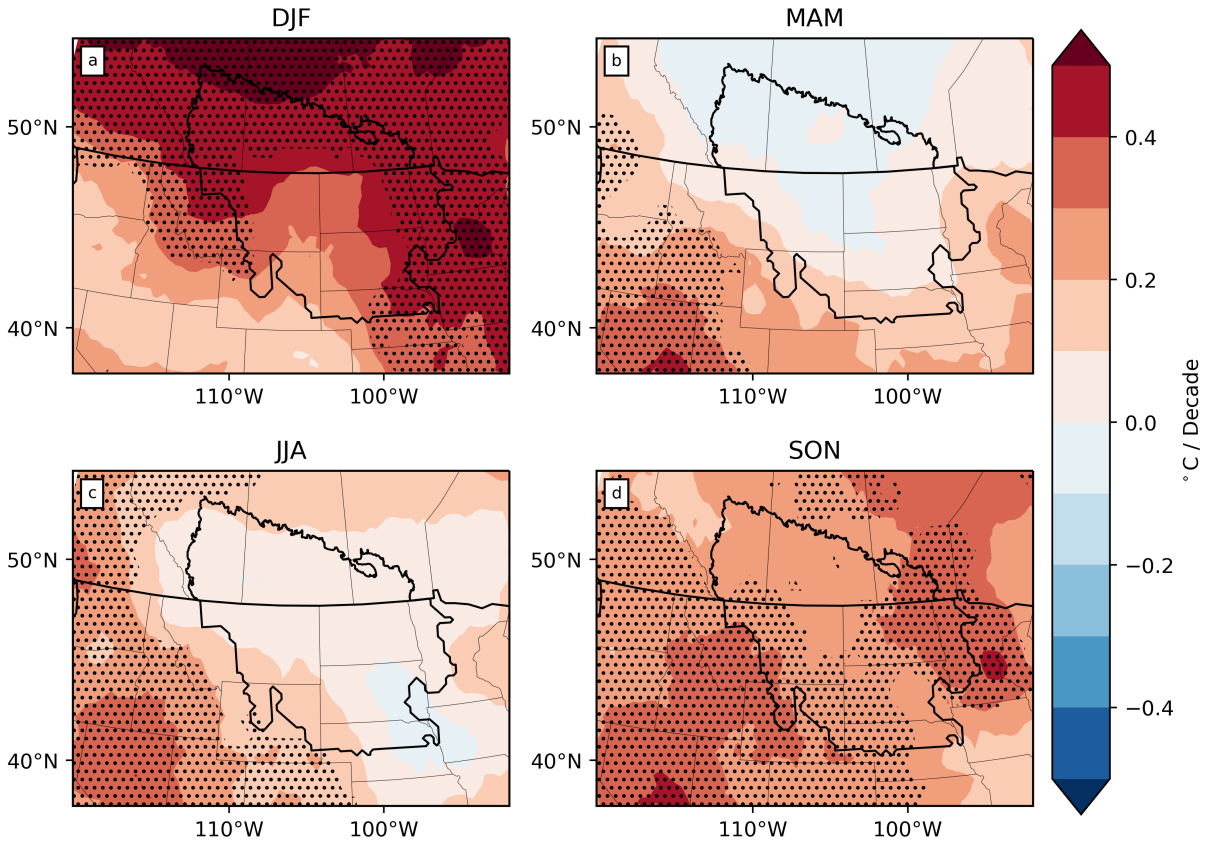


Figure 2: Trends in 2 m air temperature (T_{air}) from 1970 to 2015 across the northern North American Great Plains and surrounding regions. Stippling indicates a significant trend at $P < 0.05$ after correcting for autocorrelation (Eq. 1) against a null hypothesis of no trend.

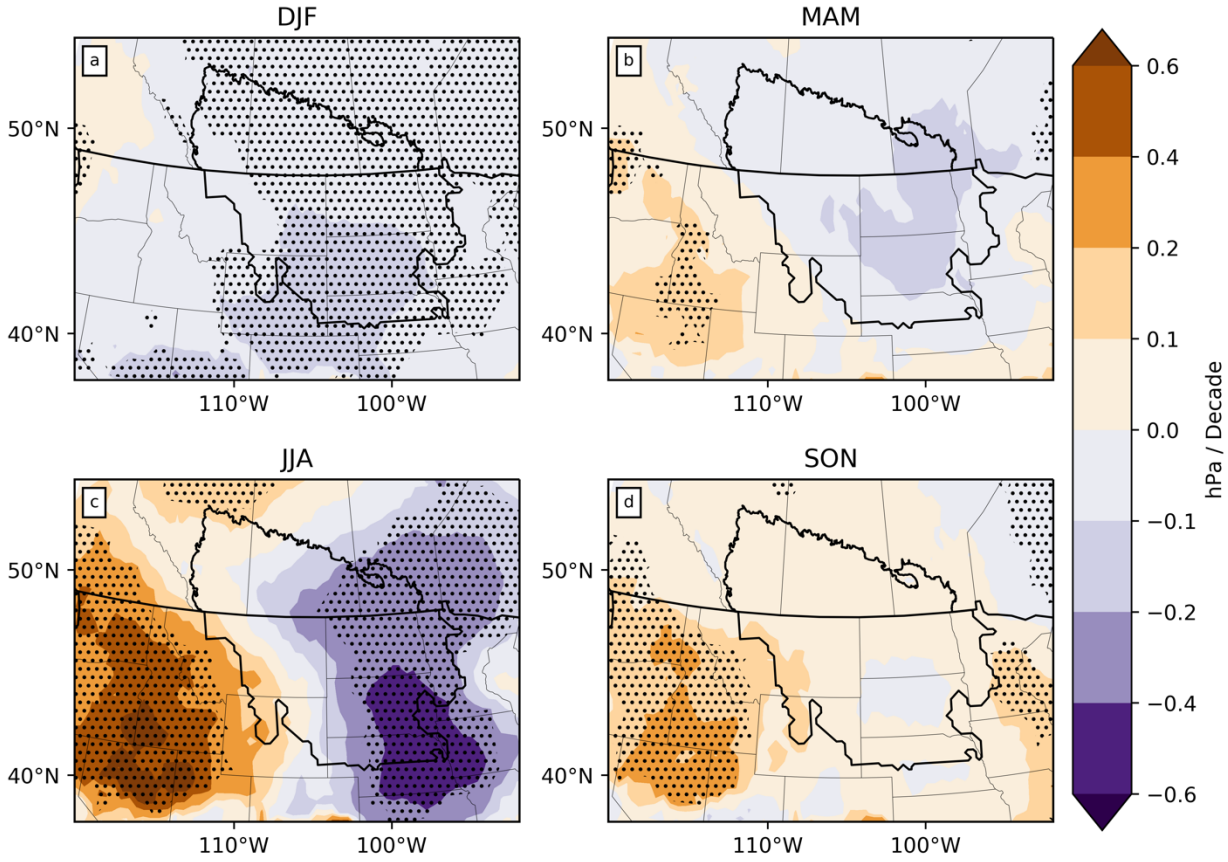


Figure 3: The same as Figure 2 but for vapor pressure deficit.

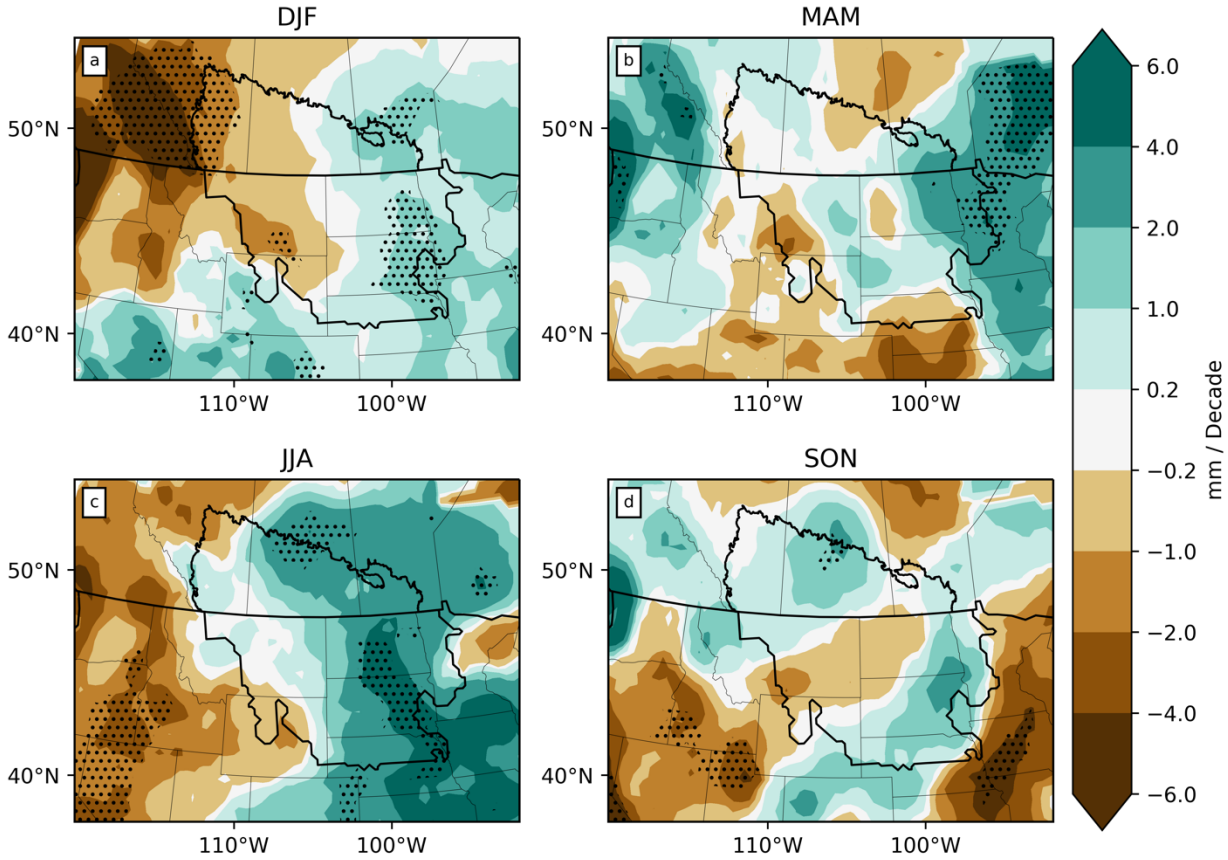


Figure 4: The same as Figure 2 but for precipitation.

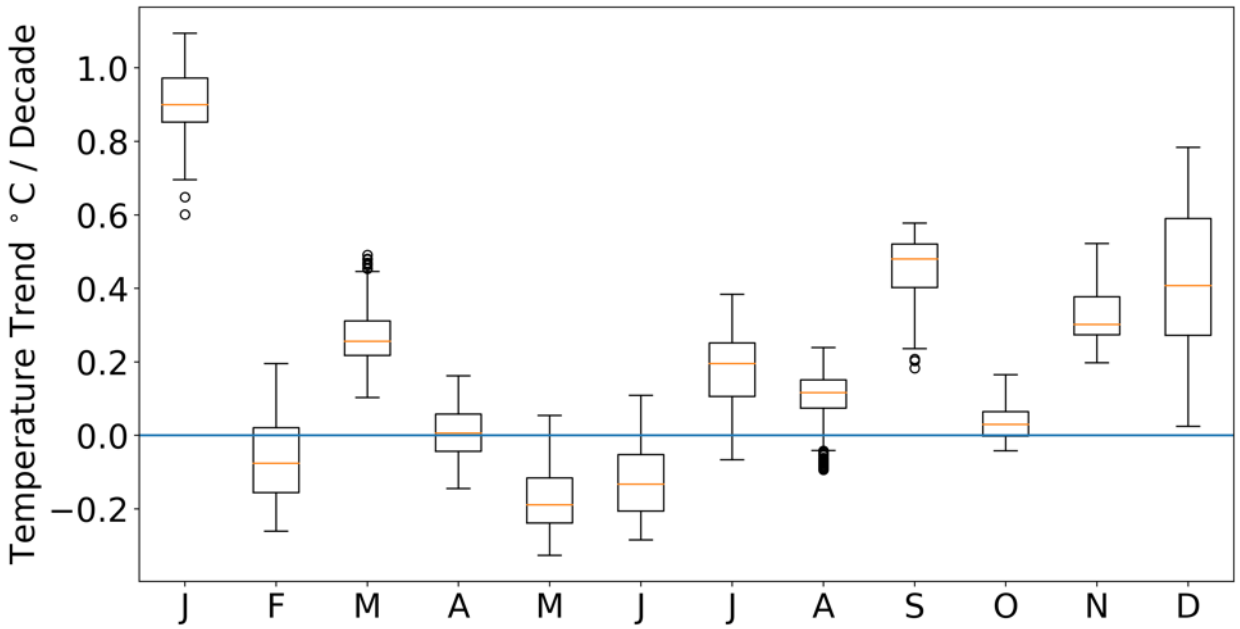


Figure 5: Monthly trends in near-surface (2 m) air temperature between 1970 and 2015 for the northern North American Great Plains (Fig. 1) from the CRU dataset. The orange lines indicate the median trend and the blue line indicates zero trend.

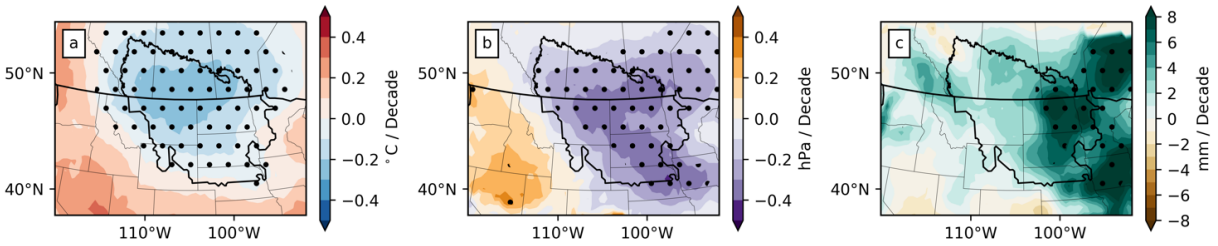


Figure 6: May and June trends in 2 m air temperature (a), vapor pressure deficit (b), and precipitation (c) from 1970-2015 in the Northern North American Great Plains (black outline, see Figure 1). (a) Stippling indicates significant ($p < 0.05$) cooling after correction for temporal autocorrelation (Eq. 1) *versus* mean global warming of 0.2 °C decade^{-1} during the commensurate period. (b,c) Stippling indicates significant trends compared to a null hypothesis of no trend.

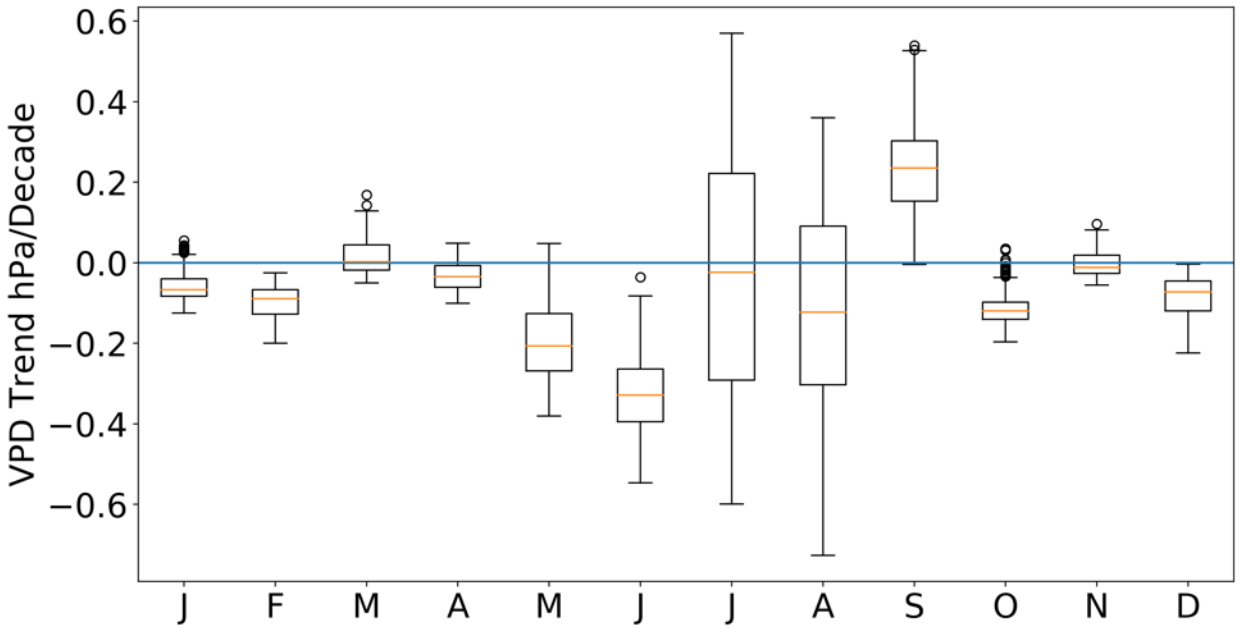


Figure 7: The same as Figure 5 but for vapor pressure deficit (VPD). The orange lines indicate the median trend and the blue line indicates zero trend.

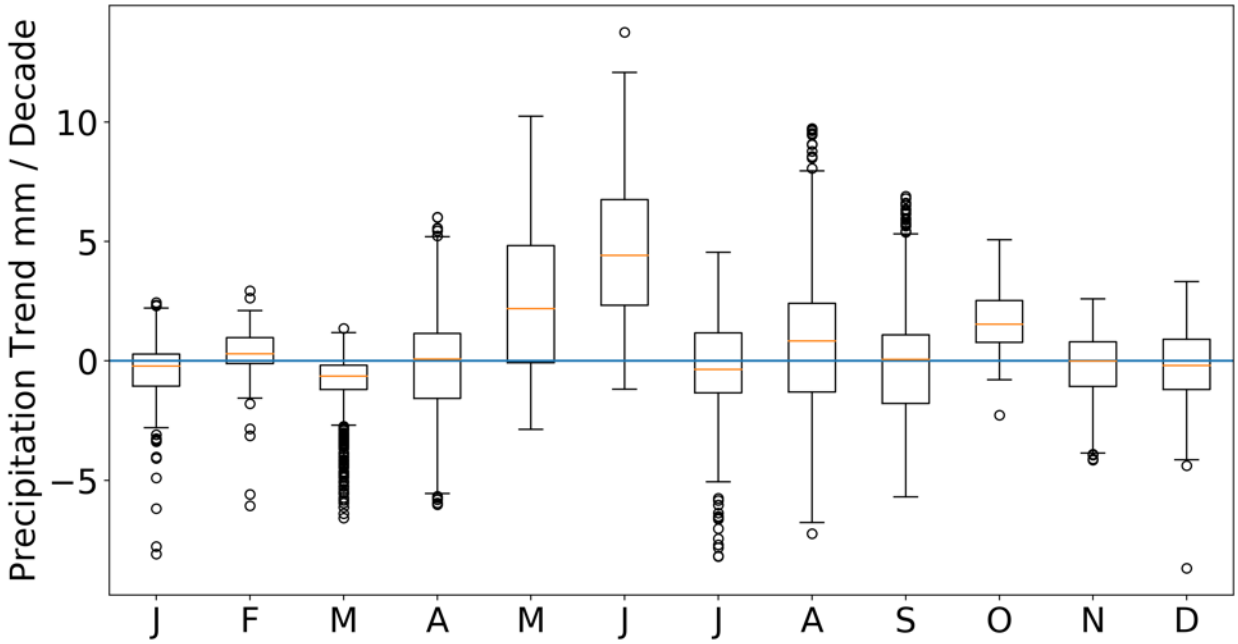


Figure 8: The same as Figure 5 but for precipitation. The orange lines indicate the median trend and the blue line indicates zero trend.

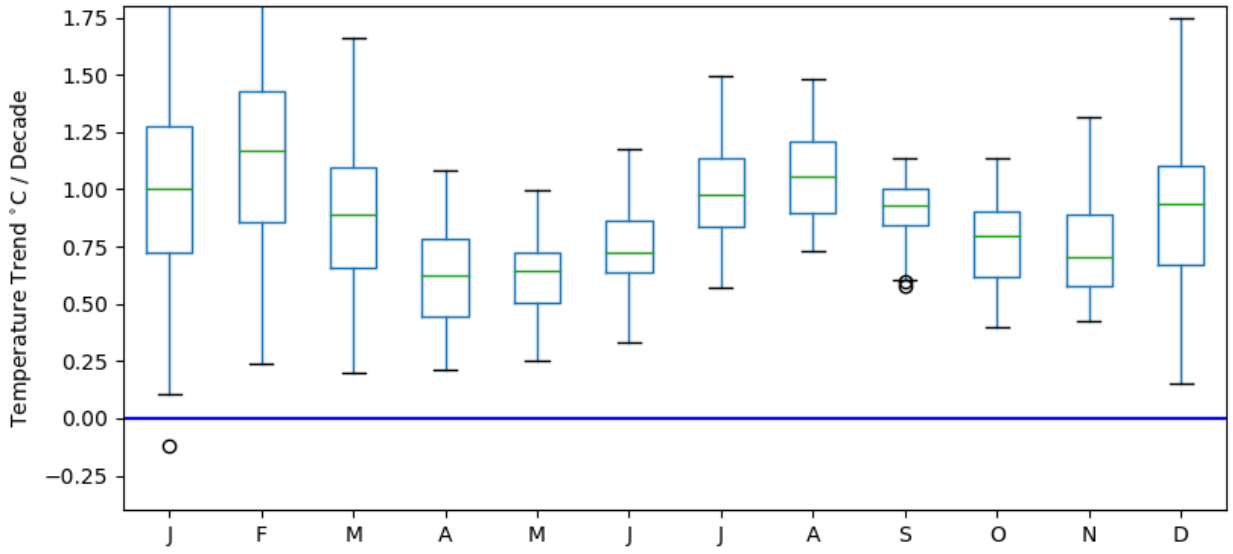


Figure 9. Trends in near surface air temperature from the CESM-LE ensemble. The boxplots show the median (green line) and variation in trends from the 39 ensemble members by month between 1970 and 2015. The trend estimates are based on averages over the grid cells that contain the NNAGP. The dark blue line indicates where a zero trend would fall.

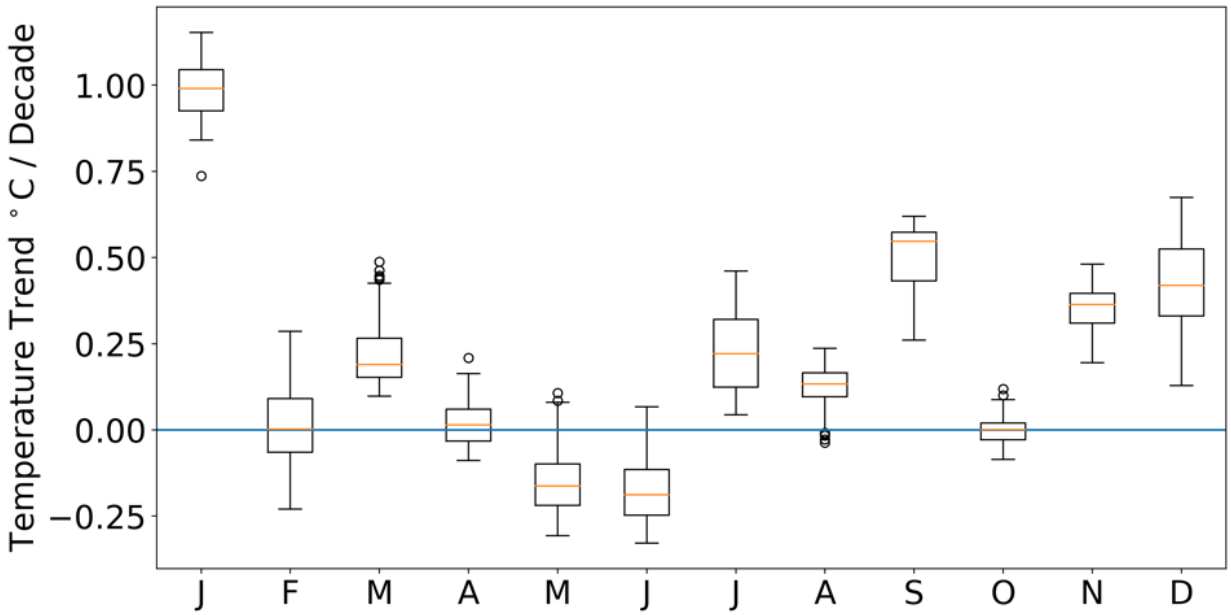


Figure A1: Trends in air temperature from 1970-2015 in the Northern North American Great Plains using Berkley Earth Surface Temperature data. The blue line indicates zero trend. The orange lines indicate the median of the distribution of trends.

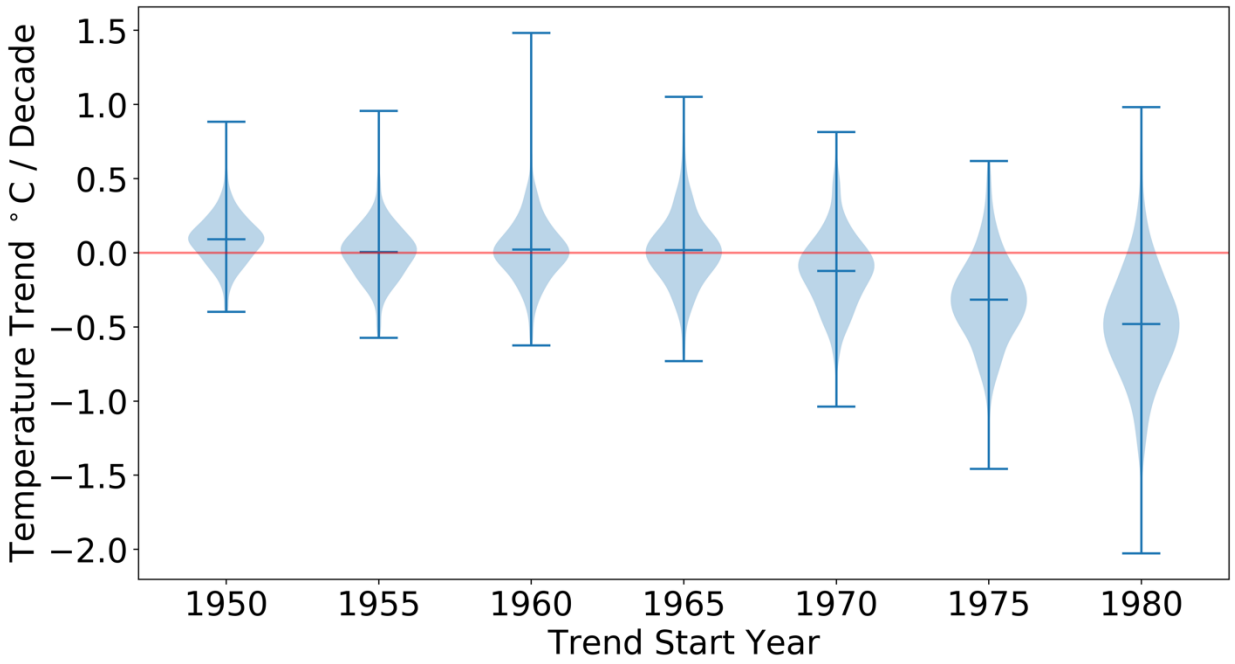


Figure A2: Near-surface (2 m) air temperature trends from 270 Global Historical Climatology Network (GHCN) sites within the NNAGP. Sites with at least 75% daily data availability from 1925-2015 were chosen for analysis. Maximum and minimum temperatures were averaged together to obtain average daily temperature. Daily data were aggregated to the May and June period and trends were calculated for each site with varying trend start years until 2015. The elongation of the violin plots is due to the shorter record from which trends were calculated, leading to more variability in trends. The distribution of the 270 trends are shown in the violin plot for each trend start year.

CHAPTER THREE

SIMULATING THE IMPACTS OF AGRICULTURAL LAND USE CHANGE ON THE CLIMATE OF THE NORTHERN NORTH AMERICAN GREAT PLAINS: VALIDATING A CONVECTION-PERMITTING CLIMATE MODEL

Contribution of Authors and Co-Authors

Manuscript in Chapter 3

Author: Gabriel T. Bromley
Contributions: Performed model simulations, analyzed model output, and wrote the first draft of the manuscript.

Co-Author: Paul C. Stoy
Contributions: Conceived study, obtained funding, discussed results and analysis, provided data, edited manuscript at all staged.

Co-Author: Andreas Prein
Contributions: Discussed results and analysis methods, edited the manuscript at all stages.

Co-Author: Shannon Albeke
Contributions: Created the fallow dataset for use within the modeling framework.

Manuscript Information

Gabriel T. Bromley, Andreas F. Prein, Shannon Albeke, more, Paul C. Stoy
Climate Dynamics

Status of Manuscript:
__X__ Prepared for submission to a peer-reviewed journal
____ Officially submitted to a peer-reviewed journal
____ Accepted by a peer-reviewed journal
____ Published in a peer-reviewed journal

Springer

CHAPTER THREE

SIMULATING THE IMPACTS OF AGRICULTURAL LAND USE CHANGE ON THE CLIMATE OF THE NORTHERN NORTH AMERICAN GREAT PLAINS PART I: VALIDATING A CONVECTION-PERMITTING CLIMATE MODEL

Abstract

Until now, there has not been an attempt to simulate the effects of summer fallow using a climate model. We utilized summer fallow data estimated from Landsat 5 for the years of 1984 and 2011 with Weather Research and Forecasting (WRF) model in a convection-permitting configuration. The vegetation fraction was adjusted to match the summer fallow for 1984 and 2011. The goal is to assess how well the WRF model performs with these different landcovers. The model had a ~3 ºC warm bias compared to Daymet in summer and a -3 ºC cold bias during winter. WRF well captures seasonal precipitation with only moderate biases during winter and spring. The vertical profile of temperature and dewpoint are within 1 ºC at upper levels but the surface warm bias is evident in the lower levels of the profiles. WRF captures the warm season sensible and latent heat flux compared to data obtained for the Lethbridge, CA eddy-covariance tower. The distribution of precipitation, including extremes, is well captured by WRF due to the use of convection-permitting grid spacing.

1. Introduction

The northern North American Great Plains (NNAGP) have experienced large shifts in land cover and land management over the past five decades (Stoy et al., 2018). These changes are coincident with cooling and moistening trends that rival global climate change in magnitude (Bromley et al. 2020; Betts et al. 2013c; Gameda et al. 2007). The NNAGP are a semi-arid region that encompasses the northern U.S. plains and the Canadian Prairies, and are primarily composed of rangeland, grassland, and cropland (Stoy et al. 2018). Many semi-arid ecosystems have been greening in the last few decades, and the NNAGP are greening at one of the fastest rates globally (Kolby Smith et al. 2016; Zhu et al. 2016; Huang et al. 2018). Nearly 19% of the land area in the

NNAGP exhibited greening, owing partially to increased productivity due to the CO_2 fertilization effect, but also due to shifts in land cover (Brookshire et al. 2020; Piao et al. 2020) and substantial shifts in agricultural land use, management, and intensification (Maaz et al. 2018; Rosenzweig and Schipanski 2019; Long et al. 2014a; Miller et al. 2002).

Prominent among these land use changes from the perspective of surface-atmosphere connections is a notable decreasing practice of summer fallow, i.e. keeping a field unsown during summer. Summer fallow has historically been very common in the agricultural areas of the NNAGP in rotation with wheat, but has steadily decreased by ~1.5% annually resulting in a reduction of nearly 250,000 km^2 since the mid 1970s (Gameda et al. 2007; Campbell et al. 2002; Betts et al. 2013c; Vick et al. 2016). Crop-fallow rotations are detrimental to soil health and have been replaced by continuous annual cropping of wheat and barley, cover cropping, and no-till agriculture (Aase and Pikul 1995; Long et al. 2014a) with uncertain impacts on regional atmospheric processes that may be pronounced given the expansive area that has shifted from an unvegetated to a vegetated state during the growing season.

Interactions between the land surface and the atmosphere have important feedbacks to the climate system, and agricultural areas can modify local and regional climate processes (Raddatz 2000b; Mueller et al. 2015b; Alter et al. 2017). Vegetation increases land surface albedo, latent heat flux, and the near surface humidity at the expense of sensible heat flux (H) while the opposite holds for fallow fields (Vick et al. 2016). The combination of these near-surface effects due to the steady decline of summer fallow are thought to contribute to an observed cooling and moistening trend over the NNAGP (Gameda et al. 2007; Betts et al. 2013c; Gerken et al. 2018c; Bromley et al. 2020). Consistent with these colling an moistening trend is an observed increase in cloud cover

and a lowering of the lifted condensation level (LCL) in the Canadian Prairies since 1992 (Betts et al. 2013c; Betts and Desjardins 2018). Higher near-surface humidity can also increase convective available potential energy and pre-condition the lower atmosphere such that convection becomes easier to trigger (Raddatz 1998b; Hanesiak et al. 2004; Brimelow et al. 2011; Shrestha et al. 2012; Gerken et al. 2018c). These changes increase the likelihood of the atmospheric boundary layer reaching the LCL: a necessary but insufficient step in forming convective precipitation (Juang et al. 2007a,c).

Convection-permitting models (CPMs) are emerging tools for studying the influence of the land surface on convective processes. CPMs use horizontal grid spacing that are small enough to explicitly resolve convective processes (several kilometers), and are also able to better capture the effects of land surface heterogeneity on precipitation (Prein et al. 2015; Vanden Broucke and Van Lipzig 2017). CPMs are able to reduce critical near-surface biases found in coarse resolution models by improving the representation of surface energy fluxes of heterogeneous landscapes (Vanden Broucke et al. 2015; Vanden Broucke and Van Lipzig 2017). Soil moisture is a heterogeneous land surface property that is impacted by land management and that can strongly modulate convective processes through soil-vegetation-boundary-layer interactions (Findell and Eltahir 2003c,d; Taylor et al. 2013; Klein and Taylor 2020). Hohenegger et al. (2009) found that by explicitly resolving convection, the precipitation response to soil moisture anomalies reversed signs compared to a coarse resolution simulation with a convective parameterization. CPMs have been used to study impacts of soil moisture on convection and land-surface coupling across global ecosystems due to their advantages in simulating deep convective and boundary-layer processes (Hohenegger et al. 2009; Zhang et al. 2020; Chen et al. 2019).

The semi-arid NNAGP exhibits seasonally strong land-atmosphere coupling (Koster 2004; Betts 2009; Betts and Desjardins 2018; Chen and Dirmeyer 2017). Convection-permitting simulations of convection in the Sahel (another semi-arid area) showed improvement over coarse resolution models that parameterize convection, better-capturing surface convergence processes, and convection initiation due to land surface heterogeneity (Birch et al. 2014; Maurer et al. 2017). There is evidence that dry soil moisture anomalies in the Sahel trigger and intensify convective storms by increasing wind shear, destabilizing the lower atmosphere through more boundary layer warming, and organizing moisture convergence through meridional temperature gradients (Taylor et al. 2006, 2012; Klein and Taylor 2020). Convection-permitting simulations in the NNAGP might improve our understanding of the land-atmosphere-precipitation interactions in semi-arid biomes and their responses to land cover change across the globe, but the role of land use change in the NNAGP and its impact on these interactions has not been studied to date.

Liu et al. (2017), hereafter L17, created the first convection-permitting simulations of North America under past and future climate conditions. Convective precipitation intensities and the diurnal cycle of convective precipitation were well captured, but the frequency of summer MCSs in the central U.S. were lower than observed (Prein et al. 2017a). The retrospective control simulation was run for the water years 2001-2013 but did not take land use or land cover change into account. Here we present a pair of convective-permitting simulations that follow the methods developed by L17 but with the goal of representing the climate under land use change scenarios observed in the NNAGP, namely different historical summer fallow amounts. These simulations are intended to act as control simulations for further work in understanding the role of summer

fallow reduction in the near surface energy balance, boundary layer interactions, and convective precipitation.

2. Model Parameters and Observational Data

a. Model setup and domain information

The Advanced Research Weather Research and Forecasting model version 4.1 (WRF) was used in a convection-permitting configuration with 4 km horizontal grid spacing. The study domain consists of 796 × 496 grid cells, 51 vertical levels up to 50 hPa, and covers the entirety of the northern North American Great Plains between 95°W and 115°W and from 40°N to 55°N (Bromley et al., 2020) (Figure S1). The domain was selected to have at least 40 grid cells between the domain boundary and the study area to avoid model spin-up issues. The European Center for Medium-Range Weather Forecasting's (ECMWF) ERA5 dataset was used as initial and lateral boundary conditions (Hersbach et al.). The high resolution of ERA5 (~31 km) allows us to directly downscale to 4 km grid spacing without an intermediate nest. The model parameterizations follow those used by L17, including the YSU boundary scheme (Hong et al. 2006), Thompson microphysics scheme(Thompson et al. 2008), and the RRTMG radiation scheme(Iacono et al. 2008). We did not use spectral nudging due to the limited size of the domain.

The Noah-MP land surface model was used with dynamic vegetation options turned off. Vegetation fraction was fixed at the annual maximum in order to facilitate the experiments that focus on the vegetative growing season. Leaf area index is provided by table values for each land use category. The TOPMODEL ground water scheme was utilized, which was found to reduce summertime biases (Niu et al. 2007; Barlage et al. 2015, 2021). The control simulations were

continuously run from October 2010 to October 2013 (current simulations) and from October 1982 – October 1985 (historical simulations). The analysis is focused on the warm season, and the first 3 months of the simulations are utilized for model spinup.

b. Creation of the fallow dataset

We obtained Landsat 5 imagery for 1984 and 2011 for the period between May 1 and August 31. Using visual cues, we digitized polygons for every LS Tile/Year and every landcover type (e.g. Crop, Fallow, Forest, Grass, Shrub, Water). Before fitting each model, each image was corrected for surface reflectance for each band. These polygons were then used to randomly sample each tile for each sample date within a year (1984 *versus* 2011). After fitting a Random Forest model for each tile and sample date within that tile, we used the model to predict cover classes to the entire image and for each date combination. This predicted raster was then saved to disk. Next, for each tile within a year, all of the predicted rasters were stacked (e.g. for 1984 and Tile 1, all six raster time series were stacked into one object) and the classifications through time were combined into a string (for example fallow, crop, crop, crop, crop, fallow). We then established rules that follow from the time series for each pixel. Once all of the tiles for a given year were classified into a single layer from the time series, we mosaicked them together into a single file. Finally, using the NLCD 2011 urban classification, we overwrote pixels classified as urban given that urban land cover classifications make up a trivial proportion of the NNAGP (Stoy et al., 2018). The vegetation fractions were adjusted to match published agricultural statistics (Vick et al. 2016) on a state and province basis with the approximate location estimated via Landsat.

The 30 m summer fallow dataset was interpolated to the 4 km model domain using a conservative remap approach. The Noah-MP land surface model uses a split-cell design where the vegetated fraction of the cell undergoes separate calculations from the non-vegetation fraction. We replaced the default vegetation fraction by setting vegetation fraction equal to 1 – fallow area in pixels for which fallow area was greater than 0 (Figure 1). The October 2010 – 2013 simulation uses the estimated fallow for 2011 and is called the control 2011 simulation (C11). The October 1982-1985 simulation uses the estimated fallow from 1984 and is called the control 1984 simulation (C84).

Multiple studies have documented the reduction in summer fallow in the NNAGP and its impact on atmospheric boundary layer processes (Raddatz 1998b; Campbell et al. 2002; Gameda et al. 2007; Betts et al. 2013c; Vick et al. 2016; Bromley et al. 2020). These estimates come from state and province -level agricultural census data. Summer fallow has been reduced since the mid-1970s and we assume that the results reported in the census are largely accurate, but the uncertainty lies in the exact timing and location of the changes. The agricultural statistics are conducted every 5 years in the U.S., but the spatial locations of fallow fields within those five years can change considerably. Summer fallow is a part of a wheat-fallow rotation, which makes it difficult to replicate the exact amount of land area under summer fallow for the intervening years between agricultural census surveys and makes specific attribution in any single year a challenge. Our approach to use fallow statistics to adjust Landsat-based estimates is designed to ensure that the total amount of reported fallow is represented in the simulations, but spatial uncertainties exist due to the intermittent overpass of Landsat (Figure 1). Additionally, the timing of planting and

harvesting varies with the weather of any given year which further obscures what is summer fallow and what is a field that hasn't been planted.

c. Observational Verification Data

We compare the temperature and precipitation from model simulations to several observational datasets to understand potential model biases. Daymet is a gridded observational dataset that uses a Gaussian filter to interpolate between station observations and accounts for elevation using a 30 arc-second digital elevation model (Thornton et al. 2016).. The horizontal grid spacing is 1 km and the dataset contains daily maximum (Tmax) and minimum (Tmin) air temperature, vapor pressure, and precipitation among other variables. The daily mean temperature was created by averaging daily Tmax and Tmin (Thornton et al. 1997). The CRU dataset is a 0.5 degree global dataset interpolating meteorological station data from multiple sources to a grid using angular distance weighting (Harris et al. 2020b). Monthly mean temperature, vapor pressure, and precipitation are used from the CRU dataset. The Gridded Meteorological Ensemble Tool described by Newman et al., 2015 a,b (hereafter GMET) interpolates North American station observations to a 0.125 degree grid (nominally 14 km grid). The dataset contains 100 ensemble members that are generated based on uncertainty in the interpolation routines as well as measurement uncertainty. We also used the Global Precipitation Climatology Centre monthly precipitation dataset (Rustemeier et al. 2020) for the validation of the precipitation output to create a more robust comparison. All datasets are individually upscaled to match the 0.5-degree monthly means of CRU and the GPCC dataset and remapped using a flux conservation algorithm for both temperature and precipitation using the Climate Data Operators software (Schulzweida 2019).

Vapor pressure deficit (VPD) is an important variable concerning vegetative growth and crop yields (Yuan et al. 2019; Rigden et al. 2020). Plant stomata will close if VPD is too high and there is evidence that VPD is decreasing in the NNAGP (Bromley et al. 2020; Ficklin and Novick 2017). Since VPD is calculated using the saturation vapor pressure, which is exponentially dependent on temperature via the Clauisus-Clapeyron relationship, VPD model biases are dominated by the temperature bias. Vapor pressure is calculated internally in WRF using mixing ratio and surface pressure, reducing the. We assess vapor pressure biases compared to Daymet and CRU as described in the Appendix.

To test the significance of model biases, we first conservatively remap the model simulation data to a 0.5-degree regular grid to match the coarsest observational datasets. Monthly-averaged two-meter temperature (T2) and precipitation (P) from the model are compared to Daymet, CRU, GPCC, and all 100 GMET ensemble members. The maximum and minimum values found across all observational datasets for each month and grid point are used as estimate for observational uncertainties. Model biases are significant if they exceed the range of observational uncertainties. This method is also used by L17 to test the significance of the 13-year convection permitting simulations of the continental United States.

To test whether WRF can reproduce extreme precipitation, the control simulations (C11 and C84) are compared to the station-based hourly precipitation dataset NCEI DSI 3240 (Hammer and Steurer 1997). An inverse distance weighting average of the nearest four grid cells are employed to create the model estimate at the station location. NCEI DSI 3240 only provides stations in the U.S. A kernel density estimate is used to create empirical density functions for the U.S. portion of the study area compared to the modeled probability density functions. Only

overlapping time periods are used for verification and station completeness needs to be at 90% for the comparison. We limit the analysis to the warm season (MJJA) as we are primarily interested in the climate impacts of agricultural management. The early warm season (AMJ) tends to be dominated by frontal rainfall and convection that is initiated by upper level forcing, whereas the late warm season (JAS) tends to be dry and the little rain that falls is predominantly from convection (Gerken et al. 2018c).

The vertical structure of the atmosphere is assessed using observed vertical profiles of temperature and dew point temperature from sounding locations within the NNAGP. Profiles are obtained for Glasgow, Montana, USA (GGW), Bismarck, North Dakota, USA (BIS), and Edmonton, Alberta, Canada, (WSE) from the Integrated Global Radiosonde Archive (Durre et al. 2006). The modeled vertical profiles are found via nearest neighbor search for the grid cell closest to the observational sounding location. The profiles from both the observational soundings and the model simulations are log-interpolated to common levels and only the 00UTC and the 12UTC model hours are used for the comparison. Each profile is differenced with the corresponding observational sounding profile and then the difference is averaged across pressure levels for a given month to create a composite profile.

Finally, surface energy flux data was obtained from a grassland eddy covariance site near Lethbridge, Canada, 'CA-Let', for the years 2011-2013 (Flanagan et al. 2002). Observed latent heat flux (LE) and H values were adjusted using the Twine et al. (2000) method, which adjusts these fluxes while keeping the observed Bowen ratio constant to achieve energy balance closure; the observed energy balance of most eddy covariance research sites is not closed (e.g. Stoy et al. 2013). The data were filtered by removing data with a friction velocity (u*) of less than 0.25 m/s

to ensure sufficient turbulence and removing datapoints where the energy balance ratio exceeded 1.5 to avoid anomalous measurements. Comparisons of the surface fluxes between WRF and CA-Leth for the entire simulation period were made using a maximum-likelihood robust linear estimator noting that robust regression is preferred to standard least squared approaches given the Laplacian (double-exponential) error distribution of eddy covariance measurements (Richardson et al. 2006). Since eddy-covariance data does not exist for the C84 simulation, comparisons are only made for the C11 simulations.

3. Results

Results of comparing seasonal temperature and precipitation differences between the simulations (C11 and C84) and the Daymet dataset are presented (we show the CRU dataset comparisons in the Appendix). Hourly precipitation, vertical profiles of temperature and dewpoint from soundings, and surface fluxes are compared for the warm season.

A. Seasonal Temperature

Figure 2 compares T2 between the C11 simulation and Daymet. C11 is 2.9 +/− 0.81 ℃ colder than Daymet within the study area during winter (Figure 2c). In the Rocky Mountains, immediately outside of the study area, the winter biases are stronger (< – 5℃) as also found by L17. A lake temperature model was not employed so a warm bias was found over Lake Winnipeg, but since this location is downstream of the study area, there were no negative effects on the simulations. While not explicitly in the study area, the Rocky Mountains are important for seasonal runoff and for influencing air masses that approach the study area from the West. C11 is about –0.69 ℃ cooler than observations in Spring (MAM) and capture the spatial pattern well (r=0.94) (Figure 2f). The

largest warm season biases are present during the summer (JJA), an issue also found by L17. Summer temperatures are generally 3 and 4 ℃ too warm across the majority of the study area with a few exceptions (Figure 2i). The largest bias when compared to Daymet is found in the lee of the Rocky Mountains on the western side of the study area and is in excess of 5 ℃ too warm but this might be due to the re-gridding process averaging temperatures across elevational gradients. Fall shows very little bias, with temperature differences between −1 and 1 ℃ (Figure 2l).

The C84 performs less well than the C11 simulations for the seasonal temperature averages with stronger biases in Winter, Spring and Fall (Figure 3). The overall spatial pattern of temperature is captured as evidenced by strong positive correlation coefficients for all seasons ($r > 0.88$). Winter has a strong cold bias despite a high correlation coefficient. The C84 bias on eastern side of the domain is about –3-4 ℃ colder than observations with the bias increasing to the southeast (Figure 3c). Saskatchewan performs the best during winter with only a –2 ℃ cold bias. Spring generally performs well with a modest –0.7 ℃ cold bias averaged across the domain (Figure 3f). The south-western parts of Alberta and Saskatchewan have insignificant bias, generally less than 2 ℃ warmer than Daymet. Summer temperatures are 2.7 ℃ warmer than Daymet and also exhibits the lowest spatial correlation ($r=0.88$)(Figure 3i). The mountains and the accompanying lee side warming are in excess of 5 ℃ too warm, as found with C11. Fall biases are less than -1 ℃ (Figure 3l). The southern half of the study area shows good agreement with observations during Fall.

b. Seasonal Precipitation

The C11 seasonal precipitation totals compare favorably with Daymet, especially during the warm season, with some biases that are important to note (Figure 4). Wintertime wet biases between C11

and Daymet are large on a percent basis but total seasonal accumulation differences are comparatively small (<20 mm) (Figure 4d). A moderate (34%) wet bias occurred during spring months, which amounts to ~30 mm. A minor (–11%) dry bias is apparent in Summer. Fall has the smallest bias of only –2%. The spatial correlation coefficients are ~0.6 in Winter, Spring and Fall and 0.81 in Summer.

The C84 simulation has a larger wet bias than the C11 simulation but follows similar seasonal patterns (Figure 5). Wintertime biases appear strong, but the total winter precipitation accumulation for the study areas is less than 20 mm (Figure 5c) like C11. Spring has a strong (>50%) wet bias over northeastern Montana and South Dakota and parts of Nebraska (Figure 5h). The Canadian Prairies exhibit better representation with only a slight wet springtime bias in Alberta. Summer shows a slight (– 4.6%) dry bias (Figure 5l). Fall is well captured with a low overall bias (~16%) with a few areas of a wet bias on the Montana-North Dakota border as well as central South Dakota (Figure 5p). Correlation coefficients for all seasons match the pattern seen in the C11 simulation with Summer having the highest coefficient (0.79) and the others lower (~0.6).

c. Seasonal Vapor Pressure

The C11 simulation performs well in Fall and Winter with biases generally less than 0.1 kPa, while there are stronger biases present in Spring and Summer (Figure 6). Spring is notably more humid by over 0.3 kPa for most of the study area and beyond (Figure 6f). When compared to the CRU vapor pressure data product, the C11 simulation is unbiased during spring (Figure SCRUVP) indicating variability in the observational datasets. C11 has a dry bias compared to Daymet, especially in the plains east of the Rocky Mountain. A north-south moisture bias gradient is evident

in the Canadian Prairies but is generally less than 0.1 kPa (Figure 6i). The CRU dataset agrees with Daymet in that the summer is dry-biased but puts the region of greatest bias over the eastern side of the study area instead (Figure SCRUVP).

The C84 simulation is in good agreement with Daymet for Fall and Winter, but Spring and Summer show a humid and dry bias respectively (Figure 7). Spring shows a humid bias in excess of 0.3 kPa similar to the vapor pressure results from C11 but the region of strongest bias is situated over northeastern Montana (Figure 7f). C84 shows a bias of less than 0.1 kPa during Spring compared to CRU (Figure SCRUVP1980), as was also found for C11. Summer is simulated well when compared to Daymet (Figure 7j). CRU finds WRF to be dry biased in summer by about 0.2 kPa but less than in the C11 simulation (Figure SCRUVP1980).

d. Precipitation intensities

C11 generally captures the distribution of precipitation intensities but under predicts moderate intensity precipitation (Figure 8). The relatively short simulation period does not allow for an extensive record of extreme precipitation, but the C11 confidence interval does overlap the confidence interval of hourly precipitation station observations. The C84 performance is similar to the C11 simulation but overpredicts intensities around ~30mm hr^{-1}(Figure 9). Low intensities are similarly overpredicted while moderate intensities are under-predicted.

e. Soundings

Figure 10 shows the C11 composite dewpoint profile differences for AMJ and JAS compared to sounding observations. There is considerable variation with almost a 20 ℃ spread in the 95% confidence interval. AMJ has a wet bias at each sounding location through most of the atmosphere, with a more pronounced moist bias in the upper levels of the troposphere. JAS has a 3-5 ℃ dry

bias at the surface but then more closely follows the profile for AMJ higher than 700 hPa. Differences in the vertical profile of temperature for the C11 simulation follow the bias pattern seen in the 2 m temperature figures (Figure 11). AMJ shows minimal bias through most of the troposphere with the exception of WSE which shows a 1 ℃ cool bias from near the surface up to 850 hPa (Figure 11c).

The C84 simulation shows little bias in the dewpoint profiles for AMJ but a dry bias in the lower parts of the atmosphere for JAS (Figure 12). (Both GGW and BIS profiles did not report above about 300 hPa in the 1980's (Figure 12 a,b); the WSE profile does go past 300 hPa but the data quality is lower.) The C84 temperature profiles show a warm bias for both AMJ (0.5 - 1 ℃) and JAS (2 ℃) at the GGW and BIS locations (Figure 13 a,b). The warm bias is present from the surface to 600 hPa with the strength of the bias decreasing with height. WSE shows a –0.5℃ cool bias near the surface for AMJ and a 1℃ bias for JAS (Figure 13c). All locations show a –1℃ cool bias above 300 hPa, which is likely near the tropopause on average.

e. Surface fluxes

Surface fluxes influence boundary-layer temperature and the development and formation of convective precipitation (Santanello et al. 2017). C11 LE and H are compared to the CA-Leth eddy covariance site for overlapping years in Figure 14. H is generally under-estimated averaged over the simulation period while the 2011 warm season shows that the C11 simulation underestimates H from April to June by –26 W m^{-2} but comes into much better agreement from June to August with a mean difference of 11 W m^{-2}. When comparing fluxes across the entire simulation period, a robust linear regression of the model simulated H compared to the observed eddy covariance H results in a slope 0.81, indicating the model underestimates H compared to observations. Latent

heat flux is generally better-represented by the model but follows an opposite pattern compared to H. C11 overestimates April to July LE by ~40 W m^{-2} WRF while the July to September LE is underestimated by –40 W m^{-2}. When comparing the model estimated LE and the observed LE over the entire simulation period using a robust linear regression, the slope is 0.87 indicating that the model better represents LE but still underestimates overall. Overall, for both H and LE, WRF can reproduce weekly and seasonal changes in surface energy fluctuations reasonably well.

4. Discussion

a. Comparison with other Convection-Permitting Simulations

The C11 and C84 simulations have predictable biases that are comparable to other convection-permitting simulations but generally well represent temperature and precipitation during the simulated time periods within the northern North American Great Plains (Liu et al. 2017; Wang et al. 2018). Here we compare the results to those of other convection permitting simulations over the same area noting that the source of differences between the simulations cannot be fully ascertained since the model version, parameters, land surface datasets, and domain size all differ.

The pattern of biases evident in the C11 simulation follows those found by L17, namely that Winter and Summer biases are larger than Spring and Fall. The C11 simulation generally has better representations of the shoulder seasons in that minimum (slightly cool) biases are found compared to L17. The L17 simulation uses spectral nudging above the boundary layer for large wavelengths (> 2000 km) which limits the model drift from long simulations but allows for variability at smaller spatial scales (Liu et al. 2012; Spero et al. 2014). L17 found that spectral

nudging of geopotential, wind, and temperature reduced the summertime temperature bias most. Spectral nudging also would limit the bias in upper levels of the atmosphere, meaning that atmospheric soundings would likely converge to the driving data, whereas the C11 and C84 simulations both show ± 2℃ spread at upper levels in both temperature and dewpoint (Figures 10,12). Both simulations use a groundwater scheme within the land surface model that has been shown to reduce summertime warm biases by 2-3ºC (Barlage et al. 2021). In summary the model biases presented here are on similar order of magnitudes of biases seen in L17 and are reasonable enough to allow further analysis looking into the impact of changing land use conditions on the regional climate.

b. Summer Warm Bias

Regional and global climate models have a well-known warm bias in the Great Plains of the United States. This is likely due to multiple factors including near-surface energy balance issues, the under-representation of groundwater and irrigation (Lin et al. 2017; Cheruy et al. 2014; Qian et al. 2020). Nine regional and global climate models across a variety of spatial resolutions, including WRF at Δx = 36 km, were compared to understand the source of the Great Plains warm bias common to all of the models (Ma et al. 2018). All models over-predicted the incoming shortwave radiation and the warm bias was tied to biases in evaporative fraction. Land cover representation is another potential source of bias in regional climate models. WRF was found to not be particularly sensitive to the different default landcovers at a coarse resolution (Δx = 36 km) but the sensitivity might increase at fine spatial scales (Mallard et al., 2018). Taking land use and land cover change into account during WRF simulations at 12km grid spacing found differences in

temperature on the order of 1 ℃ and reduced the model bias compared to observations Huang et al., (2020). At convective permitting resolutions, WRF was more sensitive to increasing the spatial resolution of topography and soil moisture than to increasing the resolution of the land cover representation (i.e. more heterogeneous land cover) (Knist et al., 2020), but the NNAGP represents a relatively extreme case of recent land cover change.

Convection permitting models more realistically capture precipitation and especially MCSs which make up a dominant portion of summertime rainfall (Prein et al. 2017a). In integral part of capturing these precipitation processes is the use of a ground water scheme, which reduces precipitation biases by half and reduces summertime temperature biases by 2-3ºC (Barlage et al. 2021).

The summer warm bias seems confined to July, August, September; April, May, and June are less biased compared to Daymet. The comparison to eddy-covariance data in Figure 14 shows that H is underestimated overall (slope = 0.81), with slight under estimations for April, May, June, while H is better simulated for July, August, September. Latent heat flux appears to have a seasonal bias compared to the observations (slope =0.88), showing a systematic over-estimation early in the warm season and a systematic under-estimation in the late part of the warm season. In the C11 simulation the relatively unbiased H in the late warm season plus the negative bias in LE might contribute to too much surface warming. This relationship might be exacerbated where summer fallow is misrepresented since the surface energy balance within Noah-MP is averaged between the bare and vegetated fractions of the grid cell.

d. Representation of Convective Precipitation

In both the C11 simulation and the C84 simulation, the spring precipitation is well capture in C11(within observational uncertainties) but C84 has a 34% wet bias. Summer precipitation is well captured in both C11 and C84 with a 7% and 12% dry bias respectively (Figures 4,5). Spring in the NNAGP sees many passing upper air disturbances which bring frontal rainfall, while summer rain is more convectively driven. The JAS profiles of C11 and C84 show warmer and drier conditions than observations (Figures 10-13). This warmer and drier surface may suppress some amount of the convection by drying out the boundary layer and possibly leading to reduced rainfall rates in the convection that does form. Summer rainfall rates are generally under-predicted at moderate intensities (5-15 mm hr^{-1}) (Figures 8,9) but do fall within the 95% confidence interval of the observations, which was also found by Prein et al., 2017.

c. The Impact of Fallow Representation

The surface energy calculations that are conducted by Noah-MP would likely increase the near-surface bias where the location and timing of summer fallow was mis-represented, while it might reduce the bias in areas where it was well captured. Surface energy fluxes play a large part on the near surface climate. Surface fluxes within WRF are calculated using the Noah-MP land surface model which uses split-cell calculations, differentiating between the vegetated portion of the grid cell and the bare ground portion of the grid cell. The approach presented here adjusts this fraction of vegetation and bare ground to try and match the summer fallow amounts for the corresponding time periods. Where there is agreement, the model bias would be systematic, i.e. bias due to the modeling system alone, where there is not good agreement, the bias would be higher.

5. Summary and Conclusion

Here we present a pair of three-year historical convection-permitting simulations that simulate mean climate under two different vegetation fractions that have been created to estimate historical summer fallow amounts. The simulations were compared to a collection of observational datasets and assessed for bias in near surface temperature, near-surface vapor pressure, and precipitation. Surface fluxes for the simulation focused on the early 2010s were compared to eddy-covariance data from the CA-Leth grassland eddy covariance site for the overlapping time period. Vertical profiles of temperature and dewpoint were compared to sounding profiles from several locations within the study area. The findings are summarized as:

- WRF captures the precipitation well in all seasons for the C11 simulation and performs well in Summer and Fall for the C84 simulation. In the C84 simulation, Winter and Spring contain positive precipitation biases.
- WRF represents near-surface temperature well in spring and fall but has a ~–3ºC cold bias in winter and a ~3ºC warm bias in late summer, similar to other WRF modeling efforts over this region.
- Compared to vertical profiles of temperature and dewpoint from soundings, WRF has ± 1.5°C bias in temperature throughout most of the troposphere and a ± 2.5°C bias in dewpoint temperature.
- WRF underestimates H in the early warm season (April – June) but better captures H in the late warm season (July-September) compared to eddy-covariance measurements from a grassland site in southern Alberta. LE is out of phase with observations, resulting in an

overestimation of LE in the early warm season (April – July) and an underestimation of LE in the late warm season (July- September).

The simulations provide a rough estimate of mean climate after accounting for changes to summer fallow. The fallow estimates are too aggressive in several areas such as in Minnesota, Manitoba and Nebraska, but match expected patterns for other areas. These simulations will act as controls for further ongoing simulations that will estimate the exact contributions of summer fallow to near-surface climate, boundary layer processes, and convection. These simulations will be run for the same time periods as presented here, but the vegetation fractions will be swapped such that C11 climate will be matched with the C84 land surface. This will control for the previously described biases. Future work will focus on reducing the uncertainty in summer fallow representation and reducing model bias in the northern North American Great Plains.

Supplementary Information

Simulation Name	***C11***	***F11***	***C84***	***MF84***
Time Period	**10/2010 - 10/2013**	**10/2010 - 10/2013**	**10/1982 - 10/1985**	**10/1982 - 10/1985**
Fallow Year	**2011**	**1984**	**1984**	**2011**
Land Surface Model	**Noah-MP**	**Noah-MP**	**Noah-MP**	**Noah-MP**
Radiation Scheme	**RRTM**	**RRTM**	**RRTM**	**RRTM**
Boundary Layer	**YSU**	**YSU**	**YSU**	**YSU**
Microphysics	**Thompson**	**Thompson**	**Thompson**	**Thompson**

Table S1: Names and parameters for each simulation. The only differences between the simulations are the time periods and the fallow estimate. Only the control simulations are discussed in this chapter.

Figures

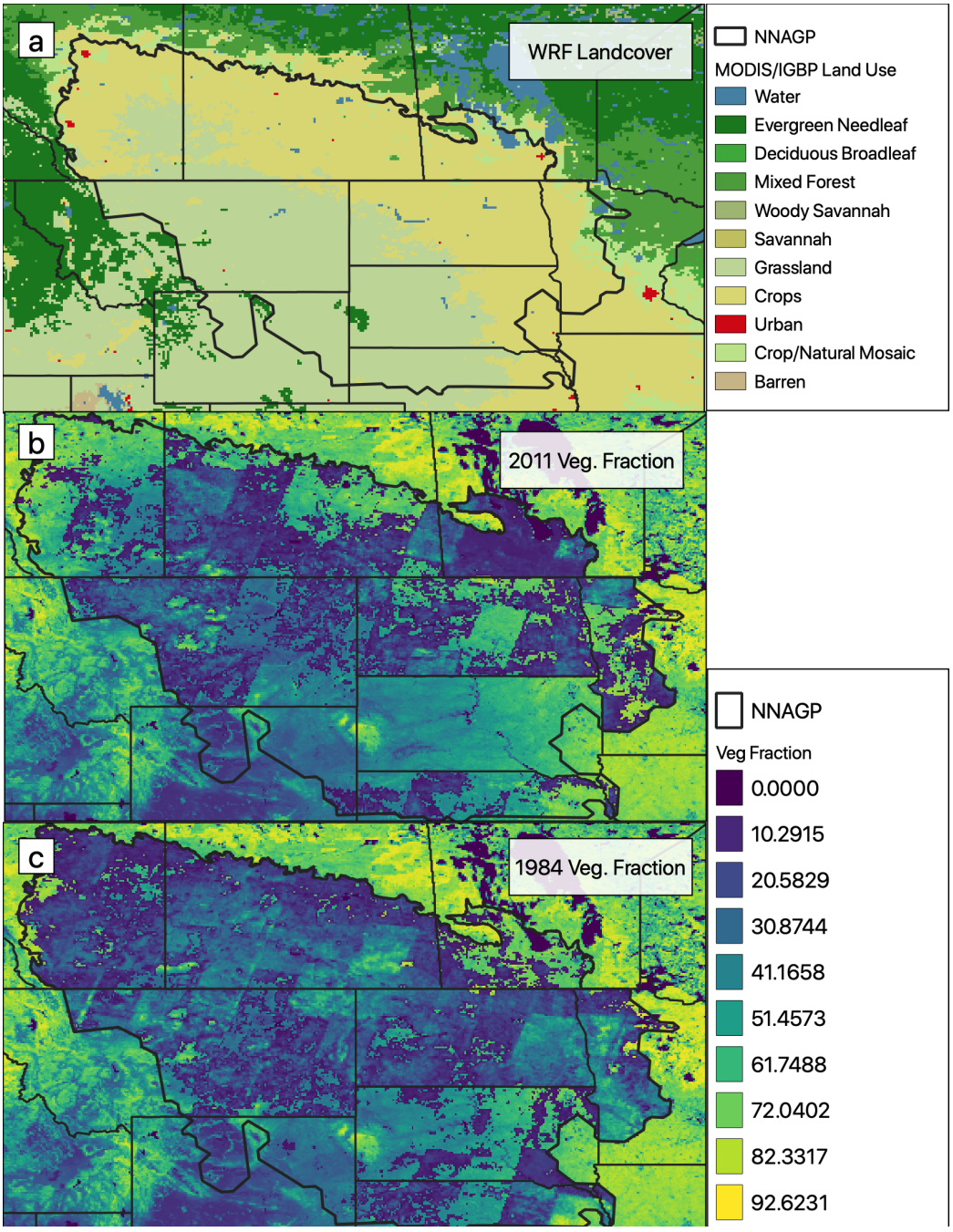


***Figure 1**: (**a**) WRF landcover for the northern North American Great Plains following Bromley et al. (2020), outlined in black. (**b**) Vegetation fraction used with the C11 simulation. (**c**) Vegetation fraction used with the C84 simulation.*

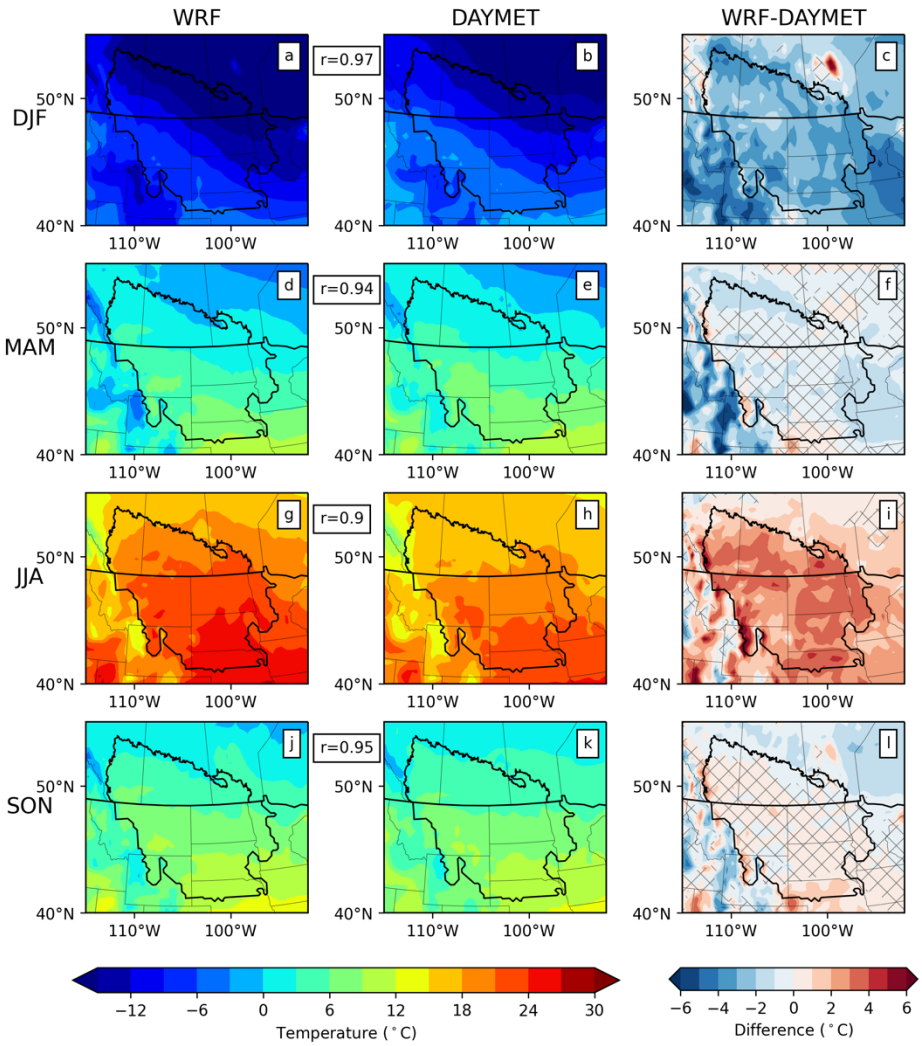


***Figure 2**: **(a)** Mean temperature for DJF 2010-2013 for the C11 WRF simulation, observed by Daymet **(b)** and the difference between simulated and observed temperature **(c)**. **(d-f)** Same as **(a-c)** but for MAM. **(g-i)** same as **(a-c)** but for JJA. **(j-k)** same as **(a-c)** but for SON. Pearson's r correlation coefficients shown between columns 1 and 2. Non-significant bias is marked by a cross hatch pattern. WRF and Daymet were conservatively remapped to 0.5-degree regular grid.*

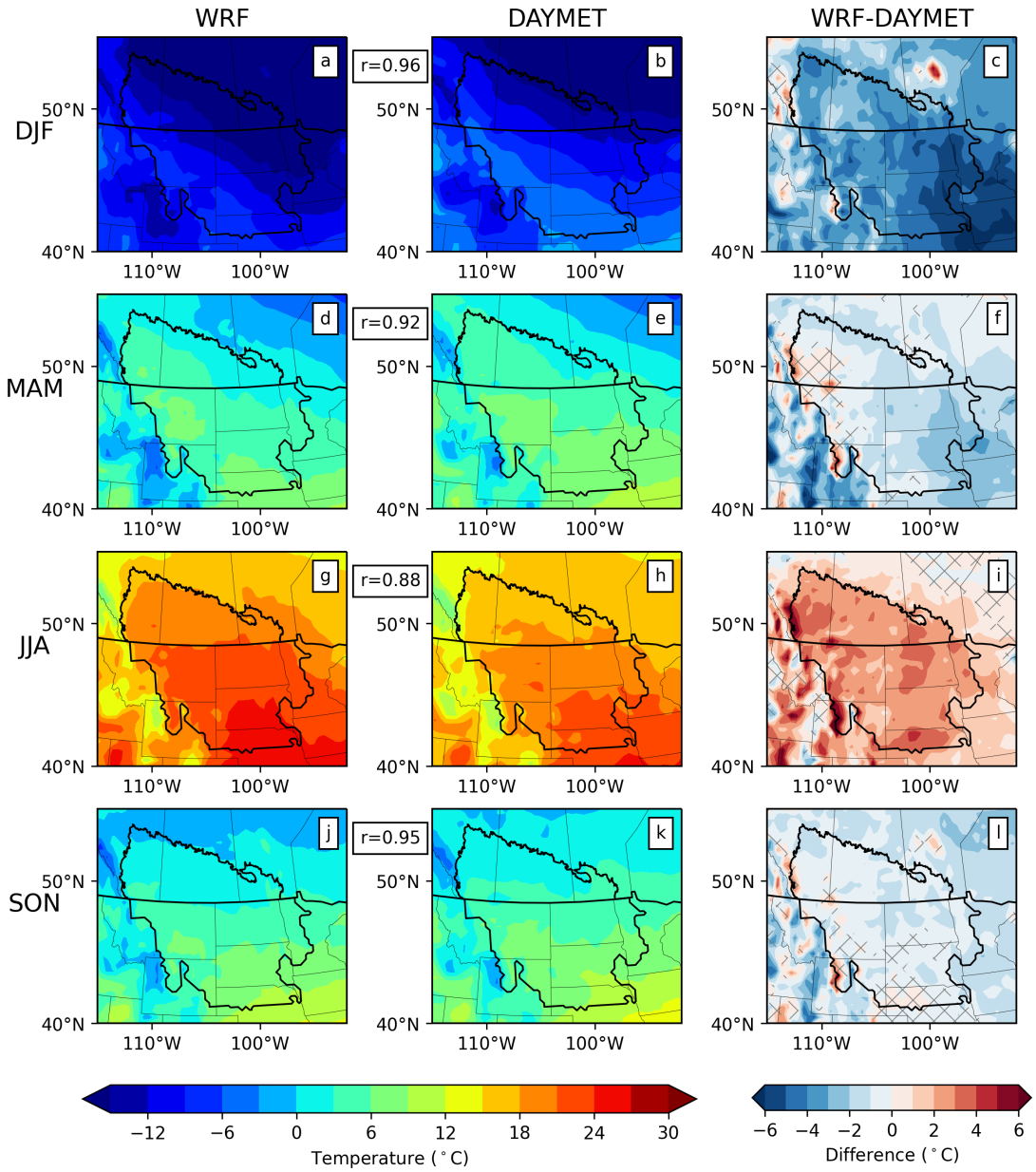


***Figure 3**: Same as in **Figure 2** but for the C84 simulation.*

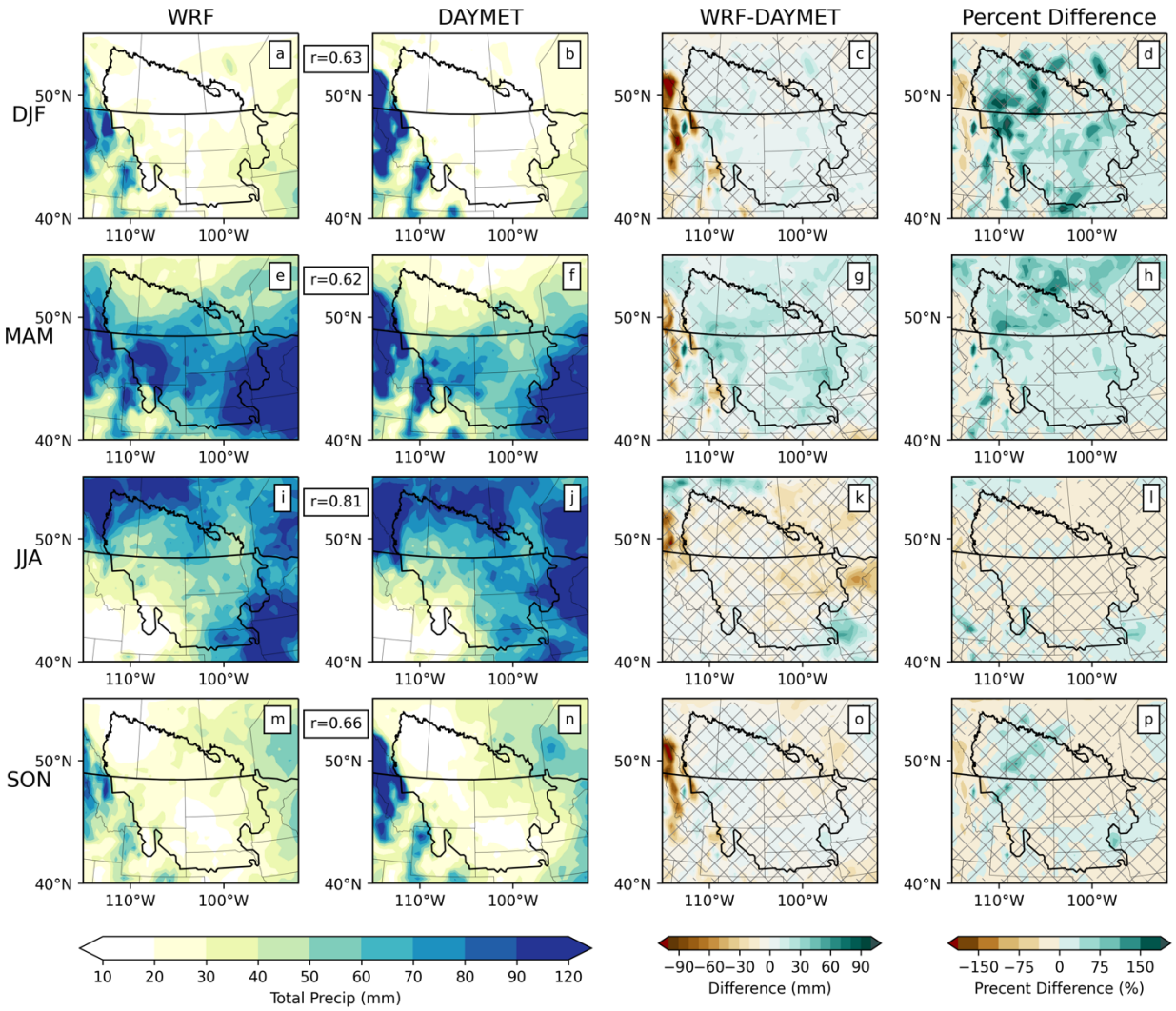


***Figure 4**: **(a)** C11 WRF simulated accumulated precipitation for DJF averaged over 2010-2013. **(b)** Daymet estimated accumulated precipitation for DJF averaged over 2010-2013. **(c)** Absolute differences between WRF and Daymet. **(d)** Percent difference between WRF and Daymet. Pearson's r correlation coefficient shown between **(a)** and **(b)**. **(e-f)** Same as **(a-d)** but for MAM. **(i-l)** Same as **(a-d)** but for JJA. **(m-p)** Same as **(a-d)** but for SON. Non-significant bias is marked by a cross hatch pattern. Both WRF and Daymet were conservatively remapped to a 0.5-degree regular grid.*

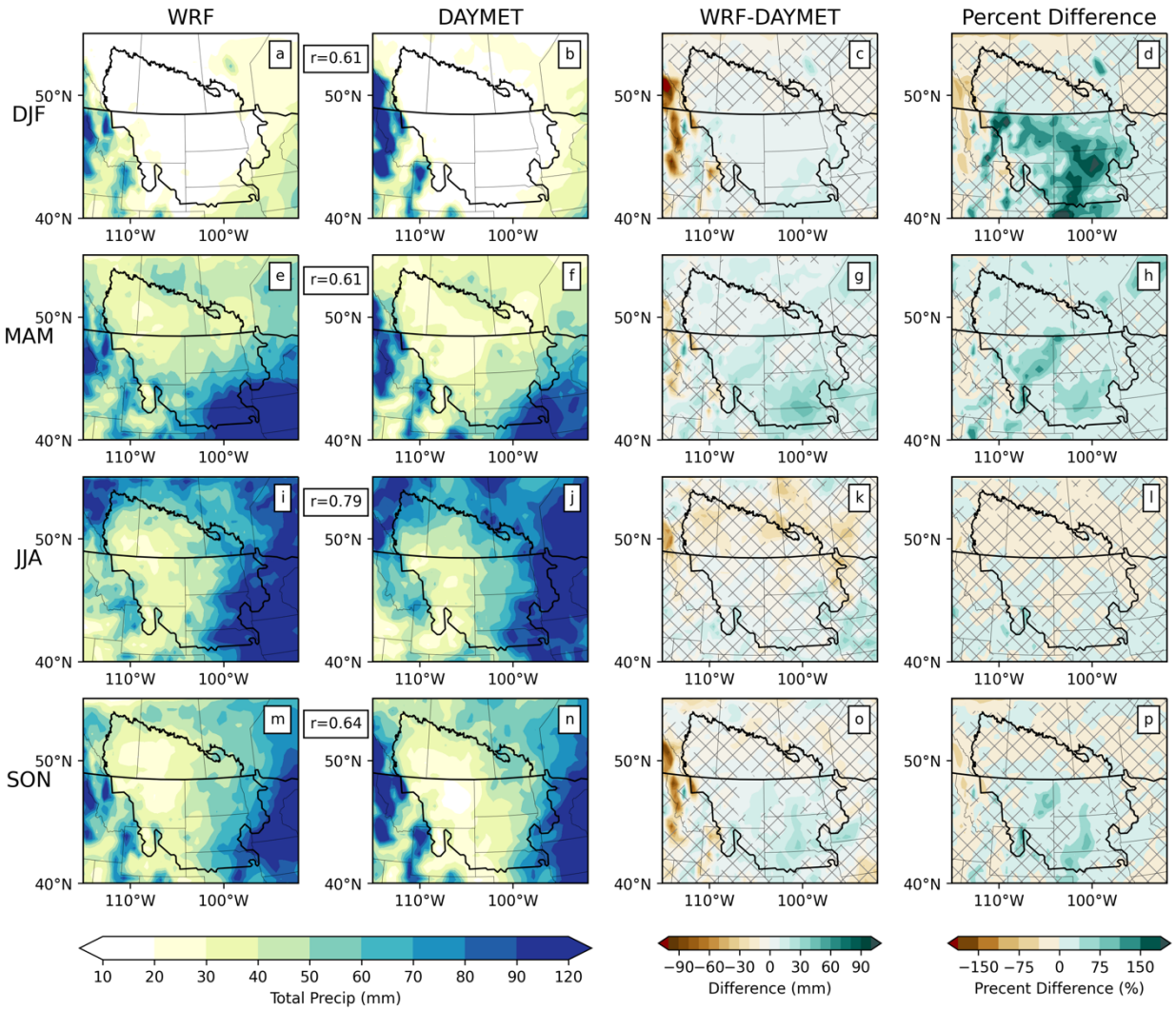


***Figure 5**: Same as **Figure 4** but for the C84 simulation.*

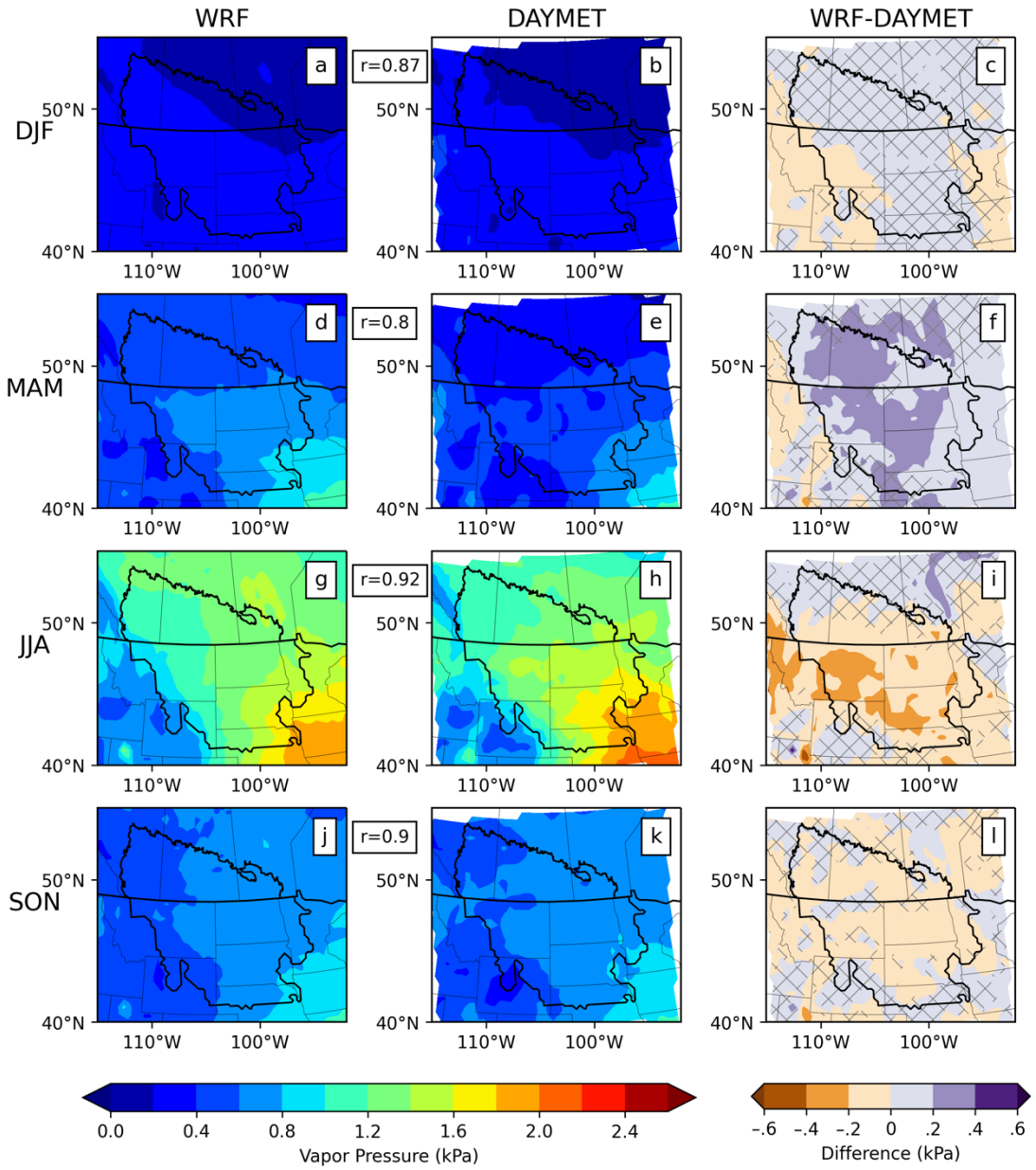


***Figure 6**: Mean vapor pressure for DJF 2010-2013 for the C11 WRF simulation **(a)** observed by Daymet **(b)** and the difference between simulated and observed vapor pressure **(c)**. **(d-f)** Same as **(a-c)** but for MAM. **(g-i)** same as **(a-c)** but for JJA. **(j-k)** same as **(a-c)** but for SON. Pearson's r correlation coefficients shown between columns 1 and 2. Areas where the difference between WRF and Daymet is less than the differences between CRU and Daymet are marked by a cross hatch pattern. Pearson's r correlation coefficient shown between columns 1 and 1. WRF and Daymet were conservatively remapped to 0.5-degree regular grid.*

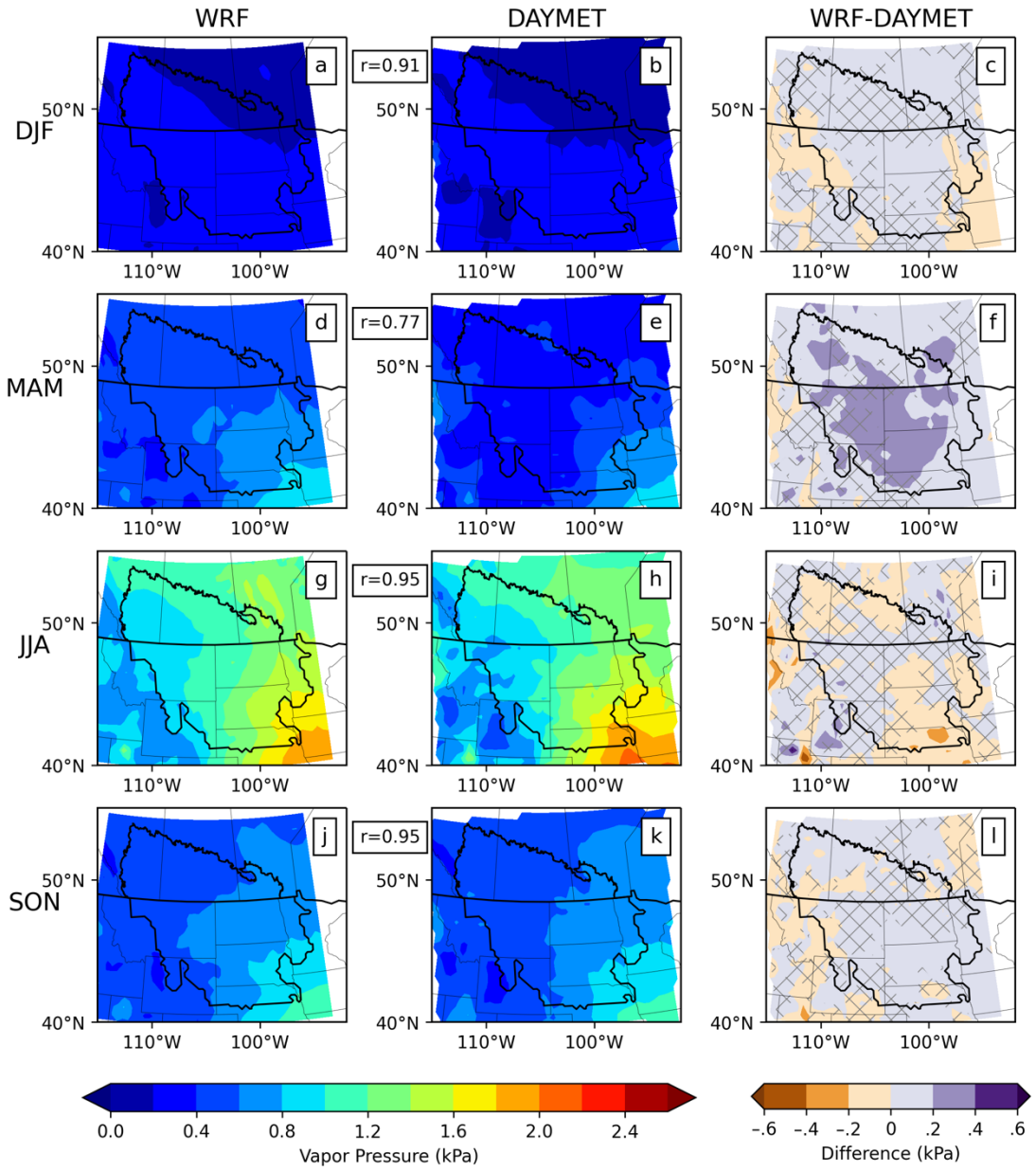


***Figure 7**: Same as **Figure 6** but for the C84 simulation.*

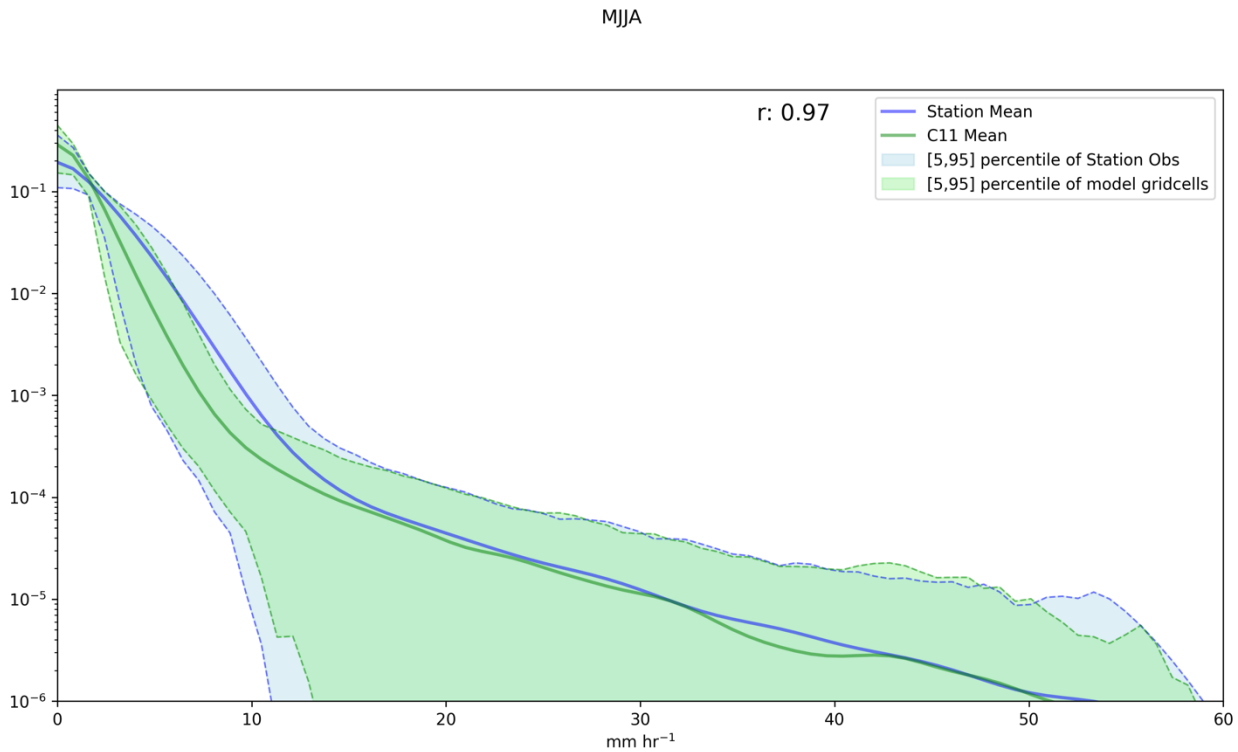


***Figure 8**: Probability densities of hourly precipitation from the C11 simulations and the U.S. hourly station observations. The solid Blue (Green) line is the average PDF of all of the station (simulation) grid cells. Dashed lines represent the spread between the [5,95] percentile PDF distributions of stations (blue) and model estimates at the station locations (green). Pearson's r correlation coefficient shown next to the legend.*

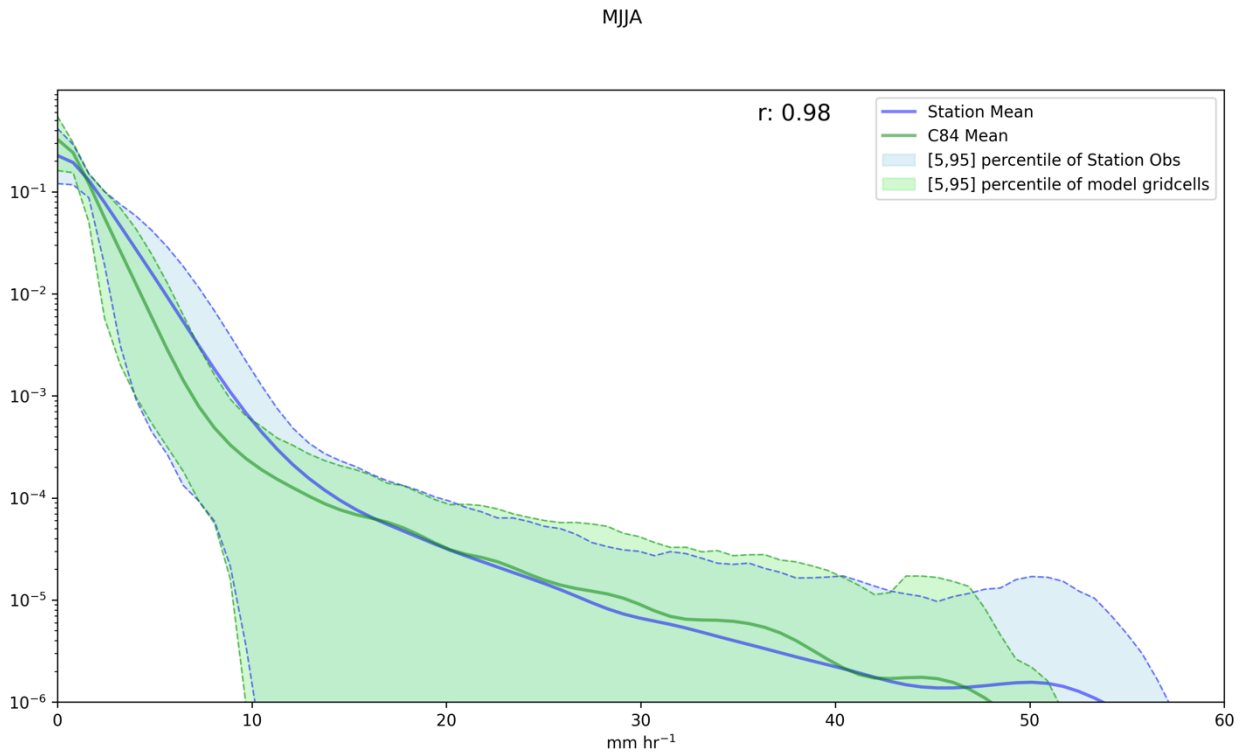


***Figure 9**: Same as **Figure 8** but for the C84 simulation.*

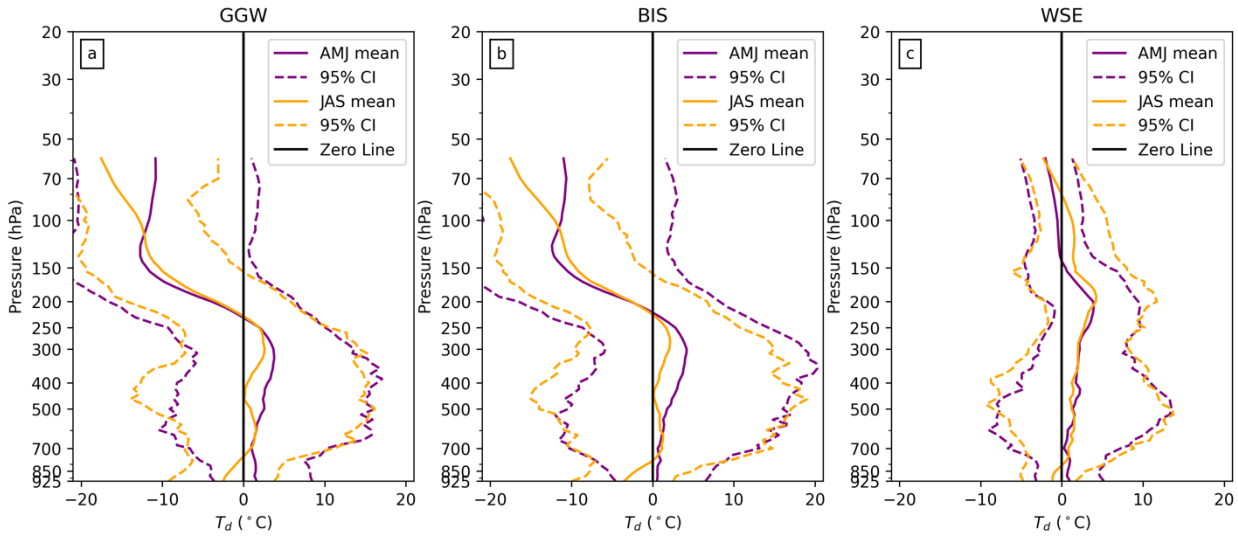


***Figure 10**: Vertical profiles from C11 of dewpoint temperature compared to the Glasgow, MT sounding location (GGW), the Bismarck, ND sounding location (BIS), Edmonton, AB, sounding location (WSE). The 2010-2013 AMJ average is shown in purple and the 2010-2013 JAS average is shown in gold. Dashed lines represent the 95% confidence interval of the mean.*

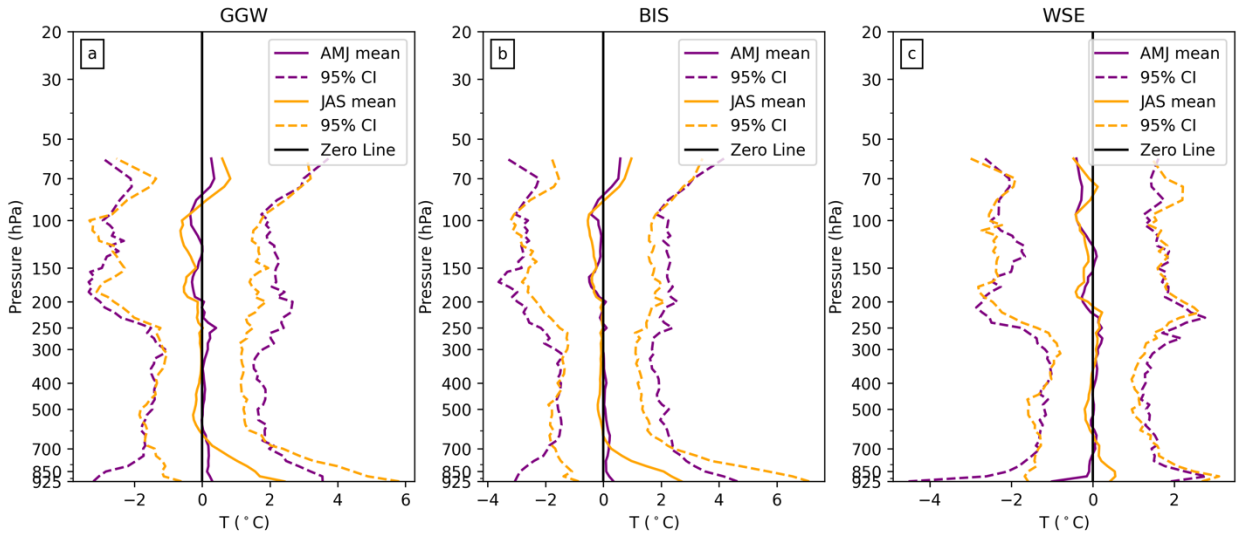


***Figure 11**: Same as **Figure 10** but for temperature.*

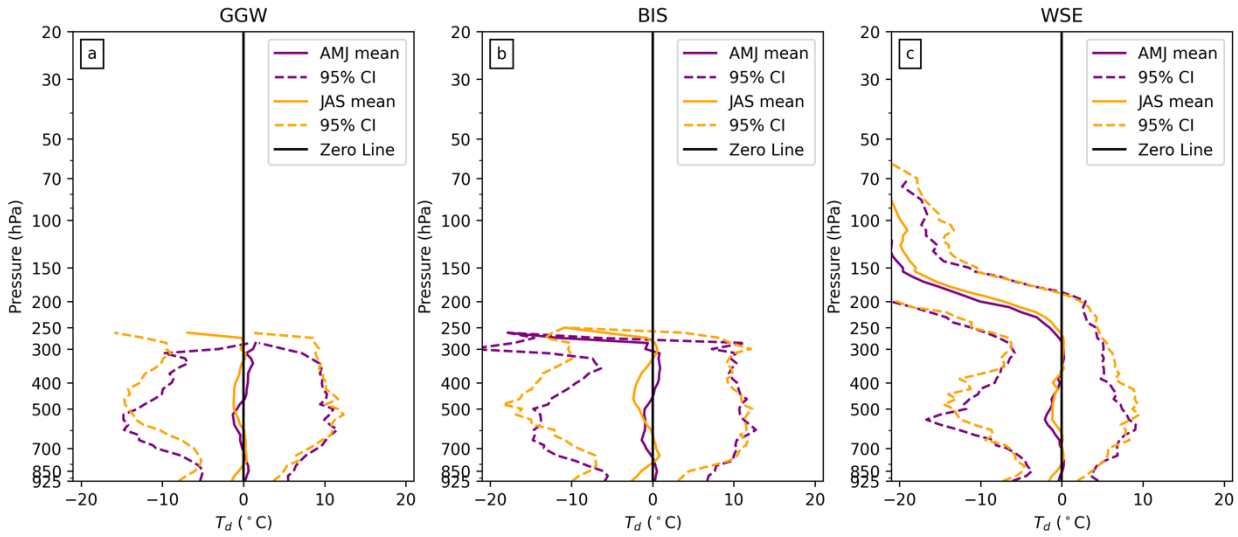


***Figure 12**: Same as Figure 10 but for the C84 simulation.*

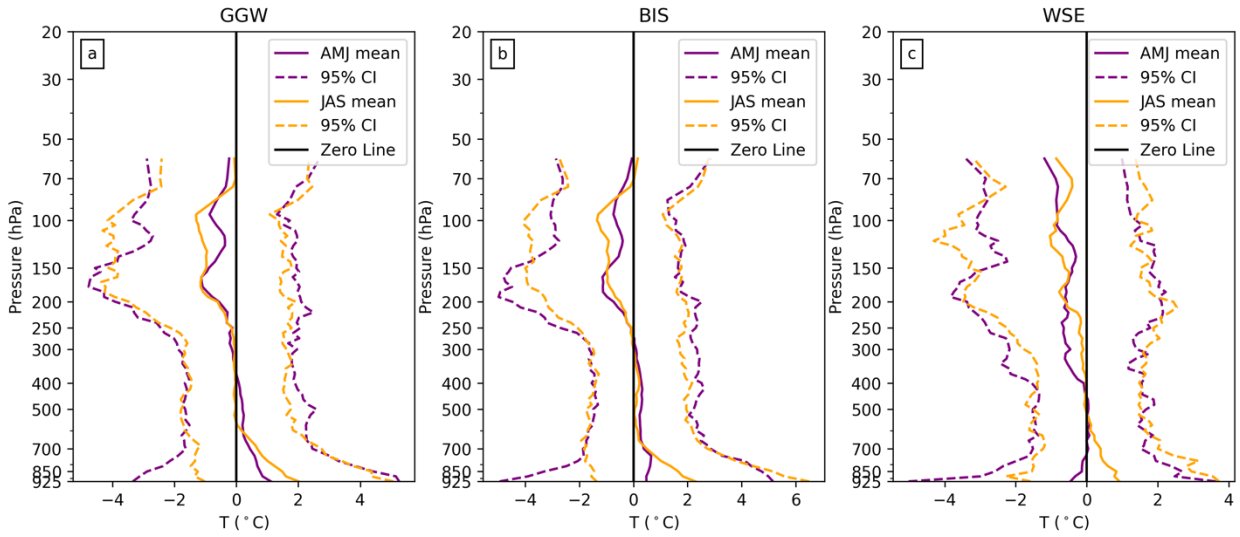


***Figure 13**: Same as **Figure 11** but for the C84 Simulation.*

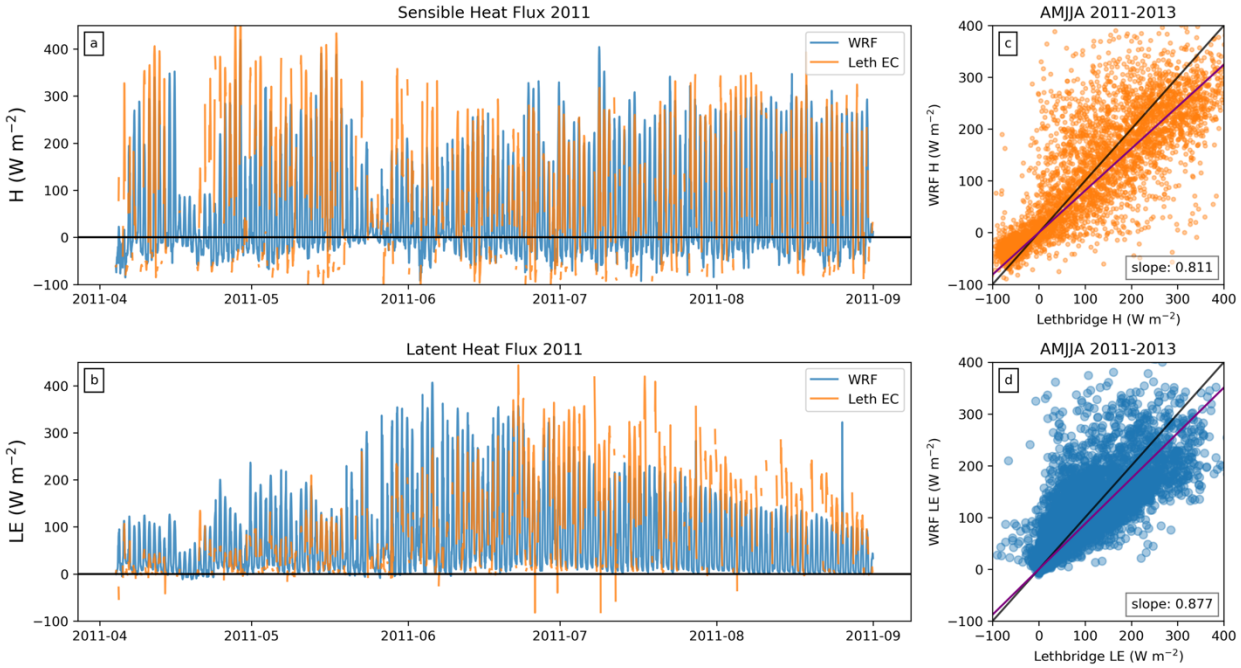


Figure 14: *Sensible heat flux (H) (a) and latent heat flux (LE) (b) from WRF (blue) and CA-Leth (orange) shown for the 2011 warm season, taken here to be AMJJA. The relationship between H (c) and LE (d) simulated by WRF and observed at CA-Leth for the 2011-2013 warm seasons, the slope of the robust linear regression shown in the bottom left.*

APPENDIX

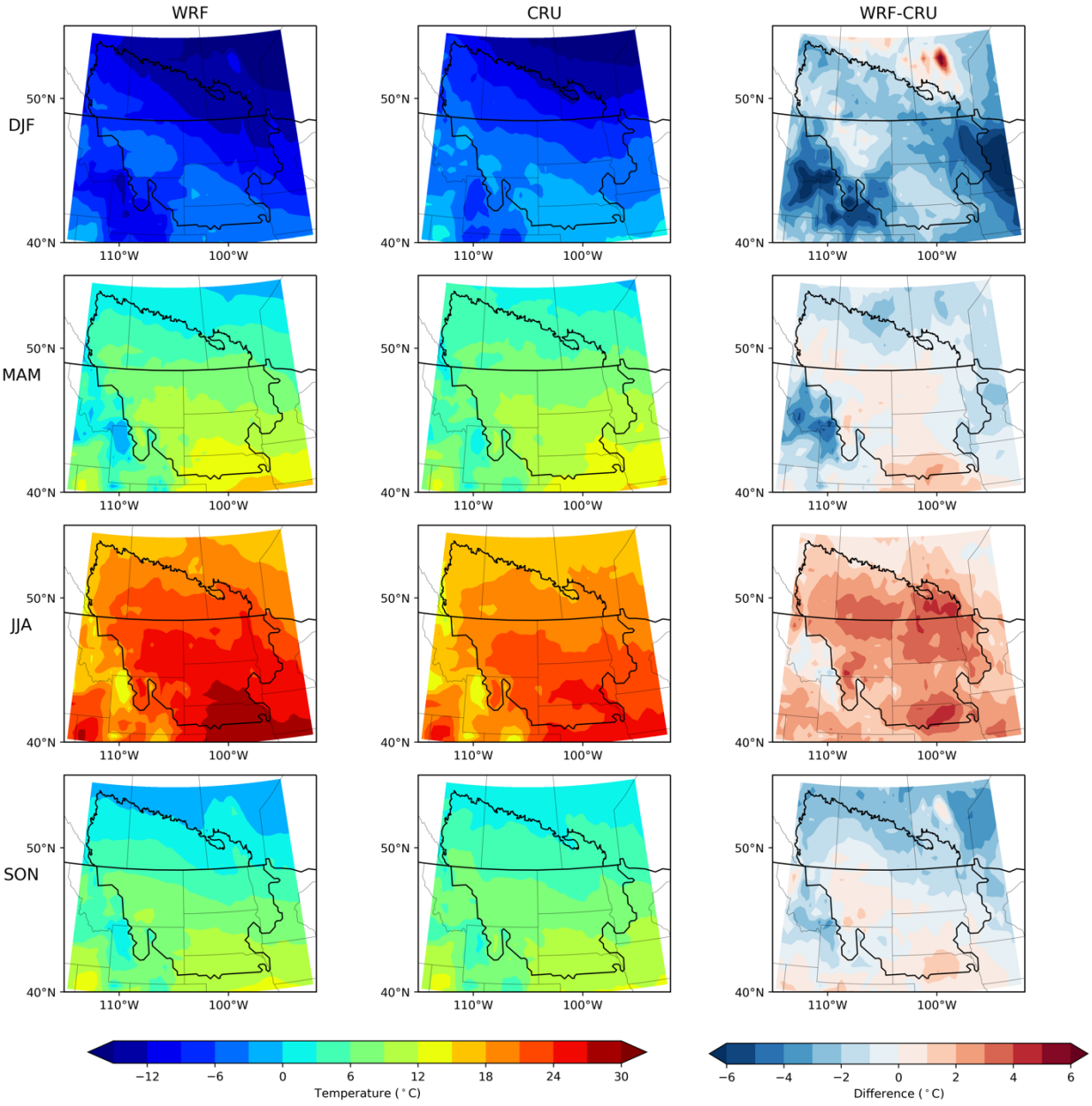


Figure S1: Same as in Figure 2 but for the CRU dataset. The CRU dataset is distributed in a .5 degree regular grid, so remapping was not performed.

d

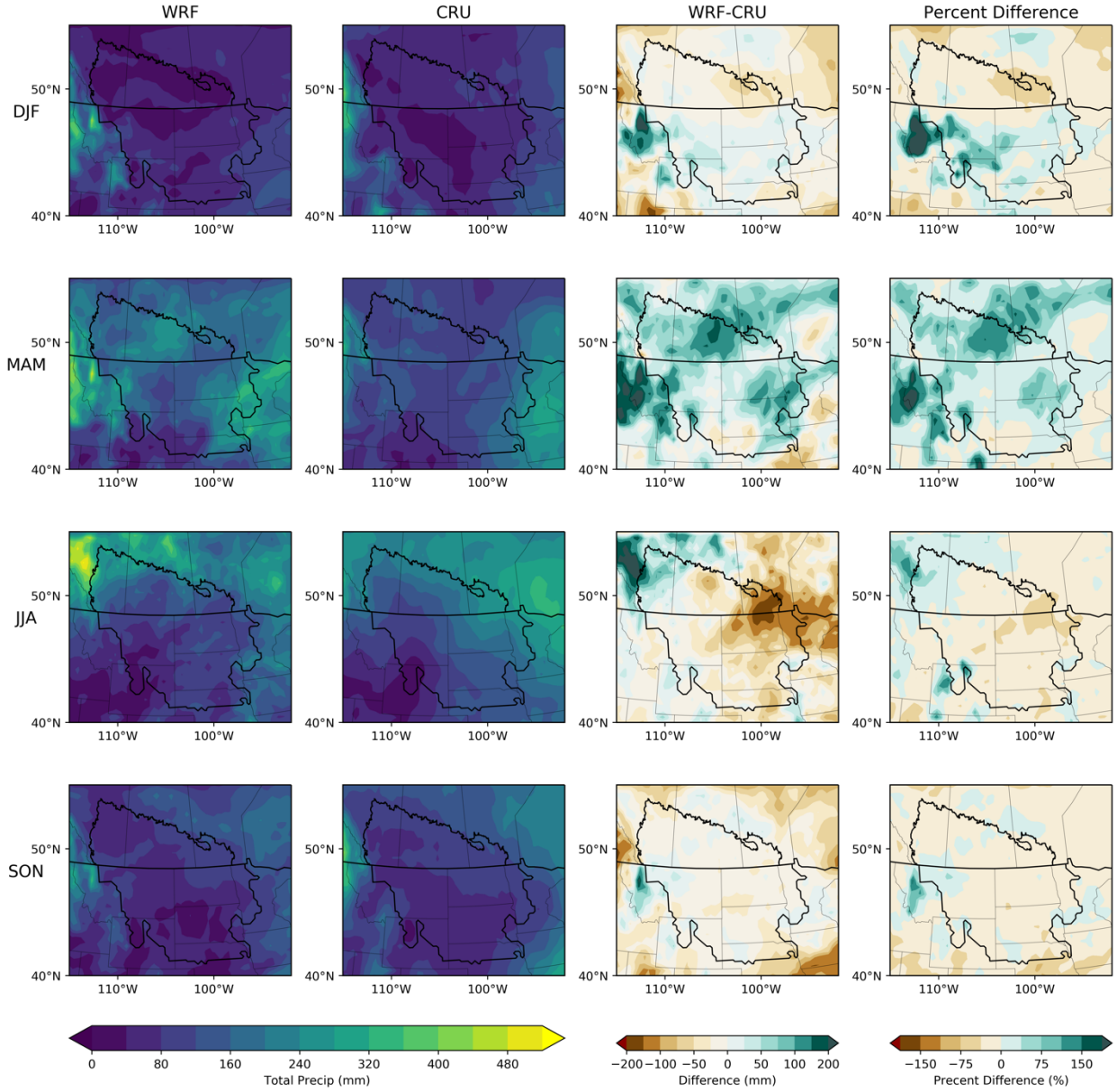


Figure S2: Same as in Figure 4 but with the CRU dataset. CRU is distributed in a .5 degree regular grid so it was not remapped.

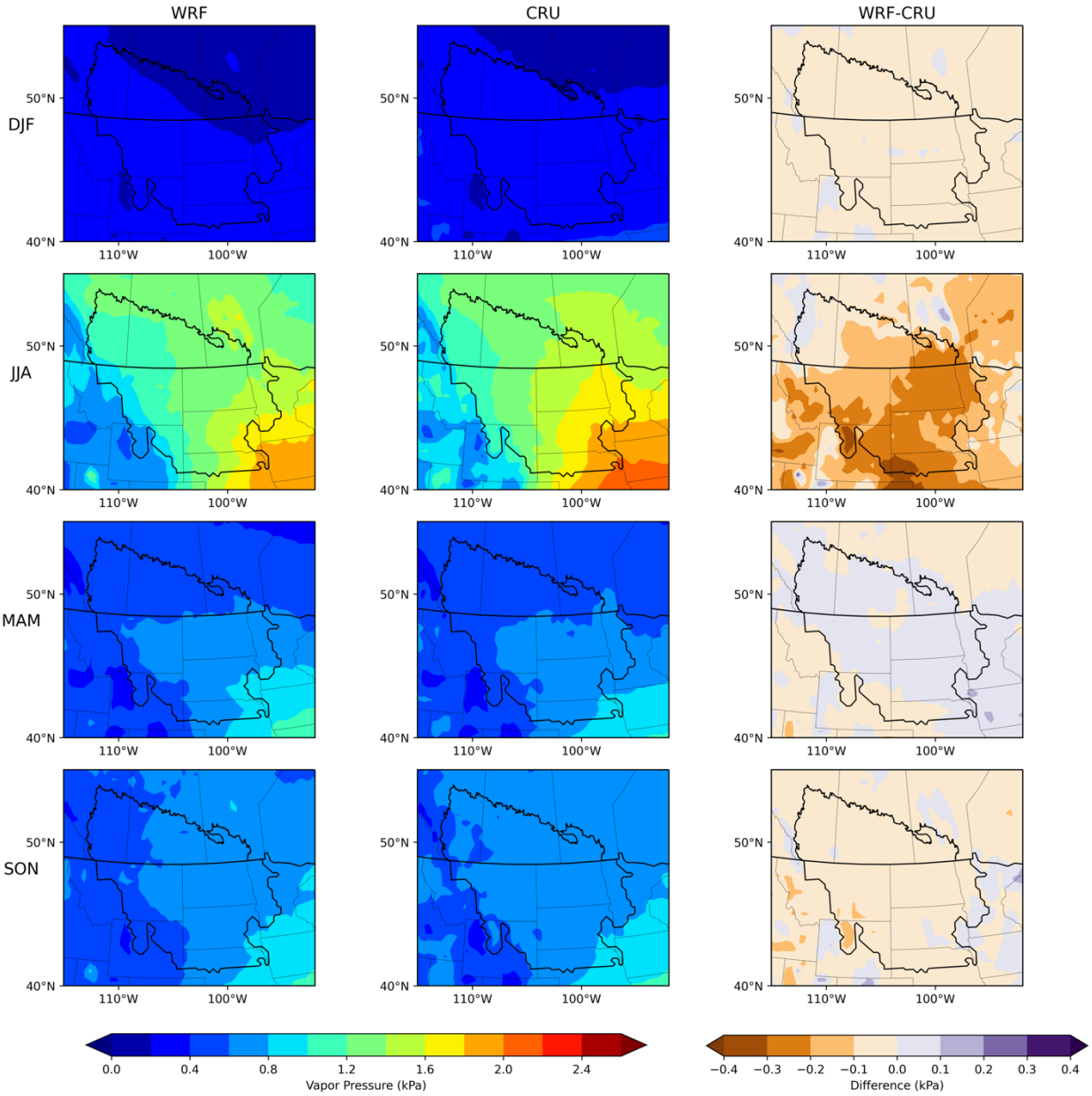


Figure S3: Difference in vapor pressure between C11 WRF simulation and the CRU 4.01 vapor pressure deficit. WRF was conservatively remapped to a .5 degree grid to match CRU.

References

Aase, J. K., and J. L. Pikul, 1995: Crop and Soil Response to Long-Term Tillage Practices in the Northern Great Plains. *Agron. J.*, **87**, 652–656, https://doi.org/10.2134/agronj1995.00021962008700040008x.

Alter, R. E., H. C. Douglas, J. M. Winter, and E. A. B. Eltahir, 2017: 20th-century regional climate change in the central United States attributed to agricultural intensification. *Geophys. Res. Lett.*, 1–9, https://doi.org/10.1002/2017GL075604.

Barlage, M., M. Tewari, F. Chen, G. Miguez-Macho, Z.-L. Yang, and G.-Y. Niu, 2015: The effect of groundwater interaction in North American regional climate simulations with WRF/Noah-MP. *Clim. Change*, **129**, 485–498, https://doi.org/10.1007/s10584-014-1308-8.

——, F. Chen, R. Rasmussen, Z. Zhang, and G. Miguez-Macho, 2021: The Importance of Scale-Dependent Groundwater Processes in Land-Atmosphere Interactions Over the Central United States. *Geophys. Res. Lett.*, **48**, e2020GL092171, https://doi.org/10.1029/2020GL092171.

Betts, A. K., 2009: Land-Surface-Atmosphere Coupling in Observations and Models. *J. Adv. Model. Earth Syst.*, **1**, 1–18, https://doi.org/10.3894/JAMES.2009.1.4.

——, and R. L. Desjardins, 2018: Understanding Land–Atmosphere–Climate Coupling from the Canadian Prairie Dataset. *Environments*, **5**, 129, https://doi.org/10.3390/environments5120129.

Betts, A. K., R. Desjardins, D. Worth, and D. Cerkowniak, 2013: Impact of land use change on the diurnal cycle climate of the Canadian Prairies. *J. Geophys. Res. Atmospheres*, **118**, 11996–12011, https://doi.org/10.1002/2013JD020717.

Birch, C. E., J. H. Marsham, D. J. Parker, and C. M. Taylor, 2014: The scale dependence and structure of convergence fields preceding the initiation of deep convection. *Geophys. Res. Lett.*, **41**, 4769–4776, https://doi.org/10.1002/2014GL060493.

Brimelow, J. C., J. M. Hanesiak, and W. R. Burrows, 2011: Impacts of Land–Atmosphere Feedbacks on Deep, Moist Convection on the Canadian Prairies. *Earth Interact.*, **15**, 1–29, https://doi.org/10.1175/2011EI407.1.

Bromley, G. T., T. Gerken, A. F. Prein, and P. C. Stoy, 2020: Recent Trends in the Near-Surface Climatology of the Northern North American Great Plains. *J. Clim.*, **33**, 461–475, https://doi.org/10.1175/JCLI-D-19-0106.1.

Brookshire, E. N. J., P. C. Stoy, B. Currey, and B. Finney, 2020: The greening of the Northern Great Plains and its biogeochemical precursors. *Glob. Change Biol.*, **26**, 5404–5413, https://doi.org/10.1111/gcb.15115.

Campbell, C. A., R. P. Zentner, S. Gameda, B. Blomert, and D. D. Wall, 2002: Production of annual crops on the Canadian prairies: Trends during 1976–1998. *Can. J. Soil Sci.*, **82**, 45–57, https://doi.org/10.4141/S01-046.

Chen, L., and P. A. Dirmeyer, 2017: Impacts of Land-Use/Land-Cover Change on Afternoon Precipitation over North America. *J. Clim.*, **30**, 2121–2140, https://doi.org/10.1175/JCLI-D-16-0589.1.

——, Y. Li, F. Chen, M. Barlage, Z. Zhang, and Z. Li, 2019: Using 4-km WRF CONUS simulations to assess impacts of the surface coupling strength on regional climate simulation. *Clim. Dyn.*, **53**, 6397–6416, https://doi.org/10.1007/s00382-019-04932-9.

Cheruy, F., J. L. Dufresne, F. Hourdin, and A. Ducharne, 2014: Role of clouds and land-atmosphere coupling in midlatitude continental summer warm biases and climate change amplification in CMIP5 simulations. *Geophys. Res. Lett.*, **41**, https://doi.org/10.1002/2014GL061145.

Daly, C., M. Halbleib, J. I. Smith, W. P. Gibson, M. K. Doggett, G. H. Taylor, J. Curtis, and P. P. Pasteris, 2008: Physiographically sensitive mapping of climatological temperature and precipitation across the conterminous United States. *Int. J. Climatol.*, **28**, 2031–2064, https://doi.org/10.1002/joc.1688.

Durre, I., R. S. Vose, and D. B. Wuertz, 2006: Overview of the Integrated Global Radiosonde Archive. *J. Clim.*, **19**, 53–68, https://doi.org/10.1175/JCLI3594.1.

Ficklin, D. L., and K. A. Novick, 2017: Historic and projected changes in vapor pressure deficit suggest a continental-scale drying of the United States atmosphere. *J. Geophys. Res. Atmospheres*, **122**, 2061–2079, https://doi.org/10.1002/2016JD025855.

Findell, K. L., and E. A. B. Eltahir, 2003a: Atmospheric Controls on Soil Moisture–Boundary Layer Interactions. Part I: Framework Development. *J. Hydrometeorol.*, **4**, 552–569, https://doi.org/10.1175/1525-7541(2003)004<0552:ACOSML>2.0.CO;2.

Findell, K. L., and E. a. B. Eltahir, 2003b: Atmospheric Controls on Soil Moisture–Boundary Layer Interactions. Part II: Feedbacks within the Continental United States. *J. Hydrometeorol.*, **4**, 570–583, https://doi.org/10.1175/1525-7541(2003)004<0570:ACOSML>2.0.CO;2.

Flanagan, L. B., L. A. Wever, and P. J. Carlson, 2002: Seasonal and interannual variation in carbon dioxide exchange and carbon balance in a northern temperate grassland. *Glob. Change Biol.*, **8**, 599–615, https://doi.org/10.1046/j.1365-2486.2002.00491.x.

Gameda, S., B. Qian, C. A. Campbell, and R. L. Desjardins, 2007: Climatic trends associated with summerfallow in the Canadian Prairies. *Agric. For. Meteorol.*, **142**, 170–185, https://doi.org/10.1016/j.agrformet.2006.03.026.

Gerken, T., G. T. Bromley, and P. C. Stoy, 2018: Surface Moistening Trends in the Northern North American Great Plains Increase the Likelihood of Convective Initiation. *J. Hydrometeorol.*, **19**, 227–244, https://doi.org/10.1175/JHM-D-17-0117.1.

Hammer, G., and P. Steurer, 1997: Data set documentation for hourly precipitation data.

Hanesiak, J. M., R. L. Raddatz, and S. Lobban, 2004: Local Initiation of Deep Convection on the Canadian Prairie Provinces. *Bound.-Layer Meteorol.*, **110**, 455–470, https://doi.org/10.1023/B:BOUN.0000007242.89023.e5.

Harris, I., T. J. Osborn, P. Jones, and D. Lister, 2020: Version 4 of the CRU TS monthly high-resolution gridded multivariate climate dataset. *Sci. Data*, **7**, 109, https://doi.org/10.1038/s41597-020-0453-3.

Hersbach, H., and Coauthors, 2020: The ERA5 global reanalysis. *Q. J. R. Meteorol. Soc.*, **146**, 1999–2049, https://doi.org/10.1002/qj.3803.

Hohenegger, C., P. Brockhaus, C. S. Bretherton, and C. Schär, 2009: The Soil Moisture–Precipitation Feedback in Simulations with Explicit and Parameterized Convection. *J. Clim.*, **22**, 5003–5020, https://doi.org/10.1175/2009JCLI2604.1.

Hong, S.-Y., Y. Noh, and J. Dudhia, 2006: A New Vertical Diffusion Package with an Explicit Treatment of Entrainment Processes. *Mon. Weather Rev.*, **134**, 2318–2341, https://doi.org/10.1175/MWR3199.1.

Huang, B., X. Hu, G.-A. Fuglstad, X. Zhou, W. Zhao, and F. Cherubini, 2020: Predominant regional biophysical cooling from recent land cover changes in Europe. *Nat. Commun.*, **11**, 1066, https://doi.org/10.1038/s41467-020-14890-0.

Huang, K., and Coauthors, 2018: Enhanced peak growth of global vegetation and its key mechanisms. *Nat. Ecol. Evol.*, **2**, 1897–1905, https://doi.org/10.1038/s41559-018-0714-0.

Iacono, M. J., J. S. Delamere, E. J. Mlawer, M. W. Shephard, S. A. Clough, and W. D. Collins, 2008: Radiative forcing by long-lived greenhouse gases: Calculations with the AER radiative transfer models. *J. Geophys. Res. Atmospheres*, **113**, https://doi.org/10.1029/2008JD009944.

Juang, J. Y., G. G. Katul, A. Porporato, P. C. Stoy, M. S. Siqueira, M. Detto, H. S. Kim, and R. Oren, 2007a: Eco-hydrological controls on summertime convective rainfall triggers. *Glob. Change Biol.*, **13**, 887–896, https://doi.org/10.1111/j.1365-2486.2007.01315.x.

——, A. Porporato, P. C. Stoy, M. S. Siqueira, A. C. Oishi, M. Detto, H. S. Kim, and G. G. Katul, 2007b: Hydrologic and atmospheric controls on initiation of convective precipitation events. *Water Resour. Res.*, **43**, 1–10, https://doi.org/10.1029/2006WR004954.

Klein, C., and C. M. Taylor, 2020: Dry soils can intensify mesoscale convective systems. *Proc. Natl. Acad. Sci.*, **117**, 21132–21137, https://doi.org/10.1073/pnas.2007998117.

Knist, S., K. Goergen, and C. Simmer, 2020: Effects of land surface inhomogeneity on convection-permitting WRF simulations over central Europe. *Meteorol. Atmospheric Phys.*, **132**, 53–69, https://doi.org/10.1007/s00703-019-00671-y.

Kolby Smith, W., S. C. Reed, C. C. Cleveland, A. P. Ballantyne, W. R. L. Anderegg, W. R. Wieder, Y. Y. Liu, and S. W. Running, 2016: Large divergence of satellite and Earth system model estimates of global terrestrial CO 2 fertilization. *Nat. Clim. Change*, **6**, 306–310, https://doi.org/10.1038/nclimate2879.

Koster, R. D., 2004: Regions of Strong Coupling Between Soil Moisture and Precipitation. *Science*, **305**, 1138–1140, https://doi.org/10.1126/science.1100217.

Lin, Y., W. Dong, M. Zhang, Y. Xie, W. Xue, J. Huang, and Y. Luo, 2017: Causes of model dry and warm bias over central U.S. and impact on climate projections. *Nat. Commun.*, **8**, https://doi.org/10.1038/s41467-017-01040-2.

Liu, C., and Coauthors, 2017: Continental-scale convection-permitting modeling of the current and future climate of North America. *Clim. Dyn.*, **49**, 71–95, https://doi.org/10.1007/s00382-016-3327-9.

Liu, P., A. P. Tsimpidi, Y. Hu, B. Stone, A. G. Russell, and A. Nenes, 2012: Differences between downscaling with spectral and grid nudging using WRF. *Atmospheric Chem. Phys.*, **12**, 3601–3610, https://doi.org/10.5194/acp-12-3601-2012.

Long, J. A., R. L. Lawrence, P. R. Miller, and L. A. Marshall, 2014: Changes in field-level cropping sequences: Indicators of shifting agricultural practices. *Agric. Ecosyst. Environ.*, **189**, 11–20, https://doi.org/10.1016/j.agee.2014.03.015.

Ma, H.-Y., and Coauthors, 2018: CAUSES: On the Role of Surface Energy Budget Errors to the Warm Surface Air Temperature Error Over the Central United States. *J. Geophys. Res. Atmospheres*, **123**, 2888–2909, https://doi.org/10.1002/2017JD027194.

Maaz, T., J. D. Wulfhorst, V. McCracken, J. Kirkegaard, D. R. Huggins, I. Roth, H. Kaur, and W. Pan, 2018: Economic, policy, and social trends and challenges of introducing oilseed and pulse crops into dryland wheat cropping systems. *Agric. Ecosyst. Environ.*, **253**, 177–194, https://doi.org/10.1016/j.agee.2017.03.018.

Mallard, M. S., T. L. Spero, and S. M. Taylor, 2018: Examining WRF's Sensitivity to Contemporary Land-Use Datasets across the Contiguous United States Using Dynamical Downscaling. *J. Appl. Meteorol. Climatol.*, **57**, 2561–2583, https://doi.org/10.1175/JAMC-D-17-0328.1.

Maurer, V., I. Bischoff-Gauß, N. Kalthoff, L. Gantner, R. Roca, and H.-J. Panitz, 2017: Initiation of deep convection in the Sahel in a convection-permitting climate simulation for northern Africa. *Q. J. R. Meteorol. Soc.*, **143**, 806–816, https://doi.org/10.1002/qj.2966.

Miller, P. R., and Coauthors, 2002: Pulse Crop Adaptation in the Northern Great Plains. *Agron. J.*, **94**, 261–272, https://doi.org/10.2134/agronj2002.2610.

Mueller, N. D., E. E. Butler, K. A. Mckinnon, A. Rhines, M. Tingley, N. M. Holbrook, and P. Huybers, 2015: Cooling of US Midwest summer temperature extremes from cropland intensification. https://doi.org/10.1038/NCLIMATE2825.

Niu, G.-Y., Z.-L. Yang, R. E. Dickinson, L. E. Gulden, and H. Su, 2007: Development of a simple groundwater model for use in climate models and evaluation with Gravity Recovery and Climate Experiment data. *J. Geophys. Res. Atmospheres*, **112**, https://doi.org/10.1029/2006JD007522.

Piao, S., and Coauthors, 2020: Characteristics, drivers and feedbacks of global greening. *Nat. Rev. Earth Environ.*, **1**, 14–27, https://doi.org/10.1038/s43017-019-0001-x.

Prein, A. F., and Coauthors, 2015: A review on regional convection-permitting climate modeling: Demonstrations, prospects, and challenges. *Rev. Geophys.*, **53**, 323–361, https://doi.org/10.1002/2014RG000475.

——, C. Liu, K. Ikeda, R. Bullock, R. M. Rasmussen, G. J. Holland, and M. Clark, 2017: Simulating North American mesoscale convective systems with a convection-permitting climate model. *Clim. Dyn.*, https://doi.org/10.1007/s00382-017-3993-2.

Qian, Y., and Coauthors, 2020: Neglecting irrigation contributes to the simulated summertime warm-and-dry bias in the central United States. *Npj Clim. Atmospheric Sci.*, **3**, 1–10, https://doi.org/10.1038/s41612-020-00135-w.

Raddatz, R. L., 1998: Anthropogenic vegetation transformation and the potential for deep convection on the Canadian prairies. *Can. J. Soil Sci.*, **78**, 657–666, https://doi.org/10.4141/S98-011.

——, 2000: Summer rainfall recycling for an agricultural region of the Canadian prairies. *Can. J. Soil Sci.*, **80**, 367–373, https://doi.org/10.4141/S99-016.

Richardson, A. D., and Coauthors, 2006: A multi-site analysis of random error in tower-based measurements of carbon and energy fluxes. *Agric. For. Meteorol.*, **136**, 1–18, https://doi.org/10.1016/j.agrformet.2006.01.007.

Rigden, A. J., N. D. Mueller, N. M. Holbrook, N. Pillai, and P. Huybers, 2020: Combined influence of soil moisture and atmospheric evaporative demand is important for accurately predicting US maize yields. *Nat. Food*, **1**, 127–133, https://doi.org/10.1038/s43016-020-0028-7.

Rosenzweig, S. T., and M. E. Schipanski, 2019: Landscape-scale cropping changes in the High Plains: economic and environmental implications. *Environ. Res. Lett.*, **14**, 124088, https://doi.org/10.1088/1748-9326/ab5e8b.

Rustemeier, E., A. Becker, P. Finger, U. Schneider, and M. Ziese, 2020: GPCC Precipitation Climatology Version 2020 at 0.25°: Monthly Land-Surface Precipitation Climatology for Every Month and the Total Year from Rain-Gauges built on GTS-based and Historic Data: Globally Gridded Monthly Totals. min. 200 KByte-max. 20 MByte per gzip compressed NetCDF archive, https://doi.org/10.5676/DWD_GPCC/CLIM_M_V2020_025.

Santanello, J. A., and Coauthors, 2017: Land–Atmosphere Interactions: The LoCo Perspective. *Bull. Am. Meteorol. Soc.*, **99**, 1253–1272, https://doi.org/10.1175/BAMS-D-17-0001.1.

Schulzweida, U., 2019: CDO User Guide. https://doi.org/10.5281/ZENODO.3539275.

Shrestha, B. M., R. L. Raddatz, R. L. Desjardins, and D. E. Worth, 2012: Continuous Cropping and Moist Deep Convection on the Canadian Prairies. *Atmosphere*, **3**, 573–590, https://doi.org/10.3390/atmos3040573.

Spero, T. L., M. J. Otte, J. H. Bowden, and C. G. Nolte, 2014: Improving the representation of clouds, radiation, and precipitation using spectral nudging in the Weather Research and Forecasting model. *J. Geophys. Res. Atmospheres*, **119**, 11,682-11,694, https://doi.org/10.1002/2014JD022173.

Stoy, P. C., and Coauthors, 2013: A data-driven analysis of energy balance closure across FLUXNET research sites: The role of landscape scale heterogeneity. *Agric. For. Meteorol.*, **171–172**, 137–152, https://doi.org/10.1016/j.agrformet.2012.11.004.

Stoy, P. C., and Coauthors, 2018: Opportunities and Trade-offs among BECCS and the Food, Water, Energy, Biodiversity, and Social Systems Nexus at Regional Scales. *BioScience*, **68**, 100–111, https://doi.org/10.1093/biosci/bix145.

Taylor, C. M., and Coauthors, 2006: Frequency of Sahelian storm initiation enhanced over mesoscale soil-moisture patterns. *Nature*, **4**, 611–625, https://doi.org/10.1038/ngeo1173.

——, D. Jeu, a. M. Richard, F. Guichard, P. P. Harris, and W. a. Dorigo, 2012: Afternoon rain more likely over drier soils. *Nature*, **489**, 423–426, https://doi.org/10.1038/nature11377.

——, C. E. Birch, D. J. Parker, N. Dixon, F. Guichard, G. Nikulin, and G. M. S. Lister, 2013: Modeling soil moisture-precipitation feedback in the Sahel: Importance of spatial scale versus convective parameterization. *Geophys. Res. Lett.*, **40**, 6213–6218, https://doi.org/10.1002/2013GL058511.

Thompson, G., P. R. Field, R. M. Rasmussen, and W. D. Hall, 2008: Explicit Forecasts of Winter Precipitation Using an Improved Bulk Microphysics Scheme. Part II: Implementation of

a New Snow Parameterization. *Mon. Weather Rev.*, **136**, 5095–5115, https://doi.org/10.1175/2008MWR2387.1.

Thornton, P. E., S. W. Running, and M. A. White, 1997: Generating surfaces of daily meteorological variables over large regions of complex terrain. *J. Hydrol.*, **190**, 214–251, https://doi.org/10.1016/S0022-1694(96)03128-9.

Thornton, P. E., M. M. Thornton, B. W. Mayer, Y. Wei, R. Devarakonda, R. S. Vose, and R. B. Cook, 2016: DaymetDaymet: Daily Surface Weather Data on a 1-km Grid for North America, Version 3. 711509.8892839993 MB, https://doi.org/10.3334/ORNLDAAC/1328.

Twine, T. E., and Coauthors, 2000: Correcting eddy-covariance flux underestimates over a grassland. *Agric. For. Meteorol.*, **103**, 279–300, https://doi.org/10.1016/S0168-1923(00)00123-4.

Vanden Broucke, S., and N. Van Lipzig, 2017: Do convection-permitting models improve the representation of the impact of LUC? *Clim. Dyn.*, **49**, 2749–2763, https://doi.org/10.1007/s00382-016-3489-5.

——, S. Luyssaert, E. L. Davin, I. Janssens, and N. van Lipzig, 2015: New insights in the capability of climate models to simulate the impact of LUC based on temperature decomposition of paired site observations. *J. Geophys. Res. Atmospheres*, **120**, 5417–5436, https://doi.org/10.1002/2015JD023095.

Vick, E. S. K., P. C. Stoy, A. C. I. Tang, and T. Gerken, 2016: The surface-atmosphere exchange of carbon dioxide, water, and sensible heat across a dryland wheat-fallow rotation. *Agric. Ecosyst. Environ.*, **232**, 129–140, https://doi.org/10.1016/j.agee.2016.07.018.

Wang, Y., B. Geerts, and C. Liu, 2018: A 30-year convection-permitting regional climate simulation over the interior western United States. Part I: Validation. *Int. J. Climatol.*, **38**, 3684–3704, https://doi.org/10.1002/joc.5527.

Yuan, W., and Coauthors, 2019: Increased atmospheric vapor pressure deficit reduces global vegetation growth. *Sci. Adv.*, **5**, eaax1396, https://doi.org/10.1126/sciadv.aax1396.

Zhang, Z., Y. Li, F. Chen, M. Barlage, and Z. Li, 2020: Evaluation of convection-permitting WRF CONUS simulation on the relationship between soil moisture and heatwaves. *Clim. Dyn.*, **55**, 235–252, https://doi.org/10.1007/s00382-018-4508-5.

Zhu, Z., and Coauthors, 2016: Greening of the Earth and its drivers. *Nat. Clim. Change*, **6**, 791–795, https://doi.org/10.1038/nclimate3004.

CHAPTER FOUR

THE DECLINE IN SUMMER FALLOW IN THE NORTHERN PLAINS COOLED NEAR-SURFACE CLIMATE BUT HAD MINIMAL IMPACTS ON PRECIPITATION

Contribution of Authors and Co-Authors

Manuscript in Chapter 4

Author: Gabriel T. Bromley
Contributions: Performed model simulations, analyzed model output, and wrote the first draft of the manuscript.

Co-Author: Paul C. Stoy
Contributions: Conceived study, obtained funding, discussed results and analysis, provided data, edited manuscript at all staged.

Co-Author: Andreas Prein
Contributions: Discussed results and analysis methods, edited the manuscript at all stages.

Co-Author: Shannon Albeke
Contributions: Created the fallow dataset for use within the modeling framework.

Manuscript Information

Gabriel T. Bromley, Andreas F. Prein, Shannon Albeke, more, Paul C. Stoy
Climate Dynamics

Status of Manuscript:
___X_ Prepared for submission to a peer-reviewed journal
____ Officially submitted to a peer-reviewed journal
____ Accepted by a peer-reviewed journal
____ Published in a peer-reviewed journal

Springer

CHAPTER FOUR

THE DECLINE IN SUMMER FALLOW IN THE NORTHERN PLAINS COOLED NEAR-SURFACE CLIMATE BUT HAD MINIMAL IMPACTS ON PRECIPITATION

Abstract

Land use and landcover change impacts the near-surface energy balance and has the potential to alter regional climate. As a result, land management strategies have the potential to moderate or intensify the impacts of a warming atmosphere. Since 1982 in the northern North American Great Plains, nearly 116,000 km^2 of crop land that was once held in fallow during the summer is now planted. To simulate the impacts of this substantial land cover change on regional climate processes, convection-permitting model experiments were performed utilizing adjusted land surface vegetation fractions to simulate modern and historical amounts of summer fallow. Results of these simulations show that historical summer fallow leads to ~1.5 ºC warmer temperatures and increase in vapor pressure deficit of ~0.15 kPa compared to modern land cover during the growing season, which is consistent with observed cooling trends. The warmer and drier land surface leads to a deeper planetary boundary layer and higher lifted condensation level, creating conditions less conducive to convective cloud and precipitation development. There is little evidence of a change to mean precipitation, but this does not differentiate between synoptically- and convectively-driven precipitation. Instead, increased moisture transport by way of the Great Plains Low Level Jet is consistent with observed increases in precipitation. Our results demonstrate that land cover change is consistent with observed regional cooling in the northern North American Great Plains but changes in precipitation cannot be explained by land management alone.

1. Introduction

Global temperatures are rising, primarily due to greenhouse gas emissions from anthropogenic activities (Stocker et al. 2014). Future temperature increases are exceedingly likely (IPCC 2007), as is an increase in precipitation extremes in extratropical zones (O'Gorman and Schneider 2009). Embedded within this global context are changes to regional temperatures and precipitation (Christensen et al. 2007) that often result from the impacts of land management and land cover change (Mahmood et al. 2014b; Luyssaert et al. 2014) on regional energy balances. Some of these

regional climate changes may be beneficial to agricultural and ecosystem management objectives, such as cooling damaging extreme temperatures (e.g. (Juang et al. 2007a; Mueller et al. 2015b); others are not (e.g. (Marshall et al. 2003; Mande et al. 2015). It is important to understand how land management impacts climate processes to develop strategies to minimize the deleterious impacts of climate change and become effective stewards of the earth system.

A unique interaction between land management and climate may have emerged across the northern Great Plains of North America (hereafter the NNAGP). Beginning in the 1960s and 1970s, concerns over soil health lead to widespread changes in agricultural management away from wheat fallow rotation agriculture and toward a more diverse agricultural system that avoids bare ground by rotating wheat with pulses, cover crops, and other crops (Miller et al. 2002, 2003; Long et al. 2014b). These changes appear to have unintentionally benefitted regional climate (Gameda et al. 2007). Agricultural areas of the Canadian Prairie Provinces have experienced a 6 W m^{-2} cooling during summer across parts of this time period (Betts et al. 2013b). Summer maximum temperatures in the Canadian Prairies have decreased by nearly 2 °C and extreme temperature events have become less frequent (Betts et al. 2013b,c). These regional climate effects have been attributed to a widespread decline of summerfallow from *ca*. 110,000 km^2 (25% of Canada's cultivated lands) to some 35,000 km^2 (8%) (Gameda et al. 2007; Vick et al. 2016). In the U.S. portion of the NNAGP and across a similar time period, near-surface air temperatures have cooled by nearly 0.2 °C $decade^{-1}$ during late spring and early summer, and near-surface atmospheric vapor pressure deficit – which strongly depletes crop yields (López et al.) – has decreased by −0.04 kPa $decade^{-1}$ (Bromley et al. 2020). These changes to regional climate

encompass a period of summer fallow decline on the order of 50,000 km^2 in the United States from a peak in 1987 until 2012 (Fig. 1).

The observed changes in climate are consistent with a transition of large expanses of land away from bare ground and toward crops which actively transport water from soil to atmosphere and increase latent heat flux and evaporative cooling (Vick et al. 2016). Changes to land management have likewise decreased the surface-atmosphere flux of sensible heat to help create a moister, shallower atmospheric boundary layer during summer (Gameda et al., 2007; Vick et al., 2016) through decreases in the Bowen ratio. Combined, these changes in surface fluxes have enhanced cloud formation ((Gameda et al. 2007; Betts et al. 2013c)) and increased the probability of convective precipitation ((Gameda et al. 2007; Betts et al. 2013c). Monthly mean precipitation has increased in the Canadian Prairies by 10 mm $decade^{-1}$ (Betts et al. 2013c; Gameda et al. 2007) and the U.S. northern Great Plains by 8 mm $decade^{-1}$ (Bromley et al. 2020). Given the multitude of factors that drive precipitation change, the full suite of mechanisms that underlie these observed increases in precipitation and the potential role of land cover change remain uncertain.

Empirical observations and localized modeling studies to date have made critical inroads into our understanding of land-atmosphere-precipitation connections in the NNAGP. Planting crops at the expense of summer fallow decreases atmospheric boundary layer (ABL) height (Gameda et al. 2007; Vick et al. 2016; Gerken et al. 2018c) and, coupled with increases in humidity, lowers the lifted condensation level (LCL) (Betts et al. 2013c; Betts and Desjardins 2018). Shallow cumulus clouds can result when the ABL crosses the LCL, a ‘necessary but not sufficient condition’ for the formation of convective precipitation (Juang et al. 2007a). Calculations of ABL and LCL height based on eddy-covariance data and 1-dimensional mixed-

layer atmospheric models show that the likelihood of ABL-LCL crossings are maximized in May and June due when 'wet coupling' (Roundy et al. 2013) prevails in the NNAGP such that increased moisture increases the likelihood of convective events (Gerken et al., 2018). This contrasts the prevailing 'dry coupled' conditions later in summer when convective precipitation is unlikely (Vick et al. 2016; Gerken et al. 2018c). Mixed layer models of atmospheric boundary layer development and land-atmosphere coupling have demonstrated an increase in ABL-LCL crossings and an increase in the likelihood of convective rain events across parts of the NNAGP (Gerken et al. 2018c), but the mechanisms underlying potential changes in convective precipitation across larger regions have not been explored.

At the same time, changes to surface-atmosphere fluxes due to land cover change appear to play a minor role in key aspects of the hydroclimate of the NNAGP. Convective precipitation in the NNAGP is dominated by mesoscale convective systems that are responsible for as much as 60% of the warm season precipitation (Carbone and Tuttle 2008). These systems form in the west and propagate eastward, often overnight, and mixed layer models are generally unable to account for these dynamics (Carbone and Tuttle 2008; Gerken et al. 2018c). The buildup of convective available potential energy (CAPE) that supports the development of MCSs comes primarily from the advection of warm, moist air into the region in addition to the diabatic heating of the boundary layer by way of sensible and latent heat fluxes from the surface (Agard and Emanuel 2017). The reduction of summer fallow has the potential to influence the flux of heat and moisture into the boundary layer, leading to the buildup of CAPE. Several studies have posited that increased evapotranspiration from more continuous cropping – and less summer fallow – has led to more growing season convection and potentially stronger storms (Raddatz 1998b; Shrestha et al. 2012).

However, since the boundary layer has also become cooler and moister, the cooling may act to reduce CAPE and perhaps balance the tendency of added moisture to increase it. Increases in temperature and moisture aloft will increase convective inhibition (CIN) which may balance or even dominate the effects of any increase in CAPE. The exact response of convective processes to such changes in near-surface conditions is unclear and requires a mechanistic modeling environment that can explicitly account for the dynamics of convective precipitation across regional scales.

How do changes to agricultural management impact regional atmospheric and climate processes? We seek to understand how land management impacts the regional climate and hydrometeorology of the NNAGP, a critical global breadbasket for wheat production. To do so, we model the regional impacts of the reduction of summer fallow across the NNAGP using the Weather Research and Forecasting model (WRF) at a 4 km spatial grid to explicitly model convective precipitation processes across multiple year periods. After describing the major results of the modeling analysis, we explore reanalysis datasets for a more comprehensive view of the changing hydroclimate of the NNAGP and discuss results in the context of the local and large-scale patterns that are consistent with observed climate trends across the region.

2. Methods and Experimental Design

2.1 Study Area

We define the semi-arid NNAGP following Bromley et al. (2020) as the combination of the Canadian Prairie Ecozone and the U.S. National Ecological Observation Network (NEON) Domain 9. Briefly, the NNAGP are dominated by grasslands, shrublands, and agriculture with

minimal urban development and forests in isolated mountain ranges and river valleys (Stoy et al. 2018). The NNAGP is a critical region for the global production of wheat, pulses, and oilseeds, and corn-soy cropping is becoming increasingly common in its eastern portion (Maaz et al. 2018; Rosenzweig and Schipanski 2019) which, coupled with other management pressures (e.g. (Dolan et al. 2020), create a dynamic system characterized by notable recent changes in land management and widespread increases in vegetation greenness (Brookshire et al. 2020) and decreases in bare ground fraction (Song et al. 2018).

2.1 Model Setup

The Weather Research and Forecasting model (WRF) is a state of the art weather model that can explicitly simulate convective processes and has been increasingly used in high-resolution regional climate simulations (Skamarock et al. 2008; Liu et al. 2017; Wang et al. 2018). WRF version 4.1 was used with a horizontal grid spacing of 4 km, 51 vertical levels up to 50 hPa, and a 20 s-time step. The study domain consists of 796 × 496 grid cells and encompasses the NNAGP with at least 40 grid cells between the study area and the edge of the domain. Initial and lateral boundary conditions were provided by the European Center for Medium-range Weather Forecasting's ERA5 dataset at three-hourly intervals (Hersbach et al.). The full model setup is described by Bromley et al., (2021) and follows (Liu et al. 2017). We use the Noah-MP land surface model with dynamic vegetation options turned off and leaf area index prescribed by table values for each land cover category (dveg=4) (Niu et al. 2011). Vegetation fraction (fveg) was fixed at the annual maximum to facilitate land cover experiments.

The TOPMODEL groundwater option was turned on, as simulating groundwater and runoff helps reduce the Great Plains warm season bias that is common to many WRF simulations (Barlage et al. 2021). Sea surface temperatures were updated as well as deep soil temperature and moisture. The simulations were run for three years coinciding with the water year beginning in October. The more modern control simulation with lesser summer fallow fraction is simulated for October 2010 – October 2013, and the historical control simulation with greater summer fallow fraction is simulated for October 1982 – October 1985. It is difficult to avoid the effects of the El Nino Southern Oscillation (ENSO) in short simulations, and results are subject to ENSO forcing. The modern simulation period starts during a positive ENSO phase and then shifts to more neutral conditions, while the historical simulation starts during a negative ENSO phase and then shifts to more neutral conditions. Full three-dimensional output was saved every three hours while a subset of surface and convective data were saved at hourly outputs.

b. Land Cover Experiments

The simulations described by Bromley et al. (2021) are used here as controls for land cover change experiments that investigate the effects of differing amounts of summer fallow. Summer fallow was represented within the model by reducing the fveg parameter by the estimated fallow percentage for each grid cell. Noah-MP uses a split-cell calculation for land-atmosphere interactions, meaning fluxes are calculated for the bare ground fraction and the vegetated fraction separately and then combined to give the surface fluxes for the entire grid cell. The historical control simulation uses a fveg field that matches the estimated summer-fallow in 1984 (Figure 1), hereafter called ‘C84’, while the modern control simulation uses a fveg that matches estimated summer fallow extent in 2011 (hereafter ‘C11’). The simulation with modern climate and 1980s

summer fallow extent is called F11 and the simulation with 1980s climate and 2010s summer fallow extent is called F84. We chose 2011 to match data availability from the U.S. National Land Cover Dataset (NLCD) (Homer et al. 2015), noting that this year was subject to relatively large fallow areas in parts of Saskatchewan, Manitoba, North Dakota and Minnesota due in part to widespread spring flooding that limited planting (Figure 1) (Stadnyk et al. 2016). From this perspective, our analysis represents a conservative interpretation of fallow change from the 1980s until the 2010s. We focus our analyses on the C11 and F11 simulations to isolate the role of land cover change apart from decadal global climate change on determining regional climate changes in the NNAGP.

c. Model Validation and Analysis

The control simulations were extensively validated in Bromley et al., (2021) against observational datasets and validation will only briefly be discussed for completeness. The near surface temperature in the C11 and C84 simulations were well simulated during spring and fall with cold (warm) biases in Winter (Summer) that were similar in magnitude to other WRF simulations (Liu et al. 2017). Precipitation was well simulated in C11 for all seasons – the difference between the model and observations was smaller than the difference between observational datasets. C84 had a wet bias in Winter and Spring but performed well in Summer. Both control simulations were compared to observational atmospheric soundings from Edmonton, AB, Glasgow, MT, and Bismark, ND. C11 has a strong near surface warm bias at all locations for the late warm season, while the early warm season was well captured. C84 simulations showed less of a near-surface bias in the late warm season by a few degrees, and well captured the early warm season. Both

simulations were within 1 °C at upper levels, and surface energy fluxes largely matched eddy covariance measurements from a grassland site in Lethbridge, AB (Flanagan and Adkinson 2011).

We focus the analysis on the warm season as investigating warm season climate trends is the focus of this work, and changes to other seasons are intermittently discussed for completeness. Seasonal changes are taken to be the average change across the three-year simulation. Statistical differences between simulations were assessed using a Mann-Whitney U test on daily data. The data processing workflow relied on the Climate Data Operators package as well as several analysis packages in Python (Schulzweida 2019; Harris et al. 2020a; Hoyer and Hamman 2017; Hunter 2007; Seabold and Perktold 2010). Convective parameters, such as convective available potential energy (CAPE) and convective inhibition (CIN) are calculated using the cape_2d function from the wrf-python package (Ladwig 2017).

3. Results

3.1 Changes to summer fallow extent and representation in WRF

The extent of summer fallow in provinces and states that intersect the study area decreased from 151,900 km^2 in 1982 to 35,100 km^2 in 2012, the years closest to the study periods when data were available from the United States (data from Canada were available every year) (Figure 1). Some 45% of the total decline in fallow of 116,800 km^2 was attributable to Saskatchewan alone (53,000 km^2). These published agricultural statistics were used to nudge the Landsat fallow attribution analysis on a per-Province and per-State basis (Figure 2) which was used to adjust the bare ground fraction in Noah-MP as noted.

3.2 Changes to near-surface energy and humidity

Two-meter air temperature (T2) shows a domain-averaged increase of about 0.18 °C during the growing season in F11 relative to C11 noting that the study period includes areas that experienced both increases and decreases in summer fallow (Figures 1-3). The strongest simulated warming is limited to June, July, August (JJA), but the warming pattern begins in May and extends until September (Figure 4). T2 cooled on average by –0.5 °C in areas where fallow decreased in C11 compared to F11. The northern and western part of the NNAGP in Alberta experienced a T2 increase on the order of +1.5 °C. T2 warmed on average by about 1.0 °C in areas where fallow increased in F11 compared with C11 across the entire study domain. There is a linear relationship between fveg and T2 (Figure 3b); T2 increases by 0.69 °C for every 10% increase in summer fallow across both simulations. There is a modest cooling signal during winter indicating the more vegetated C11 simulation is warmer by 0.25 °C (Figure 4) that follows the same spatial pattern as growing season temperature changes, but opposite in sign and of a lesser magnitude.

Changes in vapor pressure deficit (VPD) between F11 and C11 follow the same spatial pattern as T2; the areas that increased in fveg became moister and the areas that decreased in fveg became drier (Figure 5b). The domain median change is –0.045 kPa and with a wide distribution that encompasses both increases and decreases in VPD (Figure 5a). The most widespread increase in VPD is in Alberta with a 0.15 kPa increase from F11 to C11 over most of the Province within the study area. The strongest increase in VPD is nearly 0.3 kPa and occurs in central and eastern South Dakota. The largest decrease in fveg from F11 to C11 occurs in Manitoba where there was an observed increase in summer fallow (Figure 1); VPD is lower there by –0.15 kPa, with areas that decrease nearly –0.2 kPa.

Study area averaged sensible heat flux (H) is higher by 10 W m^{-2} in F11 compared to C11 where fveg is lower compared to C11 (Figure 5a). The areas of largest change have magnitudes of about 20 W m^{-2}. Latent heat flux (LE) follows the same pattern as H, but the magnitudes are larger (Figure 5b). Study area averaged LE is –16 W m^{-2} lower in the F11 simulation compared to the C11 simulation. The differences in LE are larger than H, with some areas in excess of 30 W m^{-2} in C11. Eastern Montana, western South Dakota and southern Saskatchewan show smaller magnitudes of change in both H and LE compared to the areas near the border of the study area that are considered 'crop' land cover types in the land surface model.

3.3 Changes to convective environments

We separate our analyses of convective environments between the early warm season (May and June) and late warm season (July and August) given differences in surface-atmosphere coupling in the NNAGP during these periods (Gerken et al., 2018).

During May and June, monthly mean CAPE decreased in the F11 simulation relative to the C11 simulation by –3.2 J/kg averaged across the entire domain (Figure 7a). CAPE decreased the most in South Dakota where some areas decreased in excess of –10 J/kg between simulations. The changes to the magnitude of CIN during May and June are weaker than the changes to CAPE (Figure 7b). There is not a clear pattern in the changes to CIN and weak evidence that the change in fveg affected CIN. The strongest change to CIN is in North Dakota, with a 20 J kg^{-1} increase in the western side and a –20 J kg^{-1} decrease on the eastern side. The height of the lifted condensation level (LCL) is higher in F11 compared to C11 for most of the study area. The mean change to LCL height is 13m while some areas are in more than 30m (Figure 7c). Manitoba is the only area where

the LCL heights have decreased. Mean LCL heights in Manitoba decreased by 20-30m. Differences in planetary boundary layer (PBL) heights closely follow the spatial pattern of differences in LCL heights (Figure 7d) and, as a consequence, the areas that have a positive change fveg from F11 to C11 have higher PBL heights, while the opposite holds for areas that have a negative change in fveg such as Manitoba. The mean change in PBL heights within the study area is 8m but some areas change up to 30m.

Differences in convective environments in July and August are stronger on average than in May and June but follow similar patterns (Figure 8). CAPE is lower across most of the study area in the F11 simulation by –10 J/kg with minima in Alberta as well as North and South Dakota (Figure 7a). These areas show a decrease of 20-40 J kg^{-1}. Changes to CIN in July and August are again weaker than the changes to CAPE (Figure 8b). CIN is lower in the F11 simulation than the C11 simulation in Alberta and parts of Saskatchewan by over –5 J kg^{-1} on average. Manitoba and north-eastern North Dakota exhibit higher CIN in F11 than C11 by the same magnitude of about as much as 20-30 J kg^{-1}. Differences in LCL heights show a similar pattern to May and June but much stronger with F11 simulating LCL heights that are 50 m higher than C11 across most of the study area (Figure 8c). The largest differences are located along the North Dakota-South Dakota border, northern Saskatchewan, and Alberta. LCL heights in these areas are over 100m higher. PBL heights in July and August follow a similar spatial pattern as in May and June but with greater magnitude (Figure 8d). PBL heights in Alberta and northern Saskatchewan are higher in the F11 simulation than C11 by over 100 m on average. Differences in PBL height in central parts of the study area are only 10-20m higher. The only area where PBL heights are lower in F11 is in

Manitoba with an average change of about 50 m, noting again that there was an increase in simulated fallow extent in Manitoba between 1984 and 2011 (Figure 1 & 2).

3.4 Changes to Precipitation

Spatial variability in simulated precipitation is pronounced. During May and June, precipitation is 5-10 mm higher in the F11 simulation over areas that have large proportions of bare ground compared to the C11 (Figure 9c). However, the total amount of precipitation during May and June is relatively high (>120 mm) so this constitutes a small percent change. Over areas that have less summer fallow in the F11 compared to the C11 simulation, there is a decrease in precipitation by 5-10 mm, which represents a 5-10% change.

During July and August, the F11 simulation is drier than the C11 simulation (Figure 9g). Many of the areas that were wetter in F11 than C11 in May and June are now drier than C11. Saskatchewan has the largest reduction in precipitation – between 10-15 mm – which amounts to 30-50 % less precipitation compared to the C11 simulation. North Dakota and eastern Montana are also drier in the F11 simulation compared to the C11 simulation.

4. Discussion

We demonstrate using convection-permitting WRF model simulations that the impact of land management change toward continuous cropping and away from summer fallow have decreased near-surface air temperature and vapor pressure deficit but have had muted impacts on precipitation in part because increases in instability through increased boundary layer moisture have been balanced by an increase in stability through a cooler boundary layer. Larger decreases

in precipitation due to summer fallow were found during the late growing season (i.e. July and August), which is largely after the main period of vegetation growth of key crops including wheat (Vick et al., 2016). Below, we elaborate on each of these findings to describe how land cover change has changed important aspects of the regional climate of the NNAGP, especially near the land surface. We then add to emerging evidence that observed changes in precipitation are likely due to moisture advection into our study domain rather than regional surface-atmosphere interactions.

Temperature and VPD

To summarize findings on the impact of summer fallow on near-surface climate: areas that underwent a fveg increase from F11 to C11 were cooler with lower VPD (Figs. 3 & 6). Near-surface warming and drying occurred in areas where fveg decreased. These results lend evidence to the notion that a reduction in summer fallow is responsible for the cooling and moistening trend that is observed across the NNAGP. The changes to temperature are stronger than the trends calculated by Bromley et al., (2020), noting that the trends in the latter are calculated from a 1970 starting point, whereas these experiments simulate fallow reduction from the 1980s to 2010s. Temperature trends are stronger at nearly –0.5 °C decade^{-1} (Bromley et al. 2020) when calculated using 1980 as a starting point, on the order of 1 – 1.5 °C, similar to modeled changes in T2 associated with an fveg increase from F11 to C11. The temperature difference simulated here spans from May until September, but given wheat is often harvested in August (if not sooner for the case of winter wheat), the September T2 difference is likely due to the parameterized seasonal surface fluxes for each land use category.

The winter warming in the C11 simulation relative to the F11 simulation is likely due to the changes in albedo from increased fveg in the model. Since the fveg does not change based on a seasonal cycle, areas with greater fveg are assumed to be lower in albedo since the vegetation is not covered in snow. The bare ground areas are covered in snow and thus are higher in albedo. This is similar to year round cover cropping and the winter warming effect has been noted in global climate models (Lombardozzi et al. 2018). The WRF simulated winter warming signal is less than the 3 °C change found by Lombardozzi et al., (2018) which was shown to be an overestimation (Hunter et al. 2019) due in part to the challenges in simulating snow advection and the tendency of vegetation to trap blowing snow (Pomeroy et al. 1998; Pomeroy and Li 2000). Snow interactions within land surface models are tricky and multiple modifications to the Noah-MP snow physics calculations were made by Liu et al., (2017), to create more realistic surface snow-precipitation interactions and spring melt profiles.

Plant stomatal function responds strongly to VPD at the leaf level. If VPD is too high, stomata will close to avoid evaporative water losses, effectively shutting off carbon uptake by plants (Eamus et al. 2013; Grossiord et al. 2020; Novick et al. 2016a). VPD is increasing on average across the United States, except for the U.S. portions of the NNAGP which are decreasing in VPD by an average of 0.5 kPa decade^{-1} (Bromley et al. 2020; Ficklin and Novick 2017). The VPD change for an increase in fveg from F11 to C11 is on the order of –0.45 kPa which corresponds to a first order with the observed changes to VPD in the NNAGP.

Our modeling analysis suggests that the impacts of simulated fallow reduction on near surface climate has acted to create more favorable conditions for crop growth by reducing growing season temperatures and VPD (Hsiao et al. 2019). Wheat yields are differentially sensitive to

temperature at various crop growth stages, with early season days with mean temperature > 28 °C especially detrimental (Asseng et al. 2015a). The Midwest of the United States has experienced similar outcomes of agricultural intensification leading to beneficial changes in near surface climate (Mueller et al. 2015b).

Boundary layer changes

The PBL by definition is the near surface layer of the atmosphere that is strongly influenced by surface fluxes of water and energy, so it is not surprising that the systematic shift away from summer fallow would affect PBL processes. The monthly mean boundary layer heights were higher in the F11 simulation where the fallow amounts were larger; the lowering of the PBL as fallow declines was proposed to be a consequence of the changes in energy partitioning from a fallow (bare) surface and a vegetated surface (Gameda et al. 2007) which was the case in these simulations (Figure 5). The change in PBL height assessed using a simple slab modeling approach with inputs from eddy covariance observations of turbulent fluxes from wheat and fallow fields (Vick et al., 2016). These simulations suggested an increase in PBL height of about 200 m during the growing season over a fallow field versus a spring wheat field, which is higher than the 60 m difference in mean monthly PBL heights simulated here, which is perhaps not surprising given that WRF simulates a spatial mix of fallow and vegetated areas whereas Vick et al. (2016) modeled PBL impacts of fallow and vegetation separately. PBL growth is sensitive to heterogeneous landscapes and the model representation of seasonal and diurnal variations is improved if the heterogeneity of surface fluxes are captured (Rey-Sanchez et al. 2021). Using a model similar to WRF, MM5, (Mahmood et al. 2011) found that simulations of bare soil were 1.4 °C warmer than

the control simulations (present day vegetation) and the seven-day average PBL heights were ~550 m higher. They also found moister and lower PBL and a lower LCL with a higher fveg fraction, which increased the probability of cloud development and convection (Mahmood et al. 2011). Our results are consistent with the notion that summer fallow changes PBL and LCL heights but its realized impact on precipitation was relatively small and spatially variable.

Precipitation

There is weak evidence that precipitation changed appreciably between F11 and C11, but there are small changes that give insight into land-precipitation feedback processes. Broadly speaking, the precipitation response early season and late season are opposite in sign, meaning summer fallow might act to increase precipitation early season when precipitation is energy limited in the NNAGP (Gerken et al., 2018) and decrease it in the late season when it is water limited. Precipitation in the NNAGP was found to be increasing by 8 mm decade^{-1} in May and June but July and August precipitation also increased, primarily on the eastern side of the NNAGP (Bromley et al. 2020). If summer fallow might act to increase precipitation in May and June, then there should be a negative trend in precipitation. If the land surface is not appreciably changing mean precipitation, what is the source for the observed warm season precipitation increase (Bromley et al. 2020)?

Global mean precipitation has been increasing due to anthropogenic warming of the atmosphere at about a rate of 2% K^{-1} (Held and Soden 2006; Pendergrass and Hartmann 2014). This rate comes from the thermodynamic change to precipitation, but does not account for changes to the dynamic components such as changes to circulation. Precipitation in the NNAGP is largest

in the early warm season and May through September is a convectively-active period in the NNAGP (Gerken et al. 2018c). Precipitation during this time period can take the form of stratiform rain, MCSs, and organized pre-frontal convection; July and August are quite dry compared to May and June and precipitation is primarily from MCSs. The Great Plains Low Level Jet (GPLLJ) is a nocturnal wind speed maximum, positioned at about 850 hPa, that transports moisture from the Gulf of Mexico into the Great Plains. July and August MCS development in the NNAGP is usually accompanied by a strong northward-penetrating GPLLJ (Feng et al. 2019; Song et al. 2019; Feng et al. 2016). To investigate the possibility that the observed increase in precipitation in the NNAGP is consistent with additional moisture sources from the south, we investigated meridional wind and specific humidity trends in ERA5. Figure 10a shows a vertical cross-section along the 42º latitude line of 1979-2020 trends in monthly mean meridional wind and specific humidity. Due to the lack of strong trends in meridional wind, meridional moisture transport trends are only slightly positive (Figure 10b). There is not a clear signature of a strengthening GPLLJ, but the increase in surface specific humidity corroborates Bromley et al., (2020) in that near-surface conditions are moistening during May and June. Trends in the North American Regional Reanalysis (NARR) dataset shows that moisture transport northward has increased during AMJ, particularly during days with MCS initiation (Feng et al. 2019; Barandiaran et al. 2013).

Most of the MCSs in the NNAGP occur during July and August, and the northward extension of the GPLLJ is very clear in monthly mean trends (Figure 11). Specific humidity has increased at 0.3 g kg^{-1} $decade^{-1}$ while meridional wind has increased at 0.35 m s^{-1} $decade^{-1}$. These trends are likely contributing to the observed increase in precipitation on the eastern and southern boundaries of the NNAGP during summer as well as the lower VPD during JJA (Bromley et al.,

2020). The magnitude of change to CAPE was on average larger in July and August, which could mean that there are interactions between the land surface change and the GPLLJ. An analysis that tracks MCSs and looks at changes to convective environments, e.g. Feng et al, (2016), could perhaps show how much the land surface impacts these processes.

5. Summary and Conclusions

Summer fallow in the NNAGP has declined from an estimated 151,900 km^2 in the 1980s to 35,100 km^2 in the 2010s, a decline of 116,800 km^2 which is approximately the land area of Pennsylvania. To investigate the climate impacts of this reduction in summer fallow, two three-year convection-permitting WRF simulations were performed, using ERA5 as the initial and lateral boundary conditions. The vegetation fraction of each simulation was adjusted using Landsat estimated summer fallow and nudged to match published agricultural statistics for 2011 and 1984. The intention of these simulations is to understand how the near surface climate and precipitation processes have been impacted by these substantial changes in land cover. The summary of the results are listed here:

- Where fveg increased between the fallow simulation and the control simulation, two-meter air temperatures were 1-1.5ºC cooler and VPD was 0.15 kPa lower.
- The PBL and LCL were lower by 60 m, due to the cooler and more humid land surface.
- CAPE changed by 20-30 J kg^{-1} but there were minimal changes to CIN.
- Precipitation did not change appreciably between the simulations, but the fallow simulation was 10-15 mm drier during July and August.

The results of these simulations suggest that observed near-surface cooling and moistening trends in the NNAGP are largely a result of the reduction in summer fallow. The lack of evidence for a change to precipitation stands in contrast to other observational studies focused on the same region, however, this is the first modeling study looking at summer fallow reduction. Further work is needed to better understand the precipitation result, perhaps tracking the evolution of precipitating storm systems as they move over the heterogeneous fallow landscape.

Tables

	1980s meteorology (‘84’)	2010s meteorology (‘11’)
1980s fallow	C84: 1980s meteorology + 1980s fallow estimate	F11: 2010s meteorology + 1980s fallow estimate
2010s fallow	F84: 1980s meteorology + 2010s fallow estimate	C11: 2010s meteorology + 2010s fallow

Table 1: Abbreviations and explanations for each model simulation.

Figures

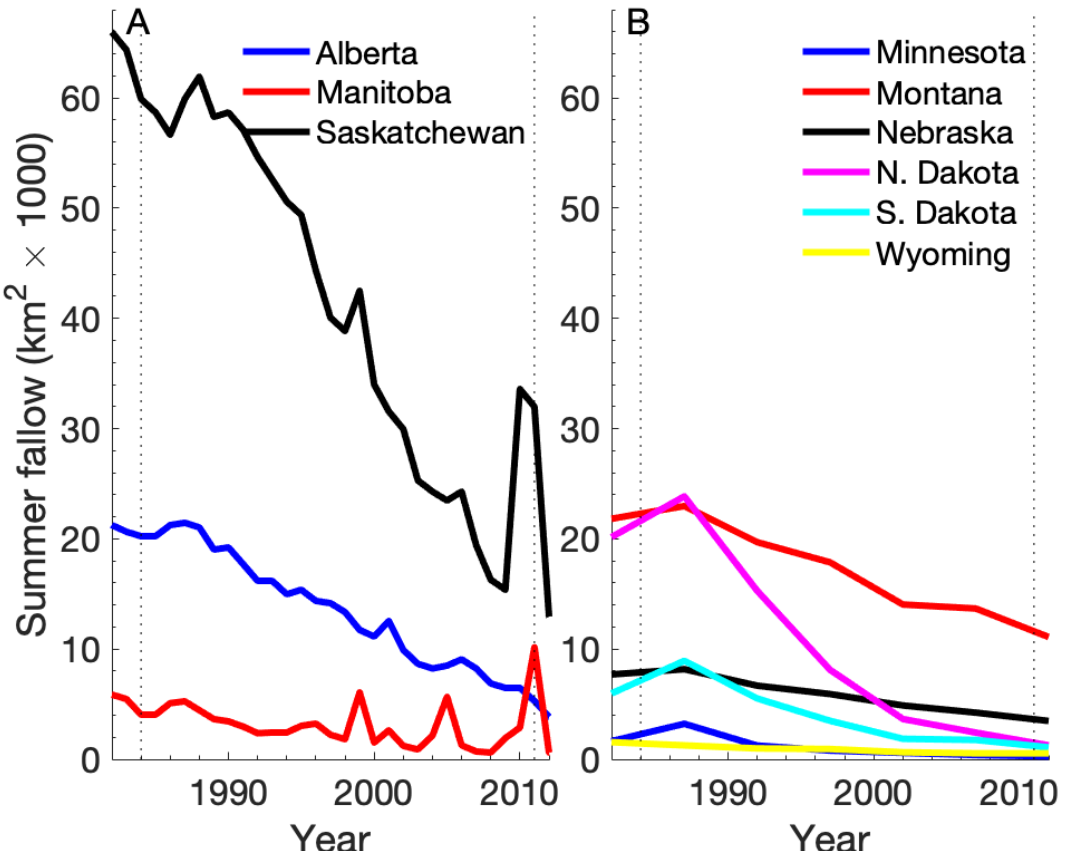


Figure 1: The area of land held in summer fallow in the (A) Canadian Prairie Provinces and (B) U.S. States of the northern North American Great Plains for the 1982 - 2012 period using data from Statistics Canada and the United States Department of Agriculture Economic Research Service following Vick et al. (2016). The primary study years, 1984 and 2011, are indicated with vertical dotted lines.

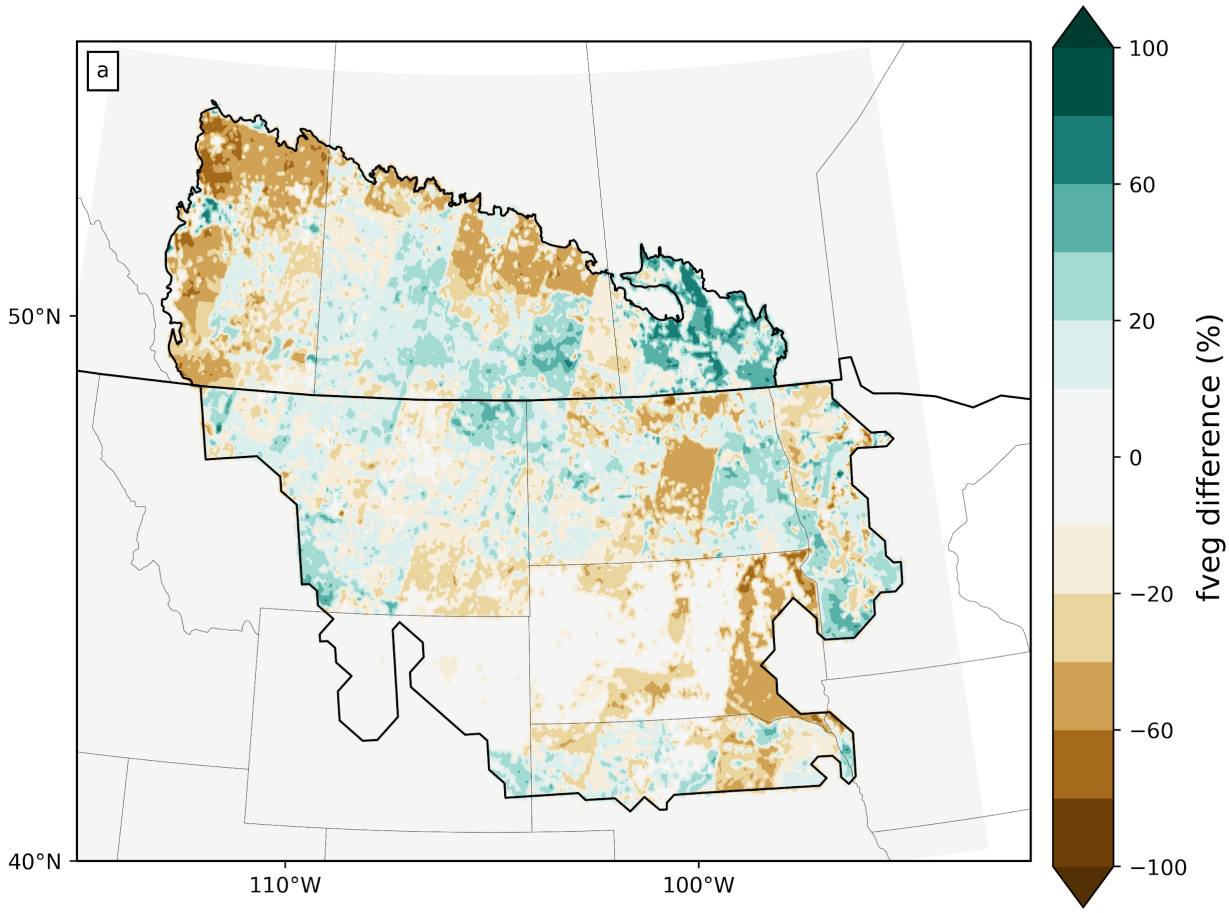


Figure 2: Differences between the 2010 fallow and 1984 vegetation fraction.

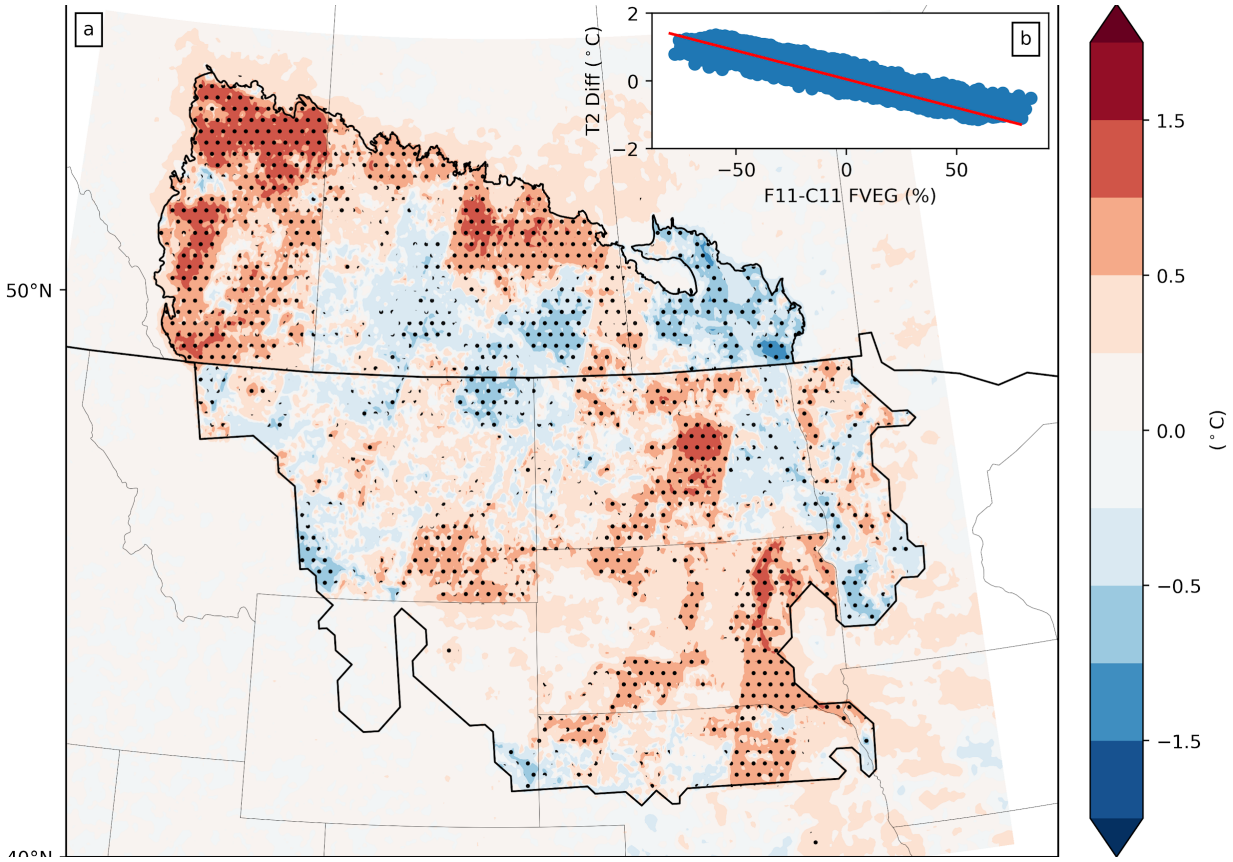


Figure 3: Two-meter temperature (T2) differences between modern (2011) fallow (F11) and control (C11) simulations averaged across the three-year simulations for MJJA.

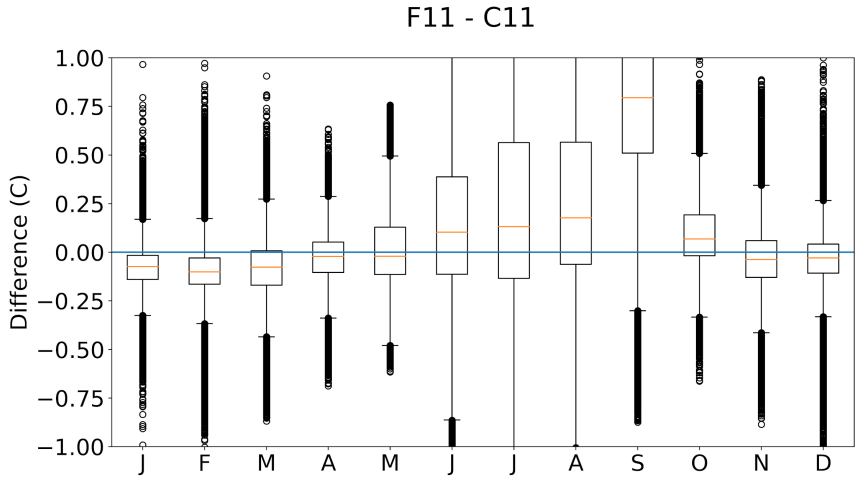


Figure 4: Monthly differences in T2 between F11 and C11. Positive values indicate the F11 simulation was warmer.

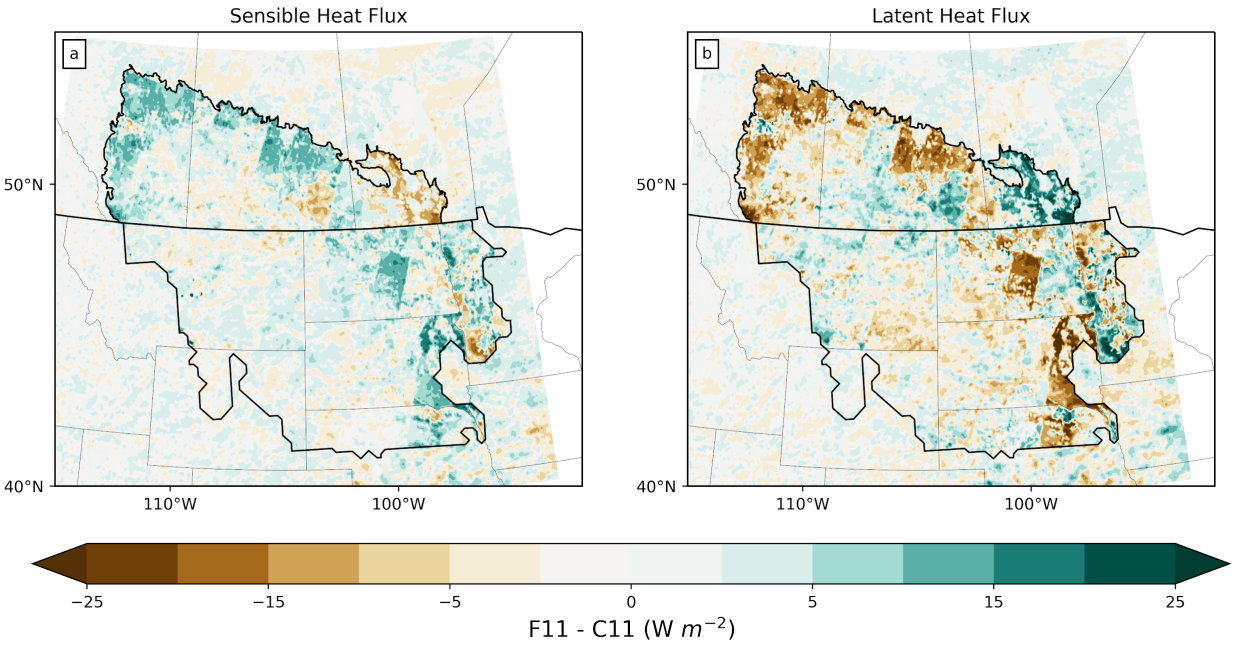


Figure 5: The difference in sensible (a) and latent (b) heat flux for MJJA between the F11 simulation and the C11 simulation.

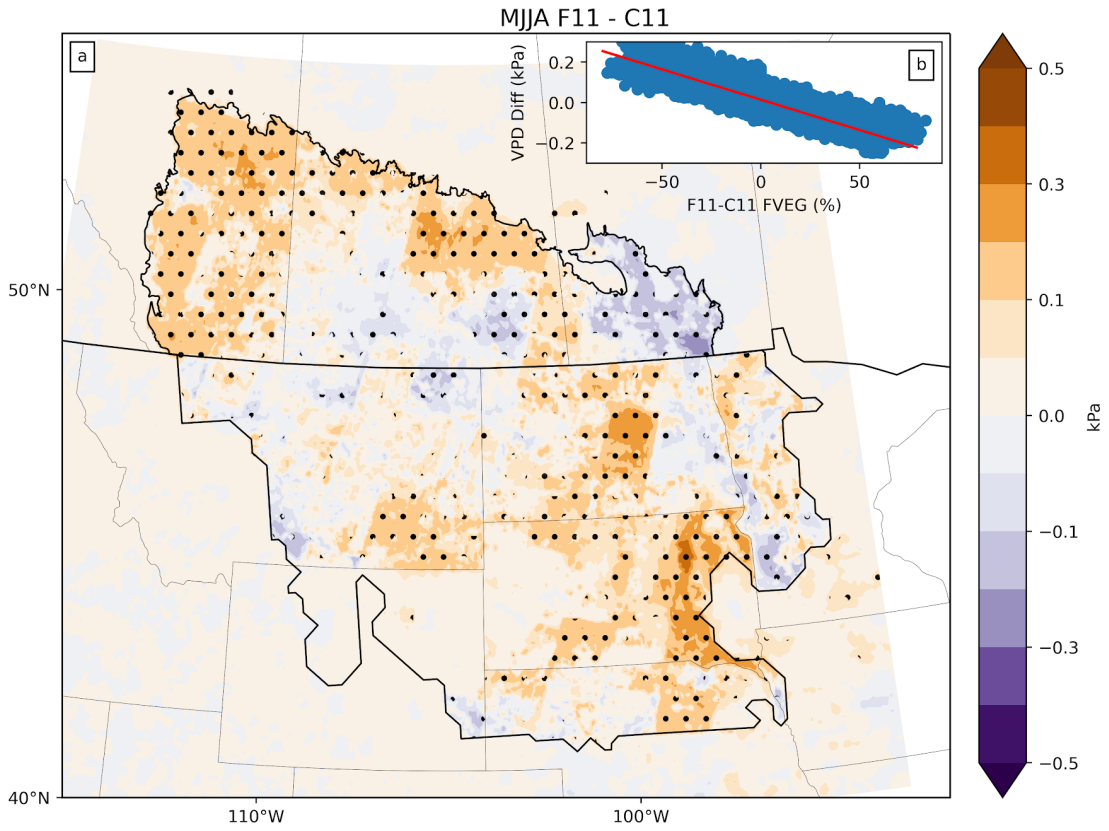


Figure 6: Two-meter vapor pressure deficit difference between the modern fallow (F11) and control (C11) simulations during the three-year simulation period for MJJA. Positive VPD values indicate the F11 simulation is drier, while negative values indicate the F11 simulation is moister.

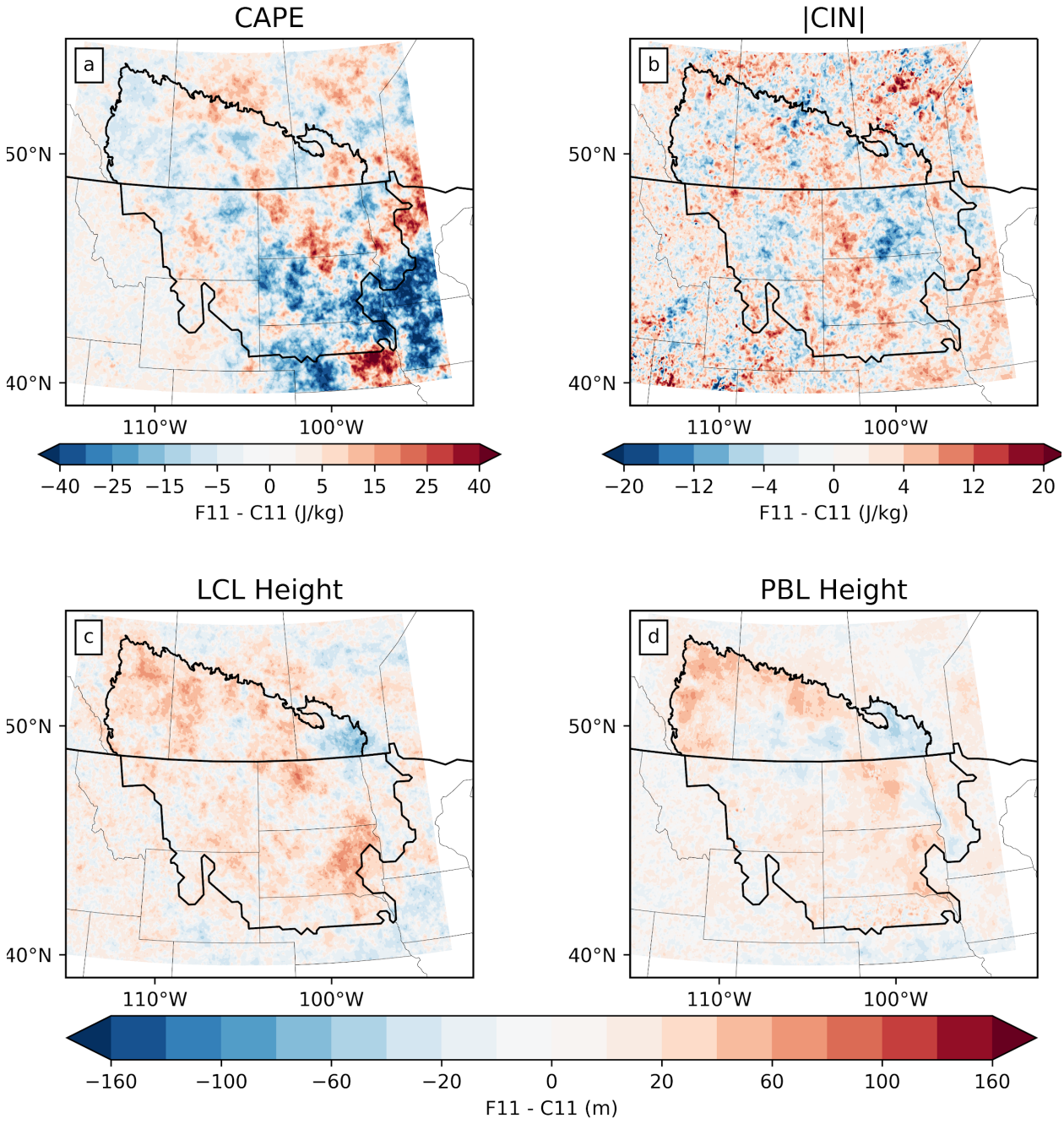


Figure 7: Changes to (a) convective available potential energy (CAPE), (b) convective inhibition (CIN), (c) lifted condensation level (LCL), and (d) planetary boundary layer (PBL) height between 2011 control and fallow simulations during May and June for the three-year simulation period.

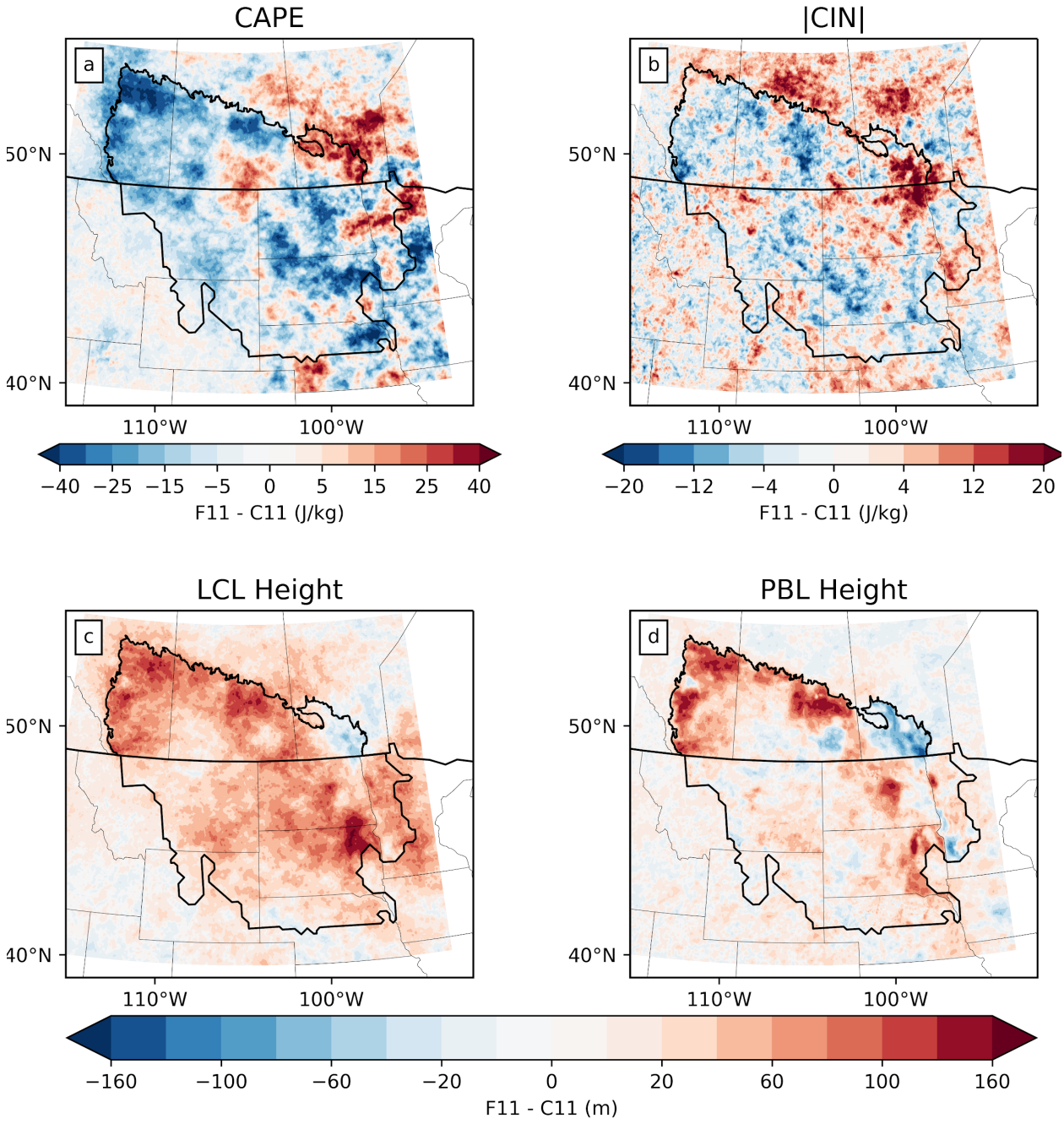


Figure 8: Same as Figure 6 but for July and August for the three-year simulation period.

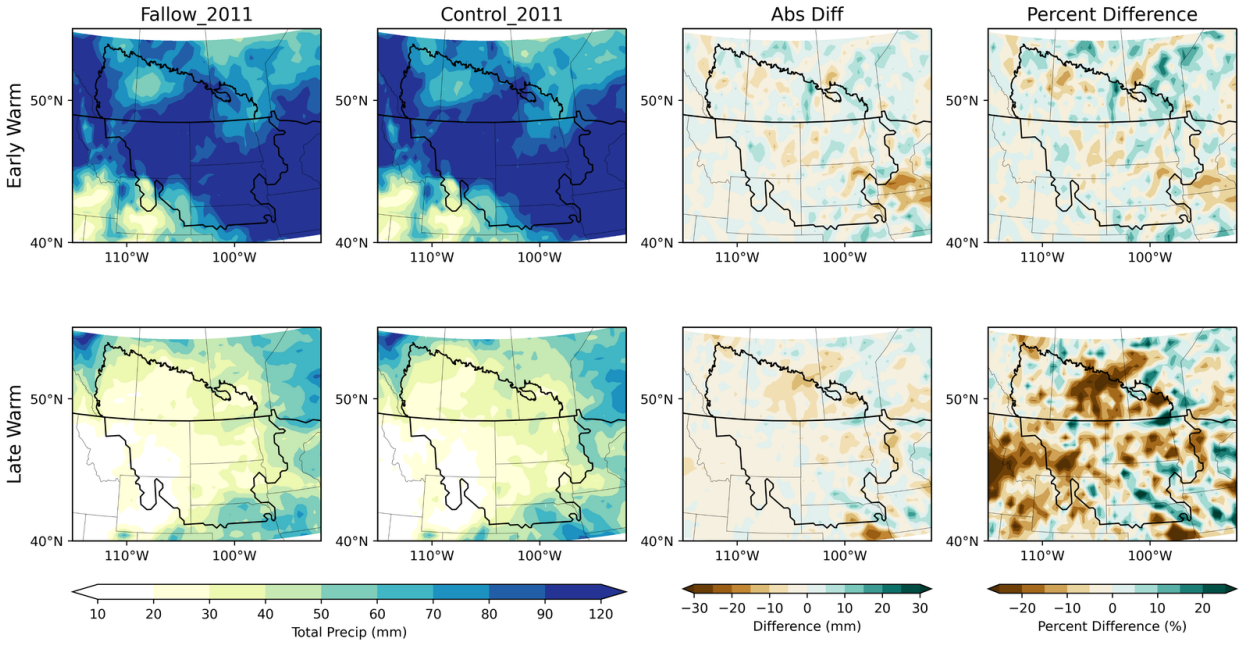


Figure 9: Changes to precipitation for May and June (Row 1) and July and August (Row 2). Precipitation was aggregated to 100km x 100km boxes to improve the signal to noise ratio.

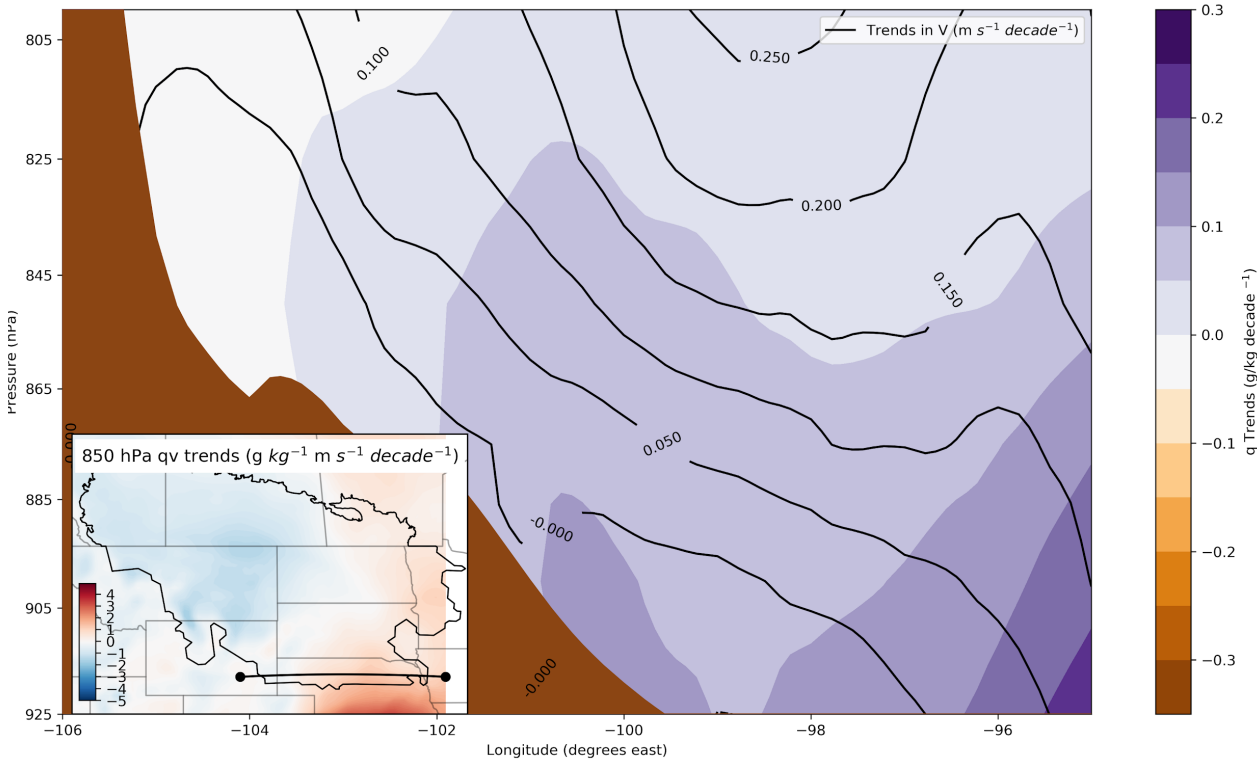


Figure 10: Vertical cross-section of 1979-2020 May and June meridional wind trends (black contours) and specific humidity trends (filled contours) for the levels between 925 hPa to 800 hPa . Inset axes show trends in meridional moisture transport (qv) for 1979-2020 and the location of the cross-section. Brown contour shows the pressure where topography is located along the cross section.

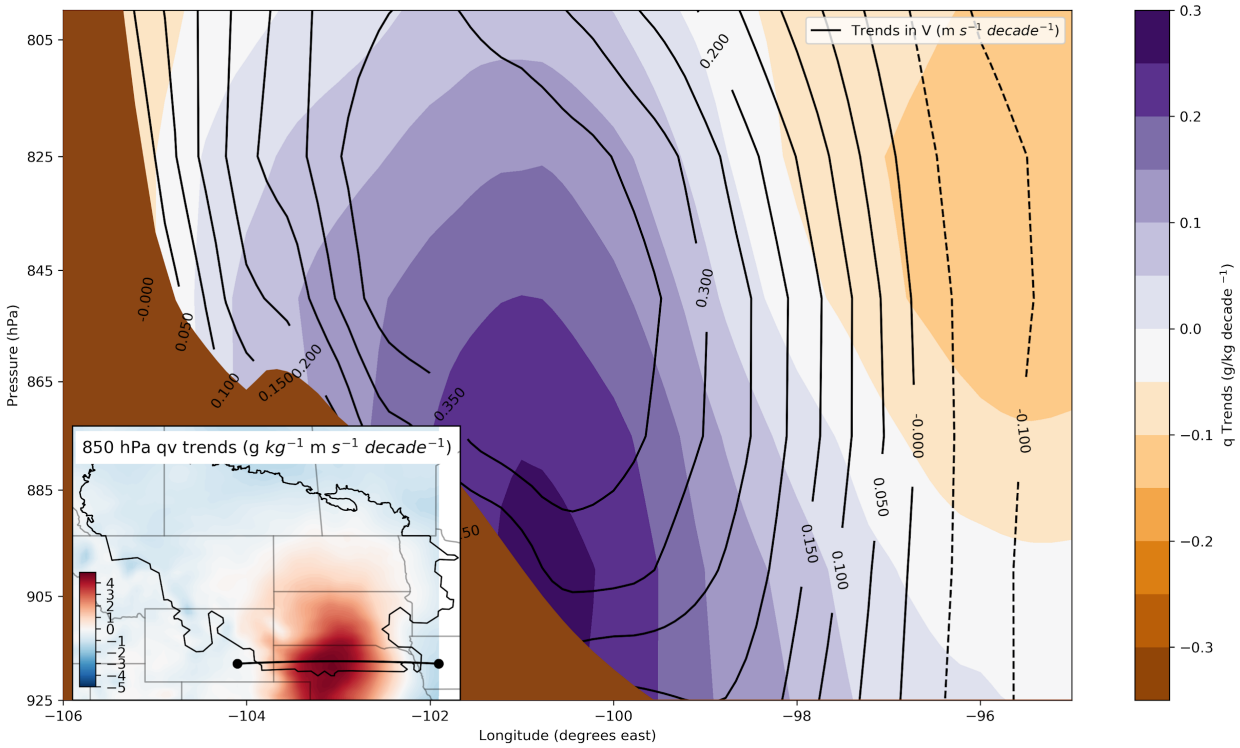


Figure 11: Same as Figure 10 but for July and August.

References

Agard, V., and K. Emanuel, 2017: Clausius–Clapeyron Scaling of Peak CAPE in Continental Convective Storm Environments. *J. Atmospheric Sci.*, **74**, 3043–3054, https://doi.org/10.1175/JAS-D-16-0352.1.

Asseng, S., and Coauthors, 2015: Rising temperatures reduce global wheat production. *Nat. Clim. Change*, **5**, 143–147, https://doi.org/10.1038/nclimate2470.

Barandiaran, D., S.-Y. Wang, and K. Hilburn, 2013: Observed trends in the Great Plains low-level jet and associated precipitation changes in relation to recent droughts. *Geophys. Res. Lett.*, **40**, 6247–6251, https://doi.org/10.1002/2013GL058296.

Barlage, M., F. Chen, R. Rasmussen, Z. Zhang, and G. Miguez-Macho, 2021: The Importance of Scale-Dependent Groundwater Processes in Land-Atmosphere Interactions Over the Central United States. *Geophys. Res. Lett.*, **48**, e2020GL092171, https://doi.org/10.1029/2020GL092171.

Betts, A. K., and R. L. Desjardins, 2018: Understanding Land–Atmosphere–Climate Coupling from the Canadian Prairie Dataset. *Environments*, **5**, 129, https://doi.org/10.3390/environments5120129.

——, R. Desjardins, and D. Worth, 2013a: Cloud radiative forcing of the diurnal cycle climate of the Canadian Prairies. *J. Geophys. Res. Atmospheres*, **118**, 8935–8953, https://doi.org/10.1002/jgrd.50593.

Betts, A. K., R. Desjardins, D. Worth, and D. Cerkowniak, 2013b: Impact of land use change on the diurnal cycle climate of the Canadian Prairies. *J. Geophys. Res. Atmospheres*, **118**, 11996–12011, https://doi.org/10.1002/2013JD020717.

Bromley, G. T., T. Gerken, A. F. Prein, and P. C. Stoy, 2020: Recent Trends in the Near-Surface Climatology of the Northern North American Great Plains. *J. Clim.*, **33**, 461–475, https://doi.org/10.1175/JCLI-D-19-0106.1.

Brookshire, E. N. J., P. C. Stoy, B. Currey, and B. Finney, 2020: The greening of the Northern Great Plains and its biogeochemical precursors. *Glob. Change Biol.*, **26**, 5404–5413, https://doi.org/10.1111/gcb.15115.

Carbone, R. E., and J. D. Tuttle, 2008: Rainfall Occurrence in the U.S. Warm Season: The Diurnal Cycle. *J. Clim.*, **21**, 4132–4146, https://doi.org/10.1175/2008JCLI2275.1.

Christensen, J. H., and Coauthors, 2007: Regional climate projections. Chapter 11.

Dolan, K. A., P. C. Stoy, and B. Poulter, 2020: Land management and climate change determine second-generation bioenergy potential of the US Northern Great Plains. *GCB Bioenergy*, **12**, 491–509, https://doi.org/10.1111/gcbb.12686.

Eamus, D., N. Boulain, J. Cleverly, and D. D. Breshears, 2013: Global change-type drought-induced tree mortality: vapor pressure deficit is more important than temperature per se in causing decline in tree health. *Ecol. Evol.*, **3**, 2711–2729, https://doi.org/10.1002/ece3.664.

Feng, Z., L. R. Leung, S. Hagos, R. A. Houze, C. D. Burleyson, and K. Balaguru, 2016: More frequent intense and long-lived storms dominate the springtime trend in central US rainfall. *Nat. Commun.*, **7**, 1–8, https://doi.org/10.1038/ncomms13429.

——, R. A. Houze, L. R. Leung, F. Song, J. C. Hardin, J. Wang, W. I. Gustafson, and C. R. Homeyer, 2019: Spatiotemporal Characteristics and Large-Scale Environments of Mesoscale Convective Systems East of the Rocky Mountains. *J. Clim.*, **32**, 7303–7328, https://doi.org/10.1175/JCLI-D-19-0137.1.

Ficklin, D. L., and K. A. Novick, 2017: Historic and projected changes in vapor pressure deficit suggest a continental-scale drying of the United States atmosphere. *J. Geophys. Res. Atmospheres*, **122**, 2061–2079, https://doi.org/10.1002/2016JD025855.

Flanagan, L. B., and A. C. Adkinson, 2011: Interacting controls on productivity in a northern Great Plains grassland and implications for response to ENSO events: CONTROLS ON GRASSLAND PRODUCTIVITY. *Glob. Change Biol.*, **17**, 3293–3311, https://doi.org/10.1111/j.1365-2486.2011.02461.x.

Gameda, S., B. Qian, C. A. Campbell, and R. L. Desjardins, 2007: Climatic trends associated with summerfallow in the Canadian Prairies. *Agric. For. Meteorol.*, **142**, 170–185, https://doi.org/10.1016/j.agrformet.2006.03.026.

Gerken, T., G. T. Bromley, and P. C. Stoy, 2018: Surface Moistening Trends in the Northern North American Great Plains Increase the Likelihood of Convective Initiation. *J. Hydrometeorol.*, **19**, 227–244, https://doi.org/10.1175/JHM-D-17-0117.1.

Grossiord, C., T. N. Buckley, L. A. Cernusak, K. A. Novick, B. Poulter, R. T. W. Siegwolf, J. S. Sperry, and N. G. McDowell, 2020: Plant responses to rising vapor pressure deficit. *New Phytol.*, **226**, 1550–1566, https://doi.org/10.1111/nph.16485.

Harris, C. R., and Coauthors, 2020: Array programming with NumPy. *Nature*, **585**, 357–362, https://doi.org/10.1038/s41586-020-2649-2.

Held, I. M., and B. J. Soden, 2006: Robust Responses of the Hydrological Cycle to Global Warming. *J. Clim.*, **19**, 5686–5699, https://doi.org/10.1175/JCLI3990.1.

Hersbach, H., and Coauthors, 2020: The ERA5 global reanalysis. *Q. J. R. Meteorol. Soc.*, **146**, 1999–2049, https://doi.org/10.1002/qj.3803.

Homer, C., and Coauthors, 2015: Completion of the 2011 National Land Cover Database for the Conterminous United States - Representing a Decade of Land Cover Change Information. *Photogramm. Eng. Remote Sens.*, **81**, 346–354, https://doi.org/10.14358/PERS.81.5.345.

Hoyer, S., and J. Hamman, 2017: xarray: N-D labeled arrays and datasets in Python. *J. Open Res. Softw.*, **5**, https://doi.org/10.5334/jors.148.

Hsiao, J., A. L. S. Swann, and S.-H. Kim, 2019: Maize yield under a changing climate: The hidden role of vapor pressure deficit. *Agric. For. Meteorol.*, **279**, 107692, https://doi.org/10.1016/j.agrformet.2019.107692.

Hunter, J. D., 2007: Matplotlib: A 2D graphics environment. *Comput. Sci. Eng.*, **9**, 90–95, https://doi.org/10.1109/MCSE.2007.55.

Hunter, M. C., C. M. White, J. P. Kaye, and A. R. Kemanian, 2019: Ground-Truthing a Recent Report of Cover Crop–Induced Winter Warming. *Agric. Environ. Lett.*, **4**, 190007, https://doi.org/10.2134/ael2019.03.0007.

Juang, J. Y., G. G. Katul, A. Porporato, P. C. Stoy, M. S. Siqueira, M. Detto, H. S. Kim, and R. Oren, 2007: Eco-hydrological controls on summertime convective rainfall triggers. *Glob. Change Biol.*, **13**, 887–896, https://doi.org/10.1111/j.1365-2486.2007.01315.x.

Ladwig, B., 2017: *wrf-python*. UCAR/NCAR,.

Liu, C., and Coauthors, 2017: Continental-scale convection-permitting modeling of the current and future climate of North America. *Clim. Dyn.*, **49**, 71–95, https://doi.org/10.1007/s00382-016-3327-9.

Lombardozzi, D. L., G. B. Bonan, W. Wieder, A. S. Grandy, C. Morris, and D. L. Lawrence, 2018: Cover Crops May Cause Winter Warming in Snow-Covered Regions. *Geophys. Res. Lett.*, **45**, 9889–9897, https://doi.org/10.1029/2018GL079000.

Long, J. A., R. L. Lawrence, P. R. Miller, L. A. Marshall, and M. C. Greenwood, 2014: Adoption of cropping sequences in northeast Montana: A spatio-temporal analysis. *Agric. Ecosyst. Environ.*, **197**, 77–87, https://doi.org/10.1016/j.agee.2014.07.022.

López, J., D. A. Way, and W. Sadok, 2021: Systemic effects of rising atmospheric vapor pressure deficit on plant physiology and productivity. *Glob. Change Biol.*, gcb.15548, https://doi.org/10.1111/gcb.15548.

Luyssaert, S., and Coauthors, 2014: Land management and land-cover change have impacts of similar magnitude on surface temperature. *Nat. Clim. Change*, **4**, 389–393, https://doi.org/10.1038/nclimate2196.

Maaz, T., J. D. Wulfhorst, V. McCracken, J. Kirkegaard, D. R. Huggins, I. Roth, H. Kaur, and W. Pan, 2018: Economic, policy, and social trends and challenges of introducing oilseed

and pulse crops into dryland wheat cropping systems. *Agric. Ecosyst. Environ.*, **253**, 177–194, https://doi.org/10.1016/j.agee.2017.03.018.

Mahmood, R., R. Leeper, and A. I. Quintanar, 2011: Sensitivity of planetary boundary layer atmosphere to historical and future changes of land use/land cover, vegetation fraction, and soil moisture in Western Kentucky, USA. *Glob. Planet. Change*, **78**, 36–53, https://doi.org/10.1016/j.gloplacha.2011.05.007.

——, and Coauthors, 2014: Land cover changes and their biogeophysical effects on climate. *Int. J. Climatol.*, **34**, 929–953, https://doi.org/10.1002/joc.3736.

Mande, T., N. C. Ceperley, G. G. Katul, S. W. Tyler, H. Yacouba, and M. B. Parlange, 2015: Suppressed convective rainfall by agricultural expansion in southeastern Burkina Faso. *Water Resour. Res.*, **51**, 5521–5530, https://doi.org/10.1002/2015WR017144.

Marshall, C. H., R. A. Pielke, and L. T. Steyaert, 2003: Crop freezes and land-use change in Florida. *Nature*, **426**, 29–30, https://doi.org/10.1038/426029a.

Miller, P. R., and Coauthors, 2002: Pulse Crop Adaptation in the Northern Great Plains. *Agron. J.*, **94**, 261–272, https://doi.org/10.2134/agronj2002.2610.

Miller, P. R., Y. Gan, B. G. McConkey, and C. L. McDonald, 2003: Pulse Crops for the Northern Great Plains: I. Grain Productivity and Residual Effects on Soil Water and Nitrogen. *Agron. J.*, **95**, 972–979, https://doi.org/10.2134/agronj2003.9720.

Mueller, N. D., E. E. Butler, K. A. Mckinnon, A. Rhines, M. Tingley, N. M. Holbrook, and P. Huybers, 2015: Cooling of US Midwest summer temperature extremes from cropland intensification. https://doi.org/10.1038/NCLIMATE2825.

Niu, G.-Y., and Coauthors, 2011: The community Noah land surface model with multiparameterization options (Noah-MP): 1. Model description and evaluation with local-scale measurements. *J. Geophys. Res. Atmospheres*, **116**, https://doi.org/10.1029/2010JD015139.

Novick, K. A., and Coauthors, 2016: The increasing importance of atmospheric demand for ecosystem water and carbon fluxes. *Nat. Clim. Change*, **6**, 1023–1027, https://doi.org/10.1038/nclimate3114.

O'Gorman, P. A., and T. Schneider, 2009: The physical basis for increases in precipitation extremes in simulations of 21st-century climate change. *Proc. Natl. Acad. Sci.*, **106**, 14773–14777, https://doi.org/10.1073/pnas.0907610106.

Pendergrass, A. G., and D. L. Hartmann, 2014: The Atmospheric Energy Constraint on Global-Mean Precipitation Change. *J. Clim.*, **27**, 757–768, https://doi.org/10.1175/JCLI-D-13-00163.1.

Pomeroy, J. W., and L. Li, 2000: Prairie and arctic areal snow cover mass balance using a blowing snow model. *J. Geophys. Res. Atmospheres*, **105**, 26619–26634, https://doi.org/10.1029/2000JD900149.

——, D. M. Gray, K. R. Shook, B. Toth, R. L. H. Essery, A. Pietroniro, and N. Hedstrom, 1998: An evaluation of snow accumulation and ablation processes for land surface modelling. *Hydrol. Process.*, **12**, 2339–2367, https://doi.org/10.1002/(SICI)1099-1085(199812)12:15<2339::AID-HYP800>3.0.CO;2-L.

Raddatz, R. L., 1998: Anthropogenic vegetation transformation and the potential for deep convection on the Canadian prairies. *Can. J. Soil Sci.*, **78**, 657–666, https://doi.org/10.4141/S98-011.

Rey-Sanchez, C., and Coauthors, 2021: Evaluation of Atmospheric Boundary Layer Height From Wind Profiling Radar and Slab Models and Its Responses to Seasonality of Land Cover, Subsidence, and Advection. *J. Geophys. Res. Atmospheres*, **126**, e2020JD033775, https://doi.org/10.1029/2020JD033775.

Rosenzweig, S. T., and M. E. Schipanski, 2019: Landscape-scale cropping changes in the High Plains: economic and environmental implications. *Environ. Res. Lett.*, **14**, 124088, https://doi.org/10.1088/1748-9326/ab5e8b.

Roundy, J. K., C. R. Ferguson, and E. F. Wood, 2013: Temporal Variability of Land–Atmosphere Coupling and Its Implications for Drought over the Southeast United States. *J. Hydrometeorol.*, **14**, 622–635, https://doi.org/10.1175/JHM-D-12-090.1.

Schulzweida, U., 2019: CDO User Guide. https://doi.org/10.5281/ZENODO.3539275.

Seabold, S., and J. Perktold, 2010: Statsmodels: Econometric and Statistical Modeling with Python. *Proc. 9th Python Sci. Conf.*, **2010**.

Shrestha, B. M., R. L. Raddatz, R. L. Desjardins, and D. E. Worth, 2012: Continuous Cropping and Moist Deep Convection on the Canadian Prairies. *Atmosphere*, **3**, 573–590, https://doi.org/10.3390/atmos3040573.

Skamarock, W. C., and Coauthors, 2008: A description of the advanced research WRF version 3, NCAR Technical Note. *Natl. Cent. Atmospheric Res. Boulder CO USA*,.

Song, F., Z. Feng, L. R. Leung, R. A. Houze Jr, J. Wang, J. Hardin, and C. R. Homeyer, 2019: Contrasting Spring and Summer Large-Scale Environments Associated with Mesoscale Convective Systems over the U.S. Great Plains. *J. Clim.*, **32**, 6749–6767, https://doi.org/10.1175/JCLI-D-18-0839.1.

Song, X.-P., M. C. Hansen, S. V. Stehman, P. V. Potapov, A. Tyukavina, E. F. Vermote, and J. R. Townshend, 2018: Global land change from 1982 to 2016. *Nature*, **560**, 639–643, https://doi.org/10.1038/s41586-018-0411-9.

Stadnyk, T., K. Dow, L. Wazney, and E.-L. Blais, 2016: The 2011 flood event in the Red River Basin: Causes, assessment and damages. *Can. Water Resour. J. Rev. Can. Ressour. Hydr.*, **41**, 65–73, https://doi.org/10.1080/07011784.2015.1008048.

Stocker, T., D. Qin, G. Plattner, and M. Tignor, 2014: *Climate Change 2013 The Physical Science Basis*.

Stoy, P. C., and Coauthors, 2018: Opportunities and Trade-offs among BECCS and the Food, Water, Energy, Biodiversity, and Social Systems Nexus at Regional Scales. *BioScience*, **68**, 100–111, https://doi.org/10.1093/biosci/bix145.

Vick, E. S. K., P. C. Stoy, A. C. I. Tang, and T. Gerken, 2016: The surface-atmosphere exchange of carbon dioxide, water, and sensible heat across a dryland wheat-fallow rotation. *Agric. Ecosyst. Environ.*, **232**, 129–140, https://doi.org/10.1016/j.agee.2016.07.018.

Wang, Y., B. Geerts, and C. Liu, 2018: A 30-year convection-permitting regional climate simulation over the interior western United States. Part I: Validation. *Int. J. Climatol.*, **38**, 3684–3704, https://doi.org/10.1002/joc.5527.

CHAPTER FIVE

RECENT ENHANCEMENT OF THERMODYNAMIC ENVIRONMENTS IN THE NORTHERN NORTH AMERICAN GREAT PLAINS

Contribution of Authors and Co-Authors

Manuscript in Chapter 5

Author: Gabriel T. Bromley
Contributions: Acquired and analyzed data, wrote first draft of the manuscript.

Co-Author: Andreas Prein
Contributions: Provided feedback on analysis methods, edited the manuscript.

Co-Author: Paul C. Stoy
Contributions: Conceived of the study, obtained funding, provided feedback on the analysis, edited the manuscript at all stages.

Manuscript Information

Gabriel T. Bromley, Andreas Prein, and Paul C. Stoy
Geophysical Research Letters

Status of Manuscript:
__X__ Prepared for submission to a peer-reviewed journal
____ Officially submitted to a peer-reviewed journal
____ Accepted by a peer-reviewed journal
____ Published in a peer-reviewed journal

American Geophysical Union

CHAPTER FIVE

RECENT ENHANCEMENT OF THERMODYNAMIC ENVIRONMENTS IN THE NORTHERN NORTH AMERICAN GREAT PLAINS

Key Points:

- **Mean annual CAPE has increased by 45 J kg^{-1} since the 1980s, with larger changes during summer.**
- **Monthly maximum CAPE distributions are shifting in favor of higher values.**
- **Future changes in CAPE are underestimated by climate models due to the difficulty of capturing changes to the Great Plains Low Level Jet.**

Abstract

Convective available potential energy (CAPE) is central to strong organized convection, such as mesoscale convective systems (MCS), and associated precipitation extremes. The northern North American Great Plains (NNAGP) are the origin of many eastward-propagating MCSs but are relatively understudied compared to the more convectively active southern and central Great Plains. Here we show that mean CAPE has increased by 45 J kg^{-1} since the 1980s at two sounding locations, Glasgow, MT (GGW) and Bismarck, ND (BIS), within the NNAGP. There has been a ~250% increase since the 1980s in the proportion of monthly maximum CAPE above 2500 J kg^{-1} at BIS and likewise for values above 1200 J kg^{-1} at GGW. Climate simulations of CAPE in the NNAGP likely underestimate its future changes due to the difficult nature of capturing the Great Plains Low Level Jet with climate models.

1 Introduction

The northern North American Great Plains (NNAGP), made up of the northern U.S. Plains and the Canadian Prairies, are a semi-arid region consisting mostly of agriculture, grasslands, and rangelands. This region has undergone substantial land use change over the past five decades by which 250,000 km^2 of agricultural land transitioned from summer fallow to planted fields; resulting in a cooler and more humid land surface (Vick et al. 2016; Gameda et al. 2007) and

increased likelihood of convective precipitation (Gerken et al., 2018). Near-surface temperatures have cooled by –0.2 °C decade^{-1} and a moistening trend has lowered vapor pressure deficit - important for plant carbon uptake and crop yields (López et al.) - by 0.15 kPa since 1970 (Bromley et al. 2020; Ficklin and Novick 2017; Betts et al. 2013c). A lowering of the Bowen ratio during the warm season has suppressed planetary boundary layer (PBL) and lifted condensation levels (LCL) heights across the NNAGP, leading to an increase in cloud cover (Betts et al. 2013c; Betts and Desjardins 2018). The likelihood of convective precipitation has increased based on evidence from slab PBL models over parts of the NNAGP (Gerken et al. 2018c; Raddatz 1998b) but it remains unclear exactly how, and if, convective processes across the entire region are impacted by changing land use patterns *versus* mechanisms consistent with global climate change.

Precipitation has increased in the NNAGP by 6-10 mm decade^{-1} since 1970 during the warm season (Bromley et al., 2020). Convective activity has increased during this time period, too (Bromley et al. 2020; Hanesiak et al. 2004; Shrestha et al. 2012), suggesting that the increase in precipitation is convectively driven. A shallower and more humid boundary layer that has resulted from land cover change (Chapter 3, this volume) might act to enrich the environment for organized convection such as mesoscale convective systems (MCSs). MCSs are responsible for 40-60% of warm-season precipitation that falls in the NNAGP (Carbone and Tuttle 2008; Feng et al. 2019) and relatively small increases in their likelihood will have relatively large impacts on dryland agriculture in this globally-important region for wheat, pulse, and oilseed production (Nielsen et al. 2005; Lauenroth et al. 2000). During spring and summer, MCSs often form in the NNAGP and propagate eastward overnight, supported by the Great Plains Low Level Jet (GPLLJ) (Feng et al. 2019). MCS rainfall intensities are increasing in the U.S. portion of the NNAGP and a greater

proportion of rainfall is coming from MCSs, owing partly to a northward extension over time of the GPLLJ into the southern portion of the NNAGP (Feng et al. 2016; Barandiaran et al. 2013).

Extreme precipitation associated with flash flooding and other damaging convective weather (Dougherty and Rasmussen 2019) also comes primarily from MCSs in the NNAGP (Stevenson and Schumacher 2014), and has been increasing with warming temperatures (Kunkel 2003; Trenberth et al. 2003; O'Gorman and Schneider 2009). Both extreme precipitation and MCS strength is heavily influenced by convective available potential energy (CAPE), with both extreme precipitation and CAPE scaling with the Clausius-Clapeyron relationship (Prein et al. 2017d,c; Lepore et al. 2015). Large values of CAPE are associated with hazardous convective weather, and understanding the factors that influence CAPE can inform our understanding of extreme precipitation.

CAPE and its counterpart convective inhibition (CIN) are useful metrics in understanding the potency of a thermodynamic environment for convection. CAPE and CIN are expected to increase with global warming due to the increase in temperatures and near surface humidity (Seeley and Romps 2014, 2015; Diffenbaugh et al. 2013; Rasmussen et al. 2017; Chen et al. 2020), but trends in CAPE and CIN in the NNAGP in response to unique warm-season cooling and moistening trends (Bromley et al., 2020) have not been quantified to date. The buildup of CAPE occurs primarily through two different mechanisms; the advection of warm and moist air into an area, and diabatic heating at the surface (Agard and Emanuel 2017). An intensifying GPLLJ would inject high-enthalpy air further into the NNAGP, while land use change might amplify the diabaticly driven destabilization of the atmosphere from the surface, acting to amplify the change

from global warming. The observed increase in moisture transport from the GPLLJ is expected to continue in response to climate change (Tang et al. 2017; Cook et al. 2008), suggesting that mechanisms underlying ongoing trends in convective environments must be understood to predict future changes. It remains unclear, however, how the thermodynamic environments of these convective storms are changing in response to the combined impacts of land use change and the intensification of the GPLLJ, and therefore, how they might continue to change in the future.

Here, we apply radiosonde, reanalysis, and climate model observations to study the changing convective environment of the NNAGP. Our goal is to characterize ongoing changes in CAPE and CIN in this relatively understudied region and discern how the future thermodynamic environments compare to recent observations.

2 Materials and Methods

2.1 *Observational and Reanalysis Data*

Twice-daily atmospheric sounding profiles were acquired for 1980-2020 from the Integrated Global Radiosonde Archive for two locations, Glasgow, MT, and Bismarck, ND. These locations were selected as the only sounding locations within the NNAGP that have a sufficiently long data record and are not subject to orographic effects. Both 00UTC and 12UTC soundings were utilized in the analysis. Data that did not pass the Tier 2 climatological checks were removed from the analysis. CAPE and CIN are calculated using the MetPy (May et al. 2016) "most_unstable_cape_cin" function. This function utilizes a profile from the layer with the highest potential temperature and then integrates CAPE between the level of free convection (LFC) and the equilibrium level (EL). CIN is integrated between the surface and the LFC. Warm season monthly maximum CAPE is modeled using a generalized extreme value distribution, parameters

for which were fit using the Scipy Stats package and the 'genextreme' function. The function chooses the generalized extreme value distribution, either Weibull or Gumbel, that best fits the data, to focus on model fit rather than assume a functional form for the distribution.

ERA5 is a high-resolution ($\Delta x \cong 31$ km) reanalysis dataset that uses the ECMWF model to integrate historical observations into continuous fields (Hersbach et al.). Monthly mean data were acquired from the Copernicus Climate Data Store. CAPE in ERA5 is calculated by lifting parcels from different model levels and retaining the maximum value. This approach is conceptually similar to the most unstable CAPE calculations performed by MetPy. Our analysis is limited to the convective season (Gerken et al., 2018) for the CAPE and moisture transport trend calculations. A robust linear regression was used for trends to reduce the effect of outliers. We define the 'northern North American Great Plains' (NNAGP) following Bromley et al. (2020) as the combination of the Canadian Prairie Province ecozone and the National Ecological Observation Network (NEON) Domain 9 (Northern Plains) in the United States.

2.2 *Simulation Data*

Data from a convection-permitting simulation of most of North America was used to assess current convective environments and understand future environments. The Weather Research and Forecasting model 3.4.1 was run with 4 km horizontal grid spacing and 51 vertical levels for 13-years from October 2000 to October 2013 (Liu et al. 2017). The fine resolutions ≤ 4 km grid spacing can explicitly resolve organized convection, such as MCSs, but will not capture smaller mesoscale circulations. The Rapid Radiative Transfer model (RRTMG), Yonsei University boundary layer model, and Thompson aerosol-aware microphysics scheme were used, as was Noah-MP as the land surface model which included a groundwater scheme known to reduce

summer temperature and precipitation biases (Barlage et al. 2021). Two simulations were run, one that represents a control simulation of the 2000-2013 time period (CTRL) and the other that represents a 'pseudo global warming' (PGW) experiment. The CTRL simulation uses six-hourly ERA-Interim data as lateral boundary conditions. The PGW simulation utilizes the same ERA-Interim data but with the CMIP5 ensemble mean climate change signal added for the RCP 8.5 emissions scenario. Nineteen ensemble members are averaged together for the 2070-2100 and 1976-2005 periods, with a perturbation field generated by taking their difference. This perturbation is then added onto the 2000-2013 ERA-Interim data. This synthetic climate change signal increases mean temperature by ~ 4 °C and relative humidity by 2-6% depending on the season (Liu et al. 2017). Since the PGW approach uses a mean climate change signal added to ERA-Interim, the goal for the experiment is to better understand the thermodynamic impacts resulting from anthropogenic warming; changes to circulation are not accounted for. A more detailed description of the model, experimental design and model validation can be found in Liu et al. (2017).

The CTRL simulation was assessed by Liu et al., (2017) and others for mean climate and how well it represents extreme precipitation and the structure of MCSs. In both cases, the model reproduces realistic precipitation distributions and MCSs, but MCS frequency is underestimated in late summer (Prein et al. 2017a,d). Vertical profiles of temperature, pressure, and mixing ratio from the model were extracted for the GGW and BIS locations using a nearest-neighbor lookup. CAPE and CIN were calculated using the "most_unstable_cape_cin" function from the MetPy python package as noted and compared against radiosonde observations.

3 Results

3.1.1 Recent and future changes to thermodynamic environments: CAPE

For both GGW and BIS, radiosonde-measured CAPE distributions have shifted toward the tails, indicating that occurrences of large CAPE values have increased in frequency in more recent decades (Figure 1). Mean CAPE at GGW has doubled from 45 J kg^{-1} to 90 J kg^{-1} between 1980-1990 and 2010-2020 (Figure 1a). The decadal distributions show that the frequency of observations larger than 1000 J kg^{-1} increased from the 1980s to the 2010s by ~250% with smaller differences between the 2000s and 2010s. The distribution of CAPE simulated by the convection-permitting CTRL simulation underestimates the frequency of CAPE values > 1200 J kg^{-1}. The simulated mean CAPE is 27 J kg^{-1}, which is ~22 J kg^{-1} lower than the 1980s mean value. The PGW simulation shows a mean CAPE of 49 J kg^{-1} which is close to the 1980s mean. The PGW distribution also closely matches the 1980s observations but under-represents the extreme occurrences of CAPE > 2000 J kg^{-1}.

Mean CAPE at BIS also increased by 45 J kg^{-1} from a mean of 115 J kg^{-1} to 160 J kg^{-1} between the 1980s to the 2010s (Figure 1b). Similar to GGW, the distributions deviate from one another at about 2000 J kg^{-1}, with the 2010s 276% more likely to have CAPE > 2000 J kg^{-1} than the 1980s. BIS has a higher mean CAPE than GGW and also experiences more events greater than 2000 J kg^{-1}. The CTRL and PGW simulations underestimate CAPE compared to the observed CAPE in the 1980s; mean CAPE for the CTRL simulation is 25 J kg^{-1} and 47 J kg^{-1} for the PGW simulation noting that the PGW simulation is designed to simulate conditions at the end of the 21st century.

The pattern in monthly maximum CAPE is similar to the change to mean CAPE. GGW maximum CAPE distributions have shifted toward higher values at the expense of low to moderate CAPE

values (Figure 2a). At GGW, the mean monthly maximum CAPE was ~1000 J kg^{-1} in the 1980s and is now ~1750 J kg^{-1}. There has been a substantial fattening of the tails of the distribution with CAPE above 1200 J kg^{-1} making up a much larger percentage in recent decades (69%) compared to the 1980s and 1990s (28%). The CTRL mean monthly maximum for GGW is 750 J kg^{-1} which is 25% lower than the observed 1980s mean monthly maximum. The PGW simulation has a mean maximum monthly CAPE of 1000 J kg^{-1} which matches the mean radiosonde-observed monthly maximum CAPE from the 1980s. The distributional change from CTRL to the PGW does show a fattening of the tails, however they both more closely match the distributions from the 1980s and 1990s than the 2000s and 2010s.

BIS is further east and is more humid than GGW and its monthly maximum CAPE distribution is broader. The mean monthly max CAPE for the 1980s is ~1600 J kg $^{-1}$ and increases to ~2450 J kg^{-1} in the 2010s. The tails of the 2000s and 2010s distributions are larger for values over 2500 J kg^{-1}. The probability of a monthly maximum CAPE value over 2500 J kg^{-1} increased by 277% from the 1980s to the 2010s and 129% from the 1990s to the 2010s. The CTRL and PGW simulations underestimate CAPE > 1500 J kg^{-1} and overestimate values less than that. The probability of monthly maximum CAPE > 2500 J kg^{-1} increases by 129% between the CTRL and the PGW simulation.

3.1.2 Recent and future changes to thermodynamic environments: CIN

Mean CIN distributions for the different decades are similar to each other at both GGW and BIS (Figure 3). The mean magnitude of CIN at GGW increased from 16 J kg^{-1} in the 1980s to 24 J kg^{-1} in the 2010s (Figure 3a). The CTRL mean CIN is 14 J kg^{-1} and increases to 25 J kg^{-1} in the PGW

simulation. Mean CIN at BIS in the 1980s was 26 J kg^{-1} and increased to 28.5 J kg^{-1} in the 2010s. The CTRL simulation mean CIN (21 J kg^{-1}) is lower than the observed 1980s CIN, and CIN in the PGW simulation at BIS strengthens to 34 J kg^{-1}.

3.2 Results from climate reanalysis

Spatial trends in convective parameters calculated from ERA5 for 1979-2020 support the changes to distributions seen in the observed atmospheric profiles. During May and June, CAPE increased by 20-50 J kg^{-1} $decade^{-1}$ in the south-central NNAGP, with the strongest trends in the most southern extent (Figure 4a). CAPE increased by 13 J kg^{-1} $decade^{-1}$ at BIS while GGW only increased by 3 J kg^{-1} $decade^{-1}$. July and August share the same spatial pattern as May and June (Figure 4b).

Vertically-integrated moisture convergence (VIMC) shows where the horizontal flux of moisture, integrated from surface to the top of the atmosphere, acts to increase or decrease total column moisture. Trends in VIMC, therefore, show where more moisture is being transported. In the NNAGP, trends in VIMC are mostly zero except over parts of North and South Dakota where VIMC increased by 0.6 mm $decade^{-1}$ over the 1980s - 2010s study period (Figure 5). These trends are immediately to the North and East of where the largest CAPE trends are located (Figures 4).

4 Discussion

The changes in CAPE highlighted at GGW and BIS illustrate how anthropogenic climate change is changing the nature of thermodynamic environments. CAPE increases in response to higher temperature and humidity and scales at the Clausius-Clapeyron relationship (Agard and Emanuel 2017) such that it can be predicted at mid-latitude continental sites from large-scale environmental parameters alone (Li and Chavas 2021) noting that recent changes to the climate of the NNAGP

are globally unique. Near-surface temperatures have been cooling during May and June and warming during July and August (Bromley et al. 2020). Surface humidity has also been increasing across the entire NNAGP during May and June and across its southern extent during July and August (Bromley et al. 2020; Gerken et al. 2018c). The moisture increase is caused by both a change to the land surface (Gameda et al. 2007; Betts et al. 2013c), and the increasing strength of the Great Plains Low Level Jet (Feng et al. 2019, 2016) consistent with a warming climate. The fingerprint of the GPLLJ is apparent in the spatial variability of CAPE trends (Figure 4) and the trends in VIMC (Figure 5), yet accurately modeling the GPLLJ is challenging for global climate models (GCM) due to their coarse resolution and likely requires downscaling the GCMs to convection-permitting resolutions (Tang et al. 2017).

The convection-permitting CTRL simulation underestimates CAPE at both GGW and BIS, which might be due to a pervasive near-surface warm bias in the Great Plains (Liu et al. 2017). If the temperatures are too high and the near-surface relative humidity is too low, a deeper boundary layer would result. The structure of the planetary boundary layer (PBL) also affects CAPE, with a shallower PBL acting to increase CAPE by increasing the depth over which CAPE is integrated. A deeper boundary layer with lower relative humidity would therefore result in lower CAPE, despite the strong relationship between higher temperatures and CAPE. Temperatures in the PGW simulation increase by an average of 3-5 °C and relative humidity increases by 3-6% depending on the season (Liu et al. 2017). The change in CAPE in PGW simulation still underestimates the 2000-2010 distribution of CAPE and is lower than the 2010-2020 for both GGW and BIS (Figure 1a,b). The likely reason for the PGW simulation showing such modest changes is the fact that it does not account for changes to circulation patterns; it looks primarily at the thermodynamic

response to a warming atmosphere and cannot account for the strengthening GPLLJ. The hypothesized cause for the strengthening of the GPLLJ is due to a westward shift in the North Atlantic Subtropical High (Cook et al. 2008; Tang et al. 2017). The conclusion then is that the PGW simulation should be taken as a conservative estimate of where circulation patterns are changing or expected to change as is occurring in the NNAGP. Changes to CAPE assessed using the CCSM4 global climate model are larger than the PGW simulation in the NNAGP, likely due to the simulated intensification of the GPLLJ (Chen et al. 2020). CAPE increases by 150-300 J kg^{-1} in the CCSM4 and shows a similar pattern to the CAPE trends shown in Figure 4, with a northwestern extension of increased CAPE into the NNAGP (Chen et al. 2020). Convection-permitting simulations of future climate that downscale global climate models also simulate changes to the GPLLJ (Hoogewind et al. 2017; Trapp et al. 2019) and estimate an increase in CAPE on the order of 600 J kg^{-1} during JJA.

Land use and land cover change might be another source of the discrepancies in recent and future thermodynamic environments. The NNAGP is a global breadbasket for wheat production, which historically included summer fallow in the crop rotation. This practice has largely disappeared in favor of continuous cropping and cover cropping during the summer and nearly 250,000 km^2 of land that used to be held in fallow during the summer is now planted, affecting surface fluxes and the boundary layer (Gerken et al. 2018c; Betts et al. 2013c; Gameda et al. 2007). Recent convection-permitting simulations of the NNAGP found that the areas that declined in summer fallow experienced an increase in mean seasonal CAPE of ~20 J kg^{-1} during May and June and up to 40 J kg^{-1} during July and August, which represents ~10% difference in CAPE (Chapter 3, this volume). This change is on the order of the increase in mean CAPE at GGW and

BIS. Trends in CAPE from ERA5 show a much broader area of CAPE increase during July and August, extending into Saskatchewan. The simulations of summer fallow in the NNAGP used a similar model setup to Liu et al. (2017) so the magnitude of CAPE change might be more uncertain than the idea that summer fallow reduction acted to increase CAPE.

5 Conclusions

The thermodynamic environments of the northern North American Great Plains have shifted toward stronger CAPE and slightly stronger CIN. Mean annual CAPE at GGW and BIS has increased by 45 J kg^{-1} with a ~250% increase in the probability of CAPE exceeding 1000 J kg^{-1} and 2000 J kg^{-1} respectively. Mean annual CIN strengthened at both GGW and BIS but only by 8 J kg^{-1} and 2 J kg^{-1} respectively. Trends in ERA5 show that an increase in strength of the GPLLJ is likely responsible for at least part of observed increases in CAPE. A 13-year convection-permitting simulation of the 2000s and of a pseudo global warming (PGW) environment both underestimated CAPE at both GGW and BIS. The PGW environment was 4 °C warmer and relative humidity increased by 2-6%, but mean annual CAPE only increased by 22 J kg^{-1} at both GGW and BIS. The changes in thermodynamic environments in the NNAGP are changing faster than some simulations of the future climate might suggest, and thus should be considered conservative estimates for future change. Global CCSM4 model estimates slightly larger CAPE change than the PGW simulation due to better capturing the dynamic changes to the GPLLJ. Downscaling global climate models using a convection-permitting models, i.e. (Hoogewind et al.

2017), to better capture the changes to the GPLLJ is a promising step understanding future thermodynamic environments in the NNAGP.

Acknowledgments

We acknowledge support from the U.S. National Science Foundation (NSF) Division of Environmental Biology (DEB) Award 1552976, the NSF Office of Integrated Activities (OIA) Award 1632810, the U.S. Department of Agriculture (USDA) National Institute of Food and Agriculture (NIFA) Hatch project 228396 and multistate project W3188, the Graduate School at Montana State University, The Montana Water Center, The National Center for Atmospheric Research, the University of Wisconsin – Madison, and the Montana Wheat and Barley Committee.

Figures

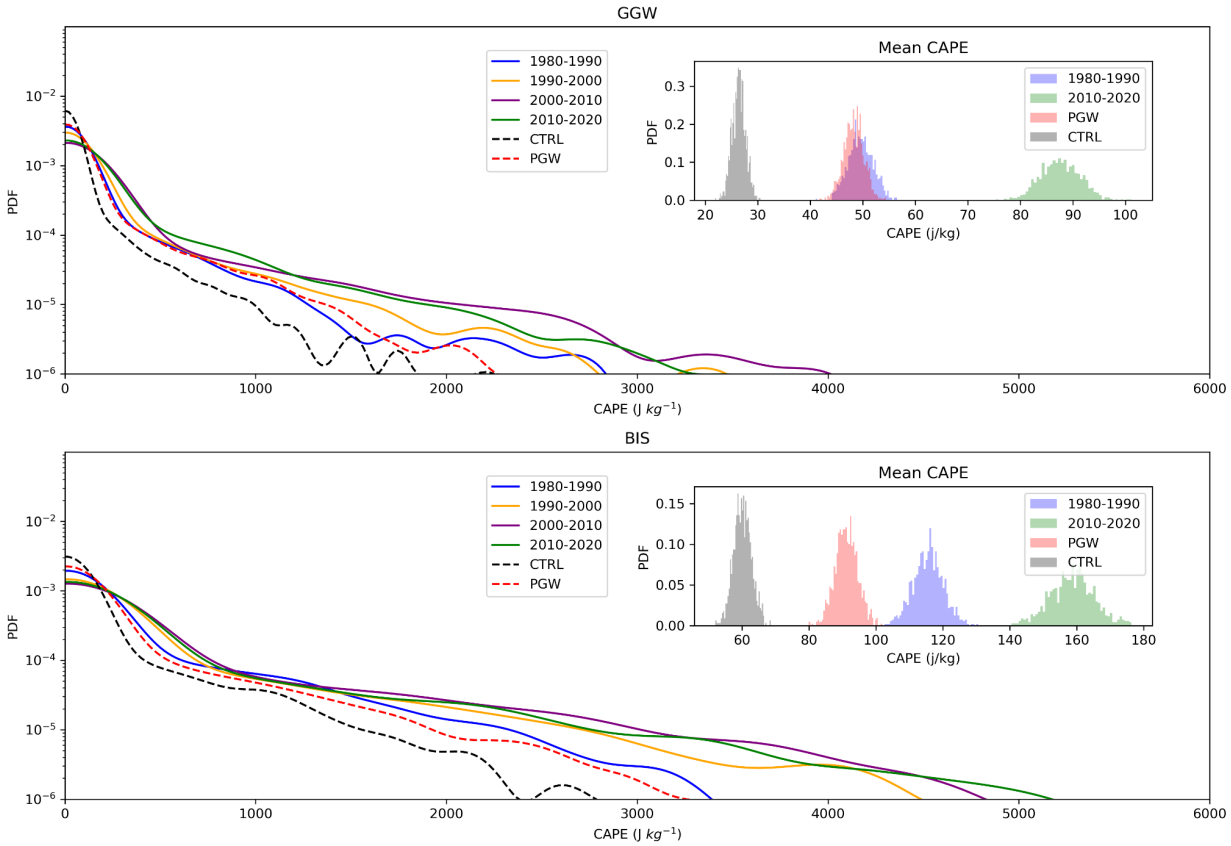


Figure 1: Empirical probability density distributions for convective available potential energy (CAPE) at (A) Glasgow, MT, USA (GGW) and (B) Bismarck, ND, USA (BIS) by decade from 1980 - 2020. CAPE distributions simulated by the control (CTRL) and pseudo global warming (PGW) Weather Research and Forecasting (WRF) model runs by Liu et al., (2017) are shown in dashed lines. Distributions include all 00 UTC and 12 UTC soundings for the entire year for every decade (n=7300). Mean CAPE distributions are calculated by bootstrap-resampling observations within the time period with replacement, as shown in the insets.

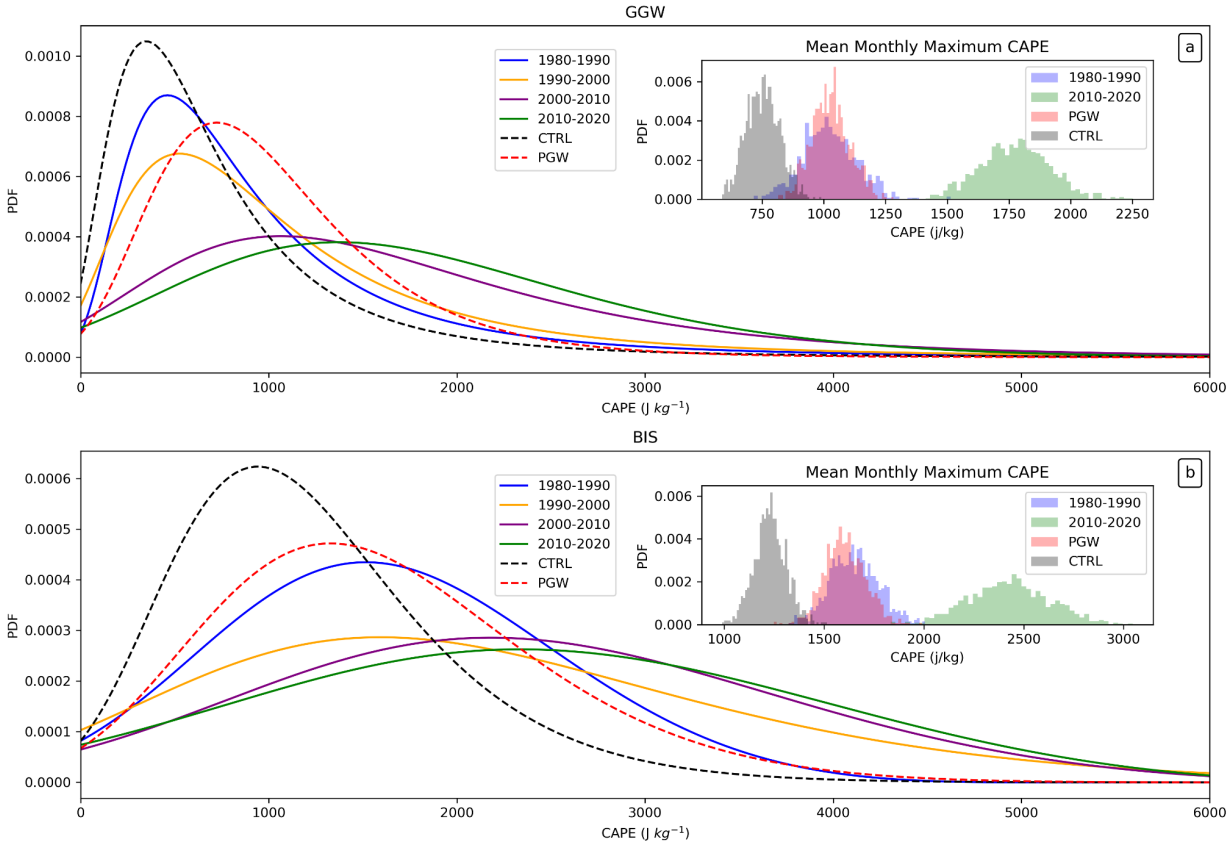


Figure 2: The same as Figure 1 but for AMJJAS monthly maximum CAPE distributions for (a) GGW and (b) BIS. Data are fit to generalized extreme value distributions. Mean monthly maximum CAPE is calculated by bootstrap resampling the monthly maximum CAPE data as shown in the insets..

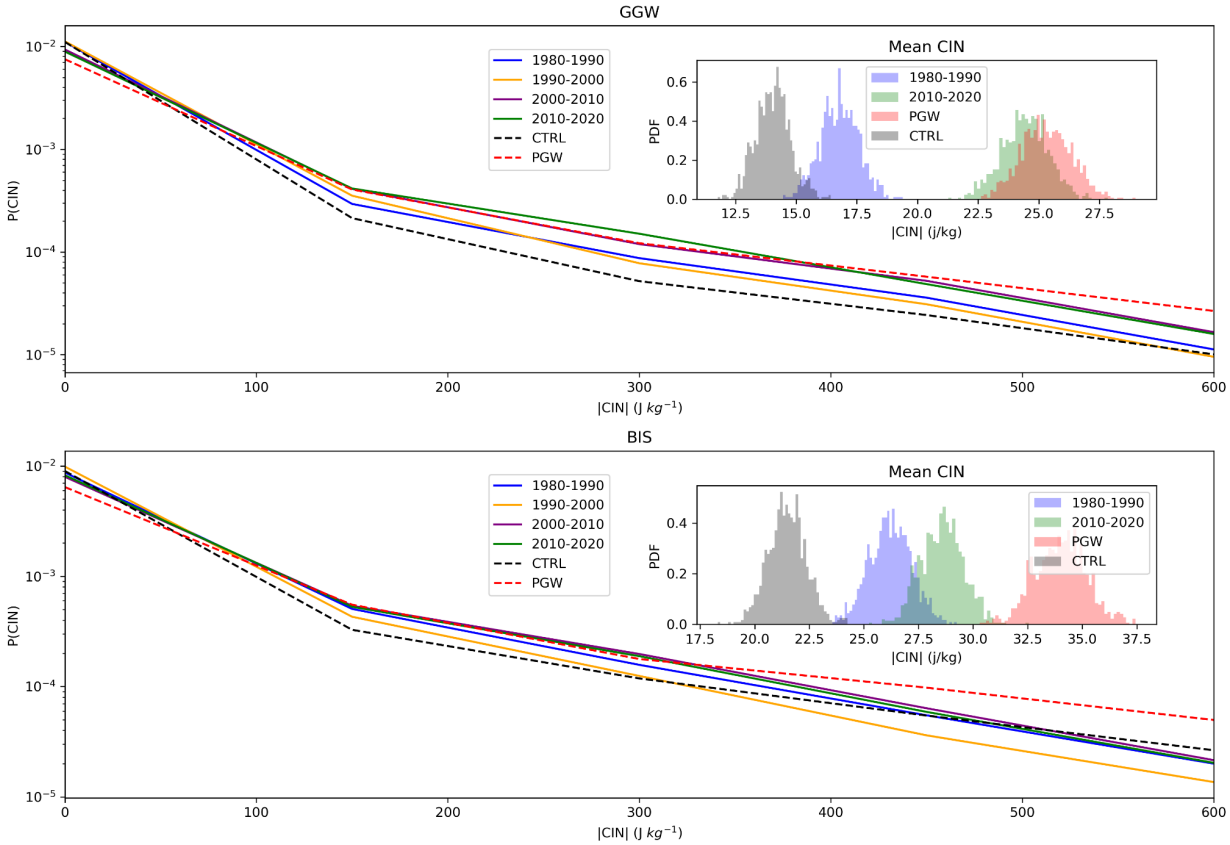


Figure 3: Same as Figure 1 but for CIN.

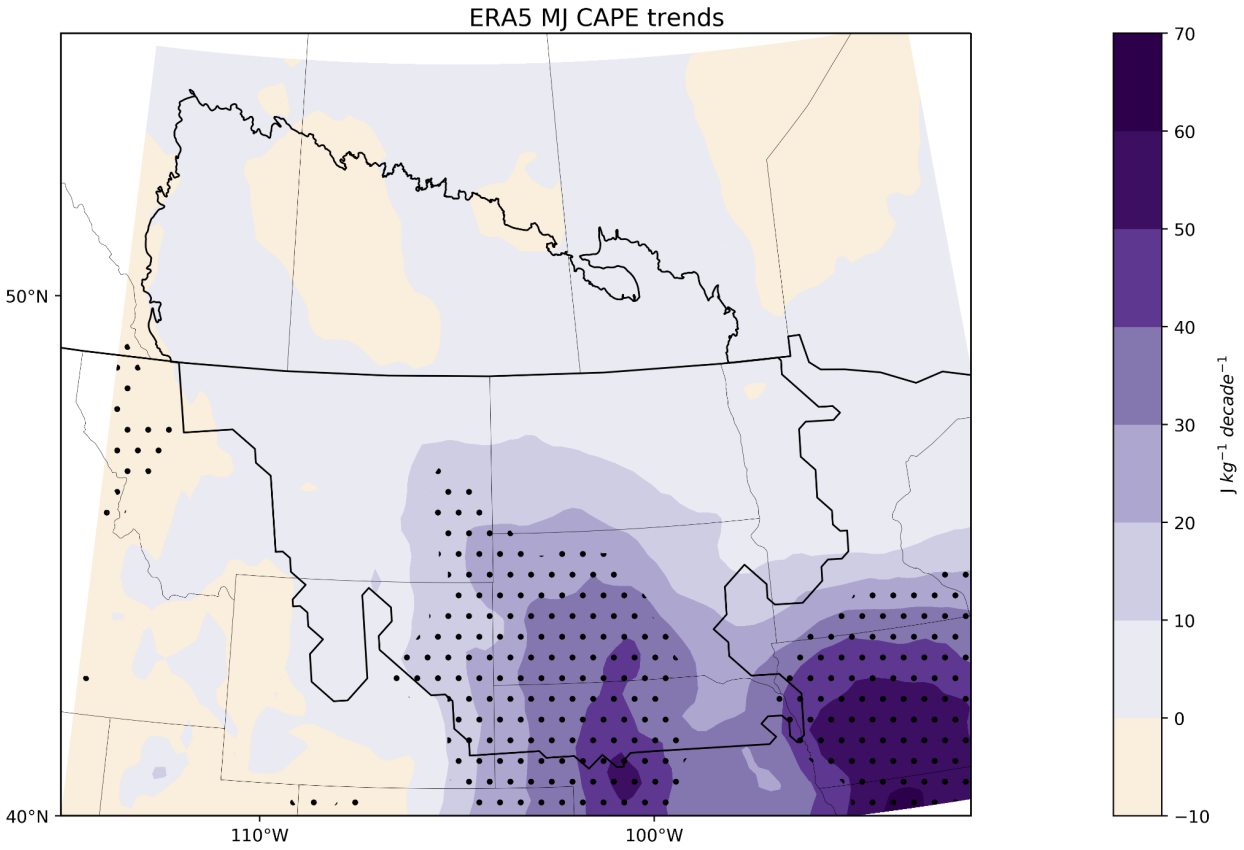


Figure 4: Trends in May and June monthly mean CAPE from the ERA5 reanalysis for the 1979-2020 period for the northern North American Great Plains (NNAGP) shown in the thick black line, and surrounds.

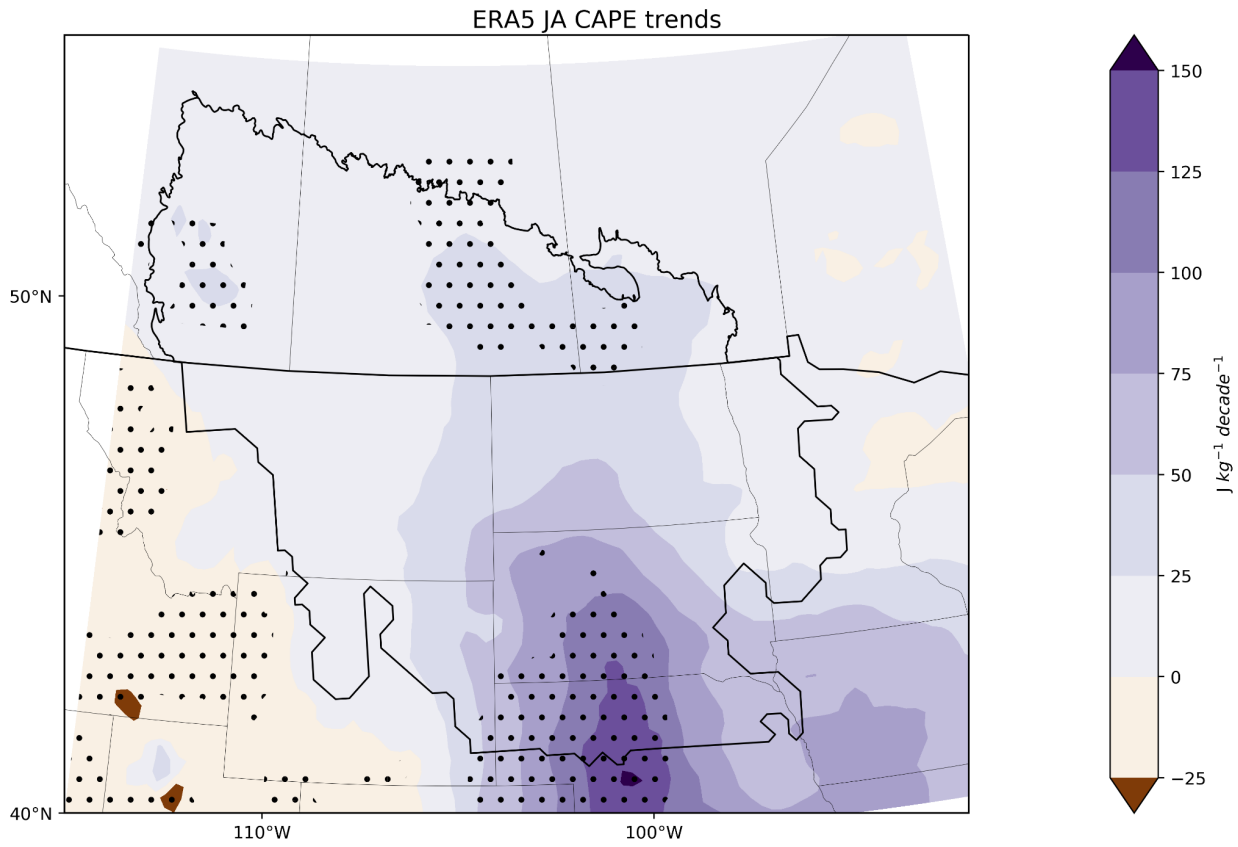


Figure 4b: Same as Figure 4a but for JA.

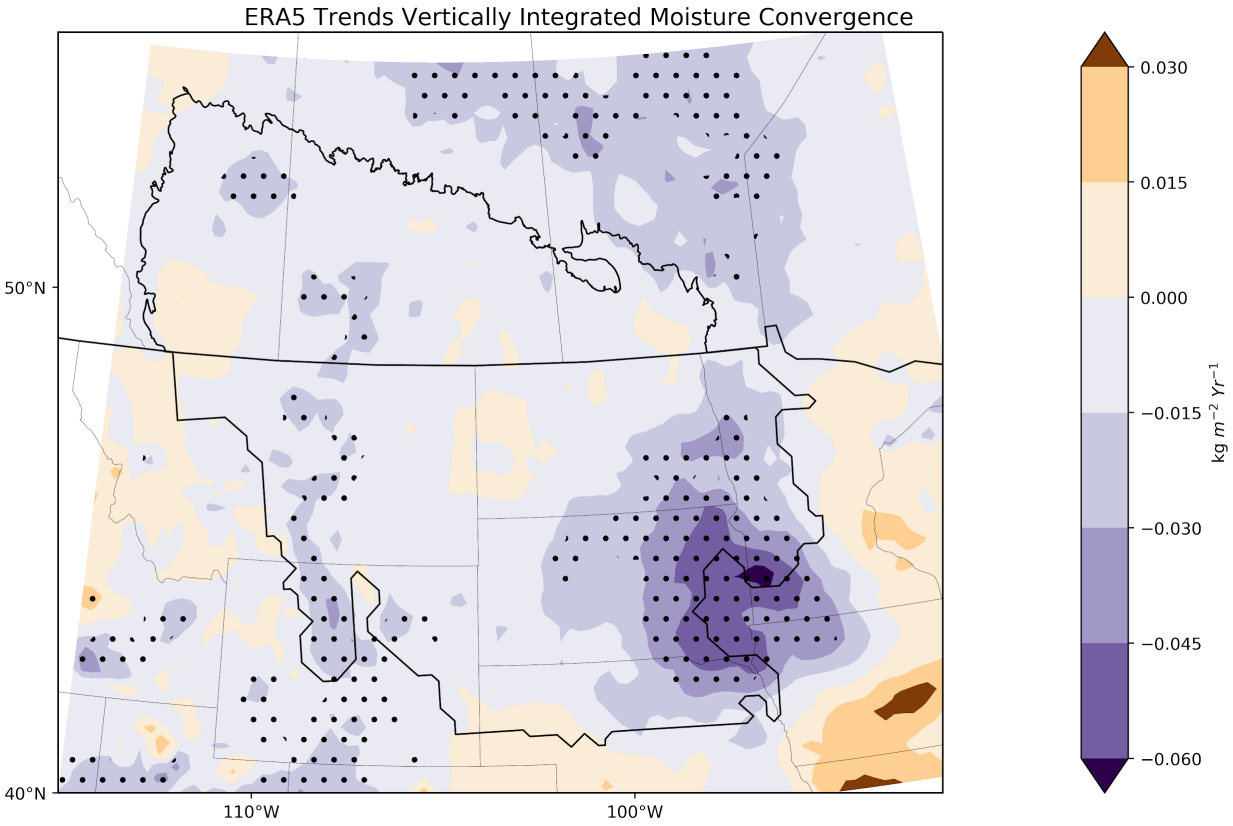


Figure 5a: Trends in AMJ horizontal moisture convergence from ERA5 1979-2020.

References

Agard, V., and K. Emanuel, 2017: Clausius–Clapeyron Scaling of Peak CAPE in Continental Convective Storm Environments. *J. Atmospheric Sci.*, **74**, 3043–3054, https://doi.org/10.1175/JAS-D-16-0352.1.

Barandiaran, D., S.-Y. Wang, and K. Hilburn, 2013: Observed trends in the Great Plains low-level jet and associated precipitation changes in relation to recent droughts. *Geophys. Res. Lett.*, **40**, 6247–6251, https://doi.org/10.1002/2013GL058296.

Barlage, M., F. Chen, R. Rasmussen, Z. Zhang, and G. Miguez-Macho, 2021: The Importance of Scale-Dependent Groundwater Processes in Land-Atmosphere Interactions Over the Central United States. *Geophys. Res. Lett.*, **48**, e2020GL092171, https://doi.org/10.1029/2020GL092171.

Betts, A. K., and R. L. Desjardins, 2018: Understanding Land–Atmosphere–Climate Coupling from the Canadian Prairie Dataset. *Environments*, **5**, 129, https://doi.org/10.3390/environments5120129.

Betts, A. K., R. Desjardins, D. Worth, and D. Cerkowniak, 2013: Impact of land use change on the diurnal cycle climate of the Canadian Prairies. *J. Geophys. Res. Atmospheres*, **118**, 11996–12011, https://doi.org/10.1002/2013JD020717.

Bromley, G. T., T. Gerken, A. F. Prein, and P. C. Stoy, 2020: Recent Trends in the Near-Surface Climatology of the Northern North American Great Plains. *J. Clim.*, **33**, 461–475, https://doi.org/10.1175/JCLI-D-19-0106.1.

Carbone, R. E., and J. D. Tuttle, 2008: Rainfall Occurrence in the U.S. Warm Season: The Diurnal Cycle. *J. Clim.*, **21**, 4132–4146, https://doi.org/10.1175/2008JCLI2275.1.

Chen, J., A. Dai, Y. Zhang, and K. L. Rasmussen, 2020: Changes in Convective Available Potential Energy and Convective Inhibition under Global Warming. *J. Clim.*, **33**, 2025–2050, https://doi.org/10.1175/JCLI-D-19-0461.1.

Cook, K. H., E. K. Vizy, Z. S. Launer, and C. M. Patricola, 2008: Springtime Intensification of the Great Plains Low-Level Jet and Midwest Precipitation in GCM Simulations of the Twenty-First Century. *J. Clim.*, **21**, 6321–6340, https://doi.org/10.1175/2008JCLI2355.1.

Diffenbaugh, N. S., M. Scherer, and R. J. Trapp, 2013: Robust increases in severe thunderstorm environments in response to greenhouse forcing. *Proc. Natl. Acad. Sci.*, **110**, 16361–16366, https://doi.org/10.1073/pnas.1307758110.

Dougherty, E., and K. L. Rasmussen, 2019: Climatology of Flood-Producing Storms and Their Associated Rainfall Characteristics in the United States. *Mon. Weather Rev.*, **147**, 3861–3877, https://doi.org/10.1175/MWR-D-19-0020.1.

Feng, Z., L. R. Leung, S. Hagos, R. A. Houze, C. D. Burleyson, and K. Balaguru, 2016: More frequent intense and long-lived storms dominate the springtime trend in central US rainfall. *Nat. Commun.*, **7**, 1–8, https://doi.org/10.1038/ncomms13429.

——, R. A. Houze, L. R. Leung, F. Song, J. C. Hardin, J. Wang, W. I. Gustafson, and C. R. Homeyer, 2019: Spatiotemporal Characteristics and Large-Scale Environments of Mesoscale Convective Systems East of the Rocky Mountains. *J. Clim.*, **32**, 7303–7328, https://doi.org/10.1175/JCLI-D-19-0137.1.

Ficklin, D. L., and K. A. Novick, 2017: Historic and projected changes in vapor pressure deficit suggest a continental-scale drying of the United States atmosphere. *J. Geophys. Res. Atmospheres*, **122**, 2061–2079, https://doi.org/10.1002/2016JD025855.

Gameda, S., B. Qian, C. A. Campbell, and R. L. Desjardins, 2007: Climatic trends associated with summerfallow in the Canadian Prairies. *Agric. For. Meteorol.*, **142**, 170–185, https://doi.org/10.1016/j.agrformet.2006.03.026.

Gerken, T., G. T. Bromley, and P. C. Stoy, 2018: Surface Moistening Trends in the Northern North American Great Plains Increase the Likelihood of Convective Initiation. *J. Hydrometeorol.*, **19**, 227–244, https://doi.org/10.1175/JHM-D-17-0117.1.

Hanesiak, J. M., R. L. Raddatz, and S. Lobban, 2004: Local Initiation of Deep Convection on the Canadian Prairie Provinces. *Bound.-Layer Meteorol.*, **110**, 455–470, https://doi.org/10.1023/B:BOUN.0000007242.89023.e5.

Hersbach, H., and Coauthors, 2020: The ERA5 global reanalysis. *Q. J. R. Meteorol. Soc.*, **146**, 1999–2049, https://doi.org/10.1002/qj.3803.

Hoogewind, K. A., M. E. Baldwin, and R. J. Trapp, 2017: The Impact of Climate Change on Hazardous Convective Weather in the United States: Insight from High-Resolution Dynamical Downscaling. *J. Clim.*, **30**, 10081–10100, https://doi.org/10.1175/JCLI-D-16-0885.1.

Kunkel, K. E., 2003: North American Trends in Extreme Precipitation. *Nat. Hazards*, **29**, 291–305, https://doi.org/10.1023/A:1023694115864.

Lauenroth, W. K., I. C. Burke, and J. M. Paruelo, 2000: Patterns of Production and Precipitation-Use Efficiency of Winter Wheat and Native Grasslands in the Central Great Plains of the United States. *Ecosystems*, **3**, 344–351, https://doi.org/10.1007/s100210000031.

Lepore, C., D. Veneziano, and A. Molini, 2015: Temperature and CAPE dependence of rainfall extremes in the eastern United States. *Geophys. Res. Lett.*, **42**, 74–83, https://doi.org/10.1002/2014GL062247.

Li, F., and D. R. Chavas, 2021: Midlatitude continental CAPE is predictable from large-scale environmental parameters. *Geophys. Res. Lett.*, **n/a**, e2020GL091799, https://doi.org/10.1029/2020GL091799.

Liu, C., and Coauthors, 2017: Continental-scale convection-permitting modeling of the current and future climate of North America. *Clim. Dyn.*, **49**, 71–95, https://doi.org/10.1007/s00382-016-3327-9.

López, J., D. A. Way, and W. Sadok, 2021: Systemic effects of rising atmospheric vapor pressure deficit on plant physiology and productivity. *Glob. Change Biol.*, gcb.15548, https://doi.org/10.1111/gcb.15548.

May, R., S. Arms, P. Marsh, E. Bruning, J. Leeman, and Z. Bruick, 2016: *MetPy: A Python Package for Meteorological Data*. UCAR/NCAR - Unidata,.

Nielsen, D. C., P. W. Unger, and P. R. Miller, 2005: Efficient Water Use in Dryland Cropping Systems in the Great Plains. *Agron. J.*, **97**, 364–372, https://doi.org/10.2134/agronj2005.0364.

O'Gorman, P. A., and T. Schneider, 2009: The physical basis for increases in precipitation extremes in simulations of 21st-century climate change. *Proc. Natl. Acad. Sci.*, **106**, 14773–14777, https://doi.org/10.1073/pnas.0907610106.

Prein, A. F., C. Liu, K. Ikeda, R. Bullock, R. M. Rasmussen, G. J. Holland, and M. Clark, 2017a: Simulating North American mesoscale convective systems with a convection-permitting climate model. *Clim. Dyn.*, https://doi.org/10.1007/s00382-017-3993-2.

——, ——, ——, S. B. Trier, R. M. Rasmussen, G. J. Holland, and M. P. Clark, 2017b: Increased rainfall volume from future convective storms in the US. *Nat. Clim. Change*, **7**, 880–884, https://doi.org/10.1038/s41558-017-0007-7.

——, R. M. Rasmussen, K. Ikeda, C. Liu, M. P. Clark, and G. J. Holland, 2017c: The future intensification of hourly precipitation extremes. *Nat. Clim. Change*, **7**, 48–52, https://doi.org/10.1038/nclimate3168.

Raddatz, R. L., 1998: Anthropogenic vegetation transformation and the potential for deep convection on the Canadian prairies. *Can. J. Soil Sci.*, **78**, 657–666, https://doi.org/10.4141/S98-011.

Rasmussen, K. L., A. F. Prein, R. M. Rasmussen, K. Ikeda, and C. Liu, 2017: Changes in the convective population and thermodynamic environments in convection-permitting regional climate simulations over the United States. *Clim. Dyn.*, **55**, 383–408, https://doi.org/10.1007/s00382-017-4000-7.

Seeley, J. T., and D. M. Romps, 2014: The Effect of Global Warming on Severe Thunderstorms in the United States. *J. Clim.*, **28**, 2443–2458, https://doi.org/10.1175/JCLI-D-14-00382.1.

——, and ——, 2015: Why does tropical convective available potential energy (CAPE) increase with warming? *Geophys. Res. Lett.*, **42**, 10,429-10,437, https://doi.org/10.1002/2015GL066199.

Shrestha, B. M., R. L. Raddatz, R. L. Desjardins, and D. E. Worth, 2012: Continuous Cropping and Moist Deep Convection on the Canadian Prairies. *Atmosphere*, **3**, 573–590, https://doi.org/10.3390/atmos3040573.

Stevenson, S. N., and R. S. Schumacher, 2014: A 10-Year Survey of Extreme Rainfall Events in the Central and Eastern United States Using Gridded Multisensor Precipitation Analyses. *Mon. Weather Rev.*, **142**, 3147–3162, https://doi.org/10.1175/MWR-D-13-00345.1.

Tang, Y., J. Winkler, S. Zhong, X. Bian, D. Doubler, L. Yu, and C. Walters, 2017: Future changes in the climatology of the Great Plains low-level jet derived from fine resolution multi-model simulations. *Sci. Rep.*, **7**, 5029, https://doi.org/10.1038/s41598-017-05135-0.

Trapp, R. J., K. A. Hoogewind, and S. Lasher-Trapp, 2019: Future Changes in Hail Occurrence in the United States Determined through Convection-Permitting Dynamical Downscaling. *J. Clim.*, **32**, 5493–5509, https://doi.org/10.1175/JCLI-D-18-0740.1.

Trenberth, K. E., A. Dai, R. M. Rasmussen, and D. B. Parsons, 2003: The Changing Character of Precipitation. *Bull. Am. Meteorol. Soc.*, **84**, 1205–1218, https://doi.org/10.1175/BAMS-84-9-1205.

Vick, E. S. K., P. C. Stoy, A. C. I. Tang, and T. Gerken, 2016: The surface-atmosphere exchange of carbon dioxide, water, and sensible heat across a dryland wheat-fallow rotation. *Agric. Ecosyst. Environ.*, **232**, 129–140, https://doi.org/10.1016/j.agee.2016.07.018.

CHAPTER SIX

CONCLUSION

Agriculture in the NNAGP has shifted away from wheat-fallow rotations and toward systems that are more diverse and benefit – or are at least less detrimental to – soil health (Engel et al. 2017; Lin and Chen 2014). Some 116,000 km^2 of land used to be fallow in the 1970s and is now planted with wheat, pulse crops, oilseeds and an increasing amount of corn and soy (Long et al. 2014a,b; Rosenzweig and Schipanski 2019; Maaz et al. 2018). These changes have been a 'win-win' for soil health and farmers checkbooks, but have these changes positively benefited climate?

In Chapters 2-4, I have shown that the regional climate of the NNAGP has cooled and become moister as a result of the reduction in summer fallow. These changes are primarily limited to May and June, but other studies have found changes outside of these months on more local scales (Bromley et al. 2020; Betts et al. 2013c; Gameda et al. 2007) and May and June are key periods for wheat growth in Montana, especially winter Wheat (Vick et al., 2016). While climate management is likely not the primary goal of individual farmers, these changes have demonstrated the power of managing the landscape for climate services which can impact climate to the same degree as land cover change (Luyssaert et al. 2014). Landscape management is not a replacement for a reduction of anthropogenic emissions, but might delay the worse effects of climate change on a region by region basis (Seneviratne et al. 2018). Key to crop success is the avoidance of temperature extremes during key growth stages (Hirsch et al. 2017; DeAngelis et al. 2010), and the cooling trends described here also help reduce the likelihood of extreme temperatures.

The precipitation response to a reduction in summer fallow is more nuanced based on the modeling analysis here. Precipitation is increasing in the NNAGP, as shown in Chapter 2, and as I showed in Chapter 5 this is likely due to the enhancement of the GPLLJ and its ability to transport moisture, rather than changes to the land surface as shown in Chapters 3 and 4. These findings contrast somewhat findings by (Gerken et al. 2018c; Gameda et al. 2007; Betts et al. 2013c; Raddatz 1998b), and more that argued that reducing summer fallow makes convective processes more likely. The WRF analysis demonstrates that this is in part due to a simultaneous increase in CIN which balances increases in CAPE. From a climate adaptation point of view, the combination of increasing precipitation, longer growing seasons that are cooling (or at minimum warming slower), and more surface humidity make the NNAGP a better place to grow crops now than 50 years prior (Bromley et al. 2020; Mueller et al. 2015a). Looking to the future, simulations of wheat yield in the NNAGP are projected to actually increase while many other areas globally are projected to decrease (Smith et al. 2013; Asseng et al. 2013a, 2015a). This places the NNAGP in a unique situation for crop growth, but it remains to be determined the degree to which an increase in favorable climate conditions – which retain the risk of severe drought (Gerken et al. 2018a) – has increased yield. As a next step, I hope to investigate the yield increase that producers unintentionally provided themselves by cooling and moistening the near-surface atmosphere during key crop growth periods to fully characterize the 'win-win-win' dynamic that has occurred as a case study in improved regional agricultural sustainability – albeit one that has an uncertain future.

Climate variability might undermine the increased suitability for growing crops in the NNAGP. The worst drought ever recorded in parts of the NNAGP occurred in 2017, and droughts

are expected to increase in severity (Gerken et al. 2018a; Bonsal et al. 2020). Simultaneously, too much precipitation to plant or harvest fields can have delirious effects on agriculture (Stadnyk et al. 2016). Future research should seek to better understand precipitation variability in the NNAGP and seek to further constrain the impacts of land use change and land management on near-surface climate.

As demonstrated in Chapter 5, the future impacts of organized convection and extreme precipitation in the NNAGP is not well studied. The GPLLJ is a major source of moisture for the MCS development in the NNAGP and changes to the GPLLJ are not well captured by global climate models (Tang et al. 2017). Out of the analyzed simulations, only the simulation that downscaled a global climate model to convection-permitting resolutions was able to accurately represent the GPLLJ (Hoogewind et al. 2017). This simulation projects that extreme precipitation, hail, and other severe convective hazards are likely to increase in the NNAGP (Trapp et al. 2019). More simulations using this approach are needed to assess the uncertainty in these projections. Since the NNAGP sits in the middle of the continent the land surface plays a critical, and still not well understood, role in strong convective events (Tan et al. 2018; Shrestha et al. 2012; Raddatz 2005, 1998b). Going forward, rigorously studying the coupling between agricultural and climate extremes in addition to trends in agroclimatology will give producers, other land managers, and policymakers more of the information that they need to make sound decisions for the future of our region.

References

Asseng, S., and Coauthors, 2013: Uncertainty in simulating wheat yields under climate change. *Nat. Clim. Change*, **3**, 827–832, https://doi.org/10.1038/nclimate1916.

——, and Coauthors, 2015: Rising temperatures reduce global wheat production. *Nat. Clim. Change*, **5**, 143–147, https://doi.org/10.1038/nclimate2470.

Betts, A. K., R. Desjardins, D. Worth, and D. Cerkowniak, 2013: Impact of land use change on the diurnal cycle climate of the Canadian Prairies. *J. Geophys. Res. Atmospheres*, **118**, 11996–12011, https://doi.org/10.1002/2013JD020717.

Bonsal, B., Z. Liu, E. Wheaton, and R. Stewart, 2020: Historical and Projected Changes to the Stages and Other Characteristics of Severe Canadian Prairie Droughts. *Water*, **12**, 3370, https://doi.org/10.3390/w12123370.

Bromley, G. T., T. Gerken, A. F. Prein, and P. C. Stoy, 2020: Recent Trends in the Near-Surface Climatology of the Northern North American Great Plains. *J. Clim.*, **33**, 461–475, https://doi.org/10.1175/JCLI-D-19-0106.1.

DeAngelis, A., F. Dominguez, Y. Fan, A. Robock, M. D. Kustu, and D. Robinson, 2010: Evidence of enhanced precipitation due to irrigation over the Great Plains of the United States. *J. Geophys. Res. Atmospheres*, **115**, https://doi.org/10.1029/2010JD013892.

Engel, R. E., P. R. Miller, B. G. McConkey, and R. Wallander, 2017: Soil Organic Carbon Changes to Increasing Cropping Intensity and No-Till in a Semiarid Climate. *Soil Sci. Soc. Am. J.*, **81**, 404–413, https://doi.org/10.2136/sssaj2016.06.0194.

Gameda, S., B. Qian, C. A. Campbell, and R. L. Desjardins, 2007: Climatic trends associated with summerfallow in the Canadian Prairies. *Agric. For. Meteorol.*, **142**, 170–185, https://doi.org/10.1016/j.agrformet.2006.03.026.

Gerken, T., G. T. Bromley, B. L. Ruddell, S. Williams, and P. C. Stoy, 2018a: Convective suppression before and during the United States Northern Great Plains flash drought of 2017. *Hydrol. Earth Syst. Sci.*, **22**, 4155–4163, https://doi.org/10.5194/hess-22-4155-2018.

——, ——, and P. C. Stoy, 2018b: Surface Moistening Trends in the Northern North American Great Plains Increase the Likelihood of Convective Initiation. *J. Hydrometeorol.*, **19**, 227–244, https://doi.org/10.1175/JHM-D-17-0117.1.

Hirsch, A. L., M. Wilhelm, E. L. Davin, W. Thiery, and S. I. Seneviratne, 2017: Can climate-effective land management reduce regional warming? *J. Geophys. Res. Atmospheres*, **122**, 2269–2288, https://doi.org/10.1002/2016JD026125.

Hoogewind, K. A., M. E. Baldwin, and R. J. Trapp, 2017: The Impact of Climate Change on Hazardous Convective Weather in the United States: Insight from High-Resolution Dynamical Downscaling. *J. Clim.*, **30**, 10081–10100, https://doi.org/10.1175/JCLI-D-16-0885.1.

Lin, R., and C. Chen, 2014: Tillage, Crop Rotation, and Nitrogen Management Strategies for Wheat in Central Montana. *Agron. J.*, **106**, 475–485, https://doi.org/10.2134/agronj2013.0316.

Long, J. A., R. L. Lawrence, P. R. Miller, and L. A. Marshall, 2014a: Changes in field-level cropping sequences: Indicators of shifting agricultural practices. *Agric. Ecosyst. Environ.*, **189**, 11–20, https://doi.org/10.1016/j.agee.2014.03.015.

——, ——, ——, ——, and M. C. Greenwood, 2014b: Adoption of cropping sequences in northeast Montana: A spatio-temporal analysis. *Agric. Ecosyst. Environ.*, **197**, 77–87, https://doi.org/10.1016/j.agee.2014.07.022.

Luyssaert, S., and Coauthors, 2014: Land management and land-cover change have impacts of similar magnitude on surface temperature. *Nat. Clim. Change*, **4**, 389–393, https://doi.org/10.1038/nclimate2196.

Maaz, T., J. D. Wulfhorst, V. McCracken, J. Kirkegaard, D. R. Huggins, I. Roth, H. Kaur, and W. Pan, 2018: Economic, policy, and social trends and challenges of introducing oilseed and pulse crops into dryland wheat cropping systems. *Agric. Ecosyst. Environ.*, **253**, 177–194, https://doi.org/10.1016/j.agee.2017.03.018.

Mueller, B., M. Hauser, C. Iles, R. H. Rimi, F. W. Zwiers, and H. Wan, 2015: Lengthening of the growing season in wheat and maize producing regions. *Weather Clim. Extrem.*, **9**, 47–56, https://doi.org/10.1016/j.wace.2015.04.001.

Raddatz, R. L., 1998: Anthropogenic vegetation transformation and the potential for deep convection on the Canadian prairies. *Can. J. Soil Sci.*, **78**, 657–666, https://doi.org/10.4141/S98-011.

Raddatz, R. L., 2005: Moisture recycling on the Canadian Prairies for summer droughts and pluvials from 1997 to 2003. *Agric. For. Meteorol.*, **131**, 13–26, https://doi.org/10.1016/j.agrformet.2005.04.007.

Rosenzweig, S. T., and M. E. Schipanski, 2019: Landscape-scale cropping changes in the High Plains: economic and environmental implications. *Environ. Res. Lett.*, **14**, 124088, https://doi.org/10.1088/1748-9326/ab5e8b.

Seneviratne, S. I., and Coauthors, 2018: Land radiative management as contributor to regional-scale climate adaptation and mitigation. *Nat. Geosci.*, **11**, 88–96, https://doi.org/10.1038/s41561-017-0057-5.

Shrestha, B. M., R. L. Raddatz, R. L. Desjardins, and D. E. Worth, 2012: Continuous Cropping and Moist Deep Convection on the Canadian Prairies. *Atmosphere*, **3**, 573–590, https://doi.org/10.3390/atmos3040573.

Smith, W. N., and Coauthors, 2013: Assessing the effects of climate change on crop production and GHG emissions in Canada. *Agric. Ecosyst. Environ.*, **179**, 139–150, https://doi.org/10.1016/j.agee.2013.08.015.

Stadnyk, T., K. Dow, L. Wazney, and E.-L. Blais, 2016: The 2011 flood event in the Red River Basin: Causes, assessment and damages. *Can. Water Resour. J. Rev. Can. Ressour. Hydr.*, **41**, 65–73, https://doi.org/10.1080/07011784.2015.1008048.

Tan, X., T. Y. Gan, and Y. D. Chen, 2018: Moisture sources and pathways associated with the spatial variability of seasonal extreme precipitation over Canada. *Clim. Dyn.*, **50**, 629–640, https://doi.org/10.1007/s00382-017-3630-0.

Tang, Y., J. Winkler, S. Zhong, X. Bian, D. Doubler, L. Yu, and C. Walters, 2017: Future changes in the climatology of the Great Plains low-level jet derived from fine resolution multi-model simulations. *Sci. Rep.*, **7**, 5029, https://doi.org/10.1038/s41598-017-05135-0.

Trapp, R. J., K. A. Hoogewind, and S. Lasher-Trapp, 2019: Future Changes in Hail Occurrence in the United States Determined through Convection-Permitting Dynamical Downscaling. *J. Clim.*, **32**, 5493–5509, https://doi.org/10.1175/JCLI-D-18-0740.1.

REFERENCES CITED

Aase, J. K., and J. L. Pikul, 1995: Crop and Soil Response to Long-Term Tillage Practices in the Northern Great Plains. *Agron. J.*, **87**, 652–656, https://doi.org/10.2134/agronj1995.00021962008700040008x.

Abatzoglou, J. T., K. T. Redmond, and L. M. Edwards, 2009: Classification of regional climate variability in the state of California. *J. Appl. Meteorol. Climatol.*, **48**, 1527–1541, https://doi.org/10.1175/2009JAMC2062.1.

Abatzoglou, J. T., D. E. Rupp, and P. W. Mote, 2014: Seasonal climate variability and change in the pacific northwest of the united states. *J. Clim.*, **27**, 2125–2142, https://doi.org/10.1175/JCLI-D-13-00218.1.

Adegoke, J. O., R. A. Pielke, J. Eastman, R. Mahmood, and K. G. Hubbard, 2003: Impact of Irrigation on Midsummer Surface Fluxes and Temperature under Dry Synoptic Conditions: A Regional Atmospheric Model Study of the U.S. High Plains. *Mon. Weather Rev.*, **131**, 556–564, https://doi.org/10.1175/1520-0493(2003)131<0556:IOIOMS>2.0.CO;2.

Agard, V., and K. Emanuel, 2017: Clausius–Clapeyron Scaling of Peak CAPE in Continental Convective Storm Environments. *J. Atmospheric Sci.*, **74**, 3043–3054, https://doi.org/10.1175/JAS-D-16-0352.1.

Alter, R. E., Y. Fan, B. R. Lintner, C. P. Weaver, R. E. Alter, Y. Fan, B. R. Lintner, and C. P. Weaver, 2015a: Observational Evidence that Great Plains Irrigation Has Enhanced Summer Precipitation Intensity and Totals in the Midwestern United States. *J. Hydrometeorol.*, **16**, 1717–1735, https://doi.org/10.1175/JHM-D-14-0115.1.

——, H. C. Douglas, J. M. Winter, and E. A. B. Eltahir, 2017: 20th-century regional climate change in the central United States attributed to agricultural intensification. *Geophys. Res. Lett.*, 1–9, https://doi.org/10.1002/2017GL075604.

Asseng, S., and Coauthors, 2013a: Uncertainty in simulating wheat yields under climate change. *Nat. Clim. Change*, **3**, 827–832, https://doi.org/10.1038/nclimate1916.

——, and Coauthors, 2015b: Rising temperatures reduce global wheat production. *Nat. Clim. Change*, **5**, 143–147, https://doi.org/10.1038/nclimate2470.

Avissar, R., and R. A. Pielke, 1989: A Parameterization of Heterogeneous Land Surfaces for Atmospheric Numerical Models and Its Impact on Regional Meteorology. *Mon. Weather Rev.*, **117**, 2113–2136, https://doi.org/10.1175/1520-0493(1989)117<2113:APOHLS>2.0.CO;2.

Avissar, R., and R. A. Pielke, 1991: The impact of plant stomatal control on mesoscale atmospheric circulations. *Agric. For. Meteorol.*, **54**, 353–372, https://doi.org/10.1016/0168-1923(91)90013-G.

Barlage, M., M. Tewari, F. Chen, G. Miguez-Macho, Z.-L. Yang, and G.-Y. Niu, 2015: The effect of groundwater interaction in North American regional climate simulations with WRF/Noah-MP. *Clim. Change*, **129**, 485–498, https://doi.org/10.1007/s10584-014-1308-8.

——, F. Chen, R. Rasmussen, Z. Zhang, and G. Miguez-Macho, 2021: The Importance of Scale-Dependent Groundwater Processes in Land-Atmosphere Interactions Over the Central United States. *Geophys. Res. Lett.*, **48**, e2020GL092171, https://doi.org/10.1029/2020GL092171.

Betts, A. K., 2009: Land-Surface-Atmosphere Coupling in Observations and Models. *J. Adv. Model. Earth Syst.*, **1**, 1–18, https://doi.org/10.3894/JAMES.2009.1.4.

——, and R. L. Desjardins, 2018: Understanding Land–Atmosphere–Climate Coupling from the Canadian Prairie Dataset. *Environments*, **5**, 129, https://doi.org/10.3390/environments5120129.

——, R. Desjardins, and D. Worth, 2013a: Cloud radiative forcing of the diurnal cycle climate of the Canadian Prairies. *J. Geophys. Res. Atmospheres*, **118**, 8935–8953, https://doi.org/10.1002/jgrd.50593.

Betts, A. K., R. Desjardins, D. Worth, and D. Cerkowniak, 2013b: Impact of land use change on the diurnal cycle climate of the Canadian Prairies. *J. Geophys. Res. Atmospheres*, **118**, 11996–12011, https://doi.org/10.1002/2013JD020717.

Birch, C. E., J. H. Marsham, D. J. Parker, and C. M. Taylor, 2014: The scale dependence and structure of convergence fields preceding the initiation of deep convection. *Geophys. Res. Lett.*, **41**, 4769–4776, https://doi.org/10.1002/2014GL060493.

Blunden, J., and D. S. Arndt, eds., 2020: State of the Climate in 2019. *Bull. Am. Meteorol. Soc.*, **101**, S1–S429, https://doi.org/10.1175/2020BAMSStateoftheClimate.1.

Bonan, G. B., 2001: Observational Evidence for Reduction of Daily Maximum Temperature by Croplands in the Midwest United States. *J. Clim.*, **14**, 2430–2442, https://doi.org/10.1175/1520-0442(2001)014<2430:OEFROD>2.0.CO;2.

——, 2008: Forests and Climate Change: Forcings, Feedbacks, and the Climate Benefits of Forests. *Science*, **320**, 1444–1449, https://doi.org/10.1126/science.1155121.

Bonetti, S., G. Manoli, J. Domec, M. Putti, M. Marani, and G. G. Katul, 2015: The influence of water table depth and the free atmospheric state on convective rainfall predisposition. *Water Resour. Res.*, **51**, 2283–2297, https://doi.org/10.1002/2014WR016431.

Bonsal, B., Z. Liu, E. Wheaton, and R. Stewart, 2020: Historical and Projected Changes to the Stages and Other Characteristics of Severe Canadian Prairie Droughts. *Water*, **12**, 3370, https://doi.org/10.3390/w12123370.

Bonsal, B. R., X. Zhang, and W. D. Hogg, 1999: Canadian Prairie growing season precipitation variability and associated atmospheric circulation. *Clim. Res.*, **11**, 191–208.

Bradshaw, B., H. Dolan, and B. Smit, 2004: Farm-Level Adaptation to Climatic Variability and Change: Crop Diversification in the Canadian Prairies. *Clim. Change*, **67**, 119–141, https://doi.org/10.1007/s10584-004-0710-z.

Bright, R. M., E. Davin, T. O'Halloran, J. Pongratz, K. Zhao, and A. Cescatti, 2017: Local temperature response to land cover and management change driven by non-radiative processes. *Nat. Clim. Change*, **7**, 296–302, https://doi.org/10.1038/nclimate3250.

Brimelow, J. C., J. M. Hanesiak, and W. R. Burrows, 2011: Impacts of Land–Atmosphere Feedbacks on Deep, Moist Convection on the Canadian Prairies. *Earth Interact.*, **15**, 1–29, https://doi.org/10.1175/2011EI407.1.

Bromley, G. T., T. Gerken, A. F. Prein, and P. C. Stoy, 2020: Recent Trends in the Near-Surface Climatology of the Northern North American Great Plains. *J. Clim.*, **33**, 461–475, https://doi.org/10.1175/JCLI-D-19-0106.1.

Brookshire, E. N. J., P. C. Stoy, B. Currey, and B. Finney, 2020: The greening of the Northern Great Plains and its biogeochemical precursors. *Glob. Change Biol.*, **26**, 5404–5413, https://doi.org/10.1111/gcb.15115.

Butler, E. E., N. D. Mueller, and P. Huybers, 2018: Peculiarly pleasant weather for US maize. *Proc. Natl. Acad. Sci.*, **115**, 11935–11940, https://doi.org/10.1073/pnas.1808035115.

Campbell, C. A., R. P. Zentner, S. Gameda, B. Blomert, and D. D. Wall, 2002: Production of annual crops on the Canadian prairies: Trends during 1976–1998. *Can. J. Soil Sci.*, **82**, 45–57, https://doi.org/10.4141/S01-046.

Carbone, R. E., and J. D. Tuttle, 2008: Rainfall Occurrence in the U.S. Warm Season: The Diurnal Cycle. *J. Clim.*, **21**, 4132–4146, https://doi.org/10.1175/2008JCLI2275.1.

Chen, J., A. Dai, Y. Zhang, and K. L. Rasmussen, 2020: Changes in Convective Available Potential Energy and Convective Inhibition under Global Warming. *J. Clim.*, **33**, 2025–2050, https://doi.org/10.1175/JCLI-D-19-0461.1.

Chen, L., and P. A. Dirmeyer, 2017: Impacts of Land-Use/Land-Cover Change on Afternoon Precipitation over North America. *J. Clim.*, **30**, 2121–2140, https://doi.org/10.1175/JCLI-D-16-0589.1.

——, ——, A. Tawfik, and D. M. Lawrence, 2017b: Sensitivities of Land Cover–Precipitation Feedback to Convective Triggering. *J. Hydrometeorol.*, **18**, 2265–2283, https://doi.org/10.1175/JHM-D-17-0011.1.

——, Y. Li, F. Chen, M. Barlage, Z. Zhang, and Z. Li, 2019: Using 4-km WRF CONUS simulations to assess impacts of the surface coupling strength on regional climate simulation. *Clim. Dyn.*, **53**, 6397–6416, https://doi.org/10.1007/s00382-019-04932-9.

Cheruy, F., J. L. Dufresne, F. Hourdin, and A. Ducharne, 2014: Role of clouds and land-atmosphere coupling in midlatitude continental summer warm biases and climate change amplification in CMIP5 simulations. *Geophys. Res. Lett.*, **41**, https://doi.org/10.1002/2014GL061145.

Christensen, J. H., and Coauthors, 2007: Regional climate projections. Chapter 11.

Chug, D., and F. Dominguez, 2019: Isolating the observed influence of vegetation variability on the climate of La Plata River Basin. *J. Clim.*, https://doi.org/10.1175/JCLI-D-18-0677.1.

Collow, T. W., A. Robock, and W. Wu, 2014: Influences of soil moisture and vegetation on convective precipitation foerecasts over the United States Great Plains. *J. Geophys. Res. Atmospheres*, **119**, 9338–9358, https://doi.org/10.1002/2014JD021454.Received.

Cook, K. H., E. K. Vizy, Z. S. Launer, and C. M. Patricola, 2008: Springtime Intensification of the Great Plains Low-Level Jet and Midwest Precipitation in GCM Simulations of the Twenty-First Century. *J. Clim.*, **21**, 6321–6340, https://doi.org/10.1175/2008JCLI2355.1.

Couzin, J., 1999: Landscape Changes Make Regional Climate Run Hot and Cold. *Science*, **283**, 317–319, https://doi.org/10.1126/science.283.5400.317.

Dai, A., 2006: Recent climatology, variability, and trends in global surface humidity. *J. Clim.*, **19**, 3589–3606, https://doi.org/10.1175/JCLI3816.1.

Davin, E. L., S. I. Seneviratne, P. Ciais, A. Olioso, and T. Wang, 2014: Preferential cooling of hot extremes from cropland albedo management. *Proc. Natl. Acad. Sci.*, **111**, 9757–9761, https://doi.org/10.1073/pnas.1317323111.

DeAngelis, A., F. Dominguez, Y. Fan, A. Robock, M. D. Kustu, and D. Robinson, 2010: Evidence of enhanced precipitation due to irrigation over the Great Plains of the United States. *J. Geophys. Res. Atmospheres*, **115**, https://doi.org/10.1029/2010JD013892.

Desai, A. R., K. J. Davis, C. J. Senff, S. Ismail, E. V. Browell, D. R. Stauffer, and B. P. Reen, 2006: A case study on the effects of heterogeneous soil moisture on mesoscale boundary-layer structure in the Southern Great Plains, U.S.A. Part I: Simple prognostic model. *Bound.-Layer Meteorol.*, **119**, 195–238, https://doi.org/10.1007/s10546-005-9024-6.

Deser, C., A. Phillips, V. Bourdette, and H. Teng, 2012: Uncertainty in climate change projections: the role of internal variability. *Clim. Dyn.*, **38**, 527–546, https://doi.org/10.1007/s00382-010-0977-x.

Dickens, J. M., B. T. Forbes, D. S. Cobean, and S. Tadayon, 2011: *Documentation of methods and inventory of irrigation data collected for the 2000 and 2005 U.S. Geological Survey Estimated use of water in the United States, comparison of USGS-compiled irrigation data to other sources, and recommendations for future compilations*. http://pubs.usgs.gov/sir/2011/5166/.

Diffenbaugh, N. S., 2009: Influence of modern land cover on the climate of the United States. *Clim. Dyn.*, **33**, 945–958, https://doi.org/10.1007/s00382-009-0566-z.

Diffenbaugh, N. S., M. Scherer, and R. J. Trapp, 2013: Robust increases in severe thunderstorm environments in response to greenhouse forcing. *Proc. Natl. Acad. Sci.*, **110**, 16361–16366, https://doi.org/10.1073/pnas.1307758110.

Dolan, K. A., P. C. Stoy, and B. Poulter, 2020: Land management and climate change determine second-generation bioenergy potential of the US Northern Great Plains. *GCB Bioenergy*, **12**, 491–509, https://doi.org/10.1111/gcbb.12686.

Dominguez, F., G. Miguez-Macho, and H. Hu, 2016: WRF with Water Vapor Tracers: A Study of Moisture Sources for the North American Monsoon. *J. Hydrometeorol.*, **17**, 1915–1927, https://doi.org/10.1175/JHM-D-15-0221.1.

Dougherty, E., and K. L. Rasmussen, 2019: Climatology of Flood-Producing Storms and Their Associated Rainfall Characteristics in the United States. *Mon. Weather Rev.*, **147**, 3861–3877, https://doi.org/10.1175/MWR-D-19-0020.1.

Draper, C. S., R. H. Reichle, and R. D. Koster, 2017: Assessment of MERRA-2 Land Surface Energy Flux Estimates. *J. Clim.*, **31**, 671–691, https://doi.org/10.1175/JCLI-D-17-0121.1.

Durre, I., R. S. Vose, and D. B. Wuertz, 2006: Overview of the Integrated Global Radiosonde Archive. *J. Clim.*, **19**, 53–68, https://doi.org/10.1175/JCLI3594.1.

Eamus, D., N. Boulain, J. Cleverly, and D. D. Breshears, 2013: Global change-type drought-induced tree mortality: vapor pressure deficit is more important than temperature per se in causing decline in tree health. *Ecol. Evol.*, **3**, 2711–2729, https://doi.org/10.1002/ece3.664.

Engel, R. E., P. R. Miller, B. G. McConkey, and R. Wallander, 2017: Soil Organic Carbon Changes to Increasing Cropping Intensity and No-Till in a Semiarid Climate. *Soil Sci. Soc. Am. J.*, **81**, 404–413, https://doi.org/10.2136/sssaj2016.06.0194.

ESA, 2017: Land Cover CCI Product User Guide Version 2.

Fall, S., D. Niyogi, A. Gluhovsky, R. A. Pielke, E. Kalnay, and G. Rochon, 2010: Impacts of land use land cover on temperature trends over the continental United States: assessment using the North American Regional Reanalysis. *Int. J. Climatol.*, **30**, 1980–1993, https://doi.org/10.1002/joc.1996.

Feng, Z., L. R. Leung, S. Hagos, R. A. Houze, C. D. Burleyson, and K. Balaguru, 2016: More frequent intense and long-lived storms dominate the springtime trend in central US rainfall. *Nat. Commun.*, **7**, 1–8, https://doi.org/10.1038/ncomms13429.

——, R. A. Houze, L. R. Leung, F. Song, J. C. Hardin, J. Wang, W. I. Gustafson, and C. R. Homeyer, 2019: Spatiotemporal Characteristics and Large-Scale Environments of Mesoscale Convective Systems East of the Rocky Mountains. *J. Clim.*, **32**, 7303–7328, https://doi.org/10.1175/JCLI-D-19-0137.1.

Ficklin, D. L., and K. A. Novick, 2017: Historic and projected changes in vapor pressure deficit suggest a continental-scale drying of the United States atmosphere. *J. Geophys. Res. Atmospheres*, **122**, 2061–2079, https://doi.org/10.1002/2016JD025855.

Findell, K. L., and E. a. B. Eltahir, 2003a: Atmospheric Controls on Soil Moisture–Boundary Layer Interactions. Part I: Framework Development. *J. Hydrometeorol.*, **4**, 552–569, https://doi.org/10.1175/1525-7541(2003)004<0552:ACOSML>2.0.CO;2.

——, and ——, 2003b: Atmospheric Controls on Soil Moisture–Boundary Layer Interactions. Part II: Feedbacks within the Continental United States. *J. Hydrometeorol.*, **4**, 570–583, https://doi.org/10.1175/1525-7541(2003)004<0570:ACOSML>2.0.CO;2.

Flanagan, L. B., and A. C. Adkinson, 2011: Interacting controls on productivity in a northern Great Plains grassland and implications for response to ENSO events: CONTROLS ON GRASSLAND PRODUCTIVITY. *Glob. Change Biol.*, **17**, 3293–3311, https://doi.org/10.1111/j.1365-2486.2011.02461.x.

——, L. A. Wever, and P. J. Carlson, 2002: Seasonal and interannual variation in carbon dioxide exchange and carbon balance in a northern temperate grassland. *Glob. Change Biol.*, **8**, 599–615, https://doi.org/10.1046/j.1365-2486.2002.00491.x.

Francis, J. A., and S. J. Vavrus, 2015: Evidence for a wavier jet stream in response to rapid Arctic warming. *Environ. Res. Lett.*, **10**, 014005, https://doi.org/10.1088/1748-9326/10/1/014005.

Friedl, M. A., D. Sulla-Menashe, B. Tan, A. Schneider, N. Ramankutty, A. Sibley, and X. Huang, 2010: MODIS Collection 5 global land cover: Algorithm refinements and characterization of new datasets. *Remote Sens. Environ.*, **114**, 168–182, https://doi.org/10.1016/j.rse.2009.08.016.

Gameda, S., B. Qian, C. A. Campbell, and R. L. Desjardins, 2007: Climatic trends associated with summerfallow in the Canadian Prairies. *Agric. For. Meteorol.*, **142**, 170–185, https://doi.org/10.1016/j.agrformet.2006.03.026.

Gao, H., and G. Jia, 2013: Assessing disagreement and tolerance of misclassification of satellite-derived land cover products used in WRF model applications. *Adv. Atmospheric Sci.*, **30**, 125–141, https://doi.org/10.1007/s00376-012-2037-4.

Garcia-Carreras, L., D. J. Parker, C. M. Taylor, C. E. Reeves, and J. G. Murphy, 2010: Impact of mesoscale vegetation heterogeneities on the dynamical and thermodynamic properties of the planetary boundary layer. *J. Geophys. Res. Atmospheres*, **115**, 1–12, https://doi.org/10.1029/2009JD012811.

Gauthier, D. A., and E. B. Wiken, 2003: Monitoring the Conservation of Grassland Habitats, Prairie Ecozone, Canada. *Environ. Monit. Assess.*, **88**, 343–364.

Gentine, P., A. A. M. Holtslag, F. D'Andrea, and M. Ek, 2013: Surface and Atmospheric Controls on the Onset of Moist Convection over Land. *J. Hydrometeorol.*, **14**, https://doi.org/10.1175/JHM-D-12-0137.1.

Gerken, T., G. T. Bromley, B. L. Ruddell, S. Williams, and P. C. Stoy, 2018a: Convective suppression before and during the United States Northern Great Plains flash drought of 2017. *Hydrol. Earth Syst. Sci.*, **22**, 4155–4163, https://doi.org/10.5194/hess-22-4155-2018.

——, ——, and P. C. Stoy, 2018b: Surface Moistening Trends in the Northern North American Great Plains Increase the Likelihood of Convective Initiation. *J. Hydrometeorol.*, **19**, 227–244, https://doi.org/10.1175/JHM-D-17-0117.1.

Grimberg, B., S. Ahmed, C. Ellis, Z. Miller, and F. Menalled, 2018: Climate Change Perceptions and Observations of Agricultural Stakeholders in the Northern Great Plains. *Sustainability*, **10**, 1687, https://doi.org/10.3390/su10051687.

Grossiord, C., T. N. Buckley, L. A. Cernusak, K. A. Novick, B. Poulter, R. T. W. Siegwolf, J. S. Sperry, and N. G. McDowell, 2020: Plant responses to rising vapor pressure deficit. *New Phytol.*, **226**, 1550–1566, https://doi.org/10.1111/nph.16485.

Hammer, G., and P. Steurer, 1997: Data set documentation for hourly precipitation data.

Hammermeister, A. M., 2001: An Ecological analysis of prairie rehabilitation on petroleum wellsites in southeast Alberta. *Can. Univ. Alta.*,.

Hanesiak, J. M., R. L. Raddatz, and S. Lobban, 2004: Local Initiation of Deep Convection on the Canadian Prairie Provinces. *Bound.-Layer Meteorol.*, **110**, 455–470, https://doi.org/10.1023/B:BOUN.0000007242.89023.e5.

Harding, K. J., P. K. Snyder, K. J. Harding, and P. K. Snyder, 2012: Modeling the Atmospheric Response to Irrigation in the Great Plains. Part II: The Precipitation of Irrigated Water and Changes in Precipitation Recycling. *J. Hydrometeorol.*, **13**, 1687–1703, https://doi.org/10.1175/JHM-D-11-099.1.

Harris, C. R., and Coauthors, 2020a: Array programming with NumPy. *Nature*, **585**, 357–362, https://doi.org/10.1038/s41586-020-2649-2.

Harris, I., P. D. Jones, T. J. Osborn, and D. H. Lister, 2014: Updated high-resolution grids of monthly climatic observations - the CRU TS3.10 Dataset. *Int. J. Climatol.*, **34**, 623–642, https://doi.org/10.1002/joc.3711.

Harris, I., T. J. Osborn, P. Jones, and D. Lister, 2020b: Version 4 of the CRU TS monthly high-resolution gridded multivariate climate dataset. *Sci. Data*, **7**, 109, https://doi.org/10.1038/s41597-020-0453-3.

Held, I. M., and B. J. Soden, 2006: Robust Responses of the Hydrological Cycle to Global Warming. *J. Clim.*, **19**, 5686–5699, https://doi.org/10.1175/JCLI3990.1.

Hersbach, H., and Coauthors, The ERA5 Global Reanalysis. *Q. J. R. Meteorol. Soc.*, **n/a**, https://doi.org/10.1002/qj.3803.

Hirsch, A. L., M. Wilhelm, E. L. Davin, W. Thiery, and S. I. Seneviratne, 2017: Can climate-effective land management reduce regional warming? *J. Geophys. Res. Atmospheres*, **122**, 2269–2288, https://doi.org/10.1002/2016JD026125.

Hochman, Z., D. L. Gobbett, and H. Horan, 2017: Climate trends account for stalled wheat yields in Australia since 1990. *Glob. Change Biol.*, **23**, 2071–2081, https://doi.org/10.1111/gcb.13604.

Hohenegger, C., P. Brockhaus, C. S. Bretherton, and C. Schär, 2009: The Soil Moisture–Precipitation Feedback in Simulations with Explicit and Parameterized Convection. *J. Clim.*, **22**, 5003–5020, https://doi.org/10.1175/2009JCLI2604.1.

Homer, C., and Coauthors, 2015: Completion of the 2011 National Land Cover Database for the Conterminous United States - Representing a Decade of Land Cover Change Information. *Photogramm. Eng. Remote Sens.*, **81**, 346–354, https://doi.org/10.14358/PERS.81.5.345.

Hong, S.-Y., Y. Noh, and J. Dudhia, 2006: A New Vertical Diffusion Package with an Explicit Treatment of Entrainment Processes. *Mon. Weather Rev.*, **134**, 2318–2341, https://doi.org/10.1175/MWR3199.1.

Hoogewind, K. A., M. E. Baldwin, and R. J. Trapp, 2017: The Impact of Climate Change on Hazardous Convective Weather in the United States: Insight from High-Resolution Dynamical Downscaling. *J. Clim.*, **30**, 10081–10100, https://doi.org/10.1175/JCLI-D-16-0885.1.

Hoyer, S., and J. Hamman, 2017: xarray: N-D labeled arrays and datasets in Python. *J. Open Res. Softw.*, **5**, https://doi.org/10.5334/jors.148.

Hsiao, J., A. L. S. Swann, and S.-H. Kim, 2019: Maize yield under a changing climate: The hidden role of vapor pressure deficit. *Agric. For. Meteorol.*, **279**, 107692, https://doi.org/10.1016/j.agrformet.2019.107692.

Hu, Q., A. Weiss, S. Feng, and P. S. Baenziger, 2005: Earlier winter wheat heading dates and warmer spring in the U.S. Great Plains. *Agric. For. Meteorol.*, **135**, 284–290, https://doi.org/10.1016/j.agrformet.2006.01.001.

Huang, B., X. Hu, G.-A. Fuglstad, X. Zhou, W. Zhao, and F. Cherubini, 2020: Predominant regional biophysical cooling from recent land cover changes in Europe. *Nat. Commun.*, **11**, 1066, https://doi.org/10.1038/s41467-020-14890-0.

Huang, K., and Coauthors, 2018: Enhanced peak growth of global vegetation and its key mechanisms. *Nat. Ecol. Evol.*, **2**, 1897–1905, https://doi.org/10.1038/s41559-018-0714-0.

Huber, D., D. Mechem, and N. Brunsell, 2014: The Effects of Great Plains Irrigation on the Surface Energy Balance, Regional Circulation, and Precipitation. *Climate*, **2**, 103–128, https://doi.org/10.3390/cli2020103.

Hunter, J. D., 2007: Matplotlib: A 2D graphics environment. *Comput. Sci. Eng.*, **9**, 90–95, https://doi.org/10.1109/MCSE.2007.55.

Hunter, M. C., C. M. White, J. P. Kaye, and A. R. Kemanian, 2019: Ground-Truthing a Recent Report of Cover Crop–Induced Winter Warming. *Agric. Environ. Lett.*, **4**, 190007, https://doi.org/10.2134/ael2019.03.0007.

Iacono, M. J., J. S. Delamere, E. J. Mlawer, M. W. Shephard, S. A. Clough, and W. D. Collins, 2008: Radiative forcing by long-lived greenhouse gases: Calculations with the AER radiative transfer models. *J. Geophys. Res. Atmospheres*, **113**, https://doi.org/10.1029/2008JD009944.

IPCC, ed., 2013: *Climate Change 2013 - The Physical Science Basis: Working Group I Contribution to the Fifth Assessment Report of the Intergovernmental Panel on Climate Change*. Cambridge University Press,.

——, 2014: *AR5 Climate Change 2014: Impacts, Adaptation, and Vulnerability — IPCC*. IPCC, https://www.ipcc.ch/report/ar5/wg2/ (Accessed January 8, 2019).

Jones, P., 2016: The reliability of global and hemispheric surface temperature records. *Adv. Atmospheric Sci.*, **33**, 269–282, https://doi.org/10.1007/s00376-015-5194-4.

Juang, J. Y., G. G. Katul, A. Porporato, P. C. Stoy, M. S. Siqueira, M. Detto, H. S. Kim, and R. Oren, 2007a: Eco-hydrological controls on summertime convective rainfall triggers. *Glob. Change Biol.*, **13**, 887–896, https://doi.org/10.1111/j.1365-2486.2007.01315.x.

——, A. Porporato, P. C. Stoy, M. S. Siqueira, A. C. Oishi, M. Detto, H. S. Kim, and G. G. Katul, 2007b: Hydrologic and atmospheric controls on initiation of convective precipitation events. *Water Resour. Res.*, **43**, 1–10, https://doi.org/10.1029/2006WR004954.

Kanamori, H., T. Kumagai, H. Fujinami, T. Hiyama, and T. Yasunari, 2018: Effects of Long- and Short-Term Atmospheric Water Cycles on the Water Balance over the Maritime Continent. *J. Hydrometeorol.*, **19**, 1413–1427, https://doi.org/10.1175/JHM-D-18-0052.1.

Karl, T. R., and K. Trenberth, 2003: Modern Global Climate Change. *Science*, **302**, 1719–1723.

Kay, J. E., and Coauthors, 2015: The Community Earth System Model (CESM) Large Ensemble Project: A Community Resource for Studying Climate Change in the Presence of Internal Climate Variability. *Bull. Am. Meteorol. Soc.*, **96**, 1333–1349, https://doi.org/10.1175/BAMS-D-13-00255.1.

Keller, M., D. S. Schimel, W. W. Hargrove, and F. M. Hoffman, 2008: A continental strategy for the National Ecological Observatory Network. *Front. Ecol. Environ.*, **6**, 282–284, https://doi.org/10.1890/1540-9295(2008)6[282:ACSFTN]2.0.CO;2.

Klein, C., and C. M. Taylor, 2020: Dry soils can intensify mesoscale convective systems. *Proc. Natl. Acad. Sci.*, **117**, 21132–21137, https://doi.org/10.1073/pnas.2007998117.

Klemm, T., and R. A. McPherson, 2017: The development of seasonal climate forecasting for agricultural producers. *Agric. For. Meteorol.*, **232**, 384–399, https://doi.org/10.1016/j.agrformet.2016.09.005.

Knist, S., K. Goergen, and C. Simmer, 2020: Effects of land surface inhomogeneity on convection-permitting WRF simulations over central Europe. *Meteorol. Atmospheric Phys.*, **132**, 53–69, https://doi.org/10.1007/s00703-019-00671-y.

Kolby Smith, W., S. C. Reed, C. C. Cleveland, A. P. Ballantyne, W. R. L. Anderegg, W. R. Wieder, Y. Y. Liu, and S. W. Running, 2016: Large divergence of satellite and Earth system model estimates of global terrestrial CO 2 fertilization. *Nat. Clim. Change*, **6**, 306–310, https://doi.org/10.1038/nclimate2879.

Koster, R. D., 2004: Regions of Strong Coupling Between Soil Moisture and Precipitation. *Science*, **305**, 1138–1140, https://doi.org/10.1126/science.1100217.

Kucharik, C. J., 2008: Contribution of Planting Date Trends to Increased Maize Yields in the Central United States. *Agron. J.*, **100**, 328–336, https://doi.org/10.2134/agronj2007.0145.

Kunkel, K. E., 2003: North American Trends in Extreme Precipitation. *Nat. Hazards*, **29**, 291–305, https://doi.org/10.1023/A:1023694115864.

Ladwig, B., 2017: *wrf-python*. UCAR/NCAR,.

Lanning, S. P., K. Kephart, G. R. Carlson, J. E. Eckhoff, R. N. Stougaard, D. M. Wichman, J. M. Martin, and L. E. Talbert, 2010: Climatic Change and Agronomic Performance of Hard Red Spring Wheat from 1950 to 2007. *Crop Sci.*, **50**, 835, https://doi.org/10.2135/cropsci2009.06.0314.

Lark, T. J., J. Meghan Salmon, and H. K. Gibbs, 2015: Cropland expansion outpaces agricultural and biofuel policies in the United States. *Environ. Res. Lett.*, **10**, 044003, https://doi.org/10.1088/1748-9326/10/4/044003.

Lauenroth, W. K., I. C. Burke, and J. M. Paruelo, 2000: Patterns of Production and Precipitation-Use Efficiency of Winter Wheat and Native Grasslands in the Central Great Plains of the United States. *Ecosystems*, **3**, 344–351, https://doi.org/10.1007/s100210000031.

Lawrimore, J. H., M. J. Menne, B. E. Gleason, C. N. Williams, D. B. Wuertz, R. S. Vose, and J. Rennie, 2011: An overview of the Global Historical Climatology Network monthly mean temperature data set, version 3. *J. Geophys. Res. Atmospheres*, **116**, 1–18, https://doi.org/10.1029/2011JD016187.

Lepore, C., D. Veneziano, and A. Molini, 2015: Temperature and CAPE dependence of rainfall extremes in the eastern United States. *Geophys. Res. Lett.*, **42**, 74–83, https://doi.org/10.1002/2014GL062247.

Li, F., and D. R. Chavas, 2021: Midlatitude continental CAPE is predictable from large-scale environmental parameters. *Geophys. Res. Lett.*, **n/a**, e2020GL091799, https://doi.org/10.1029/2020GL091799.

Li, Z., Y. Li, B. Bonsal, A. H. Manson, and L. Scaff, 2018: Combined impacts of ENSO and MJO on the 2015 growing season drought on the Canadian Prairies. *Hydrol. Earth Syst. Sci.*, **22**, 5057–5067, https://doi.org/10.5194/hess-22-5057-2018.

Lin, R., and C. Chen, 2014: Tillage, Crop Rotation, and Nitrogen Management Strategies for Wheat in Central Montana. *Agron. J.*, **106**, 475–485, https://doi.org/10.2134/agronj2013.0316.

Lin, Y., W. Dong, M. Zhang, Y. Xie, W. Xue, J. Huang, and Y. Luo, 2017: Causes of model dry and warm bias over central U.S. and impact on climate projections. *Nat. Commun.*, **8**, 881, https://doi.org/10.1038/s41467-017-01040-2.

Liu, C., and Coauthors, 2017: Continental-scale convection-permitting modeling of the current and future climate of North America. *Clim. Dyn.*, **49**, 71–95, https://doi.org/10.1007/s00382-016-3327-9.

Liu, P., A. P. Tsimpidi, Y. Hu, B. Stone, A. G. Russell, and A. Nenes, 2012: Differences between downscaling with spectral and grid nudging using WRF. *Atmospheric Chem. Phys.*, **12**, 3601–3610, https://doi.org/10.5194/acp-12-3601-2012.

Lobell, D. B., and C. Bonfils, 2008: The Effect of Irrigation on Regional Temperatures: A Spatial and Temporal Analysis of Trends in California, 1934–2002. *J. Clim.*, **21**, 2063–2071, https://doi.org/10.1175/2007JCLI1755.1.

Lobell, D. B., G. Bala, and P. B. Duffy, 2006: Biogeophysical impacts of cropland management changes on climate. *Geophys. Res. Lett.*, **33**, https://doi.org/10.1029/2005GL025492.

Lobell, D. B., C. J. Bonfils, L. M. Kueppers, and M. A. Snyder, 2008: Irrigation cooling effect on temperature and heat index extremes. *Geophys. Res. Lett.*, **35**, https://doi.org/10.1029/2008GL034145.

Lobell, D. B., W. Schlenker, and J. Costa-Roberts, 2011: Climate Trends and Global Crop Production Since 1980. *Science*, **333**, 616–620, https://doi.org/10.1126/science.1204531.

Lombardozzi, D. L., G. B. Bonan, W. Wieder, A. S. Grandy, C. Morris, and D. L. Lawrence, 2018: Cover Crops May Cause Winter Warming in Snow-Covered Regions. *Geophys. Res. Lett.*, **45**, 9889–9897, https://doi.org/10.1029/2018GL079000.

Long, J. A., R. L. Lawrence, P. R. Miller, and L. A. Marshall, 2014a: Changes in field-level cropping sequences: Indicators of shifting agricultural practices. *Agric. Ecosyst. Environ.*, **189**, 11–20, https://doi.org/10.1016/j.agee.2014.03.015.

——, ——, ——, ——, and M. C. Greenwood, 2014b: Adoption of cropping sequences in northeast Montana: A spatio-temporal analysis. *Agric. Ecosyst. Environ.*, **197**, 77–87, https://doi.org/10.1016/j.agee.2014.07.022.

López, J., D. A. Way, and W. Sadok, Systemic effects of rising atmospheric vapor pressure deficit on plant physiology and productivity. *Glob. Change Biol.*, **n/a**, https://doi.org/10.1111/gcb.15548.

Lu, Y., K. Harding, and L. Kueppers, 2017: Irrigation effects on land-atmosphere coupling strength in the United States. *J. Clim.*, **30**, 3671–3685, https://doi.org/10.1175/JCLI-D-15-0706.1.

Luyssaert, S., and Coauthors, 2014: Land management and land-cover change have impacts of similar magnitude on surface temperature. *Nat. Clim. Change*, **4**, 389–393, https://doi.org/10.1038/nclimate2196.

Ma, H.-Y., and Coauthors, 2018: CAUSES: On the Role of Surface Energy Budget Errors to the Warm Surface Air Temperature Error Over the Central United States. *J. Geophys. Res. Atmospheres*, **123**, 2888–2909, https://doi.org/10.1002/2017JD027194.

Maaz, T., J. D. Wulfhorst, V. McCracken, J. Kirkegaard, D. R. Huggins, I. Roth, H. Kaur, and W. Pan, 2018: Economic, policy, and social trends and challenges of introducing oilseed and pulse crops into dryland wheat cropping systems. *Agric. Ecosyst. Environ.*, **253**, 177–194, https://doi.org/10.1016/j.agee.2017.03.018.

Mahmood, R., K. G. Hubbard, R. D. Leeper, and S. A. Foster, 2008: Increase in Near-Surface Atmospheric Moisture Content due to Land Use Changes: Evidence from the Observed Dewpoint Temperature Data. *Mon. Weather Rev.*, **136**, 1554–1561, https://doi.org/10.1175/2007MWR2040.1.

——, and Coauthors, 2010: Impacts of Land Use/Land Cover Change on Climate and Future Research Priorities. *Bull. Am. Meteorol. Soc.*, **91**, 37–46, https://doi.org/10.1175/2009BAMS2769.1.

——, R. Leeper, and A. I. Quintanar, 2011: Sensitivity of planetary boundary layer atmosphere to historical and future changes of land use/land cover, vegetation fraction, and soil moisture in Western Kentucky, USA. *Glob. Planet. Change*, **78**, 36–53, https://doi.org/10.1016/j.gloplacha.2011.05.007.

——, T. Keeling, S. A. Foster, and K. G. Hubbard, 2013: Did irrigation impact 20th century air temperature in the High Plains aquifer region? *Appl. Geogr.*, **38**, 11–21, https://doi.org/10.1016/j.apgeog.2012.11.002.

——, and Coauthors, 2014a: Land cover changes and their biogeophysical effects on climate. *Int. J. Climatol.*, **34**, 929–953, https://doi.org/10.1002/joc.3736.

Mallard, M. S., T. L. Spero, and S. M. Taylor, 2018: Examining WRF's Sensitivity to Contemporary Land-Use Datasets across the Contiguous United States Using Dynamical Downscaling. *J. Appl. Meteorol. Climatol.*, **57**, 2561–2583, https://doi.org/10.1175/JAMC-D-17-0328.1.

Mande, T., N. C. Ceperley, G. G. Katul, S. W. Tyler, H. Yacouba, and M. B. Parlange, 2015: Suppressed convective rainfall by agricultural expansion in southeastern Burkina Faso. *Water Resour. Res.*, **51**, 5521–5530, https://doi.org/10.1002/2015WR017144.

Manoli, G., J. C. Domec, K. Novick, A. C. Oishi, A. Noormets, M. Marani, and G. Katul, 2016: Soil-plant-atmosphere conditions regulating convective cloud formation above southeastern US pine plantations. *Glob. Change Biol.*, **22**, 2238–2254, https://doi.org/10.1111/gcb.13221.

Marshall, C. H., R. A. Pielke, and L. T. Steyaert, 2003: Crop freezes and land-use change in Florida. *Nature*, **426**, 29–30, https://doi.org/10.1038/426029a.

Maurer, V., I. Bischoff-Gauß, N. Kalthoff, L. Gantner, R. Roca, and H.-J. Panitz, 2017: Initiation of deep convection in the Sahel in a convection-permitting climate simulation for northern Africa. *Q. J. R. Meteorol. Soc.*, **143**, 806–816, https://doi.org/10.1002/qj.2966.

May, R., S. Arms, P. Marsh, E. Bruning, J. Leeman, and Z. Bruick, 2016: *MetPy: A Python Package for Meteorological Data*. UCAR/NCAR - Unidata,.

Miller, P. R., and Coauthors, 2002: Pulse Crop Adaptation in the Northern Great Plains. *Agron. J.*, **94**, 261–272, https://doi.org/10.2134/agronj2002.2610.

Miller, P. R., Y. Gan, B. G. McConkey, and C. L. McDonald, 2003: Pulse Crops for the Northern Great Plains: I. Grain Productivity and Residual Effects on Soil Water and Nitrogen. *Agron. J.*, **95**, 972–979, https://doi.org/10.2134/agronj2003.9720.

Millett, B., · W Carter Johnson, G. Guntenspergen, W. C. Johnson, and G. Guntenspergen, 2009: Climate trends of the North American prairie pothole region 1906–2000. *Clim. Change*, **93**, https://doi.org/10.1007/s10584-008-9543-5.

Mishra, V., J. M. Wallace, and D. P. Lettenmaier, 2012: Relationship between hourly extreme precipitation and local air temperature in the United States. *Geophys. Res. Lett.*, **39**, https://doi.org/10.1029/2012GL052790.

Mueller, B., M. Hauser, C. Iles, R. H. Rimi, F. W. Zwiers, and H. Wan, 2015a: Lengthening of the growing season in wheat and maize producing regions. *Weather Clim. Extrem.*, **9**, 47–56, https://doi.org/10.1016/j.wace.2015.04.001.

Mueller, N. D., E. E. Butler, K. A. Mckinnon, A. Rhines, M. Tingley, N. M. Holbrook, and P. Huybers, 2015b: Cooling of US Midwest summer temperature extremes from cropland intensification. https://doi.org/10.1038/NCLIMATE2825.

Mueller, N. D., A. Rhines, E. E. Butler, D. K. Ray, S. Siebert, N. M. Holbrook, and P. Huybers, 2017: Global Relationships between Cropland Intensification and Summer Temperature Extremes over the Last 50 Years. *J. Clim.*, **30**, 7505–7528, https://doi.org/10.1175/JCLI-D-17-0096.1.

Muhlbauer, A., P. Spichtinger, and U. Lohmann, 2009: Application and Comparison of Robust Linear Regression Methods for Trend Estimation. *J. Appl. Meteorol. Climatol.*, **48**, 1961–1970, https://doi.org/10.1175/2009JAMC1851.1.

Nielsen, D. C., P. W. Unger, and P. R. Miller, 2005: Efficient Water Use in Dryland Cropping Systems in the Great Plains. *Agron. J.*, **97**, 364–372, https://doi.org/10.2134/agronj2005.0364.

Niu, G.-Y., Z.-L. Yang, R. E. Dickinson, L. E. Gulden, and H. Su, 2007: Development of a simple groundwater model for use in climate models and evaluation with Gravity Recovery and Climate Experiment data. *J. Geophys. Res. Atmospheres*, **112**, https://doi.org/10.1029/2006JD007522.

——, and Coauthors, 2011: The community Noah land surface model with multiparameterization options (Noah-MP): 1. Model description and evaluation with

local-scale measurements. *J. Geophys. Res. Atmospheres*, **116**, https://doi.org/10.1029/2010JD015139.

Novick, K. A., and Coauthors, 2016a: The increasing importance of atmospheric demand for ecosystem water and carbon fluxes. *Nat. Clim. Change*, **6**, 1023–1027, https://doi.org/10.1038/nclimate3114.

O'Gorman, P. A., and T. Schneider, 2009: The physical basis for increases in precipitation extremes in simulations of 21st-century climate change. *Proc. Natl. Acad. Sci.*, **106**, 14773–14777, https://doi.org/10.1073/pnas.0907610106.

Ortiz, R., and Coauthors, 2008: Climate change: Can wheat beat the heat? https://doi.org/10.1016/j.agee.2008.01.019.

Partridge, T. F., J. M. Winter, E. C. Osterberg, D. W. Hyndman, A. D. Kendall, and F. J. Magilligan, 2018: Spatially Distinct Seasonal Patterns and Forcings of the U.S. Warming Hole. *Geophys. Res. Lett.*, **45**, 2055–2063, https://doi.org/10.1002/2017GL076463.

Pendergrass, A. G., and D. L. Hartmann, 2014: The Atmospheric Energy Constraint on Global-Mean Precipitation Change. *J. Clim.*, **27**, 757–768, https://doi.org/10.1175/JCLI-D-13-00163.1.

Piao, S., and Coauthors, 2020: Characteristics, drivers and feedbacks of global greening. *Nat. Rev. Earth Environ.*, **1**, 14–27, https://doi.org/10.1038/s43017-019-0001-x.

Pielke, R. A., 2001: Influence of the spatail distribution of vegetation and soils on the predictions of cumulus convective rainfall. *Rev. Geophys.*, **39**, 151–177, https://doi.org/10.1029/1999RG000072.

——, Sr, R. Avissar, M. Raupach, A. J. Dolman, X. Zeng, and A. S. Denning, 1998: Interactions between the atmosphere and terrestrial ecosystems: influence on weather and climate. *Glob. Change Biol.*, **4**, 461–475, https://doi.org/10.1046/j.1365-2486.1998.t01-1-00176.x.

Pielke, R. A., J. Adegoke, A. Beltrán-Przekurat, C. A. Hiemstra, J. Lin, U. S. Nair, D. Niyogi, and T. E. Nobis, 2007: An overview of regional land-use and land-cover impacts on rainfall. *Tellus Ser. B Chem. Phys. Meteorol.*, **59**, 587–601, https://doi.org/10.1111/j.1600-0889.2007.00251.x.

Pomeroy, J. W., and L. Li, 2000: Prairie and arctic areal snow cover mass balance using a blowing snow model. *J. Geophys. Res. Atmospheres*, **105**, 26619–26634, https://doi.org/10.1029/2000JD900149.

——, D. M. Gray, K. R. Shook, B. Toth, R. L. H. Essery, A. Pietroniro, and N. Hedstrom, 1998: An evaluation of snow accumulation and ablation processes for land surface modelling.

Hydrol. Process., **12**, 2339–2367, https://doi.org/10.1002/(SICI)1099-1085(199812)12:15<2339::AID-HYP800>3.0.CO;2-L.

Prasanna, V., and T. Yasunari, 2009: Time-Space Characteristics of Seasonal and Interannual Variations of Atmospheric Water Balance over South Asia. *J. Meteorol. Soc. Jpn.*, **87**, 263–287, https://doi.org/10.2151/jmsj.87.263.

Prein, A. F., and Coauthors, 2015: A review on regional convection-permitting climate modeling: Demonstrations, prospects, and challenges. *Rev. Geophys.*, **53**, 323–361, https://doi.org/10.1002/2014RG000475.

——, C. Liu, K. Ikeda, R. Bullock, R. M. Rasmussen, G. J. Holland, and M. Clark, 2017a: Simulating North American mesoscale convective systems with a convection-permitting climate model. *Clim. Dyn.*, https://doi.org/10.1007/s00382-017-3993-2.

——, ——, ——, S. B. Trier, R. M. Rasmussen, G. J. Holland, and M. P. Clark, 2017b: Increased rainfall volume from future convective storms in the US. *Nat. Clim. Change*, **7**, 880–884, https://doi.org/10.1038/s41558-017-0007-7.

——, R. M. Rasmussen, K. Ikeda, C. Liu, M. P. Clark, and G. J. Holland, 2017c: The future intensification of hourly precipitation extremes. *Nat. Clim. Change*, **7**, 48–52, https://doi.org/10.1038/nclimate3168.

Qian, Y., and Coauthors, 2020: Neglecting irrigation contributes to the simulated summertime warm-and-dry bias in the central United States. *Npj Clim. Atmospheric Sci.*, **3**, 1–10, https://doi.org/10.1038/s41612-020-00135-w.

Quiring, S. M., and T. N. Papakyriakou, 2005: Characterizing the spatial and temporal variability of June-July moisture conditions in the Canadian prairies. *Int. J. Climatol.*, **25**, 117–138, https://doi.org/10.1002/joc.1104.

Quiring, S. M., and D. B. Kluver, 2009: Relationship between Winter/Spring Snowfall and Summer Precipitation in the Northern Great Plains of North America. https://doi.org/10.1175/2009JHM1089.1.

Raddatz, R. L., 1998a: Anthropogenic vegetation transformation and the potential for deep convection on the Canadian prairies. *Can. J. Soil Sci.*, **78**, 657–666, https://doi.org/10.4141/S98-011.

——, 2000a: Summer rainfall recycling for an agricultural region of the Canadian prairies. *Can. J. Soil Sci.*, **80**, 367–373, https://doi.org/10.4141/S99-016.

Raddatz, R. L., 2005: Moisture recycling on the Canadian Prairies for summer droughts and pluvials from 1997 to 2003. *Agric. For. Meteorol.*, **131**, 13–26, https://doi.org/10.1016/j.agrformet.2005.04.007.

Ramsey, F., and D. Schafer, 2012: *The Statistical Sleuth: A Course in Methods of Data Analysis*. 4th ed.

Rasmussen, K. L., A. F. Prein, R. M. Rasmussen, K. Ikeda, and C. Liu, 2017: Changes in the convective population and thermodynamic environments in convection-permitting regional climate simulations over the United States. *Clim. Dyn.*, **55**, 383–408, https://doi.org/10.1007/s00382-017-4000-7.

Reidmiller, D. R., C. W. Avery, D. R. Easterling, K. E. Kunkel, K. L. M. Lewis, T. K. Maycock, and B. C. Stewart, 2018: *Impacts, Risks, and Adaptation in the United States: The Fourth National Climate Assessment, Volume II*. U.S. Global Change Research Program,.

Rey-Sanchez, C., and Coauthors, 2021: Evaluation of Atmospheric Boundary Layer Height From Wind Profiling Radar and Slab Models and Its Responses to Seasonality of Land Cover, Subsidence, and Advection. *J. Geophys. Res. Atmospheres*, **126**, e2020JD033775, https://doi.org/10.1029/2020JD033775.

Richardson, A. D., and Coauthors, 2006: A multi-site analysis of random error in tower-based measurements of carbon and energy fluxes. *Agric. For. Meteorol.*, **136**, 1–18, https://doi.org/10.1016/j.agrformet.2006.01.007.

Rigden, A. J., N. D. Mueller, N. M. Holbrook, N. Pillai, and P. Huybers, 2020: Combined influence of soil moisture and atmospheric evaporative demand is important for accurately predicting US maize yields. *Nat. Food*, **1**, 127–133, https://doi.org/10.1038/s43016-020-0028-7.

Rodell, M., and J. S. Famiglietti, 2002: The potential for satellite-based monitoring of groundwater storage changes using GRACE: the High Plains aquifer, Central US. *J. Hydrol.*, **263**, 245–256, https://doi.org/10.1016/S0022-1694(02)00060-4.

——, ——, D. N. Wiese, J. T. Reager, H. K. Beaudoing, F. W. Landerer, and M. H. Lo, 2018: Emerging trends in global freshwater availability. *Nature*, **557**, 651–659, https://doi.org/10.1038/s41586-018-0123-1.

Rohde, R., R. A. Muller, R. Jacobsen, E. Muller, and C. Wickham, 2013: A New Estimate of the Average Earth Surface Land Temperature Spanning 1753 to 2011. *Geoinformatics Geostat. Overv.*, **01**, https://doi.org/10.4172/2327-4581.1000101.

Rosenzweig, S. T., and M. E. Schipanski, 2019: Landscape-scale cropping changes in the High Plains: economic and environmental implications. *Environ. Res. Lett.*, **14**, 124088, https://doi.org/10.1088/1748-9326/ab5e8b.

Rossum, G., 1995: *Python Reference Manual*. CWI (Centre for Mathematics and Computer Science),.

Roundy, J. K., C. R. Ferguson, and E. F. Wood, 2013: Temporal Variability of Land–Atmosphere Coupling and Its Implications for Drought over the Southeast United States. *J. Hydrometeorol.*, **14**, 622–635, https://doi.org/10.1175/JHM-D-12-090.1.

Rustemeier, E., A. Becker, P. Finger, U. Schneider, and M. Ziese, 2020: GPCC Precipitation Climatology Version 2020 at 0.25°: Monthly Land-Surface Precipitation Climatology for Every Month and the Total Year from Rain-Gauges built on GTS-based and Historic Data: Globally Gridded Monthly Totals. min. 200 KByte-max. 20 MByte per gzip compressed NetCDF archive, https://doi.org/10.5676/DWD_GPCC/CLIM_M_V2020_025.

Sacks, W. J., and C. J. Kucharik, 2011: Crop management and phenology trends in the U.S. Corn Belt: Impacts on yields, evapotranspiration and energy balance. *Agric. For. Meteorol.*, **151**, 882–894, https://doi.org/10.1016/j.agrformet.2011.02.010.

Santanello, J. A., and Coauthors, 2017: Land–Atmosphere Interactions: The LoCo Perspective. *Bull. Am. Meteorol. Soc.*, **99**, 1253–1272, https://doi.org/10.1175/BAMS-D-17-0001.1.

Santer, B. D., T. M. L. Wigley, J. S. Boyle, D. J. Gaffen, J. J. Hnilo, D. Nychka, D. E. Parker, and K. E. Taylor, 2000: Statistical significance of trends and trend differences in layer-average atmospheric temperature time series. *J. Geophys. Res.*, **105**, 7337–7356, https://doi.org/10.1029/1999JD901105.

Schlenker, W., M. J. Roberts, and V. K. Smith, 2009: Nonlinear temperature effects indicate severe damages to U.S. crop yields under climate change.

Schulzweida, U., 2019: CDO User Guide. https://doi.org/10.5281/ZENODO.3539275.

Seabold, S., and J. Perktold, 2010: Statsmodels: Econometric and Statistical Modeling with Python. *Proc. 9th Python Sci. Conf.*, **2010**.

Seager, R., J. Feldman, N. Lis, M. Ting, A. P. Williams, J. Nakamura, H. Liu, and N. Henderson, 2018a: Whither the 100th Meridian? The Once and Future Physical and Human Geography of America's Arid–Humid Divide. Part II: The Meridian Moves East. *Earth Interact.*, **22**, 1–24, https://doi.org/10.1175/EI-D-17-0012.1.

Seeley, J. T., and D. M. Romps, 2014: The Effect of Global Warming on Severe Thunderstorms in the United States. *J. Clim.*, **28**, 2443–2458, https://doi.org/10.1175/JCLI-D-14-00382.1.

——, and ——, 2015: Why does tropical convective available potential energy (CAPE) increase with warming? *Geophys. Res. Lett.*, **42**, 10,429-10,437, https://doi.org/10.1002/2015GL066199.

Segal, M., Z. Pan, R. W. Turner, and E. S. Takle, 1998: On the Potential Impact of Irrigated Areas in North America on Summer Rainfall Caused by Large-Scale Systems. *J. Appl. Meteorol.*, **37**, 325–331, https://doi.org/10.1175/1520-0450-37.3.325.

Seneviratne, S. I., D. Lüthi, M. Litschi, and C. Schär, 2006: Land-atmosphere coupling and climate change in Europe. *Nature*, **443**, 205–209, https://doi.org/10.1038/nature05095.

Seneviratne, S. I., and Coauthors, 2018: Land radiative management as contributor to regional-scale climate adaptation and mitigation. *Nat. Geosci.*, **11**, 88–96, https://doi.org/10.1038/s41561-017-0057-5.

Sertel, E., A. Robock, and C. Ormeci, 2010: Impacts of land cover data quality on regional climate simulations. *Int. J. Climatol.*, **30**, 1942–1953, https://doi.org/10.1002/joc.2036.

Shrestha, B. M., R. L. Raddatz, R. L. Desjardins, and D. E. Worth, 2012: Continuous Cropping and Moist Deep Convection on the Canadian Prairies. *Atmosphere*, **3**, 573–590, https://doi.org/10.3390/atmos3040573.

Skamarock, W. C., and Coauthors, 2008: A description of the advanced research WRF version 3, NCAR Technical Note. *Natl. Cent. Atmospheric Res. Boulder CO USA*,.

Smith, W. N., and Coauthors, 2013: Assessing the effects of climate change on crop production and GHG emissions in Canada. *Agric. Ecosyst. Environ.*, **179**, 139–150, https://doi.org/10.1016/j.agee.2013.08.015.

Song, F., Z. Feng, L. R. Leung, R. A. Houze Jr, J. Wang, J. Hardin, and C. R. Homeyer, 2019: Contrasting Spring and Summer Large-Scale Environments Associated with Mesoscale Convective Systems over the U.S. Great Plains. *J. Clim.*, **32**, 6749–6767, https://doi.org/10.1175/JCLI-D-18-0839.1.

Song, X.-P., M. C. Hansen, S. V. Stehman, P. V. Potapov, A. Tyukavina, E. F. Vermote, and J. R. Townshend, 2018: Global land change from 1982 to 2016. *Nature*, **560**, 639–643, https://doi.org/10.1038/s41586-018-0411-9.

Spera, S. A., J. M. Winter, and J. W. Chipman, 2018: Evaluation of Agricultural Land Cover Representations on Regional Climate Model Simulations in the Brazilian Cerrado. *J. Geophys. Res. Atmospheres*, **123**, 5163–5176, https://doi.org/10.1029/2017JD027989.

Spero, T. L., M. J. Otte, J. H. Bowden, and C. G. Nolte, 2014: Improving the representation of clouds, radiation, and precipitation using spectral nudging in the Weather Research and Forecasting model. *J. Geophys. Res. Atmospheres*, **119**, 11,682-11,694, https://doi.org/10.1002/2014JD022173.

Stadnyk, T., K. Dow, L. Wazney, and E.-L. Blais, 2016: The 2011 flood event in the Red River Basin: Causes, assessment and damages. *Can. Water Resour. J. Rev. Can. Ressour. Hydr.*, **41**, 65–73, https://doi.org/10.1080/07011784.2015.1008048.

Stein, A. F., R. R. Draxler, G. D. Rolph, B. J. B. Stunder, M. D. Cohen, and F. Ngan, 2015: NOAA's HYSPLIT Atmospheric Transport and Dispersion Modeling System. *Bull. Am. Meteorol. Soc.*, **96**, 2059–2077, https://doi.org/10.1175/BAMS-D-14-00110.1.

Stevenson, S. N., and R. S. Schumacher, 2014: A 10-Year Survey of Extreme Rainfall Events in the Central and Eastern United States Using Gridded Multisensor Precipitation Analyses. *Mon. Weather Rev.*, **142**, 3147–3162, https://doi.org/10.1175/MWR-D-13-00345.1.

Stocker, T., D. Qin, G. Plattner, and M. Tignor, 2014: *Climate Change 2013 The Physical Science Basis*.

Stoy, P. C., and Coauthors, 2013: A data-driven analysis of energy balance closure across FLUXNET research sites: The role of landscape scale heterogeneity. *Agric. For. Meteorol.*, **171–172**, 137–152, https://doi.org/10.1016/j.agrformet.2012.11.004.

Stoy, P. C., and Coauthors, 2018: Opportunities and Trade-offs among BECCS and the Food, Water, Energy, Biodiversity, and Social Systems Nexus at Regional Scales. *BioScience*, **68**, 100–111, https://doi.org/10.1093/biosci/bix145.

Sun, Q., C. Miao, Q. Duan, H. Ashouri, S. Sorooshian, and K.-L. Hsu, 2018: A Review of Global Precipitation Data Sets: Data Sources, Estimation, and Intercomparisons. *Rev. Geophys.*, **56**, 79–107, https://doi.org/10.1002/2017RG000574.

Tan, X., T. Y. Gan, and Y. D. Chen, 2018: Moisture sources and pathways associated with the spatial variability of seasonal extreme precipitation over Canada. *Clim. Dyn.*, **50**, 629–640, https://doi.org/10.1007/s00382-017-3630-0.

Tang, Y., J. Winkler, S. Zhong, X. Bian, D. Doubler, L. Yu, and C. Walters, 2017: Future changes in the climatology of the Great Plains low-level jet derived from fine resolution multi-model simulations. *Sci. Rep.*, **7**, 5029, https://doi.org/10.1038/s41598-017-05135-0.

Taylor, C. M., and Coauthors, 2006: Frequency of Sahelian storm initiation enhanced over mesoscale soil-moisture patterns. *Nature*, **4**, 611–625, https://doi.org/10.1038/ngeo1173.

——, D. Jeu, a. M. Richard, F. Guichard, P. P. Harris, and W. a. Dorigo, 2012: Afternoon rain more likely over drier soils. *Nature*, **489**, 423–426, https://doi.org/10.1038/nature11377.

——, C. E. Birch, D. J. Parker, N. Dixon, F. Guichard, G. Nikulin, and G. M. S. Lister, 2013: Modeling soil moisture-precipitation feedback in the Sahel: Importance of spatial scale versus convective parameterization. *Geophys. Res. Lett.*, **40**, 6213–6218, https://doi.org/10.1002/2013GL058511.

Thompson, G., P. R. Field, R. M. Rasmussen, and W. D. Hall, 2008: Explicit Forecasts of Winter Precipitation Using an Improved Bulk Microphysics Scheme. Part II: Implementation of a New Snow Parameterization. *Mon. Weather Rev.*, **136**, 5095–5115, https://doi.org/10.1175/2008MWR2387.1.

Thornton, P. E., S. W. Running, and M. A. White, 1997: Generating surfaces of daily meteorological variables over large regions of complex terrain. *J. Hydrol.*, **190**, 214–251, https://doi.org/10.1016/S0022-1694(96)03128-9.

Thornton, P. E., M. M. Thornton, B. W. Mayer, Y. Wei, R. Devarakonda, R. S. Vose, and R. B. Cook, 2016: DaymetDaymet: Daily Surface Weather Data on a 1-km Grid for North America, Version 3. 711509.8892839993 MB, https://doi.org/10.3334/ORNLDAAC/1328.

Trapp, R. J., K. A. Hoogewind, and S. Lasher-Trapp, 2019: Future Changes in Hail Occurrence in the United States Determined through Convection-Permitting Dynamical Downscaling. *J. Clim.*, **32**, 5493–5509, https://doi.org/10.1175/JCLI-D-18-0740.1.

Trenberth, K. E., A. Dai, R. M. Rasmussen, and D. B. Parsons, 2003: The Changing Character of Precipitation. *Bull. Am. Meteorol. Soc.*, **84**, 1205–1218, https://doi.org/10.1175/BAMS-84-9-1205.

Twine, T. E., and Coauthors, 2000: Correcting eddy-covariance flux underestimates over a grassland. *Agric. For. Meteorol.*, **103**, 279–300, https://doi.org/10.1016/S0168-1923(00)00123-4.

Vanden Broucke, S., and N. Van Lipzig, 2017: Do convection-permitting models improve the representation of the impact of LUC? *Clim. Dyn.*, **49**, 2749–2763, https://doi.org/10.1007/s00382-016-3489-5.

——, S. Luyssaert, E. L. Davin, I. Janssens, and N. van Lipzig, 2015: New insights in the capability of climate models to simulate the impact of LUC based on temperature decomposition of paired site observations. *J. Geophys. Res. Atmospheres*, **120**, 5417–5436, https://doi.org/10.1002/2015JD023095.

Vick, E. S. K., P. C. Stoy, A. C. I. Tang, and T. Gerken, 2016: The surface-atmosphere exchange of carbon dioxide, water, and sensible heat across a dryland wheat-fallow rotation. *Agric. Ecosyst. Environ.*, **232**, 129–140, https://doi.org/10.1016/j.agee.2016.07.018.

Wang, Y., B. Geerts, and C. Liu, 2018: A 30-year convection-permitting regional climate simulation over the interior western United States. Part I: Validation. *Int. J. Climatol.*, **38**, 3684–3704, https://doi.org/10.1002/joc.5527.

Wiken, E. B., and Canadian Council on Ecological Areas, eds., 1996: *A perspective on Canada's ecosystems: an overview of the terrestrial and marine ecozones*. Canadian Council on Ecological Areas, 95 pp.

Xie, S.-P., and Coauthors, 2015: Towards predictive understanding of regional climate change. *Nat. Clim. Change*, **5**, 921–930, https://doi.org/10.1038/nclimate2689.

Yang, Z., F. Dominguez, X. Zeng, H. Hu, H. Gupta, and B. Yang, 2017: Impact of Irrigation over the California Central Valley on Regional Climate. *J. Hydrometeorol.*, **18**, 1341–1357, https://doi.org/10.1175/JHM-D-16-0158.1.

Yin, J., J. D. Albertson, J. R. Rigby, and A. Porporato, 2015: Land and atmospheric controls on initiation and intensity of moist convection: CAPE dynamics and LCL crossings. *Water Resour. Res.*, **51**, 8476–8493, https://doi.org/10.1002/2015WR017286.

Yuan, W., and Coauthors, 2019: Increased atmospheric vapor pressure deficit reduces global vegetation growth. *Sci. Adv.*, **5**, eaax1396, https://doi.org/10.1126/sciadv.aax1396.

Zhang, Z., Y. Li, F. Chen, M. Barlage, and Z. Li, 2020: Evaluation of convection-permitting WRF CONUS simulation on the relationship between soil moisture and heatwaves. *Clim. Dyn.*, **55**, 235–252, https://doi.org/10.1007/s00382-018-4508-5.

Zhao, C., and Coauthors, 2017: Temperature increase reduces global yields of major crops in four independent estimates. *Proc. Natl. Acad. Sci.*, **114**, 9326–9331, https://doi.org/10.1073/pnas.1701762114.

Zhu, Z., and Coauthors, 2016: Greening of the Earth and its drivers. *Nat. Clim. Change*, **6**, 791–795, https://doi.org/10.1038/nclimate3004.

Downloaded from. https://doi.org/10.1126/science.1251423.